

**Some parts of this thesis may have been removed for copyright restrictions.**

If you have discovered material in AURA which is unlawful e.g. breaches copyright, (either yours or that of a third party) or any other law, including but not limited to those relating to patent, trademark, confidentiality, data protection, obscenity, defamation, libel, then please read our [Takedown Policy](#) and [contact the service](#) immediately

STUDIES OF THE RESIDENCE-TIME DISTRIBUTION  
FOR THE DRYING OF DROPS IN SPRAY  
DRYING TOWERS

by

Ayokunle Olu Ade-John, B.Sc., M.Sc., Dip.Chem.Eng.

203623 30 MAR 1977  
660.47791 ADE

A thesis submitted to the University of Aston in  
Birmingham for the degree of Doctor of Philosophy.

DEPARTMENT OF CHEMICAL ENGINEERING,  
THE UNIVERSITY OF ASTON IN BIRMINGHAM

October, 1976.

**VOLUME CONTAINS CLEAR OVERLAYS**  
**OVERLAYS SCANNED SEPERATELY AND**  
**OVER THE RELEVANT PAGE.**

DEDICATED TO MY FAMILY



SUMMARY

A review of the literature pertaining to the drying of single drops and the drying of clouds of droplets in spray drying towers has been reported with reference to the residence-time distribution of the drops and air in the tower.

The experimental investigation on the drying characteristics of single crust-forming drops has been carried out on sodium sulphate decahydrate drops.

A 9' x 4' diameter P.V.C. spray drying tower was designed and operated to study the residence-time distribution and flow patterns of the drops and the air in the tower.

A mathematical model for evaluating the mass transfer coefficient, at high rates of heat and mass transfer through the sodium sulphate crust has been proposed. The crust thickness and porosity were evaluated from the stereoscan photomicrographs. The porosity was found to be independent of the drop diameter, while the crust thickness decreased as the drop diameter increased. Hence the mass transfer coefficient increased with an increase in drop diameter.

The flow patterns of the air in the tower were identified by injecting thick clouds of smoke into different parts of the tower. The volumes of the various sections were measured and correlations predicting these volumes have been presented. A mathematical model to predict the exit concentration profile as a function of

time of a pulse of tracer inserted into the air in the tower was derived. It was based on the volumes obtained from the smoke experiments. The experimental values showed a good agreement with the theoretical predictions. A tracer technique has also been applied for the determination of the residence-time distribution of sprays of pure water and sodium carbonate slurries.

A design model for the spray drying tower has been developed and tested with data supplied by an industrial company from an existing pilot plant spray tower. The agreement between experimental and predicted results was extremely good.

### ACKNOWLEDGEMENTS

The author wishes to express his sincere gratitude to:-

Professor G. V. Jeffreys, Head of the Department of Chemical Engineering, University of Aston in Birmingham, for his continual interest, encouragement and personal supervision of this research programme.

Mr. N. Roberts, Chief Technician in the Department of Chemical Engineering and the entire members of the Technical Staff for their help and advice.

Mr. C. Stewart, of the Department of Metallurgy for his assistance in the use of the stereoscan equipment.

The Kwara State Government of Nigeria, for awarding me a Postgraduate Scholarship to pursue this research programme.

Miss C. E. Estien, for typing the thesis with extreme care.

CONTENTS

	<u>Page</u>
<u>CHAPTER 1</u>	
Introduction	1
<u>CHAPTER 2</u>	
<u>Literature Survey</u>	
2.1 Evaporation From Drops	3
2.1.1 Theoretical Considerations	4
2.1.2 Forced Convection	5
2.1.3 Natural Convection	6
2.2 Drying of Drops containing Dissolved and suspended Solids.	9
2.2.1 Effect of Dissolved and Suspended Solids.	10
2.2.2 Drying and Evaporation in Superheated Vapours.	11
2.2.3 Estimation of Drying Time	13
2.3 Evaporation of Liquids into turbulent Gas Streams	16
2.3.1 The j-Factor of Chilton and Colburn.	17
2.3.2 The j-factor for Heat Transfer	19
2.3.3 The j-factor for Mass Transfer	20
2.4 Mass Transfer Across a Phase Boundary	22
2.4.1 The Two-Film Theory of Whitman	23
2.4.2 Higbie Penetration Theory	24



	<u>Page</u>
2.4.3 The Film-Penetration Model	25
2.4.4 Mass Transfer Coefficients	26
2.5 Flow Characteristics of Drops and Air in Spray Drier.	29
2.5.1 Flow patterns of air in spray drying towers.	30
2.5.2 Residence-time analysis of air in Spray Driers.	31
2.5.3 Hydrodynamic Behaviour of Spray Droplets.	33
2.6 Spray Drying Of Droplets and Dissolved Solids.	39
2.6.1 Heat and Mass Transfer in Spray Drying.	39
2.6.2 Factors Affecting the Properties of Spray-dried Materials.	42
2.7 Conclusions	44
 <u>CHAPTER 3</u>	
<u>Mathematical Models</u>	46
3.1 Momentum - Heat Transfer Model	46
3.2 Air Residence-Time Model	51
3.3 Spray Tower Design Model	59
 <u>CHAPTER 4</u>	
<u>Experimental Equipment, Procedure and Measurements</u>	66
4.1 Description of Experimental Equipment	66

	<u>Page</u>
4.1.1 Experimental apparatus for the Drying of Single Drops.	66
4.1.2 Overall experimental equipment for the Spray Drying System.	73
4.1.3 The Gas Analysis Equipment	77
4.1.4 The Spray Tower	79
4.1.5 The Spray Nozzles	85
4.1.6 The Katharometer	88
4.1.7 The Smoke Generator	88
4.2 Calibration of Measuring Instruments For Studies of the Drying of Single Drops.	91
4.2.1 The Feed Device	91
4.2.2 Rotameter	91
4.2.3 Dew-Point Meter	92
4.3 Calibration of Measuring Instruments For Studies in The Spray Drying Tower.	93
4.3.1 Rotameter	93
4.3.2 The Dall Tube Meter	93
4.3.3 Two-Pen Potentiometric Recorder	94
4.4 Experimental Procedure and Measurements.	95
4.4.1 Drying of Single Sodium Sulphate Drops.	95
4.4.2 Estimation Of Volumes In the Spray Tower.	98
4.4.3 Air Residence-Time Analysis	101

	<u>Page</u>
4.4.4 Residence-Time, Analysis For Pure Water Spray.	104
4.4.5 Residence-Time Analysis For Sprays of Sodium Carbonate Slurries.	104
 <u>CHAPTER 5</u>	
<u>Presentation And Analysis Of Experimental Results</u>	111
5.1 Drying of Single Drops of Sodium Sulphate Decahydrate.	111
5.2 Hydrodynamic Behaviour of Drops and Air in The Spray Tower.	118
5.2.1 Effect of Air Flowrate	118
5.2.2 Effect of Liquid Feed Flowrate	118
5.2.3 Effect of Reynolds Number	124
5.2.4 Effect of Superficial Velocity	124
5.2.5 Correlations	124
5.3 Exit Response Analysis of Air	129
5.3.1 Effect of Air Flowrate	129
5.3.2 Comparison of Predicted with Experimental Exit Concentration Profile..	155
5.4 Exit Response Analysis of Liquid Spray	161
5.4.1 Residence-Time Analysis For Pure Water Spray.	161
5.4.2 Residence-Time Analysis For Sodium Carbonate Slurries.	161

	<u>Page</u>
 <u>CHAPTER 6</u>	
Application of the Spray Tower Design Model	165
6.1 Discussion on the Design Model	174
 <u>CHAPTER 7</u>	
<u>Discussion</u>	176
7.1 Drying of Single Sodium Sulphate Drops	176
7.2 Hydrodynamic Behaviour of Drops and Air in the Spray Drying Tower.	177
7.2.1 Residence-Time Analysis of Air	177
7.2.2 Residence-Time Analysis of Liquid Spray.	178
7.3 Comparison of Experimental Techniques	180
 <u>CHAPTER 8</u>	
<u>Conclusions And Recommendations</u>	
8.1 Conclusions	183
8.2 Recommendations for Future Work	185
 <u>APPENDICES</u>	
Appendix A	187
Appendix B	195
Appendix C	216
 NOMENCLATURE	 255
REFERENCES	261



	<u>List of Figures</u>	<u>Page</u>
Figure 2.1	Mass Transfer from a liquid drop.	24
Figure 3.1	Crust-forming Hemispherical Drop.	47
Figure 3.2	Air Residence-Time Distribution Model.	52
Figure 3.3	Heat and Mass Balance on Spray Drier.	60
Figure 4.1	Overall Flow Diagram - Single Drop Experiment.	67
Figure 4.2	Constant Temperature Unit.	71
Figure 4.3	Flow Diagram of Overall Experimental Equipment.	74
Figure 4.4	Diagram of Equipment for the Analysis of CO <sub>2</sub> in Air.	76
Figure 4.5	The Spray Drying Tower.	78
Figure 4.6	Dished-End of Spray Drying Tower	81
Figure 4.7	Conical Base and Ring Main of P.V.C. Spray Tower.	82
Figure 4.8	Conical Base and Ring Main of S/S Spray Tower.	83
Figure 4.9	Katharometer.	87
Figure 4.10	Thickness of By-pass Stream from Spray Chamber Wall.	103
Figures 5.2.1-5	Plots of $V_i/\epsilon_V$ Versus Reynolds Number.	113

		$\frac{\rho_g U_g}{\rho_l U_l}$	<u>Page</u>
Figures 5.2.6-10	Plots of $V_i/\Sigma V$ Versus		119
Figures 5.3.1-25	Air Residence Time Distribution		130
Figures 5.4.1-5	Residence Time Distribution for Water Spray.		156
Figures 5.4.6-7	Residence Time Distribution for Sodium Carbonate Slurries.		112

	<u>List Of Plates</u>	<u>Page</u>
Plate 4.1	Overall Experimental Apparatus - Single Drop.	65
Plate 4.2	Feeding device.	69
Plate 4.3	Constant Temperature Unit.	72
Plate 4.4	Spray Drying Tower.	75
Plate 4.5	Spray Nozzles	84
Plate 4.6	The Katharometer and 6-way Manifold	86
Plate 4.7	The Smoke Generator	89
Plate 4.8	Lee's Disc Apparatus	97
Plate 4.9	A Typical Water Spray	100
Plate 4.10	Control Panel	105
Plates 5.1-4	Stereoscan Photomicrographs	107
Plates 5.5-6	Input/Output Response graphs.	127

## CHAPTER ONE

### INTRODUCTION

## 1. INTRODUCTION

Among the many drying methods available, the growing importance of spray drying is abundantly evident from the increasing number of its industrial applications, ranging from production in the most delicate conditions in food and pharmaceutical manufacture, through to the high outputs required in such heavy chemical fields as detergent and inorganic salt manufacture.

In spray drying, as in most other drying problems, simultaneous heat and mass transfer takes place; heat being transferred first by convection from the hot gas to the drop surface and then by conduction into the drop while vapour is transferred by diffusion and convection back to the gas stream. The first period of drying, termed the constant-rate period when a free liquid interface exists, is susceptible to a simple analysis, but as soon as the drop concentrates beyond saturation a crust begins to form and an additional resistance is created to reduce the rate of mass transfer from the drop. Thus the drying characteristics are determined by the nature of the solid structure. The rate of mass transfer through the crust so formed, depends on the material being dried and the temperature difference between the drop and gas. Previous investigators (1,10,11,25) on the drying of single drops have based their analyses on low rates of heat and mass transfer when a small temperature difference prevails.



A review of the literature has shown that the manner in which the sprayed droplets and the drying air contact one another is an important factor in spray drier design.

The experimental investigation has therefore been carried out under the following sections;

- (1) Drying of single crust-forming sodium sulphate drops at high rates of transfer.
- (2) The Flow characteristics and the residence-time distribution of the drops and air in a 9' x 4' diameter spray drying tower.
- (3) A design model incorporating (1) and (2) was developed and tested with experimental data from an existing spray drying tower.

A mathematical model for calculating the mass transfer coefficient from the amount of water evaporated from a single crust-forming drop has been developed in section (3.1).

A mathematical model for predicting the exit concentration profile of tracer in air in the spray tower has also been developed in section (3.2).

The results of this study have been presented graphically in chapter 5, and correlations for predicting the volumes of the various flow patterns in the spray tower are also presented in section (5.2.5).

CHAPTER TWO

LITERATURE SURVEY

## 2.1 EVAPORATION FROM DROPS

Studies of the factors affecting the rate of evaporation of drops of pure water and the rate of evaporation of water drops containing dissolved and suspended solids have been carried out by Ranz and Marshall (1). Their investigation was restricted to the Reynolds number range usually encountered in Spray drying operations. Independent correlations of heat and mass transfer rates have been presented. The results obtained showed that drops containing dissolved solids such as ammonium nitrate and sodium chloride, evaporated initially as though they were saturated throughout, despite the fact that the average concentration was less than Saturation. However, for drops containing insoluble materials, the initial evaporation rate was found to correspond to that for pure water.

Methods for predicting the evaporation rates of a single drop and of the phenomena associated with the evaporation process are of importance in the analysis of many chemical engineering operations involving the dispersion of liquids in gases. Thus, fundamental data on the factors influencing the rate of heat and mass transfer for droplets are important to the operations of spray drying, spray cooling, humidification, spray absorption, spray extraction, combustion, crystallization, transfer in fluidised beds, and other operations where transfer occurs between a continuous gas phase and a discontinuous phase appearing as spherical particles.

The fundamental study of the evaporation from drops can be divided into the following parts:



- (1) Rate of heat transfer to the drop surface.
- (2) Rate of evaporation and mass transfer from the drop surface.
- (3) Temperature and Concentration at the drop surface during evaporation.
- (4) Effect on evaporation rate of the original drop temperature, heats of solution and crystallization, and the manner in which solid surfaces are formed.

### 2.1.1 Theoretical Considerations

The evaporation of a liquid drop is an operation in which simultaneous heat and mass transfer takes place; heat being transferred by convection from the hot air stream to the drop surface, then by conduction into the drop for its evaporation. At the same time, due to this evaporation, vapour is transferred from the drop, first through the drop and then by convection into the hot air stream. The rate of transfer per unit area of interface is a function of temperature, humidity, and transport properties of the gas, the diameter, temperature and velocity of the gas over the drop. Thus, Fuchs (2) presented a theoretical treatment of mass transfer for evaporation of drops in still air, and found that the rate of change of surface area of a pure liquid drop, was constant during evaporation and that the total lifetime of the drop was proportional to the square of the initial drop diameter. This agreed favourably with the theoretical investigations made by Froessling (5), Langmuir (100) and Williams (14).

Kramers (3) and Meyer (4) presented heat transfer data

in the low Reynolds number range and analysed the data on free convection from spherical drops respectively. However, the diameters of the spherical drops studied, were quite different from the range used by Ranz and Marshall (1). Also free convection obscured the true effect of the velocity of the fluid stream. Boundary layer theory (5) indicates that the rate of transfer is maximum on the front side of the drop facing the on-coming air stream, decreases to a minimum value near the separation point and increases to another, but lower, maximum rate on the trailing face which experiences velocities in the reverse direction. This type of distribution of mass-transfer rates was investigated by Froessling (5) through the sublimation of a naphthalene bead, but since his results were largely based on the evaporation of materials of low volatility, the problem was restricted only to mass transfer. Froessling first cited the equations for correlating data on heat and mass transfer. These equations were later used by Ranz and Marshall (1), for correlating their experimental data, as quoted in section (2.1.2) below.

### 2.1.2 Forced Convection

Experimental data on mass-transfer rates from spherical drops of pure water and benzene were correlated by Ranz and Marshall (1), by an empirical equation similar to the one used by Froessling (5). Thus, for mass transfer;

$$\text{Nu}' = 2.0 + 0.6 (\text{Sc})^{0.33} (\text{Re})^{0.5} \quad (2.1)$$



and by analogy, heat-transfer data should be correlated by a corresponding equation.

$$\text{Nu} = 2.0 + 0.6 (\text{Pr})^{0.33} (\text{Re})^{0.5} \quad (2.2)$$

Where the symbols are, as given, in the nomenclature. Equations (2.1) and (2.2) are both consistent with the theoretical requirement that, at zero Reynolds Number,

$$\text{Nu}' = \text{Nu} = 2.0 \quad \text{at } \text{Re} = 0 \quad (2.3)$$

At high values of Reynolds Number, however, the constant term becomes less significant and hence equations (2.1) and (2.2) can be converted through the well-known j-factor equations of Chilton and Colburn (6,7) which will be discussed in section (2.3).

### 2.1.3. Natural Convection

In cases where heat transfer is by conduction and mass transfer is by diffusion, at zero relative velocity the relation

$$\text{Nu} = \text{Nu}' = 2.0 \quad \text{at } V_o = 0 \quad (2.4)$$

applies. In the practical case, however, the existence of a density difference across the transfer path, and a fluid velocity caused by free convection contribute to the transfer rate. Ranz and Marshall (1) accounted for this buoyancy effect by proposing that the velocity term

in the Reynolds Number, could be taken as the vector sum  $|\bar{V}_O + \bar{V}_{fc}|$ ; where  $\bar{V}_{fc}$  is a velocity component due to free convection parallel to gravity.

$$\text{If } |\bar{V}_{fc}| = (D_p g_c \sigma \Delta\theta)^{0.5} \quad (2.5)$$

and  $V_O = 0$ , then equations (2.1) and (2.2) become:-

$$Nu' = 2.0 + 0.6 (Sc)^{0.33} (Gr)^{0.25} \quad (2.6)$$

$$Nu = 2.0 + 0.6 (Pr)^{0.33} (Gr)^{0.25} \quad (2.7)$$

Thus by substituting the velocity term proposed in equation (2.5) into the Reynolds Number, Ranz and Marshall obtained equations (2.6) and (2.7) in which the Reynolds Number was replaced by the Grashof Number, thus

$$Gr = (D_p^3 \rho_g^2 g_c \sigma \Delta\theta) / \mu^2 \quad (2.8)$$

Equations (2.6) and (2.7) are quite consistent with standard correlations for natural convection (8,12). For simultaneous heat and mass transfer at high temperature and concentration driving forces however, corrections for sensible heat carried by the vapour molecules and by diffusion due to thermal gradients must be considered (9,55). It is however worth noting the factors which might have contributed to errors in the experimental data presented by Ranz and Marshall (1) and

anomalies in heat and mass transfer analogy. These are:-

- (1) Inaccurate values of diffusivity might have been used.
- (2) Secondly, the value of the partial pressure of diffusing vapour at the interface might not have been the saturation vapour pressure.
- (3) The partial pressure of water vapour in air might have been zero at low air rates where the air stream velocity and the velocity of natural convection were of the same order of magnitude, and water vapour from the surrounding might have diffused into the jet.
- (4) Free convection may have been significant at low values of air velocity.

Although the data for heat transfer may have involved inherently inaccurate corrections for sensible heat, this correction was small, and since the values of thermal conductivity are much more reliable than values of diffusivity, the heat transfer points are believed to be more accurate than the mass transfer points when both the  $Nu$  and  $Nu'$  numbers are plotted (1) against the products of  $(Pr)^{0.33} (Re)^{0.5}$  and  $(Sc)^{0.33} (Re)^{0.5}$  for heat and mass transfer respectively.



## 2.2. DRYING OF DROPS CONTAINING DISSOLVED AND SUSPENDED SOLIDS

A lot of work appears to have been carried out on the drying of pure liquid drops which is less complex than the drying of drops containing dissolved and suspended solids. In spray drying, as in most drying problems, the first period of drying usually termed the constant-rate period (10,15,16,17) is amenable to a simple analysis. However, as soon as the droplet concentrates to the point where it no longer presents a free liquid surface to the hot air stream, it becomes a particle with drying characteristics determined by the nature of the solid structure - that is the critical point (21,22,23). The particle enters a period in which the rate of drying decreases with decreasing moisture content.

For a clear understanding of the evaporation of drops containing dissolved solids, a study of the drying characteristics of drops of pure solvent must first be investigated (11). Then, a free liquid interface is initially presented to the air stream during drying, so that the evaporation takes place in a similar manner as from pure water drops until the crust begins to form (15,24). At this stage, however, the drying characteristics of the crust-forming drop will depend on the type of material dissolved in the drop. For example Audu and Jeffreys (11,45), found that the crusts formed when drops of detergent slurries were dried were not as porous as those of sodium sulphate, and in some cases, appear to be somewhat

plastic.

The work of Charlesworth and Marshall (10), on the drying of single drops containing dissolved sodium chloride, copper sulphate, ammonium sulphate, potassium nitrate, and whole fresh milk shows that a significant amount of resistance to evaporation through the crust exists. An internal stress developed in the drop due to pressure build-up as a result of the crust being impermeable to the easy flow of liquid or vapour through its pores. Hence, in most cases the skin then ruptured and collapsed.

#### 2.2.1 Effect of Dissolved and Suspended Solids

Some dissolved materials in a droplet lower the vapour pressure of the liquid. This depends on both the interfacial temperature as well as the concentration of the nonvolatile component in the surface. In these circumstances the drop evaporates as if it were saturated throughout, because the diffusion coefficients of the dissolved materials are so small that solids concentrate in the surface by evaporating much faster than they can diffuse towards the centre of the drop.

The work of Williams and Schmit (13,14) showed that sometimes the heat of crystallization is significant compared with the latent heat of evaporation and that the constant-rate period (1,10) has to be treated as two separate periods with different interfacial temperatures for each.



### 2.2.2 Drying and Evaporation in Superheated Vapours

Trommelen and Crosby (25), investigated the evaporation of pure liquid drops and the drying of drops containing dissolved and suspended solids, as well as drops containing food products in a medium of superheated vapour. They found that the rate of evaporation of water was much lower in superheated steam than in a hot air stream, although the medium in which a faster rate of drying took place depended on the type of material being dried. They also discovered that the final product showed no major differences for the two drying media, except that some materials yielded denser particles in superheated steam than in the hot air stream. A complete history of the drying from single drops containing dissolved solids was only obtained (25), when drying took place very slowly. At high temperatures, drying took place quite rapidly even though the drop was in an atmosphere of negligible velocity.

Investigations by Chu et al (26,27), Toei et al (28), and Wenzel (29) reveal that when a pure liquid evaporates into a gas stream of dissimilar vapour, it attains dynamic equilibrium at a temperature somewhat below the dry bulb temperature due to the combined resistances to heat and mass transfer in the drying medium. On the other hand when the liquid evaporates into a medium of its own vapour the resistance to mass transfer is extremely small, and the temperature of the liquid is of the same order as that of its saturated vapour at its ambient pressure. Charlesworth, Ranz and Marshall (1,10) discovered similar thermal effects during the first period of drying (18,19,20) in which



dissolved materials were present, even though the length of this period of drying was a short one.

Toei et al (28) evaporated pure water into superheated steam and mixtures of steam and air at  $9 \leq Re \leq 120$ , and  $0.7 \leq Pr \leq 1.0$  and obtained the following correlations for heat and mass transfer, similar to those of Ranz and Marshall (1). For heat transfer;

$$Nu = 2.0 + 0.65 (Re)^{0.5} (Pr)^{0.33} \quad (2.9)$$

and for mass transfer;

$$Sh (p_{av}/\Pi)^{-0.2} = 2.0 + 0.65 (Re)^{0.5} (Sc)^{0.33} \quad (2.10)$$

Where  $\Pi$ , is the total pressure of the system. The above correlations are in good agreement with those of Keey and Glen (30), Rowe et al (31) and Hughmark (32) who concluded that, for  $1 \leq Re \leq 450$  and  $Sc$  or  $Pr \leq 250$ , the Ranz and Marshall correlations were applicable.

Lee and Ryley (33), also studied the evaporation of non-spherical water drops in superheated steam and they obtained correlations for heat and mass transfer, similar to those of Ranz and Marshall (1); except that the empirical factor in the correlations was found to be 0.74 instead of 0.6.

For drops containing food products such as sucrose, tomato juice, coffee extract and milk, Trommelen and Crosby (25) studied the effect of temperature and drying medium on their drying characteristics. They discovered that the

drops generally did not exhibit any constant temperature period, near the saturation temperature when drying took place in air. The drop temperature rose continuously to that of the air throughout the course of drying. When drying took place in superheated steam, however, a constant temperature period occurred near the saturation temperature of the steam.

As far as the evaporation of drops containing dissolved and suspended solids is concerned, the work by Zak (34) appears to be inconclusive and offer no basis for the prediction and explanation of the phenomena associated with the constant-rate period. Keen (15), Fisher (16,17) and Sherwood (18,19,20), indicated that under steady state conditions, the drying process could be divided into a constant rate and one or two falling-rate periods. The results obtained from the studies of Van Krevelin (35) on the drying of single drops seem applicable.

### 2.2.3 Estimation Of Drying Time

The evaporation rate for the first period of drying of a single aqueous droplet can be obtained from the equation for the rate of heat transfer,

$$q = h A (\theta_o - \theta_i) \quad (2.11)$$

Since radiation transfer is negligible, the heat transfer coefficient, can be estimated from the relation;

$$h = \frac{k}{D_p} = (2.0 + 0.54 (Re)^{0.5}) \quad (2.12)$$

The above relation, however, is restricted to aqueous drops (1), thus it can not be applied to all cases of drying.

In spray drying where atomisation produces drop diameters in the region of  $10^{-4}$ m, with cocurrent operations, the heat transfer coefficient,  $h$ , can be calculated from a simpler relation using the limiting value of;

$$Nu = (h D_p / k) = 2.0 \quad \text{at } Re = 0 \quad (2.13)$$

The first period of drying may be terminated before conditions of uniform saturation throughout the drop are even reached. Ranz and Marshall (1) reported that this created an unusual porosity for the final product.

Equation (2.11) is applicable for the estimation of the rate of drying of the falling rate period if an accurate value of the temperature difference can be determined.

A heat balance for drying in still air gives the following expression for the falling rate;

$$\frac{dW}{dt} = \frac{6h}{\lambda D_{pc}} \frac{(\Delta\theta)}{\rho_s} + \frac{Cs}{\lambda} \frac{d(\Delta\theta)}{dt} \quad (2.14a)$$

This equation is applicable for practical spray drying operations (1). For materials which do not crystallize from solution to give extraneous heat effects, however, the falling rate drying time for drops can be estimated from the relation;



$$(t_f - t_c) = \frac{\lambda D_{pc} \rho_s (W_c - W_f)}{6h \Delta\theta_{av}} \quad (2.14b)$$

Hence an estimation of the total drying time  $t_T$ , at low Reynolds Number for drops containing suspended solids is given by:

$$t_T = \frac{\lambda_i \rho_l ((D_{p1})^2 - (D_{pc})^2)}{8k \cdot (\theta_o - \theta_i)} + \frac{\lambda (W_c - W_f) \rho_s (D_{pc})^2}{12k \cdot \Delta\theta_{av}} \quad (2.15)$$

In spray drying, where high temperature is most frequently necessary, especially for cocurrent flow operation, it has been generally observed (1), that the air temperature falls much more rapidly than the particle temperature increases. This problem must therefore be considered when using equation (2.15). Hence the average temperature difference,  $(\theta_o - \theta_i)$ , is used during the constant-rate period, while the logarithmic mean average of the temperature difference during the falling rate period will be more appropriate.

### 2.3 EVAPORATION OF LIQUIDS INTO TURBULENT GAS STREAMS

For the design of equipment for the process industries, it is essential that the problems of heat transfer, mass transfer and fluid flow are taken into consideration. A number of experimental studies on heat transfer with different fluids flowing in tubes and passing various solid shapes, as well as studies on mass transfer in many types of equipment have been carried out (36). It has been found that mass transfer, heat transfer and fluid flow are closely related, and a complete understanding of turbulent flow conditions near phase boundaries could provide a sound basis for the development of the theory of interphase transfer. Maisel and Sherwood (36), made a contribution to this subject by evaporating water, carbon tetrachloride and benzene from flat surfaces, cylinders and spheres into turbulent streams of different gases. They obtained experimental data on the effect of both scale and intensity of turbulence on the rate of mass transfer. Gilliland and Sherwood (38) presented the following correlation

$$\frac{K_G D}{D_v} = 0.023 (\text{Re})^{0.83} (\text{Sc})^{0.44} \quad (2.16)$$

for vapourisation of liquid into air in a wetted-wall column.

Sherwood (37), developed a theoretical expression for mass transfer in turbulent flow in the form;

$$\frac{K_c p_b \gamma}{V_o P} = f/2 \quad (2.17)$$

Where  $\gamma$  is a function of  $f$ ,  $Re$  and  $Sc$ . The above equations formed the basis of analysis that produced the  $j$ -factors of Chilton and Colburn (6).

### 2.3.1. The $j$ -Factor Of Chilton And Colburn

Chilton and Colburn (6) suggested that the empirical function  $(Sc)^{0.67}$ , could be used in place of  $\gamma$ , in equation (2.17) and thereby, correlated the data in terms of the dimensionless group  $j_D$ , where:

$$j_D = \frac{K_c p_b Sc^{0.67}}{V_o P} = f(Re) \quad (2.18)$$

The correlation agreed favourably with those of Maisel and Sherwood (36) in treating their experimental data. Maisel and Sherwood (36) also modified Pohlhausen's (39), theoretical relation for heat transfer and derived the following correlation for mass transfer;

$$j_D = 0.323 (Re)^{-0.5} \left(1 - \left(\frac{l_o}{l_t}\right)^{0.75}\right)^{-0.5} \quad (2.19)$$

The empirical constant of 0.323 obtained, differs from the



value of 0.332 obtained by Pohlhausen (39). This is because he had assumed different velocity and temperature profiles. Equation (2.19) also has its short-coming, as it cannot be applied to cases where the boundary layer is turbulent. Hence, it is confined to laminar boundary layer. Jacob and Dow (40), followed the same reasoning and correlated their data on heat transfer to a cylinder placed parallel to an air stream and obtained;

$$\frac{hl_t}{k} = 0.028 (Re)^{0.8} (1 + 0.4(l_o/l_t)^{2.75}) \quad (2.20)$$

The data correlated by Powell (41) agreed favourably with the correlations obtained by Maisel and Sherwood (36) and Jacob and Dow(40).

Similar investigation of the effect of the Schmidt group on mass transfer in turbulent flow was made by Linton and Sherwood (42). Objects of various size and shape were placed in water and tested both in streamline and turbulent flow. The data at low water flowrates were in good agreement with the theory for streamline flow. The data obtained in turbulent flow agreed favourably with that of Chilton and Colburn involving the  $(Sc)^{0.67}$  group. Linton and Sherwood, however, found that in streamline flow for  $Re \leq 2100$ , no radial mixing occurred and that the transfer of solute from the tube wall into the fluid stream was entirely by molecular diffusion.

Colburn (44,46) derived a method for correlating the data from forced convection heat transfer and made a

comparison of the correlation with fluid friction. He obtained a correlation in the form:

$$\text{St} (\text{Pr})^{0.67} = 0.023 (\text{Re})^{-0.2} \quad (2.21)$$

Where:  $\text{St} = \left( \frac{h}{c_p \rho u} \right)$ , Stanton Number

The above equation has been modified to give the well-known  $j$ -factor for heat transfer.

### 2.3.2. The $j$ -Factor For Heat Transfer

By modifying equation (2.21) Chilton and Colburn (6), obtained a correlation in dimensionless form for heat transfer by convection to a fluid flowing through a tubular passage.

$$\text{Nu} = 0.023 (\text{Re})^{0.8} (\text{Pr})^{0.33} \quad (2.22)$$

Dividing both sides of equation (2.22) by the product  $(\text{Re} \cdot \text{Pr})$ , Chilton and Colburn obtained the correlation for the  $j$ -factor for heat transfer,  $j_h$

$$j_h = 0.023 (\text{Re})^{-0.2} \quad (2.23)$$

They also made a plot of  $j_h$  against  $\text{Re}$  and found that the curve obtained was in good agreement with the friction chart for flow through tubes.



### 2.3.3. The j-Factor For Mass Transfer

By analogy to heat transfer under forced convection, an expression for the rate of mass transfer is;

$$\frac{K_G d_p}{D_v} = f(\text{Re } \text{Sc}) \quad (2.24)$$

This relation was confirmed by Gilliland and Sherwood (23), who correlated experimental data on the vapourisation of liquids into air in a wetted-column.

Chilton and Colburn (6), later derived the j-factor for mass transfer,  $j_D$ , by analogy to that obtained for heat transfer:

$$j_D = \frac{K_G p_b}{G_s} \quad (2.25)$$

When expressed as  $j_D$ ,  $j_h$  or  $f/2$ , data on mass transfer, heat transfer and friction are in close agreement in the range  $1000 \leq \text{Re} \leq 30000$  for single cylinders placed normal to turbulent gas stream. Maisel and Sherwood (36), obtained correlations for the rates of mass transfer for various liquids evaporating from different surfaces. They found that the j-factors for heat and mass transfer were approximately equal. Hence the values of mass transfer coefficients could be obtained from the corresponding values of the heat transfer coefficients and vice versa.

The application of the j-factors however, has its limitations. Thus when a droplet containing dissolved solids is being dried it concentrates to such a point (10), where it no longer presents a free liquid-vapour interface to the air stream, then the j-factors are no longer applicable. This is due to the drag (1) caused by the eddies set up as a result of the air impinging on an obstruction - that is the resistance caused by the crust of the drop. Another reason is due to the difference in the transfer paths for the heat and mass transfer. Heat being transferred by conduction through the crust, while vapour is transferred through the pores of the crust.

## 2.4 MASS TRANSFER ACROSS A PHASE BOUNDARY

In most important applications of mass transfer, it has been found that material is transferred across a phase boundary. When a liquid droplet is evaporating into still air, vapour is transferred from the surface to the bulk of the gas due to the concentration gradient. This process continues until the evaporation of all the liquid is complete or until the gas is saturated and the concentration gradient is reduced to zero (46). The rate of mass transfer between two fluid phases, is dependent upon the following:

- (1) The physical properties of the two phases concerned.
- (2) The concentration difference
- (3) The interfacial area
- (4) The degree of turbulence in each fluid.

Due to the pioneering work of Maxwell (47), on mass transfer from spherical particles, an expression for the mass transfer coefficient,  $K_i$ , was obtained by solving the equations describing radial molecular diffusion analytically.

$$K_i = \frac{2 C D_v}{D_p} \quad (2.26)$$

This theoretical treatment, however, is closely related to mass transfer within a single phase in which no discontinuities occur. A reasonable number of mechanisms have been suggested to represent conditions existing in the



phase boundary region (46,52,108). These include the Two-Film Theory propounded by Whitman (48), which states that the resistance to transfer in each phase could be regarded as lying in a thin film close to the interface. Goodridge and Brickwell (49) investigated the interfacial resistance in carbon dioxide-water system, and found that it was not high. Higbie (50) also suggested the film Penetration Theory and reported that the transfer process was largely due to new material transported by eddies to the interface and molecular diffusion across the interface, where unsteady state transfer took place for a fixed period at the freshly exposed surface. Danckwerts (53), however, considered a modification of the theory by reporting that the material brought to surface remained there for varying periods of time. The Film-penetration Theory propounded by Toor and Manchello (54), has revealed that each of the earlier theories has its limitations.

#### 2.4.1 The Two-Film Theory of Whitman

The Whitman Two-film theory (48), treated the problem of mass transfer from one fluid stream to another, by assuming that turbulence faded away at the interface, and that a laminar layer existed in each fluid. The existence of turbulent eddies beyond the laminar layer however, created a decrease in the resistance to mass transfer. The theory also assumed that the regions where resistance to transfer occurred could be replaced by two hypothetical layers, one on either side of the interface.



### 2.4.2 Higbie Penetration Theory

Higbie (50), propounded his theory after studying the existence of a resistance to transfer of a pure liquid drop, exposed to a gas for a specific period. This theory was based on the assumption that the eddies in the fluid carried an element of fluid to the interface where it was exposed to the second phase for a specific time interval, and then the surface element was mixed with the bulk once more.

Thus the rate of mass transfer for a surface element moving from A to B in time  $t$ , of a pure liquid drop shown in Figure 2.1 could be expressed as;

$$N_A = 2 (C_i - C_o) \cdot \left( \frac{D_v}{\pi t} \right)^{0.5} \quad (2.27)$$

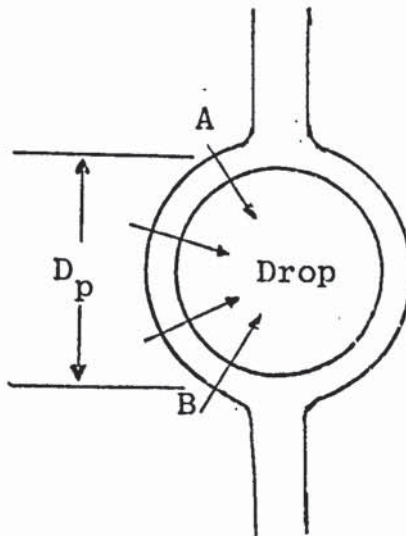


Figure 2.1 Mass Transfer From A Liquid Drop

where the time of exposure of the surface element was given by:

$$t = \frac{D_p}{V} \quad (2.28)$$

A concentration gradient occurred across the surface of the liquid drop.

Danckwerts (53), however, presented a modified form of Higbie's theory, by suggesting that each fluid element of the surface would not be exposed equally, but that the ages were randomly distributed.

#### 2.4.3. The Film-Penetration Model

Toor and Marchelo (54), combined some of the principles in the theories of Whitman (48) and Higbie (50). Similar to the Whitman's Two-film theory, they suggested that the total resistance to transfer was close to the laminar film at the interface, but failed to agree with the Whitman's theory that mass transfer was a steady state process. They also agreed with Higbie's Penetration Theory on mass transfer, but that resistance to mass transfer was restricted to the finite film. Toor and Marchelo therefore concluded that neither the Two-film theory nor the Penetration theory could be treated separately, as they both occurred depending on the time of exposure.

#### 2.4.4. Mass Transfer Coefficients

From all the theories of mass transfer, it is evident that the rate of mass transfer,  $N_A$ , in the absence of bulk flow, was directly proportional to the concentration driving force, which could be expressed as the molar concentration difference:

$$N_A = K_i (C_i - C_o) \quad (2.29)$$

Where  $K_i$  is the mass transfer coefficient and  $C_i$ ,  $C_o$ , are the molar concentrations of the diffusing species in the interface and the bulk phase respectively. The mass transfer coefficient,  $K_i$ , was directly proportional to the diffusivity and inversely proportional to the film thickness (46), in the case of the Two-Film Theory. For the Penetration Theory, however, it was found to be proportional to the square root of the diffusivity and inversely proportional to the square root of the time of exposure when all surface elements were exposed at equal time, whereas it was found to be proportional to the square root of the rate of renewal when random surface renewal was assumed.

With mass transfer across a phase boundary (46), however, when there was no accumulation of material at the interface, the mass transfer on either side of the phase boundary could be expressed in the form:



$$N_A = k_1 (C_{01} - C_{i1}) = k_2 (C_{i2} - C_{02}) \quad (2.30)$$

Where  $C_{i1}$  and  $C_{01}$  are the molar concentrations of the diffusing species in the interface and the bulk phase 1 respectively; and  $C_{i2}$  and  $C_{02}$ , are the concentrations in the interface and bulk phase 2 respectively.

For cases where there was no resistance to transfer at the interface, however,  $C_{i1}$  and  $C_{i2}$ , were replaced by their corresponding equilibrium values  $C_{e1}$  and  $C_{e2}$ , to obtain the equation;

$$N_A = k_1 (C_{01} - C_{e1}) = k_2 (C_{e2} - C_{02}) \quad (2.31)$$

Where  $C_{e1}$  is the concentration in phase 1, in equilibrium with  $C_{02}$  in phase 2, and  $C_{e2}$  is the concentration in phase 2 in equilibrium with  $C_{01}$  in phase 1,  $K$ , is the overall mass transfer.

For cases where the equilibrium relationship was linear, the proportionality constant  $H$ , otherwise known as Henry's Law constant could be expressed in the form;

$$H = \frac{C_{i1}}{C_{i2}} = \frac{C_{e1}}{C_{02}} = \frac{C_{01}}{C_{e2}} \quad (2.32)$$

From equations (2.30), (2.31) and (2.32) a relationship between the various transfer coefficients could be expressed as;

$$\frac{1}{K_A} = \frac{1}{Hk_1} + \frac{1}{k_2} \quad (2.33)$$



This relation between the various coefficients, is valid provided the rate of transfer is linearly related to the concentration difference,  $\Delta C$ , driving force (46).

The theories could also be applied to the mass transfer problems between a fluid and solid surface, such as would be encountered in the drying of drops containing dissolved solids.

## 2.5 FLOW CHARACTERISTICS OF DROPS AND AIR IN SPRAY DRIERS

The manner in which sprayed droplets are contacted by the drying air is an important factor in spray drier design. This plays an important part on the properties of the dried products (56), by influencing the droplet behaviour during drying. The Spray-air contact could be determined by the position of the spray nozzle in relation to the drying air inlet. Many positions for the sprayed droplets and air in the spray tower have been considered. The three major positions commonly used in the process industries are Co-current, Counter-current and Mixed flow driers. It has been found however, that counter-current flow driers, where spray and air enter the spray tower at the opposite ends, offer best performance with excellent heat utilization (57,58). Counter-current flow is commonly used with pressure spray nozzles, since an upward flow of the drying air, was found to reduce the fall velocity of the droplets in the spray, giving them sufficient residence time in the drying chamber for completion of evaporation.

A small amount of work has been done on the flow patterns of both droplets and air in spray towers. Masters (59), investigated the effects of the feed rate, air flow-rate and speed of the rotating disc atomiser on the sprayed droplets. He measured the spray impingement on wall of a 6 ft. diameter spray drier, and found that the extent of wall impingement was dependent on the operating conditions. Lapple and Shepherd (60), investigated the flow patterns

of sprayed droplets and calculated the drop trajectories from motion in a Centrifugal flow profile. Charm (61), also studied drop flow in drier designs incorporating disc atomisers. He reported that the radial distance of travel depended on the peripheral speed of the disc. Masters and Mohtadi (62), found that the drop size was inversely proportional to the disc speed, and that maximum distance was attained when the drag forces increased to give a critical drop diameter. Their results agreed favourably with those of Friedman, Gluckert and Marshall (63) at lower speeds. Gauvin and Katta (64) proposed equations for predicting the three-dimensional motion of droplets in a 1.83m x 1.22m diameter spray drier, based on the knowledge of the characteristics of the atomizing device and on the air flow patterns in the spray drying chamber. Place et al (65), however, used a tracer technique to investigate the behaviour of the air flowing through a 50' x 21' diameter spray tower. From the residence time analysis of the drying air in the spray tower, he was able to predict the exit time of the air at different parts of the tower.

#### 2.5.1. Flow Patterns Of Air In Spray Drying Towers

Spray drying has become a major operation in industry, ranging from the production in the most delicate of conditions in food and pharmaceutical manufacture, through to the high outputs required in such heavy chemical fields as detergent and inorganic salt manufacture. It is evident from the investigations of Masters (56,66) Kessler (67),



Buckham and Moulton (68), that the flow pattern of the drying air, as well as the manner in which the spray contacted the air were the main factors in the design of spray driers.

Kessler (67), investigated the airflow profile in a Co-current laboratory drier, and reported the existence of both streamline as well as a swirling motion. Buckham and Moulton (68), however, restricted their studies to air-mixing effects in a 12' x 4' diameter co-current spray drying chamber. Arni (69), reported on the effect of air-entry design on the flow patterns existing in both co-current as well as counter-current flow driers of the same dimensions as that of Buckham and Moulton.

Chaloud et al (70), reported on air flow characteristics in a co-current drying tower drying detergent formulation. They concluded that the swirling air in the spray tower increased turbulence and hence the transfer coefficients between droplets and air. This gave good mixing along the axis of flow and thereby the difference in air temperature between the top and bottom of the tower, was greatly reduced. They also reported that the swirling action of the air stabilised the flow-pattern in the tower.

#### 2.5.2 Residence Time Analysis Of Air In Spray Driers

Place, Ridgway and Danckwerts (65), made an investigation into the residence-time distribution and the flow-pattern of the drying air, in a 50' x 21' diameter spray drier (65,99) using a pulse of helium as tracer. Danckwerts (71) had earlier suggested that it was possible



to have a good knowledge about the flow-pattern of a fluid in a continuous-flow system by injecting a pulse of tracer at the inlet, and subsequently measuring the concentration profile of the tracer as a function of time, at various points inside the system.

Place et al, injected helium tracer at various points in the spray drier, and for each case, the variation of the tracer concentration with time was recorded on a mass spectrometer. The average residence time of the molecules from a desired point in the tower was determined. They displayed their results in contours of equal average exit times (65). Their result indicated that a considerable amount of channelling of the drying air near the axis of the tower, as well as stagnation at the corners occur. The disadvantage of the by-pass stream is that, the air had substantially less than the mean residence time, and was unduly hot and dry without having made a reasonable contribution to the drying process, like the well-mixed zones. This however contradicted the work of Taylor (72), who reported that the exit-time for a pulse of tracer was the same, whether the tracer was injected on the axis or near the wall because turbulence distributed the tracer rapidly, so that the mean velocity of the tracer molecules was equal to that of the air, regardless of where the tracer was injected.

From all these reports it is clear that channelling, swirling and stagnation of the drying air occur in the spray drying tower, and that at the present time the interactions of these different flows are not well understood.

### 2.5.3. Hydrodynamic Behaviour Of Spray Droplets

The studies of drop flow in spray driers could be carried out in two different stages (66). The first stage of motion would be in the close vicinity of the spray nozzle, where it was assumed that the flow pattern of the drying air has no influence on the drop trajectory. The second stage considered the drop trajectory to be that following the air flow profile in the chamber. Masters (66), also reported that the air movement in the spray chamber predetermined the rate of evaporation by influencing the passage of spray drops through the drying zone.

Fraser (73), Sivetz and Foote (74), reported their studies on drop motion in a spray drier; while Baltas and Gauvin (75,82), reviewed critically their work on transport phenomena in spray drying. Gauvin et al (76), recently reported their study on the prediction of droplet trajectories for water sprays in the nozzle zone as well as in the free-entrainment zone in a co-current spray drying chamber. Their theoretical predictions were in good agreement with experimental results.

Katta and Gauvin (64), extended the work of Gauvin et al (76), on water sprays to the spray drying of calcium lignosulphonate. They determined the maximum evaporative capacity of the chamber at steady state, according to the criterion that no incompletely dried particle should hit the walls of the chamber. This was done by increasing the feed rate until the particle started to hit the observation



windows on the chamber wall. Dried particles did not adhere to the wall as they were carried out by the air stream. They found that there was a marked decrease in capacity with an increase in the feed concentration. This was due to the fact that the average droplet size, as well as the largest droplets, increased with an increase in feed concentration; and hence, an increase in the initial momentum and the drying time of the largest droplets.

A number of studies (77,78,79), have been made on the average droplet diameter, droplet size distribution and largest droplet size, which are the important characteristics of sprayed droplets. Nukiyama and Tanasawa (77), presented an empirical correlation to predict the average droplet size, from the results of their experimental studies using pneumatic atomization. Their final correlation was:

$$d_{vs} = \frac{585}{v_{rel}} \left( \frac{\eta}{\rho_l} \right)^{0.5} + 597 \cdot \left( \frac{\mu_l}{\sqrt{\eta \rho_l}} \right)^{0.45} \cdot \left( \frac{1000 Q_l}{Q_a} \right)^{1.5} \quad (2.34)$$

Later on, Nukiyama and Tanasawa presented a second empirical equation for the size distribution of the form:

$$n_i / \Delta d = a d_i^2 e^{-(b d_i^q)} \quad (2.35)$$

Several experiments were carried out (64,78,80,81) to verify equations (2.34) and (2.35). Lewis et al.(78), proved from their experimental investigation that the value of  $q$ , was constant, for a given spray nozzle, over a wide

range of operating conditions. Katta and Gauvin (64), found that their experimental value for the Sauter mean diameter,  $d_{VS}$ , agreed favourably with that predicted by Nukiyama and Tanasawa (77), Katta and Gauvin (65) also treated the experimental data on drop size distribution for water spray droplets, and reported that the value of  $q$ , in equation (2.35) was 2 for a pneumatic nozzle. Nukiyama and Tanasawa (77), obtained the following relations for the constants  $a$  and  $b$ ,

$$b = 2.25/d_{VS}^2 \quad (2.36)$$

$$\text{and } a = 1.91b^3.V \quad (2.37)$$

Where  $V$ , was the total sample volume. The experimental work of Miyasaka (84), on the ratio of the diameter of the largest droplet,  $d_m$ , to the Sauter mean diameter,  $d_{VS}$ , showed that the value,  $d_m/d_{VS}$ , varied from 1.8 to 3.0. His result was in good agreement with those of Kim and Marshall (79) and Licht (83).

Katta and Gauvin (64), reported that the trajectories of spray droplets in spray towers, could be predicted by solving a set of simultaneous equations which were expressed in the form of; the three-dimensional motion of the droplets, their instantaneous rate of evaporation, the three-dimensional flow pattern of the drying gas and the instantaneous properties of the gas.

In both centrifugal and gravitational fields the equation of motion was expressed as (64);



$$\frac{dV_f}{dt} = g_c + r\omega^2 + \frac{V_t V_r}{r'} - \frac{C_D V_f^2 \rho_g A_p}{2W_d} + \frac{F_1}{W_d} \quad (2.38)$$

Resolving equation (2.38), in the three dimensions (64), the droplet velocities were expressed as;

Tangential Motion,

$$\frac{dV_t}{dt} = - \left( \frac{V_t V_r}{r'} \right) - \frac{3C_D \rho_g V_f}{4 d_i \rho_l} (V_t - V_{at}) \quad (2.39)$$

Radial Motion,

$$\frac{dV_r}{dt} = \frac{V_t^2}{r'} - \frac{3C_D \rho_g V_f}{4 d_i \rho_l} (V_r - V_{ar}) + \frac{F_1}{W_d} \quad (2.40)$$

and for axial motion,

$$\frac{dV_a}{dt} = g_c - \frac{3C_D \rho_g V_f}{4 d_i \rho_l} (V_a - V_{av}) \quad (2.41)$$

Where the velocity of the droplet relative to the fluid,

$V_f$  was given by;

$$V_f^2 = (V_t - V_{at})^2 + (V_a - V_{av})^2 + (V_r - V_{ar})^2 \quad (2.42)$$

Where,  $V_{at}$ ,  $V_{ar}$  and  $V_{av}$ , were the absolute values of the tangential, radial and axial velocities of air respectively.

Katta and Grauvin used the equations proposed by Beard and Pruppacher (85), to evaluate the drag coefficient,  $C_D$ ; while Saffman's (86) equation for the motion of a sphere in an unbounded shear flow:

$$F_1 = 20.25 \rho_a d_i^2 (v_a/K)^{0.5} K V_f \quad (2.43)$$

was used to estimate the shear lift force,  $F_1$ , while  $K$  was obtained from the relation,

$$K = 1.4 V_{ar} \left( \frac{r'}{r_1} \right)^2 \quad (2.44)$$

Where  $r_1$ , was the radial distance when the nozzle velocity was half its value.

Keey and Pham (87), recently reviewed some of the design methods that had been proposed, and described numerical methods for predicting the performance of spray driers. Similar to the work reported by Masters (66), Katta and Gauvin (64), Keey and Pham also identified the two distinct zones of the droplets in the spray drier. The first zone being, that close to the spray nozzle, while second stage was considered to be the free-entrainment zone in the spray drying chamber.

Although accurate prediction of the flow-patterns of the droplets and air in spray towers, is difficult, it is evident from the above reports that they form the basis for the design of spray driers. The review in this section showed that the contact between the spray droplets and the

drying air has a great effect on the drop size distribution, as well as on the general properties of the dried product; since the drying air influences the droplet behaviour during drying.

## 2.6 SPRAY DRYING OF DROPLETS AND DISSOLVED SOLIDS

In spray drying as in most drying operations, simultaneous heat and mass transfer take place. Heat for evaporation is transferred by conduction and convection from the hot gaseous atmosphere to the drop surface, while vapour is transferred by diffusion and convection back into the gas stream (88).

The work by Masters (56,66), Katta and Gauvin (64), showed that the spray-air contact has an important effect on the properties of the final products of spray dried materials. Crosby and Marshall (89,91) investigated the effects of different air temperatures, feed temperatures and feed concentrations on the size and density of spray dried sodium sulphate, coffee extract and clay slip. They found that the effects of these operating variables was dependent on the type of material being spray dried.

### 2.6.1 Heat And Mass Transfer In Spray Drying

Marshall (88), investigated the heat and mass transfer phenomena to and from pure liquid spray droplets. He presented a stepwise procedure for calculating drop size distribution. He also reported that at high evaporation rates the actual Nusselt Number in Ranz and Marshall's(1) correlation for heat transfer, was substantially less than that for low evaporation rates.

Dlouhy and Gauvin (12) studied the evaporation of spray droplets in a 14' x 0.67' diameter spray drier.



They reported that small particles less than  $3 \times 10^{-5} \text{ m}$ , produced in the drier probably had no internal diffusional resistance and hence, no significant falling-rate period was observed. This is rather strange as one would expect that the formation of a solid phase at the droplet surface introduced a diffusional resistance. This was however in contrast with their experimental work on tray-drying carried out on the same substance, under similar drying conditions where a diffusional resistance was reported. Using the approaches of Probert (92), Miesse (93), and Shapiro and Erickson (94), Dlouhy and Gauvin calculated the drying time for spray droplets, by assuming a Nusselt Number of 2.

Manning and Gauvin (95) carried out experiments to determine the rate of heat and mass transfer for sprays of pure water in the nozzle zone, using pneumatic nozzles. They presented the drop size distribution using the same method of Dlouhy and Gauvin (12). They followed the evaporation rates by injecting a red dye into the feed. The concentration was then measured colourimetrically. They estimated the air velocity from a graphical method although this was liable to errors compared with a direct method. The scatter of points about the correlation line was quite significant when their data was fitted to Ranz and Marshall's (1) correlation for heat transfer.

An extension of the work by Dlouhy and Gauvin (12 101) on heat and mass transfer coefficients in a spray drier, was carried out by Bose and Pei (96). They evaporated spray

droplets of water using sampling techniques, temperature and humidity measurements similar to those of Dlouhy and Gauvin (12). Unlike Dlouhy and Gauvin, however, they reported that the relative velocity between droplets and the air stream had a significant effect on the rate of evaporation.

Dickinson and Marshall (97), also found that when sprays of pure liquids were evaporated, those with less uniform drop size distribution, evaporated more quickly initially, than those of more uniform sprays. This was due to the fact that the smaller drops which were present initially evaporated at high rates. They also found that the air temperature fell as the spray droplets evaporated, hence the rate of evaporation decreased. At high spray velocity however, it was discovered that the distance travelled by the spray to achieve a specified degree of evaporation was much greater, especially at the start.

It is therefore evident from these studies that many factors affect the rate of heat and mass transfer in spray driers; and these include air and feed velocities, as well as air and feed temperatures. Most authors however argue that the formation of a solid phase at the droplet surface introduces a diffusional resistance which slowed down the rate of evaporation. Kirschbaum (98), attributed the fact that residual moisture was almost always found in spray-dried products to this cause.



### 2.6.2. Factors Affecting The Properties of Spray-Dried Materials

One of the important advantages in spray drying is that certain product properties and quality values such as product density, particle shape and size can be effectively controlled and varied over a wide range of operating conditions. Spray drying frequently preserves the quality of a product because drying is so rapid and the material in the hot drying zone is always so wet that it does not become overheated. Duffie and Marshall (102), studied the effect of air and feed temperatures, feed concentration and properties on the bulk densities of spray-dried water-dispersible organic dyestuff, sodium silicate and sodium chloride. They found that the bulk densities of the organic dyestuff and sodium silicate decreased with increasing drying air temperature, due mainly to increased dried-particle size. They also reported a decrease in bulk densities of the dyestuff, sodium silicate and sodium chloride with increasing feed temperature, due largely to changes in atomisation. The bulk density of the dyestuff also decreased when the feed concentration was increased. Their results agreed favourably with those reported by Wallman and Blyth (103) on similar materials. In contrast to these reports however, Marshall and Seltzer (90) reported after their investigation on other materials, that certain materials showed a significant increase in bulk densities when their feed temperatures were increased.



Crosby and Marshall (89), investigated the effect of air temperature, feed temperature and feed concentration on the size and density of spray-dried sodium sulphate, coffee extract and clay slip, in relation to the initial drop size. The results of their studies showed that the effects of the operating variables on the properties of spray dried materials were dependent upon the type of materials being dried. For crystalline materials such as sodium sulphate they found that there was no significant effect of air temperature on the particle density at very low or high feed concentrations. Whereas, for coffee extract, the inlet air temperature showed a very pronounced effect over a wide range of feed concentration. They also concluded that regardless of the type of material being dried, the final particle diameter rarely equalled the initial spray diameter, except in the case of film-forming materials such as coffee extract where the final particle diameter was often found to be either equal or greater than the initial spray droplet diameter, at high feed concentration and at temperatures above the boiling point.

## 2.7 CONCLUSIONS

The literature review indicates that the drying of drops is a very complex process, and a knowledge of the drying characteristics of a wide range of liquid drops is essential in the design of drying equipment in the process industry. The studies of the drying characteristics of drops had been made on

- (1) Single stagnant drops of pure liquid.
- (2) Single drops containing dissolved or suspended solids.
- (3) Sprays of pure liquid drops
- (4) Sprays of drops containing dissolved and suspended solids.

As discussed earlier, the drying of single drops or the spray of liquid drops in a spray drying tower, is a heat and mass transfer problem. The correlations proposed by Froessling (5) for heat and mass transfer have been applied to several experimental studies as well as for the practical cases of drying. Most of the work quoted, also support the correlations of Ranz and Marshall (1).

Previous work (65), on the flow patterns existing in the spray drying tower have shown that a reasonable amount of swirling channelling and stagnant zones exist in the tower, but to our knowledge no-one has estimated the volume of the various sections involved. The manner in which the sprays contact the air have been shown to play a very significant role in the design of spray driers, hence a good knowledge of the flow patterns in the spray drying tower is extremely

important, as this affects the properties of the final products. It is hoped therefore that the present study on the behaviour of the drops and air in the spray drying tower, as well as the residence time distribution will form the basis for future work for the design of a practical spray drier.



CHAPTER THREE

MATHEMATICAL MODELS

### 3 MATHEMATICAL MODELS

#### 3.1 Momentum - Heat Transfer Model

A number of theories (1,45) have been presented on the mechanisms of heat and mass transfer during the evaporation of drops containing dissolved solids. Ranz and Marshall (1) reported that heat was transferred from the air to the drop surface by convection, then into the drop itself by conduction for its evaporation, and that liquid or vapour was transferred back to the air by diffusion through the pores. Audu and Jeffreys (11,45), also reported from their work on drying of single drops containing dissolved solids that vapour was transferred from the drop through the pores by the same diffusional mechanism. In certain drops however, a lot of heat was transferred into the drop that the rate of formation of vapour was greater than the rate of diffusion through the crust. This resulted in a pressure build-up inside the drop (10), hence the drop collapsed and there was a flow of steam through the holes in the crust.

The model hereby proposed for the calculation of the mass transfer coefficient  $K_G$ , from the amount of water evaporated from a single sodium sulphate decahydrate drop, is based on the fact that steam was ejected through the pores in the crust by a pressure drop  $\Delta P$ , driving force, as a result of heat transferred by conduction into the wet core of the particle.

Consider a single crust-forming drop being dried in a wind tunnel by a hot air stream. The drop first evaporates as a pure liquid until the crust begins to form.

At this stage however, the rate of evaporation of liquid vapour through the pores of the crust, will depend upon the pressure drop,  $\Delta P$ , through the crust.

The diagram in Figure 3.1 represents a single crust-forming drop being dried. The air humidities upstream and downstream are taken to be,  $H_u$ , and  $H_d$ , respectively,

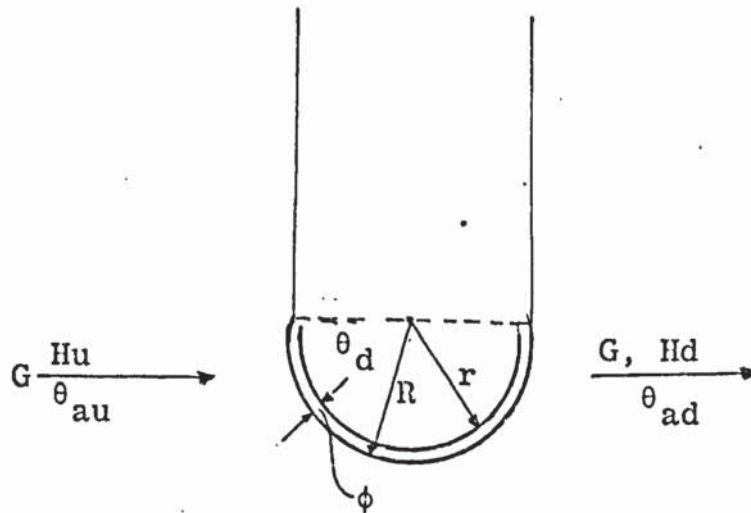


Figure 3.1 Crust-forming Hemispherical Drop

and the crust thickness is,  $\phi$ . The air temperatures upstream and downstream are,  $\theta_{au}$  and  $\theta_{ad}$  respectively.

#### Assumptions

- (1) The external radius,  $R$ , of the crust remains constant.
- (2) The air flowrate is constant
- (3) The air temperature and other physical properties of the air are constant.



- (4) The drop has a hemispherical shape.
- (5) Steady state conditions exist throughout the drying period.

A model for the quantity of heat,  $q$ , transferred through the crust can be expressed as;

$$q = \frac{k \cdot 2\pi R^2 (\theta_{au} - \theta_d) (1 - \epsilon')}{\phi} \quad (3.1)$$

where,  $\theta_{au}$  is the air temperature,  $\theta_d$ , is the temperature inside the drop, and  $\epsilon'$ , the crust porosity.

The amount of water evaporated,  $W$ , from the drop can be evaluated from the relation:

$$W = \frac{2\pi R^2 k \Delta\theta (1 - \epsilon')}{\phi \lambda} \quad (3.2)$$

The thermal conductivity,  $k$ , may be estimated from a Lee's Disc experiment using the following expression (104);

$$k = \frac{A_x e t'}{(\theta_2 - \theta_3)} \left\{ \frac{A_x}{2} \frac{(\theta_2 + \theta_3 - \theta)}{2} + A_3 (\theta_3 - \theta) \right\} \quad (3.3)$$

As explained earlier, the flow of steam through the pores of the crust, is due to the pressure drop,  $\Delta P$ , driving force inside the drop.

A number of equations had been developed by Blake and Kozeny (110,116), Kozeny and Ergun (111,115), Carman (112) and Shalhoub (113) on the flow of liquid through porous

media. These equations were not applied in this case as it was assumed that there was a laminar flow of vapour through the pores rather than a turbulent flow or a flow in the transition region.

Thus the D'arcy equation (114) for a laminar flow of vapour through channels should be applicable. This may be estimated by the relation (22,46);

$$\Delta P = 4 \left( \frac{R}{\rho V^2} \right) \frac{\phi}{d_p} \rho_g U^2 \quad (3.4)$$

and by re-arrangement the velocity,  $U$ , can be evaluated from the D'arcy equation for the laminar flow of vapour in a channel:

$$U = \left( \frac{1}{4f} \cdot \frac{d_p}{\phi \rho_g} \cdot \Delta P \right)^{0.5} \quad (3.5)$$

But the mean velocity  $U$ , of the flow of the vapour through the pores of the crust can also be expressed in terms of the amount of water evaporated,  $W$ , as:-

$$U = \frac{W}{\rho_g N \pi d_p^2} \quad (3.6)$$

where  $N$ , is the total number of pores and  $d_p$ , is the mean pore diameter.

By re-arranging equation (3.6), the amount of water vapour evaporated can be computed from the relation;

$$W = U \rho_g N \pi d_p^2 \quad (3.7)$$

The value of  $W$ , obtained from equation (3.7), can therefore be compared with experimental value obtained from equation (3.2).

Using the Ranz and Marshall equation (1), the mass transfer coefficient  $K_G$ , can be evaluated; since the amount of water evaporated can be expressed as:-

$$W = K_G \pi d_p^2 (C_1 - C_o) = K_G \pi d_p^2 (p_d - p_a) \quad (3.8)$$

or

$$W = K_G \pi d_p^2 (\Delta C) = K_G \pi d_p^2 (\Delta P) \quad (3.9)$$

Where  $\Delta C$  = Concentration difference, driving force.

$\Delta P$  = Pressure drop, driving force



### 3.2 AIR RESIDENCE-TIME MODEL

The volumes of the various flow patterns which were estimated from the experimental work using the smoke generator, formed the basis for the model hereby postulated for predicting the exit concentration profile of a pulse of tracer injected into the spray tower.

Figure 3.2 represents the flow patterns of the drying air in the spray drying tower. The model is based on the hypothesis that the spray tower is made up of a well-stirred section at the bottom and another at the top with a plug-flow region in the middle. The existence of a by-pass stream through the tower is also included in the analysis.

A number of equations had been developed on the flow characteristics of fluids in various vessels (105,109,119,120). The gamma function is however applied in this case because of its versatility. Considering the first well-stirred section at the bottom of the tower. Using the gamma function (105,107), the exit age distribution  $E(t)_\Gamma$ , of the well-mixed section is given by:-

$$E(t)_\Gamma = \frac{1}{v^p \Gamma(p)} \cdot t^{p-1} \cdot e^{-t/v} \quad (3.10)$$

where  $p$ , is the parameter related to the extent of fluid mixing in the direction of flow and  $v$  is the parameter related to the mean residence time of the system.  $\Gamma$  denotes the gamma function defined as;

$$\Gamma(p) = \int_0^{\infty} (x^{p-1} e^{-x}) dx \quad (3.11)$$

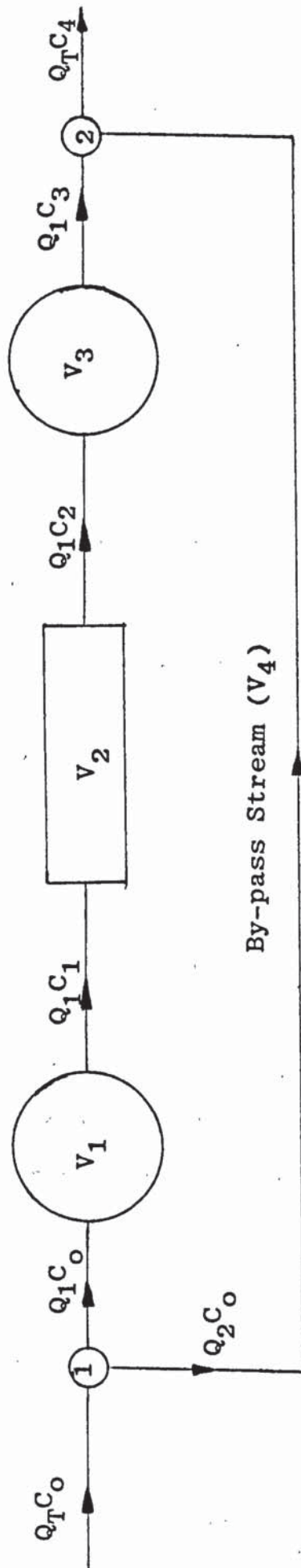


Figure 3.2 Air Residence time Distribution Model

The mean of the exit age distribution  $E(t)_T$ , of the well-mixed section is given by,

$$\bar{t}_T = v_p \quad (3.12)$$

$V_1$ ,  $V_2$ ,  $V_3$  and  $V_4$  are the volumes of the first well-stirred section, the plug-flow, the second well-stirred section, and the by-pass stream respectively.

The dimensionless residence time of the air in the plug flow section is given by:-

$$\tau = \frac{V_2}{V_T} \quad (3.13)$$

Where,  $V_T = V_1 + V_2 + V_3 + V_4$ , total volume ( $m^3$ )

$$\text{If } \epsilon = \frac{V_3}{V_T} \quad (3.14)$$

is the dimensionless residence time of air in the second stirred-tank section at the top of the tower, then the dimensionless residence time in the first stirred-tank section can be expressed as,

$$\frac{V_1}{V_T} = (1 - \tau - \epsilon) \quad (3.15)$$

Considering a closed system, then the residence time  $\bar{t}$ , of the entire system is given by:-



$$\bar{t} = \frac{V_T}{Q_T} \quad (3.16)$$

Where  $Q_T = Q_1 + Q_2$ , total volumetric flowrate

$$\text{Let } \beta = Q_1/Q_T \quad (3.17)$$

From equation (3.12), the mean of the exit age distribution, of the first well-stirred section is expressed as;

$$\begin{aligned} \bar{t}_1 = v_p &= \frac{V_1}{Q_1} \\ &= \frac{V_1}{Q_1} \cdot \frac{V_T}{V_T} \end{aligned} \quad (3.18)$$

Substituting for  $Q_1$  from equation (3.17), then we have,

$$v_p = \frac{V_1 V_T}{\beta Q_T V_T} \quad (3.19)$$

combining equations (3.16) and (3.19),

$$\text{therefore, } \bar{t}_1 = v_p = \frac{\bar{t}}{\beta} \frac{V_1}{V_T} \quad (3.20)$$

and from equations (3.15) and (3.20)

$$v_p = \frac{\bar{t}}{\beta} (1 - \tau - \epsilon) \quad (3.21)$$

therefore, 
$$v = \frac{\bar{t} (1-\tau-\epsilon)}{p\beta} \quad (3.22)$$

But  $E(\theta)_\Gamma = E(t)_\Gamma \cdot \bar{t}$  (3.23)

Where  $E(\theta)_\Gamma$ , is the exit age distribution of the first well-mixed region in terms of the dimensionless time,  $\theta$ .

Recall that,  $\theta = \frac{t}{\bar{t}}$  dimensionless time

Combining equations (3.10) and (3.22).

Therefore, 
$$E(\theta)_\Gamma = \frac{(\beta p)^p}{(1-\tau\epsilon)^p \cdot \Gamma(p)} \cdot \theta^{p-1} \cdot e^{-\frac{\beta p \theta}{(1-\tau-\epsilon)}} \quad (3.23)$$

Taking the Laplace transform of the above equation for the first well-mixed section, we have;

$$H(s)_\Gamma = E(s)_\Gamma = \frac{C_1(s)}{C_o(s)} = \left[ \frac{p\beta}{(1-\tau-\epsilon)s + p\beta} \right]^p \quad (3.24)$$

The transfer function for the plug-flow section is given by:-

$$H(s)_p = \frac{C_2(s)}{C_1(s)} = e^{-\tau s} \quad (3.25)$$

Combining equations (3.24) and (3.25), the transfer function of the first and second stages is given by;

$$H(s) = \frac{C_2(s)}{C_o(s)} = \left[ \frac{p\beta}{(1-\tau-\epsilon)s+p\beta} \right]^p e^{-\tau s} \quad (3.26)$$

Similarly, for the third stage, which is the well-mixed region at the top of the tower, the transfer function is defined as:

$$H(s)_T = E(s) = \frac{C_3(s)}{C_2(s)} = \left[ \frac{p'\beta}{\epsilon s + p'\beta} \right]^{p'} \quad (3.27)$$

Combining equations (3.26) and (3.27), therefore;

$$H(s) = \frac{C_3(s)}{C_o(s)} = \left\{ \left[ \frac{p\beta}{(1-\tau-\epsilon)s+p\beta} \right]^p \cdot \left[ \frac{p'\beta}{\epsilon s + p'\beta} \right]^{p'} \right\} \cdot e^{-\tau s} \quad (3.28)$$

A mass balance at point (2), in figure 3.2, where the by-pass stream joins the outlet stream of the second mixing section can be expressed as:

$$Q_T C_4 = Q_1 C_3 + Q_2 C_o \quad (3.29)$$

Dividing the above equation by  $Q_T$ ,

$$\text{Therefore; } C_4 = \beta C_3 + (1-\beta) C_o \quad (3.30)$$

Recall that  $\beta = Q_1/Q_T$ .

Taking the Laplace transform of both sides of equation (3.30),



$$\text{Therefore, } C_4(s) = \beta C_3(s) + (1-\beta) C_0(s) \quad (3.31)$$

Combining equations (3.28) and (3.31), therefore;

$$H(s) = \frac{C_4(s)}{C_0(s)} = \left\{ \beta \left[ \left( \frac{p\beta}{(1-\tau-\epsilon)s+p\beta} \right)^p \cdot \left( \frac{p'\beta}{\epsilon s+p'\beta} \right)^{p'} \right] \right\} e^{-\tau s} + (1-\beta) \quad (3.32)$$

It is assumed however, that the stirred-tank sections at the bottom and top of the spray drying tower are completely well-mixed.

$$\text{So that, } p = p' = 1 \quad (3.33)$$

Equation (3.32), can be expressed in terms of the exit concentration profile,  $C_4(\theta)$ , for a shot of tracer injected at the air inlet into the spray tower. Thus for a unit impulse say;

$$C_0(s) = 1 \quad (3.34)$$

$$\text{Therefore, } C_0(\theta) = \delta\theta$$

From equation (3.32) through to (3.34)

$$C_4(s) = \left\{ \beta \cdot \left[ \left( \frac{\beta}{(1-\tau-\epsilon)s+\beta} \right) \cdot \left( \frac{\beta}{\epsilon s+\beta} \right) \right] \right\} e^{-\tau s} + (1-\beta)$$

Therefore;

$$C_4(s) = \left\{ \beta \left[ \left( \frac{\alpha}{s+\alpha} \right) \cdot \left( \frac{\gamma}{s+\gamma} \right) \right] \right\} \cdot e^{-\tau s} + (1-\beta)$$

$$\text{Where: } \alpha = \frac{\beta}{(1-\tau-\epsilon)}$$

$$\gamma = \beta/\epsilon$$

$$\text{Therefore, } C_4(s) = \left\{ \alpha\beta\gamma \left[ \left( \frac{1}{s+\alpha} \right) \cdot \left( \frac{1}{s+\gamma} \right) \right] \right\} \cdot e^{-\tau s} + (1-\beta) \quad (3.35)$$

Inverting equation (3.35), using convolution (106) and the Heaviside function (117), which states that;

$$\int_0^{\theta-\tau} \left[ e^{-\tau s} \cdot f(s) \right] \equiv f(\theta-\tau) \cdot H(\theta-\tau) \quad (3.36)$$

So, equation (3.35) becomes,

$$C_4(\theta) = \frac{\alpha\beta\gamma}{\gamma-\alpha} \left[ e^{-\alpha(\theta-\tau)} - e^{-\gamma(\theta-\tau)} \right] + \delta\theta(1-\beta) \quad (3.37)$$

and hence, the exit concentration of a shot of tracer injected at the air inlet into the spray drying tower can be computed from the expression,

$$C_4(\theta) = \frac{\alpha\beta\gamma}{\gamma-\alpha} \left[ e^{\alpha(\tau-\theta)} - e^{\gamma(\tau-\theta)} \right] + \delta\theta(1-\beta) \quad (3.37)$$

in terms of the dimensionless time,  $\theta$ .

### 3.3 SPRAY TOWER DESIGN MODEL

Spray drier design is directed towards achieving desired dried product properties at the highest possible thermal efficiency. The whole basis of economic operation is the utilization of heat passed into the drier, that is - the drier heat load required for producing a unit weight of dry product. The heat load is proportional to the rate of evaporation and for a given rate is greatly affected by the solids content in the feed stream.

The heat and mass balances are hereby developed for the counter-current flow drier as shown in Figure 3.3. Thus using the volumes of the top and bottom stirred-tanks and the plug flow sections, the heat and mass balances over the various sections in relation to these capacities, the air and liquid feed flowrates, air and liquid feed temperatures, humid heat  $s$ , the heat capacity  $c_p$ , the concentration driving force  $\Delta C$ , and the residence times  $\tau$  and  $\theta$ , for the air and drops respectively.

#### Assumptions

- (1) Steady state condition exists throughout
- (2) Constant air temperature
- (3) Constant Feed temperature
- (4) Constant air flowrate
- (5) Constant Feed flowrate
- (6) Well-insulated drying chamber.



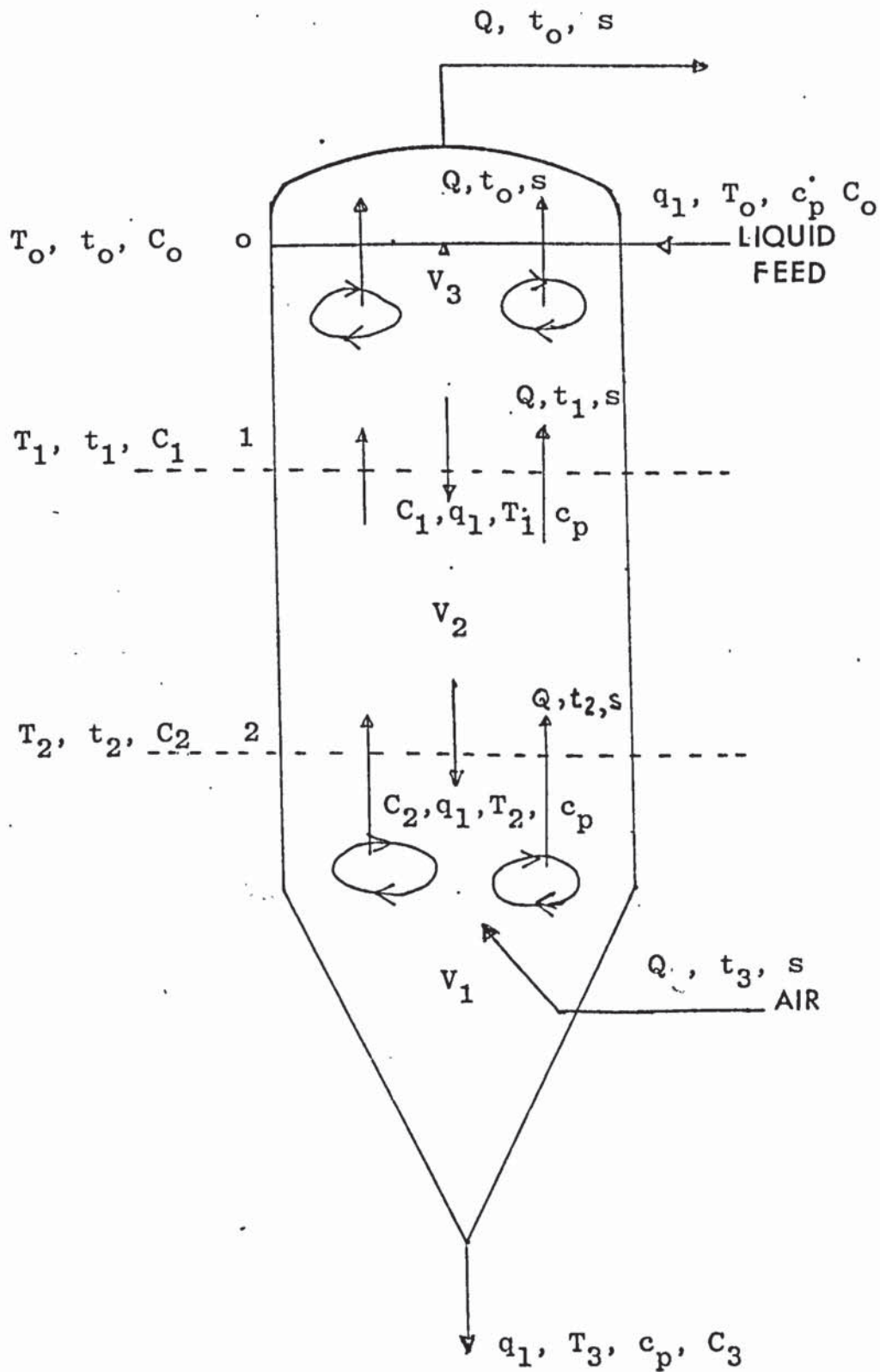


Figure 3.3 Heat and Mass Balance on the Spray Drier

A heat balance over the first stirred-tank section is given by the following equation:

$$Qs \int_9 (t_3 - t_2) \tau_1 = \int_l q_1 c_p (T_3 - T_2) \theta_2 + \int_l q_1 (C_3 - C_2) \lambda_2 \theta_2 \quad (3.38)$$

Where:  $\tau_1 = \frac{V_1}{Q}$ , residence time of air in stirred-tank section (s).

$\theta_2$  = residence time of sprayed droplets in stirred-tank section (s).

$q_1 (C_3 - C_2)$  = Rate of drying of the sprayed droplets

$(C_3 - C_2)$  = Concentration driving force (kg moisture/m<sup>3</sup> solution).

Similarly, a heat balance over the plug flow section gives:-

$$Qs \int_9 (t_2 - t_1) \tau_2 = \int_l q_1 c_p (T_2 - T_1) \theta_1 + \int_l q_1 (C_2 - C_1) \lambda_1 \theta_1 \quad (3.39)$$

Where:  $\tau_2 = V_2/Q$ , residence time of air in plug flow section (s)

$\theta_1$  = residence time of sprayed droplets in plug flow section (s).

Finally, a heat balance over the top stirred-tank section is given by:

$$Qs \int_9 (t_1 - t_o) \tau_3 = \int_l q_1 c_p (T_1 - T_o) \theta_o + \int_l q_1 (C_1 - C_o) \lambda_o \theta_o \quad (3.40)$$

Where:  $\tau_3 = V_3/Q$ , residence time of air in stirred-tank section (s)

$\theta_o =$  residence time of spray droplets in stirred-tank section (s)

Thus, an overall heat balance over the whole system is given by;

$$Q_s(t_3 - t_o)\tau = \int_0^1 q_1 c_p (T_3 - T_o) \theta + \int_0^1 q_1 (C_3 - C_o) \lambda \theta \quad (3.41)$$

Where:  $\tau = \frac{V_T}{Q}$ , the air residence time in the tower  
 $= \theta$  residence time of spray droplets in the tower.

The by-pass stream  $Q_o$ , t, s is assumed to flow out very quickly through the air exit without making any contribution to the drying process. For a well-insulated drying chamber, the heat losses are low.

The rate of mass transfer over the three sections could be evaluated from the following equations.

For the first stirred-tank section at the bottom of the tower, the rate of drying of the evaporating spray droplet is given by;

$$N_A = K_2 a (C_3 - C_2) \quad (3.42)$$

Introducing the residence time  $\theta_2$ , of the droplets in this section, then the total amount of water evaporated



in the time interval  $\theta_2$ , could be expressed in terms of

$$\text{Rate of Drying} = N_A \theta_2 = K_2 a (C_3 - C_2) \theta_2 \quad (3.43)$$

$$\begin{aligned} \text{Where } N_A &= \text{rate of mass transfer} && (\text{kg/m}^2\text{s}) \\ K_2 &= \text{mass transfer coefficient} && (\text{m/s}) \\ a &= \text{mass transfer area} && (\text{m}^2) \end{aligned}$$

Similarly, for the plug flow section, the rate of drying in the time interval  $\theta_1$  is given by:

$$N_A \theta_1 = K_1 a (C_2 - C_1) \theta_1 \quad (3.44)$$

Where  $\theta_1$  is the residence time of the sprayed droplets in the plug flow section.

Finally, for the top stirred-tank section, the rate of drying could also be expressed in the form:

$$N_A \theta_o = K_o a (C_1 - C_o) \theta_o \quad (3.45)$$

Where  $\theta_o$ , is the residence time of the sprayed droplets in the top section of the tower. Thus, equations (3.43), (3.44) and (3.45) could be represented by the general form:

$$N_A \theta_i = K_i a (C_{i+1} - C_i) \theta_i \quad (3.46)$$

So the overall mass balance over the whole system in terms of rate of drying is given by:

$$N_A \theta = K_G a (C_3 - C_O) \theta \quad (3.47)$$

Where  $\theta$  is the residence time of the sprayed droplets in the tower.

The mass transfer coefficient  $K_G$  can be calculated from the momentum heat transfer model, proposed in section (3.1).

The amount of water evaporated is given by the relation:

$$W = K_i \pi d_p^2 \cdot \Delta C_i = K_i \pi d_p^2 \cdot \Delta P_i \quad (3.48)$$

The amount of water evaporated is calculated from the equation:

$$W = U \rho_g \cdot N \pi d_p^2 \quad (3.49)$$

CHAPTER FOUR

EXPERIMENTAL EQUIPMENT, PROCEDURE  
AND MEASUREMENTS



Wind Tunnel

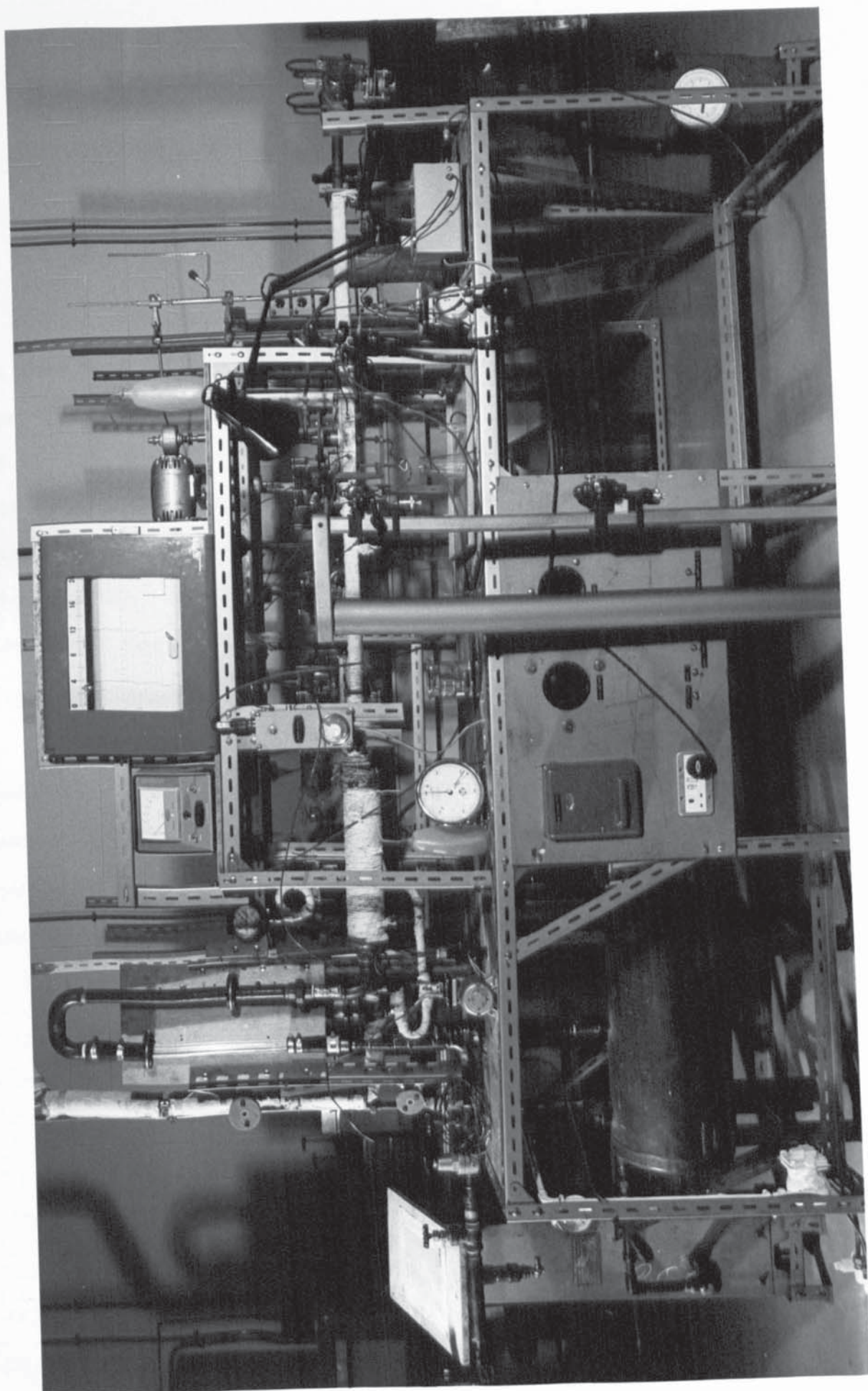


PLATE 4.1 OVERALL EXPERIMENTAL APPARATUS - SINGLE DROP

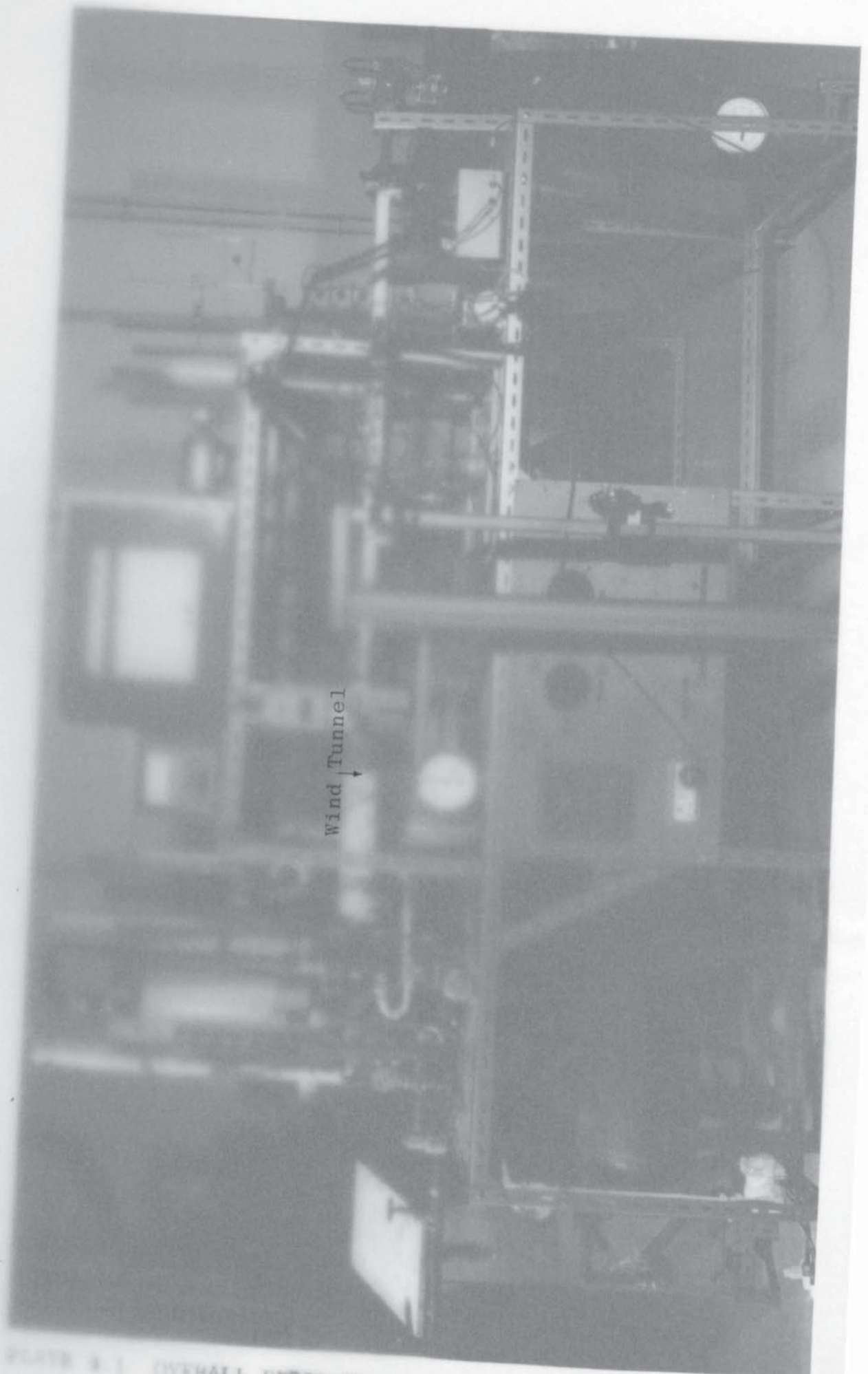


FIGURE 4.1 OVERALL EXPERIMENTAL APPARATUS -- SINGLE DROP



#### 4. EXPERIMENTAL EQUIPMENT, PROCEDURE AND MEASUREMENTS

##### 4.1 Description of Experimental Equipment

##### 4.1.1. Experimental Apparatus for the Drying of Single Drops

The photograph on plate 4.1 and the schematic diagram in figure 4.1, represent the overall experimental equipment for the drying of single drops. It consists essentially of an air receiver, a Birlec air drier, a metric type 18A rotameter, a temperature recorder, a wind tunnel, two sample pumps, a T-piece of perspex material, drop suspension device, the Shaw hygrometry unit consisting of a dew-point meter, two constant temperature units and two sensing elements.

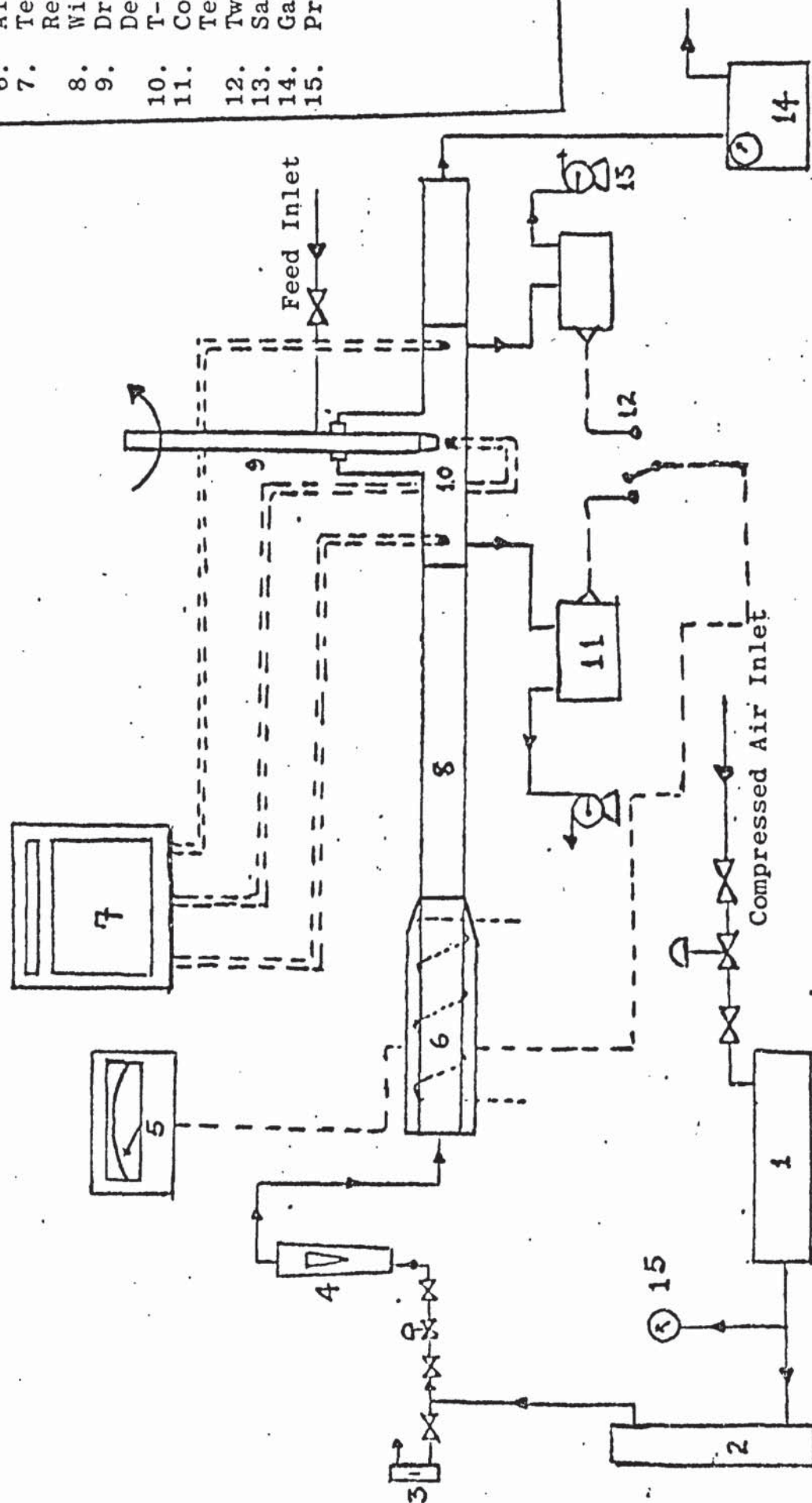
Compressed air at approximately 100 psi was passed into the air receiver from the laboratory mains supply before entry into the system. The purgerator served as a pressure regulator to achieve a steady mains air pressure. The air flowrate was measured by a metric type 18A rotameter installed at the inlet to the wind tunnel. The air flowrate was controlled by a 2.54 cm globe valve connected to the drier outlet.

The wind tunnel was 1.83m in length and was made up of mild steel with a square duct of 2.54 x 2.54 cm, which was well-lagged with asbestos. The air in the wind tunnel was heated by a 1 KW electric heater mounted at the rotameter outlet, and was controlled with a 3A, 90 Ohm Cressall Torovolt resistor with a range of 0°C to 600°C.

FIGURE 4.1 Overall Flow Diagram - Single Drop Experiment

KEY

1. Air Receiver
2. Birlec Air Dryer
3. Purgerator
4. Rotameter Type 18A
5. Hygrometer
6. Air Heater
7. Temperature Recorder
8. Wind Tunnel
9. Drop-Suspension Device
10. T-piece Perspex Constant
11. Temperature Unit
12. Two-Way Switch
13. Sample Pump
14. Gas Meter
15. Pressure Gauge





The working section was made up of a T-piece perspex material (11,104), and the air temperatures upstream and downstream were measured by thermocouple wires connected 0.1m apart. Another thermocouple wire was connected directly below the drop suspension device. These thermocouples were in turn connected to an Elliot Automation strip-chart recorder.

The photograph on plate 4.2 shows the feeding device which was designed (11,104), to maintain a constant drop size during each run. It was made up of two glass tubes connected together by a quick-fit Rotaflo valve type TF2/13, produced by Fisons Scientific Apparatus Limited. The glass piston in the larger-bore tube was used to prevent the oscillations of the drop.

The drop suspension device consisted of an 0.95 cm O.D. stainless steel tube, with an 0.16 cm diameter hole 10 cm from the nozzle. The tube was in turn placed in a 2.54 cm diameter cylindrical T-piece brazed onto a 7.6 cm diameter plate, so that the 0.16 cm diameter hole was enclosed within the cylinder. The Crane mechanical seals type IABR171/Z, provided a liquid-tight seal between the tube and cylinder, so that only the tube was rotated by coupling directly to the vertical shaft of a single phase 50 Hz Parvalux electric motor capable of a maximum speed of 100 r.p.m. The speed was controlled by a 27 Ohm, 10A Cressall Torovolt resistor connected into the armature of the motor and generally the shaft was rotated at 15 r.p.m.

**BLANK IN ORIGINAL**



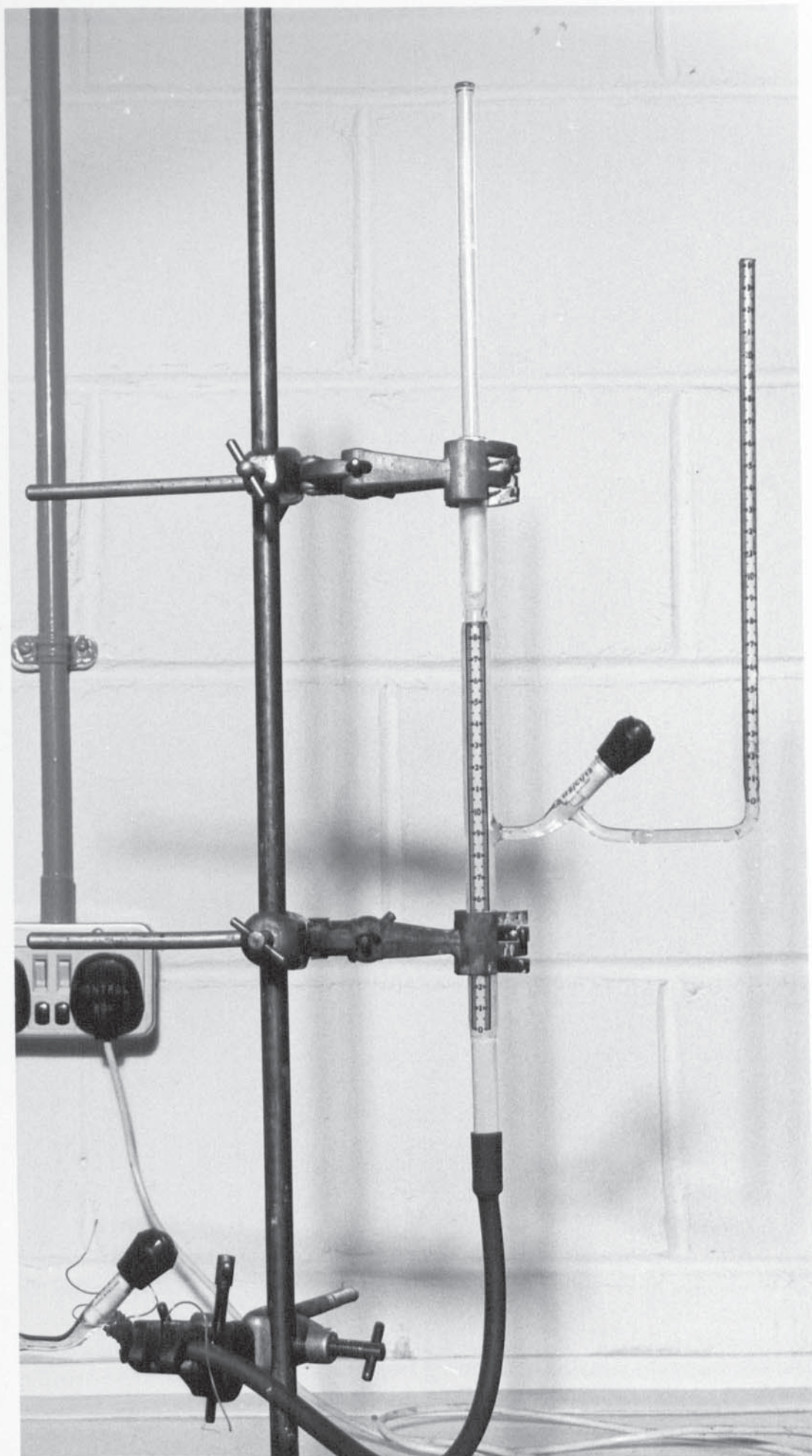


PLATE 4.2 FEEDING DEVICE

The portion of the stainless steel tube below the brass plate was threaded to take a screw-on P.T.F.E. or stainless steel nipple with an internal diameter range of 0.1 cm to 0.6 cm.

The Shaw hygrometer unit (11,104) consisted of two constant temperature units, two sample pumps, two sensing elements connected to a dew-point meter with a reading from  $-80^{\circ}\text{C}$  to  $-20^{\circ}\text{C}$ , by three coaxial cables and a two-way key. The sensing elements were each screwed into one of the constant temperature units shown in Figure 4.2 and plate 4.3. Air from the T-piece perspex working section, was drawn through the constant temperature units by two sample pumps, so that the air humidity was picked up by the sensing elements which in turn was transmitted to the dew-point meter via the coaxial cables. The constant temperature unit maintained the element temperature at a constant value, especially when there was a risk of condensation or where dew-points above ambient occurred. The sensitive thermostat maintained a constant temperature by switching the 30 KW heater on or off depending on the particular dial setting required. Fittings for 0.32 cm O.D. piping were provided on the units, so that the 0.32 cm diameter copper pipings connected to the sampling pumps were easily fitted into the units.

The Stereoscan Equipment was used as a scanning electron microscope giving a three-dimensional photograph. It had a high range of magnification from about 15 to 100,000 diameters, although the image became slightly blurred when the magnification exceeded 20,000 diameters.



# CONSTANT TEMPERATURE UNIT.

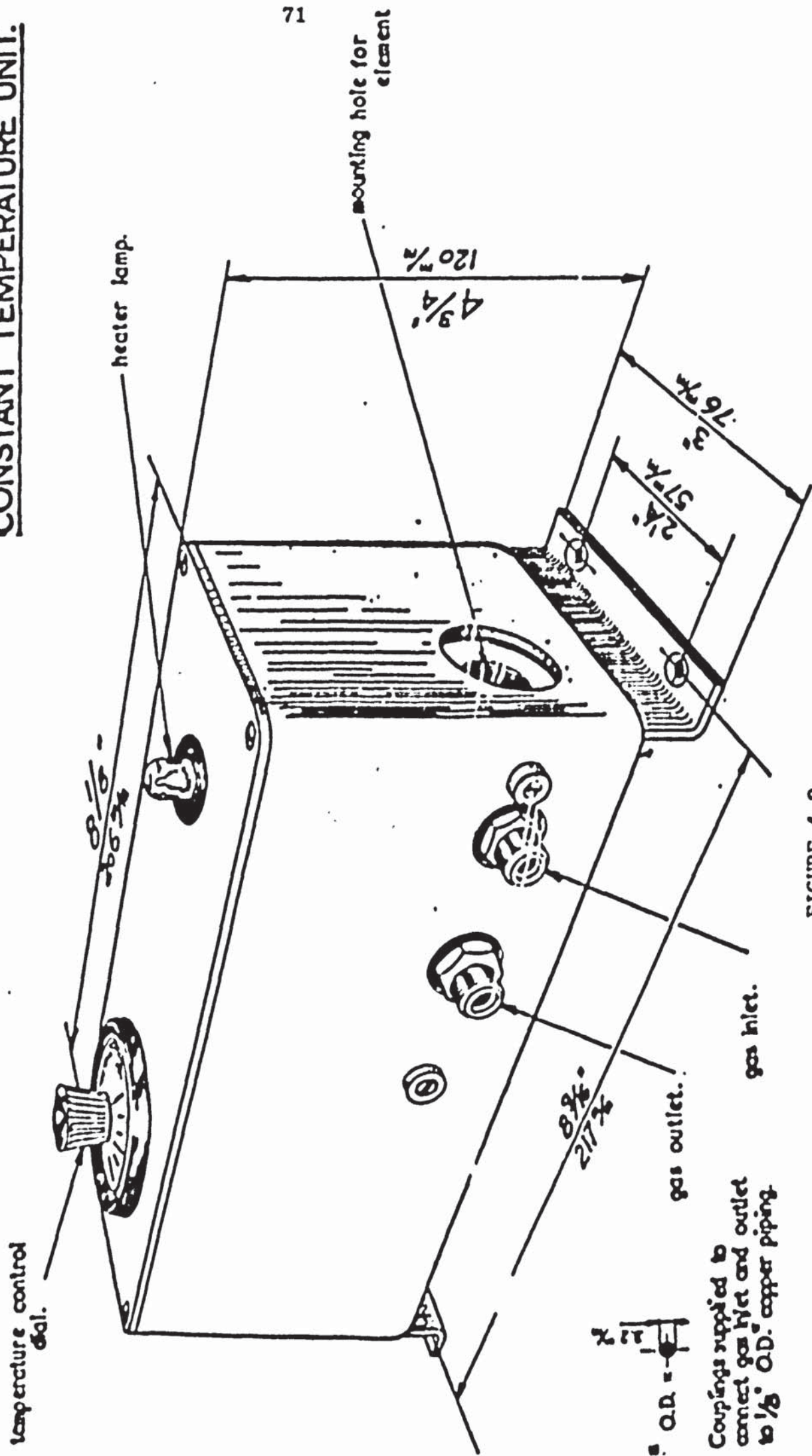


FIGURE 4.2

Sensing Element  
←



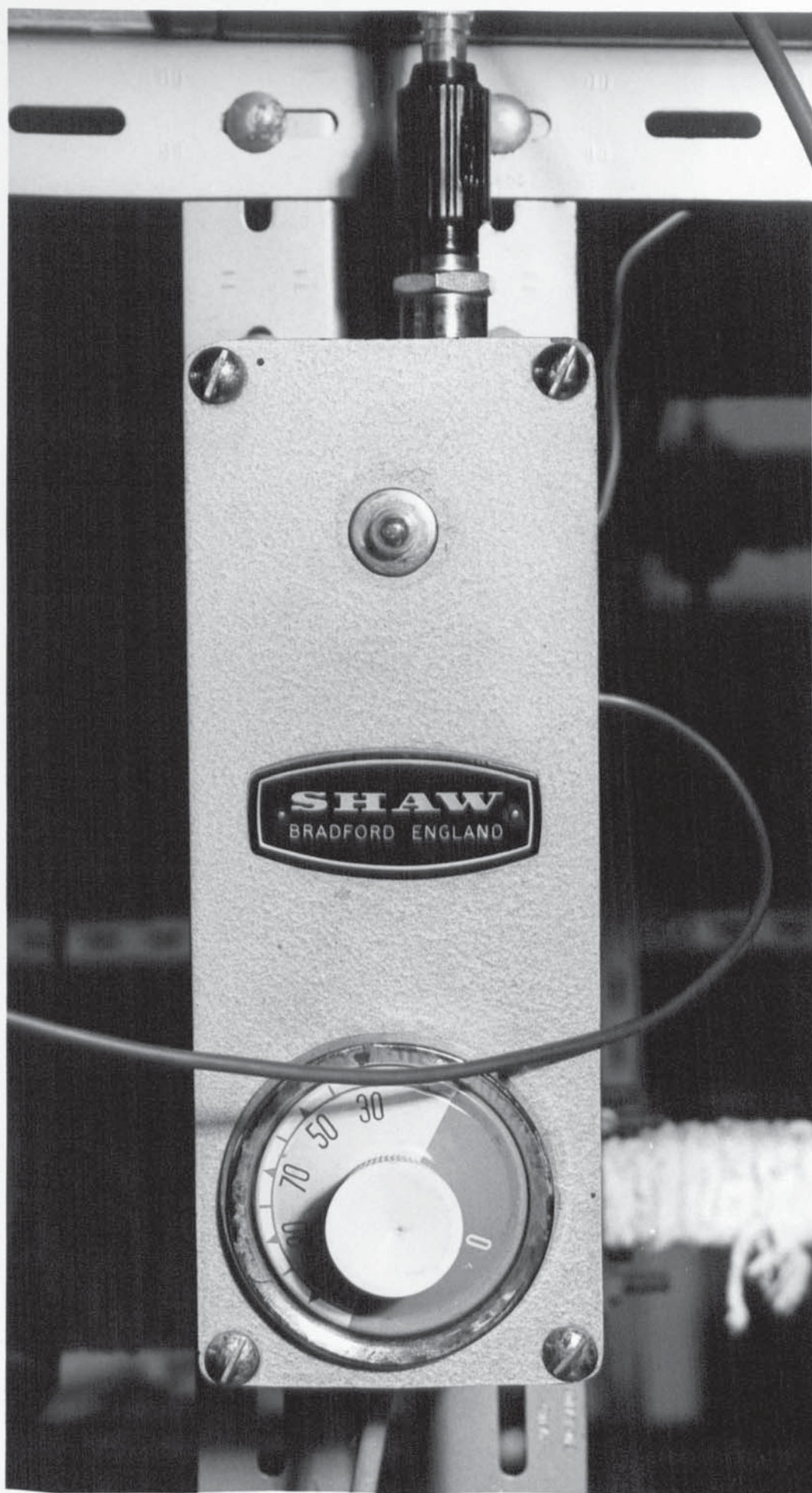


PLATE 4.3 CONSTANT TEMPERATURE UNIT

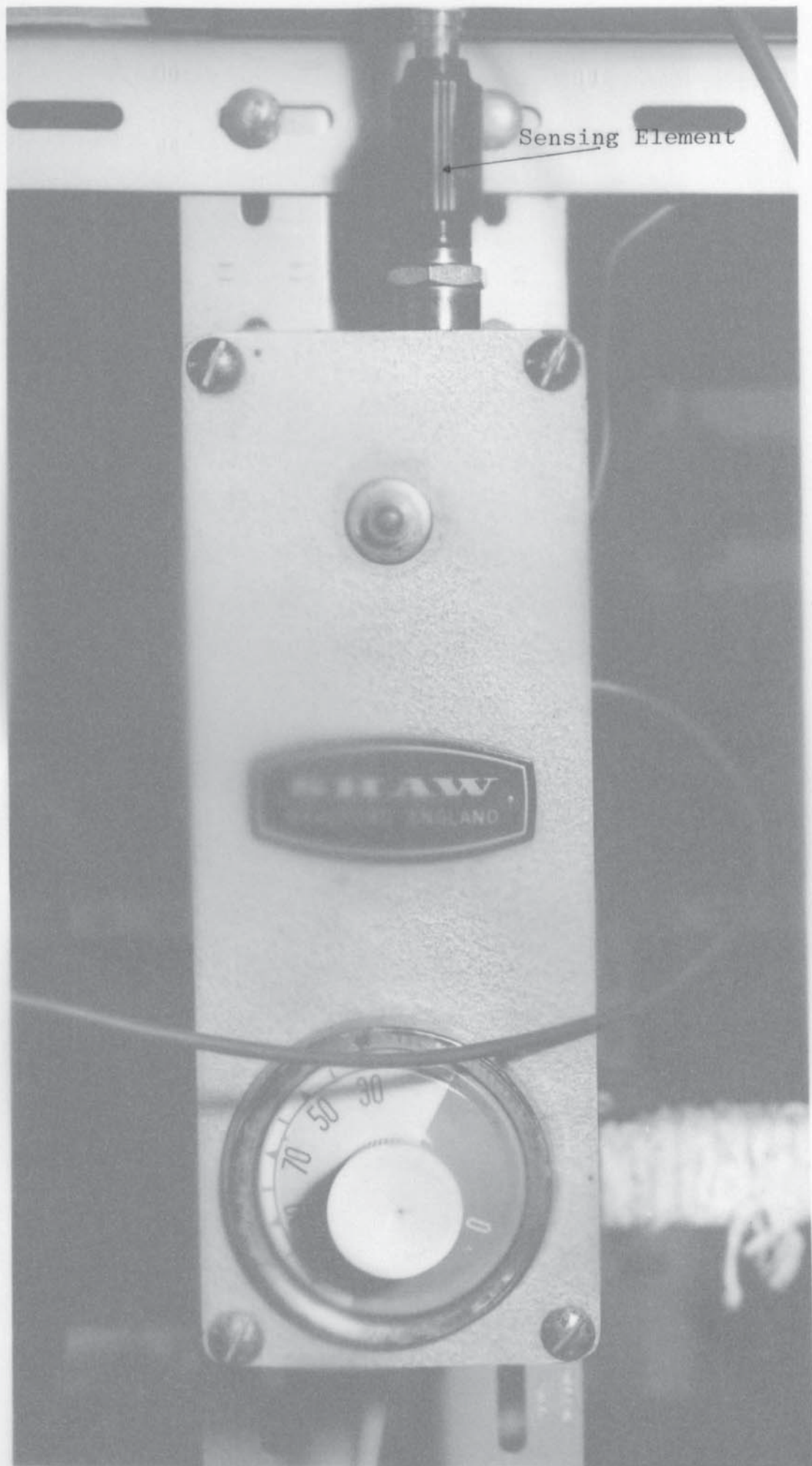


PLATE 4.3 CONSTANT TEMPERATURE UNIT



The structural analysis of the crust was obtained from this equipment.

#### 4.1.2. Overall Experimental Equipment For The Spray

##### Drying System

The schematic diagram of the overall experimental equipment is shown in figure 4.3; and the photograph on plate 4.4 presents the main features for the spray drying system. It consists essentially of an air supply fan, a quick-action valve, a Dall tube meter, two feed tanks, a temperature recorder, two heating coils and two Ether temperature controllers for the feed tanks, a feed pump, a metric type 14F rotameter, a 9' x 4' diameter P.V.C. spray drying tower, the Delavan hollow cone nozzle, the recovery tank and recirculation pump.

Atmospheric air was passed into the 4 in. diameter mild steel piping by the 20 HP, 3 phase, Parkinson air supply fan. The air flow rate was controlled by a 4 in. diameter Audco slim seal valve which was a quick-action valve. The excess air was removed by the air purgerator. The air flowrate was measured by a 4 in. diameter Dall tube meter with a bore throat of 1.83 in. diameter provided by George Kent Limited. The air was passed into the inlet piping of the spray tower via a 5 in. diameter flexible piping which was in turn connected to a reducer fitted to a 3 in. diameter air inlet duct.

The feed system consisted of two 2' x 2' x 3' stainless steel tanks each fitted with a stirrer, a heater, and an Ether temperature controller. One feed tank was used for chemicals and the other for water. The feed was piped



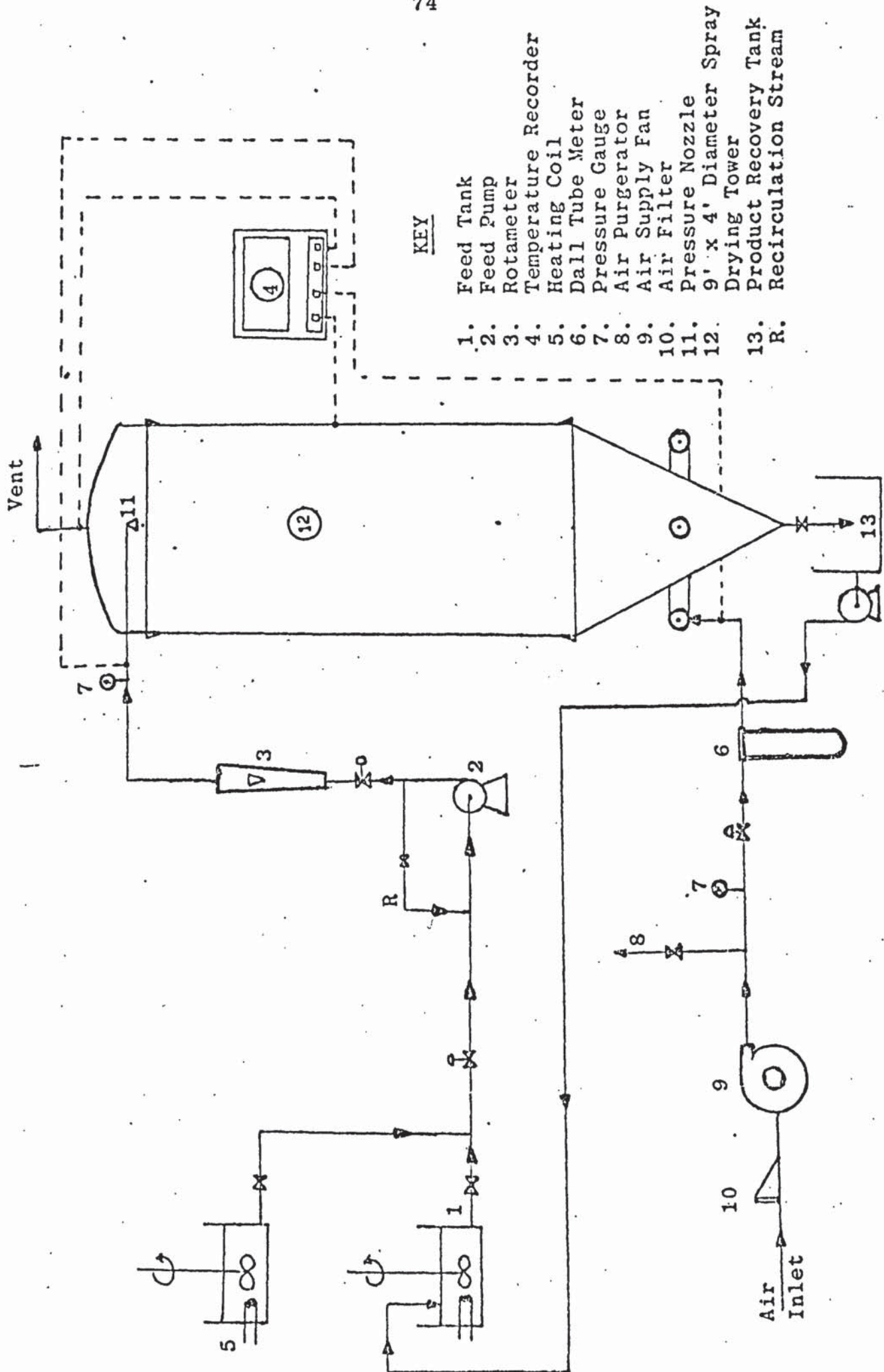


FIGURE 4.3 FLOW DIAGRAM OF OVERALL EXPERIMENTAL EQUIPMENT

**BLANK IN ORIGINAL**

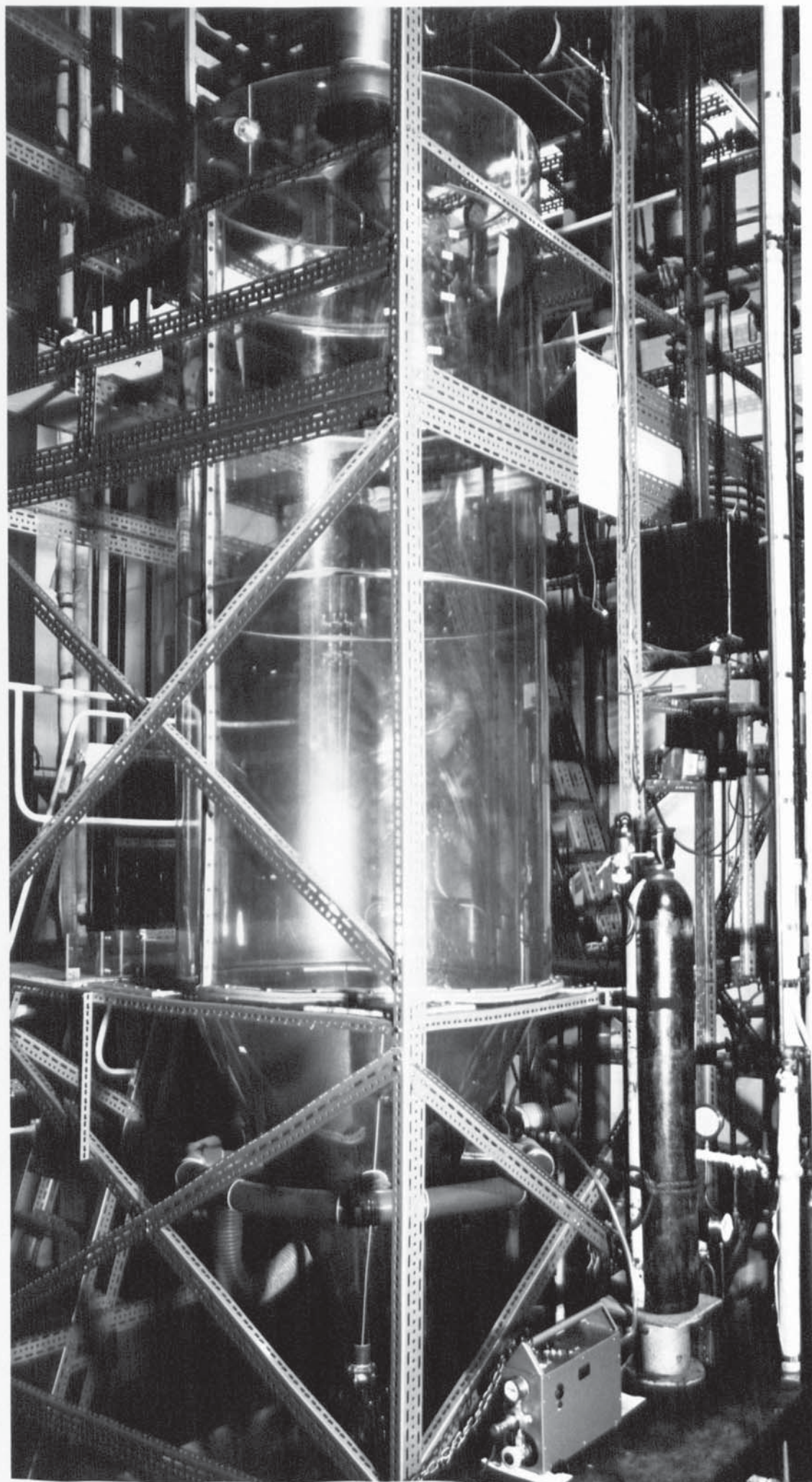


PLATE 4.4 SPRAY DRYING TOWER



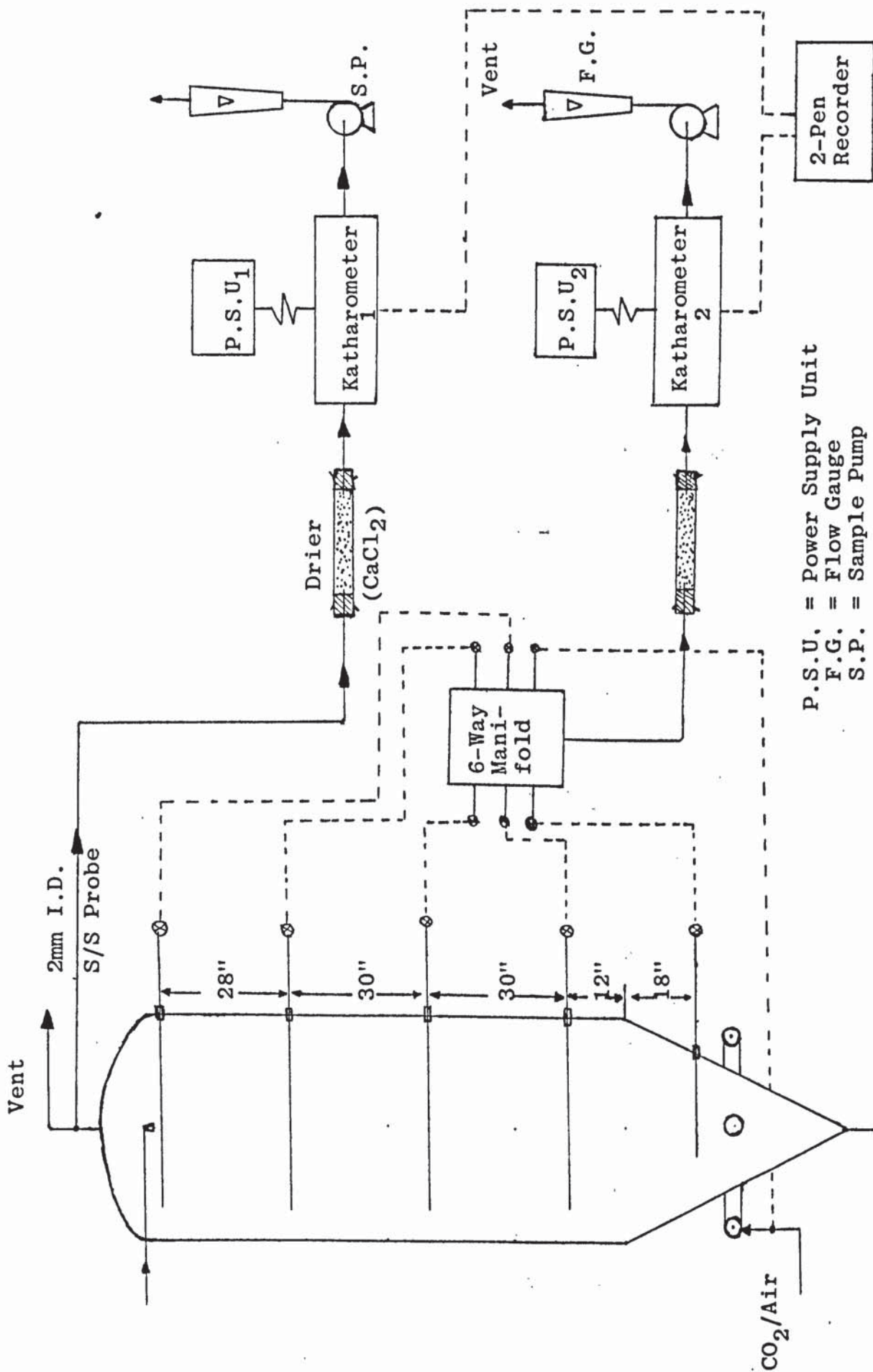


FIGURE 4.4. Diagram of Equipment For The Analysis of CO<sub>2</sub> in Air

through a 1.5 in. diameter Q.V.F. piping by a 3 phase, 50 Hz, Hoover gear pump which provided a constant evaporated load for the liquid spray. The feed flow was controlled by a Q.V.F. needle valve which was connected to the metric type 14F rotameter, while the Ether temperature controller maintained a constant feed temperature. The Delavan hollow cone nozzle provided the spray of liquid at the top of the tower.

The temperatures of the air inlet and the feed inlet into the spray tower were taken by thermocouples connected to a George Kent temperature recorder. Temperatures inside the spray tower were measured by thermocouples at 4' and 6', above the conical section of the tower. The exit temperature of the drying air was also measured in the same way.

#### 4.1.3. The Gas Analysis Equipment

The apparatus (figure 4.4) for experiments involving the analysis of carbon dioxide gas as a tracer in air, consisted of a six-way manifold, two sample pumps, two flow gauges, two thermostatically controlled katharometer analysers, two power supply units, a two-pen potentiometric indicating recorder, and five 2 mm I.D stainless steel probes, each 1.52m in length. The stainless steel probes were passed into the spray tower through 3/8' bulk head fittings fixed to the tower. These probes were in turn connected to the six-way manifold (plate 4.6), so that only one sampling probe could be used at a time.

THE SPRAY DRYING TOWER

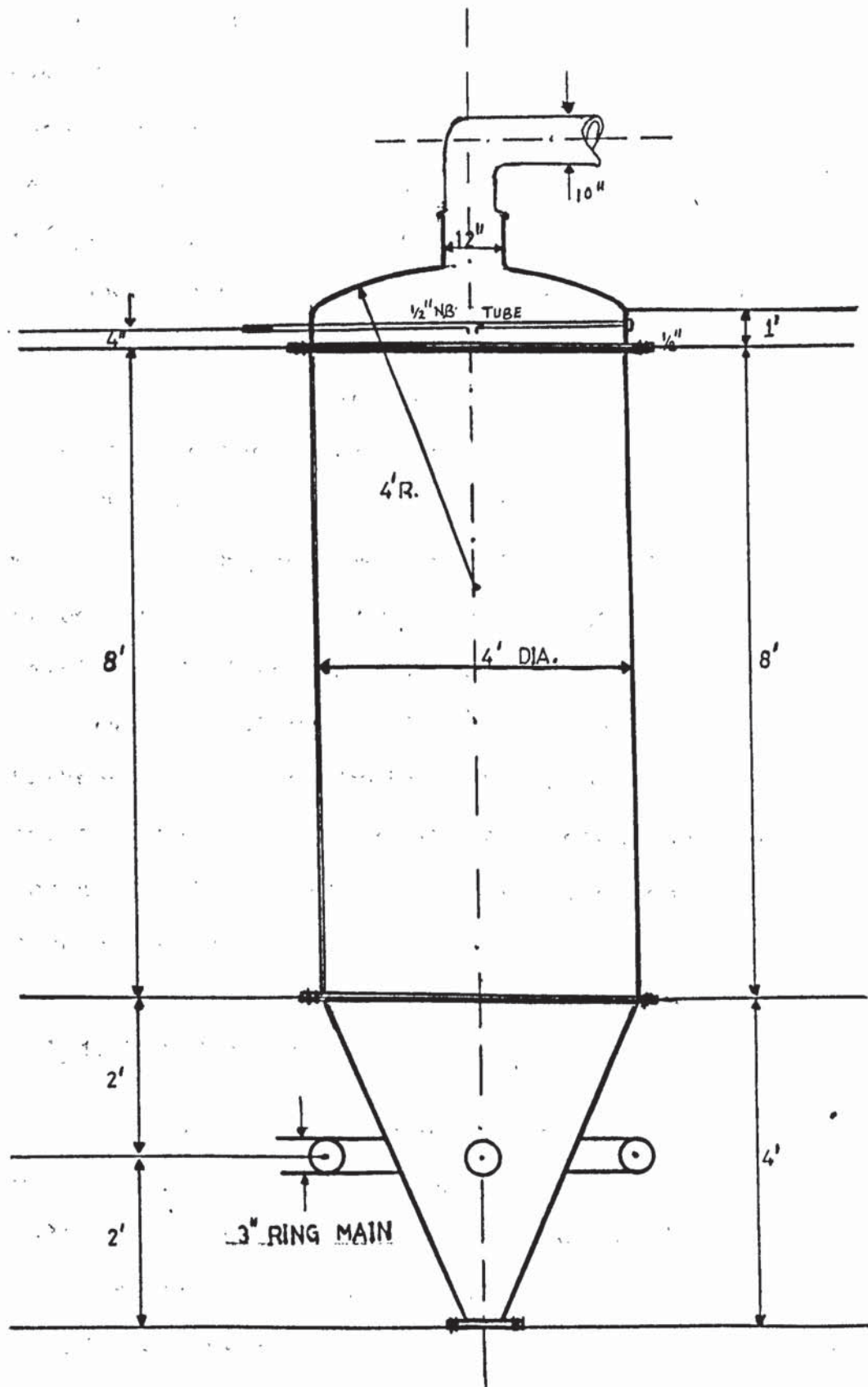


FIGURE 4.5



The sampling pump sucked the air/ $\text{CO}_2$  from the desired point in the tower and this was passed through a drier of Calcium Chloride to remove any trace of moisture. The sample was passed to the katharometer. The signal from the katharometer was then transmitted to the two-pen potentiometric indicating recorder which provided a visual display of the percentage concentration of the carbon dioxide in air. The power supply unit provided the katharometer with a stable current of 350 mA. The flow of sample through the katharometer was maintained at 100 cc/minute by a gas tap connected to the George Kent type 6525440 flow gauge.

The exit air at the top of the spray drying tower was sampled in the same way. The 2 mm I.D stainless steel probe was connected into a tapping at the exit vent. The sample of  $\text{CO}_2$ /air was again passed into the drier to remove any trace of moisture and this was passed into the katharometer for analysis, by the sampling pump. The signal was then passed into the two-pen potentiometric recorder, for a visual display of the percentage concentration of carbon dioxide in air.

#### 4.1.4. The Spray Tower

The spray drying tower designed for these studies is shown in Figure 4.5 and plate 4.4. It was made from a 3/16 in. thick clear P.V.C. As the major part of this investigation involved studies of the flow patterns and residence time distribution of both the drops and the drying air in the tower, a transparent tower gave the

greatest opportunity to make visual observation of the hydrodynamic behaviour of both phases. The main cylindrical section was 8 ft. high and 4 ft. in diameter. A 2 in. wide flange with 24, 13/32 in. diameter equally spaced holes was attached to both ends of the cylindrical section, as well as the top dished end and the conical base sections and the three sections bolted together.

The dished end section of the tower, shown in figure 4.6, was also made from a 3/16 in. thick P.V.C. It had a diameter of 4 ft. and at its top was attached a 6 in. by 12 in. diameter pipe section, onto which a metal reducer was fitted to take the 10 in. diameter bend of the air exhaust system.

The diagram in figure 4.7 illustrates the 4 ft. by 4 ft. diameter conical base of the tower. This base terminated into a 2 in. nominal bore, B.S.P. flange, which contained a 2 in. Q.V.F. valve. A 3 in. I.D. ring main was placed around the conical base at a position 2 ft. from the top. The drying air passed through this main, into four admission ports, equally spaced around the periphery of the tower base at  $90^{\circ}$  to one another. This ensured equal distribution of the air into the tower.

A stainless steel duplicate tower was also constructed in the same way, except that the height of the conical base shown in figure 4.8 was 1 ft. shorter than that of the P.V.C. tower. The stainless steel tower was however not used for these studies. It is expected that future work on spray drying of pure liquids and slurries at high

# DISHED END OF SPRAY DRYING TOWER

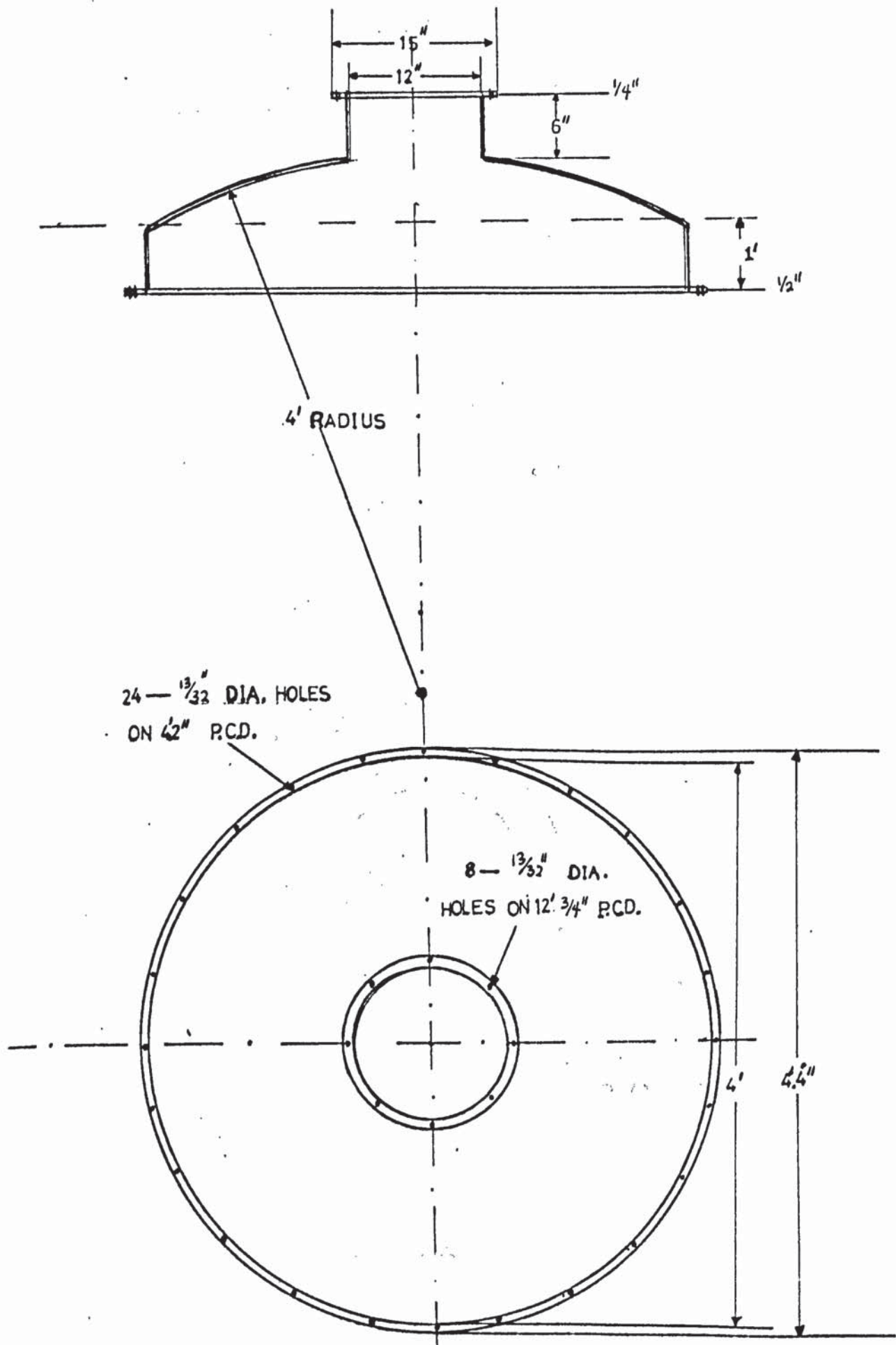


FIGURE 4.6.



CONICAL BASE AND RING MAIN FOR THE P.V.C. SPRAY TOWER

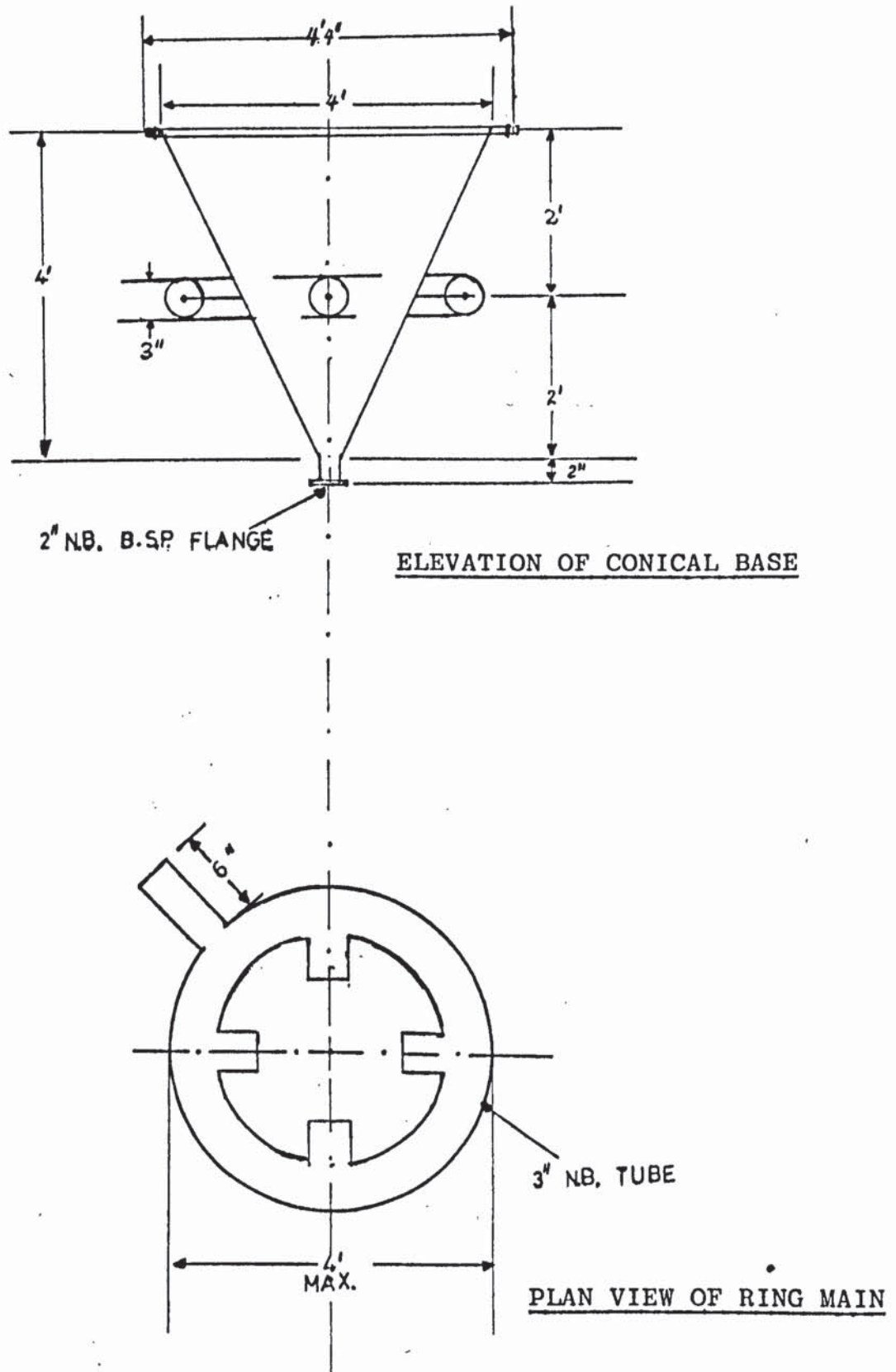


FIGURE 4.7

CONICAL BASE AND RING MAIN FOR THE S/S SPRAY TOWER

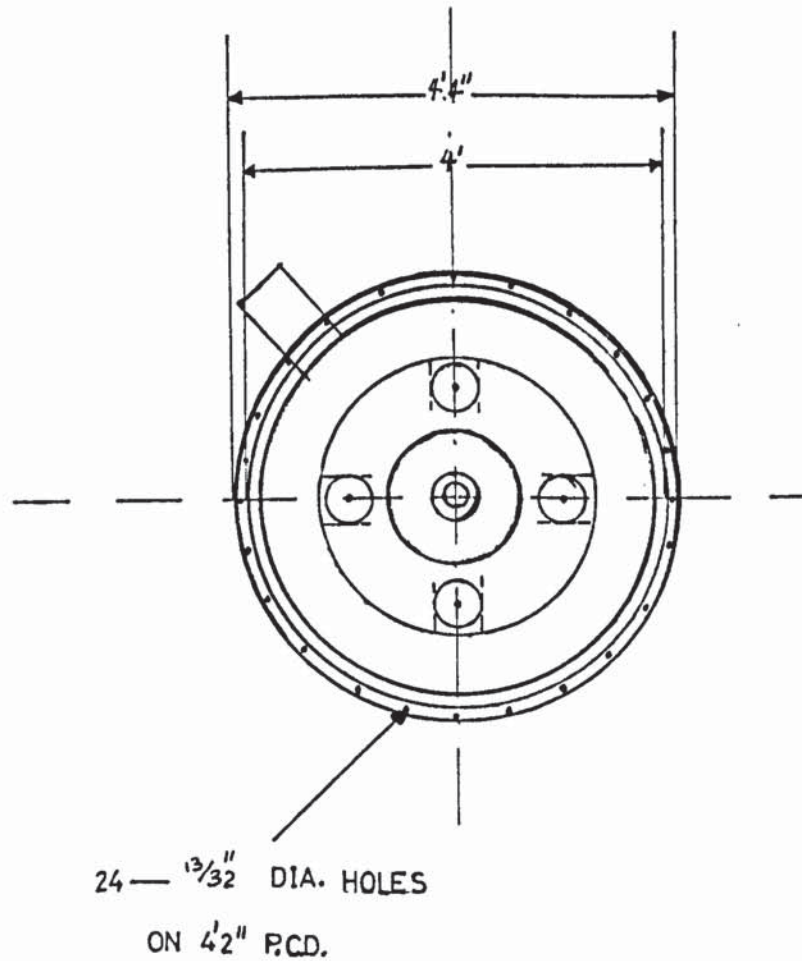
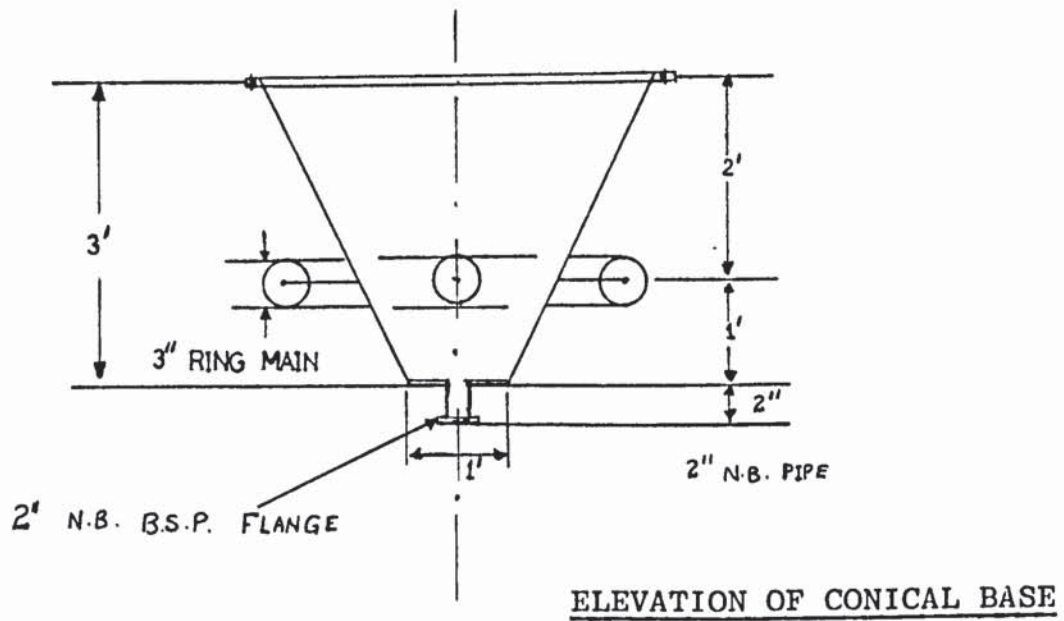
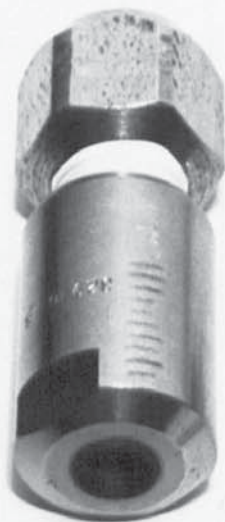


FIGURE 4.8





DELAVAN  
MINI SDX 4-6



DELAVAN  
DC 4-4



DELAVAN  
WM 4-1



PLATE 4.5 SPRAY NOZZLES

temperatures will be carried out in the spray tower.

#### 4.1.5. The Spray Nozzles

Two types of spray nozzles were used in the experimental studies. For feeds of pure water, the Delavan hollow cone nozzle type Wm 804 shown in plate 4.5 was employed. The nozzle was made from an 18-8-3 stainless steel and contained a 16.7 mm long cylindrical strainer, attached to the feed inlet, to ensure that no unwanted solid material could pass through the nozzle and thereby cause its blockage. The nozzle had a 1/4 in. B.S.P. male thread, which could be screwed into the 1/4 in. B.S.P. female thread of the feed line.

For feeds containing dissolved and suspended solids of sodium carbonate, the Delavan hollow cone nozzle type SDX 32936-11, shown in plate 4.5 was utilised. It consisted of a 303 stainless steel body and stem adaptor, a ceramic swirl chamber and an O-ring seal. The swirl chamber was the most important feature of the nozzle as it minimised plugging and was claimed to provide uniform sized drops. The orifice disc was made of tungsten carbide which was recessed to prevent damage. The stainless steel stem adaptor was fitted with a 1/4 in. B.S.P. female thread to take a male to male 1/4 in. B.S.P. stainless steel adaptor for the feed line.





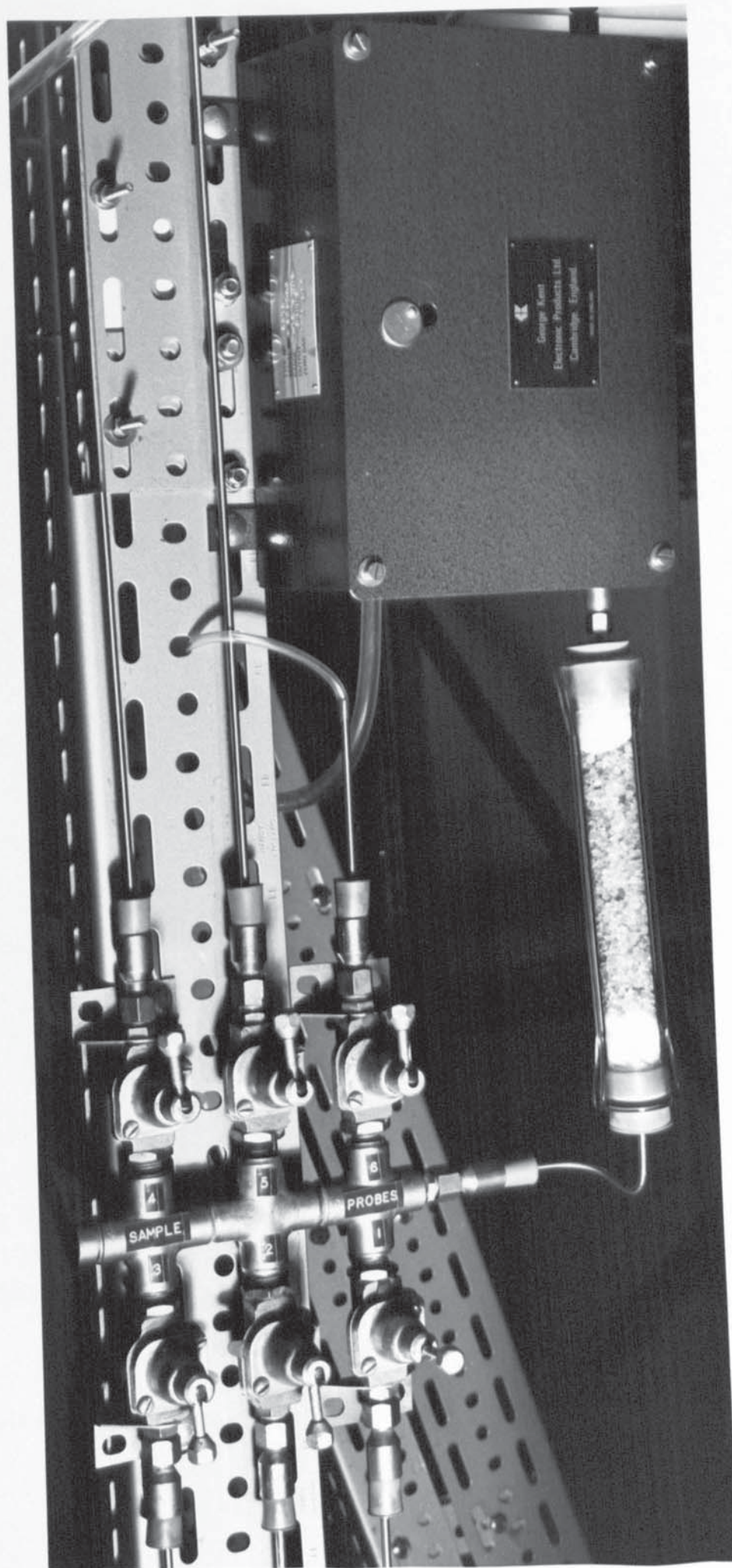
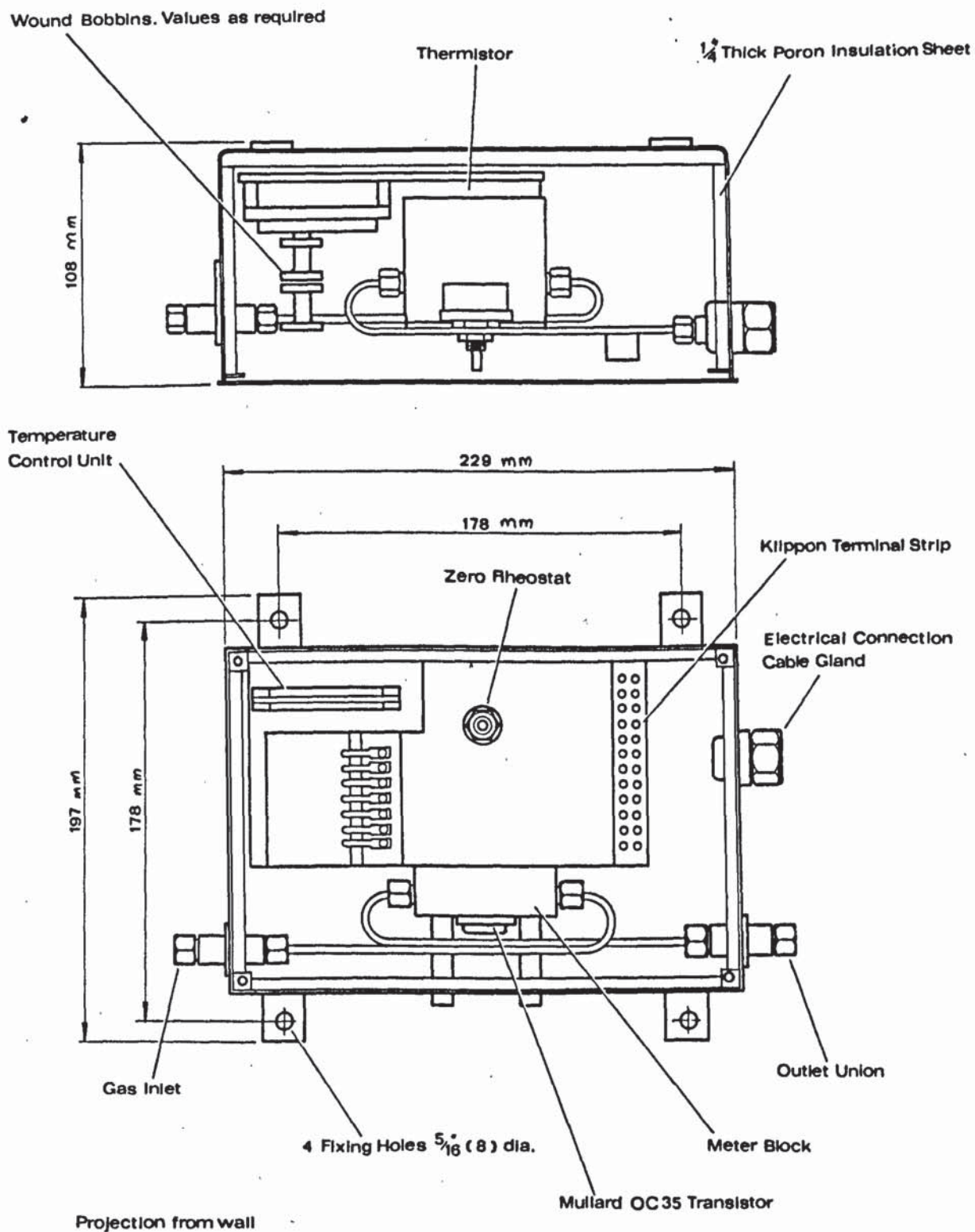


PLATE 4.6 THE KATHAROMETER AND 6-WAY MANIFOLD

# KATHAROMETER MODEL 6518



**FIGURE 4.9**



#### 4.1.6. The Katharometer

The gas analyser used for the experiment is shown in figure 4.9 and plate 4.6. It was a thermostatically controlled direct acting brass block katharometer, type 6518, supplied by George Kent Electronic Limited. The katharometer consisted of four platinum wires with identical electric and thermal characteristics, each forming an arm of a simple Wheatstone bridge. Thus, when a dry carbon dioxide-air mixture passed through the cells at a constant rate, a temperature difference developed which caused a difference between the resistances in the components of the bridge. Hence a current flowed, due to the imbalance of the bridge. The imbalance potential was dependent upon the percentage of carbon dioxide gas passing through one of the cells of the bridge. The current for the katharometer was provided by the power supply unit with a stabilised 350 mA current output for the analyser bridge circuit, as well as for the temperature control circuitry.

#### 4.1.7. The Smoke Generator

The smoke to be injected into the spray tower was provided by the 3020 smoke generator shown in plate 4.7, supplied by C. F. Taylor Limited. It consisted of a 200 ml. oil reservoir and mixing chamber which was heated electrically, a small carbon dioxide cylinder placed on the underside of the generator, a carbon dioxide pressure gauge and safety valve device. The pressurisation unit fitted



Pressurisation  
Unit






PLATE 4.7 THE SMOKE GENERATOR





PLATE 4.7 THE SMOKE GENERATOR



to the smoke outlet forced the white smoke into the tower against back pressure of the air. The oil level was measured by a dipstick fitted to the filler cap. The unit also contained a thermostat neon indicator which automatically switched off whenever the correct working temperature had been attained.

## 4.2 CALIBRATION OF MEASURING INSTRUMENTS FOR STUDIES OF THE DRYING OF SINGLE DROPS

The feed device, rotameter and the Dew-point meter were calibrated (11,104) for the experimental studies on the drying of single drops in the following manner.

### 4.2.1 The Feed Device

As shown in the photograph in plate 4.2, the glass tubes of the feeding device were graduated in centimeters by means of a scalafix. To calibrate the feeding device, the glass tubes were filled with water and the initial level on the scale was noted. The rotaflo valve was opened and the water collected in a small measuring cylinder. The final level on the scale was again recorded as well as the volume of water collected. The procedure was repeated twice, and the average volume per centimeter scale reading was obtained (104).

### 4.2.2 Rotameter

The flowrate of air in the wind tunnel was measured by the Metric type 18A rotameter with Duralumin float. The float was calibrated against the volume of air recorded by the Parkinson gas meter over a specific time interval. The procedure was repeated for six float positions and a graph of volumetric flowrate versus float position on the centimeter scale was plotted (104).

#### 4.2.3 Dew-point Meter

The Dew-point meter was calibrated by passing the air from the Birlec drier through a previously-weighed bed of alumina for a specific time interval and recording the humidity on the meter. At the end of the experiment, the moisture content of the air was calculated from the difference between the final and initial weight of the bed, and this was compared with the recorded humidity on the meter.



### 4.3 CALIBRATION OF MEASURING INSTRUMENTS FOR STUDIES IN THE SPRAY DRYING TOWER

For experiments on the studies of the residence time distribution for the drops and air in the spray drying tower, the following measuring instruments were calibrated.

#### 4.3.1 Rotameter.

The feed flowrate was measured by a metric type 14 F rotameter with Duralumin float. The float was calibrated against the volume of water collected and measured over a time interval. This was repeated for various float positions on the rotameter scale and a graph of volumetric flowrate against the float position was plotted.

#### 4.3.2 The Dall Tube Meter

The air flowrate was measured by a 4 in. Dall tube meter with a throat bore of 1.83 in. The mass flowrate of the air was calculated from the pressure drop across the Dall tube. The pressure drop was measured by a mercury manometer connected to the tappings on the 4 in. Dall tube and the throat bore. The air flowrate was increased and the manometer height was recorded. The procedure was repeated for different air flowrates and the corresponding mercury manometer height was recorded. A graph of the pressure drop against the mass flowrate of the air was then plotted.

#### 4.3.3 The Two-Pen Potentiometer Recorder

The instrument was calibrated by a Foster Cambridge portable potentiometer. It was switched on for about 10 minutes in order to stabilise the circuits. A voltage corresponding to the zero reading was then passed into the instrument and the indicating pointer was checked and adjusted if necessary to the zero mark. A voltage corresponding to the full scale reading was also passed into the recorder and the indicating pointer was checked and adjusted. The span of the instrument was checked in a similar manner.

#### 4.4 EXPERIMENTAL PROCEDURE AND MEASUREMENTS

The first part of the experimental work involved the drying of single drops of sodium sulphate decahydrate in order to test the momentum-heat transfer model discussed earlier on in Section (3.1).

The major part of the experimental work however, was on the studies of the residence time distribution of drops and air in the spray drying tower.

##### 4.4.1 Single Drops of Sodium Sulphate

A super-saturated solution of sodium sulphate decahydrate was prepared with warm distilled water. Air was passed through the wind tunnel and the heater was switched on. After steady state condition had been attained in the wind tunnel, the solution was introduced into the feeding device. The drop was suspended at the drop suspension device by careful adjustment of the rotaflo valve. The drop was rotated at 15 r.p.m. by the motor and allowed to dry at a constant temperature and air flowrate for 30 minutes. The air humidities both upstream and downstream were noted as well as the upstream and downstream temperatures by means of the thermocouples. The initial level of liquid in the feed device was read on the scale, and after each experiment, the final level was also recorded. Hence by a mass balance, the amount of water evaporated was also calculated. The temperature inside the drop was obtained by projecting the thermocouple into the drop. The drop



diameter was measured by a cathetometer. The experiment was repeated using different nozzle diameters. Drops of 2, 4, 5 and 6 mm outside diameter were dried in this way. At the end of each run the crust formed by the drop was sliced off by a guillotine device (11), onto a filter paper which absorbed the excess solution in the hollow shell of the crust.

After drying, the hemispherical sodium sulphate crusts were glued to metallic studs with araldite and coated with a thin layer of carbon and gold-palladium to maintain a constant electric potential on the crust surface. To ensure that fine details like pores or cracks were not lost the thickness of the coating was in the region of  $5 \times 10^{-9}$  m.

The specimens were then introduced into the chamber of the scanning microscope where photomicrographs were obtained on a 35 mm film. These photomicrographs were examined for internal and external structural analysis, as well as porosity and crust thickness measurements (11,104). The porosity was obtained by placing an initially weighed tracing paper of the same size on the photomicrograph and then tracing the pores on the paper. The pores traced on the paper were then carefully cut and removed. The paper was then weighed again to obtain the porosity of the crust.

For experiments involving the measurement of the thermal conductivity of the dried sodium sulphate however, a supersaturated solution of the compound was prepared



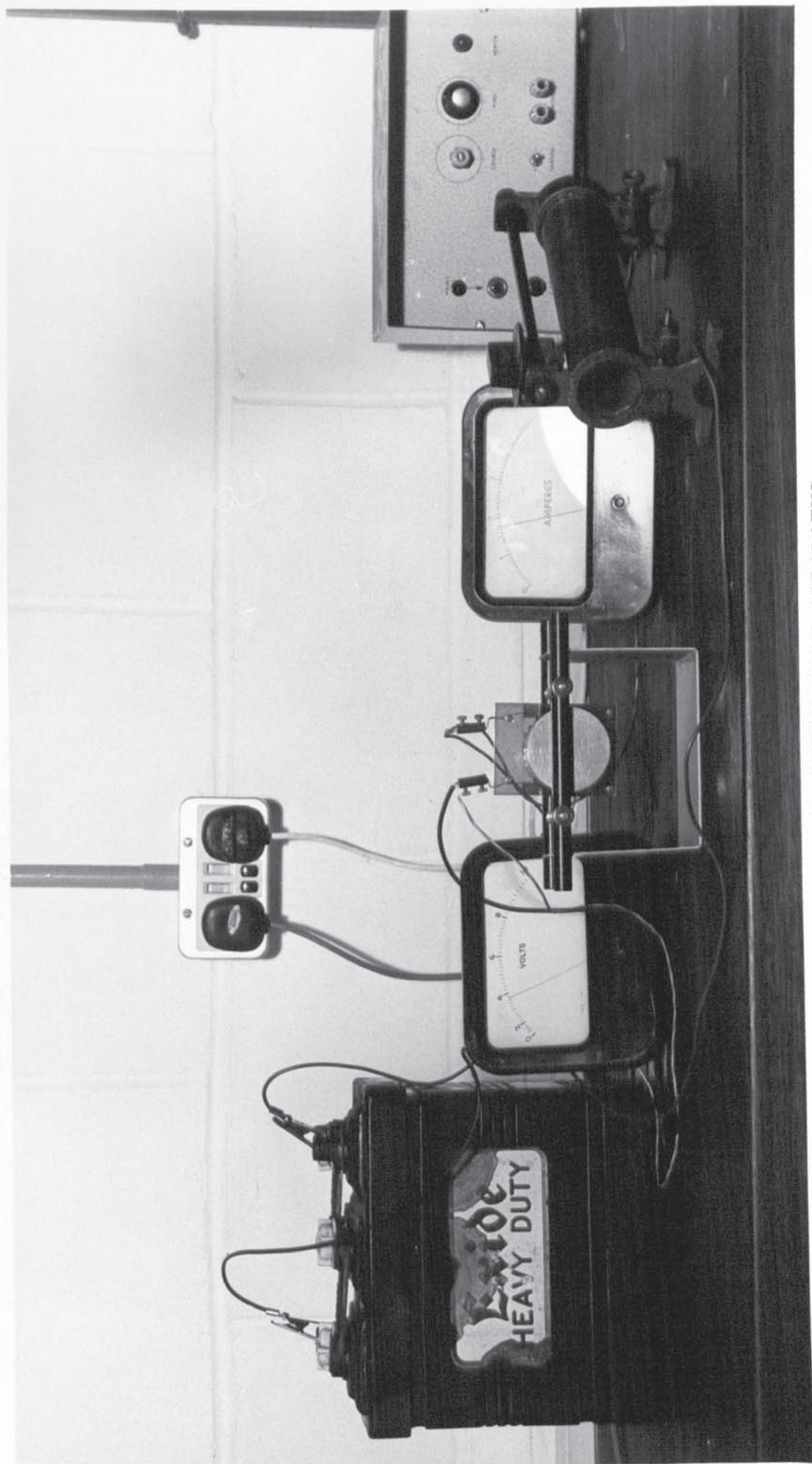


PLATE 4.8 LEE'S DISC APPARATUS



until no more could dissolve. Additional sodium sulphate was then added until a slurry was formed. This was filtered by a vacuum pump with the aid of 5.08 cm diameter filter paper placed inside a filter funnel of the same size. After the water had been well-drained, a thin layer of the sodium sulphate precipitate was placed in an oven to dry up under a low heat rate.

After drying, the thin layer of sodium sulphate was carefully removed and placed between the two discs for thermal conductivity measurements by the Lees' method. The Lees' disc apparatus is shown in the photograph in plate 4.8. It consisted of three metal discs and a small heater. The specimen was placed in between the two discs while the heater was carefully placed in between the second and third disc. These were all clamped firmly together. The heater was connected in series with an ammeter, a variable resistance and a 6 volts accumulator. A voltmeter measured the potential difference across the heater. Liquid paraffin was used in the holes of the discs in order to improve the thermal contact between the thermometers and the discs. A 3 amp current was first passed through the heating coil to raise the temperature quickly and then readjusted to 2 amp. The final readings of the three thermometers were recorded after steady state had been reached.

#### 4.4.2 Estimation Of Volumes In The Spray Tower

The advantage offered by the transparent spray drying tower was that observation of the hydrodynamic behaviour of

both phases inside the tower could be made. Thus the flow patterns of the drying air in the tower were followed by injecting clouds of smoke into the tower at the air inlet.

After steady state had been attained in the spray tower at the desired air and liquid feed flow rates and temperature, smoke from the 3020 smoke generator was injected into the tower through the air inlet. Swirling smoke clouds were observed in the conical base as well as at the top section of the tower. A plug flow region was observed in between the two well-mixed zones, with a by-pass stream across the entire length of the spray tower. The volume of the well-mixed section at the bottom of the tower was measured and recorded. The experiment was repeated with four other air flowrates while the spray was kept at a constant flowrate. The flowrate of the water spray was then varied and the corresponding volumes were measured and again recorded. The smoke was injected into the top section of the tower about 6 in. below the spray nozzle, and the volume of the well-mixed section was again measured and recorded for five different air flowrates and liquid feed flowrates. This procedure was repeated in order to estimate the plug-flow volume in the tower. These volumetric measurements as well as the volume of the by-pass stream were confirmed by the tracer technique which will be discussed in the next section.







PLATE 4.9 A TYPICAL WATER SPRAY

#### 4.4.3 Air Residence Time Analysis

Experimental work to test the model presented in section (3.2) was carried out using a tracer technique. After steady state conditions had been attained in the spray tower, a pulse of carbon dioxide was injected at the air inlet. The amount of carbon dioxide injected was measured by an integrated heater regulator type 148302. To ensure that the carbon dioxide gas injected into the tower was not absorbed by the water spray, the feed was initially saturated with carbon dioxide gas. The carbon dioxide-air mixture was then drawn through a 2 mm I.D. stainless steel probe fixed into the exit vent of the tower. This sample was drawn through a 60 cc. glass tube containing calcium chloride to remove any moisture present in the gas mixture, before it was passed through the katharometer where the concentration of carbon dioxide in air was measured. A graph of concentration against time was recorded on the chart of the continuous two-pen potentiometric recorder. The flow of gas sample through the katharometer was maintained at 100 mls per minute for each run with the aid of a 3/16 in. gas tap type D505X/12/12. The input concentration profile of the carbon dioxide tracer in air was also measured by a 2mm I.D. stainless steel probe connected to the air inlet into the tower where the gas sample was passed through the second katharometer via the 6-way manifold device. The input concentration profile was displayed on the two-pen recorder.



The experiment was repeated for the same air flowrates and feed flowrates as in section (4.4.2), and the corresponding concentration of the carbon dioxide tracer in air was obtained. After every run the air and water spray were allowed to run for about 20 minutes to ensure that there was no trace of carbon dioxide left in the spray tower.

In order to measure the thickness  $\delta t'$ , of the by-pass stream, five 2 mm 1.D. stainless steel probes each 1.524m in length were placed horizontally along the spray tower as shown in Figure 4.10. The probes were passed through 3/16 in. bulk head fittings type D 400/12/12, and were connected by 1/8 in. 1.D. P.V.C. tubes to the 6-way manifold so that the probes could be moved horizontally to any desired point in the tower. After steady state had been reached in the tower, a shot of carbon dioxide was again injected at the air inlet, and the concentration profile of the tracer in the by-pass stream was measured by placing the probe near the wall of the tower. This procedure was repeated for different positions of the probe near the wall until a point was reached where the residence time of the air was quite short. At this stage the length of the probe was measured to obtain the thickness and hence the volume of the by-pass stream around the tower wall. The experiment was repeated with the other probes along the tower and in each case, since the residence time of the well-stirred section of the tower was longer than that of the by-pass stream, the two sections were quite distinguishable.



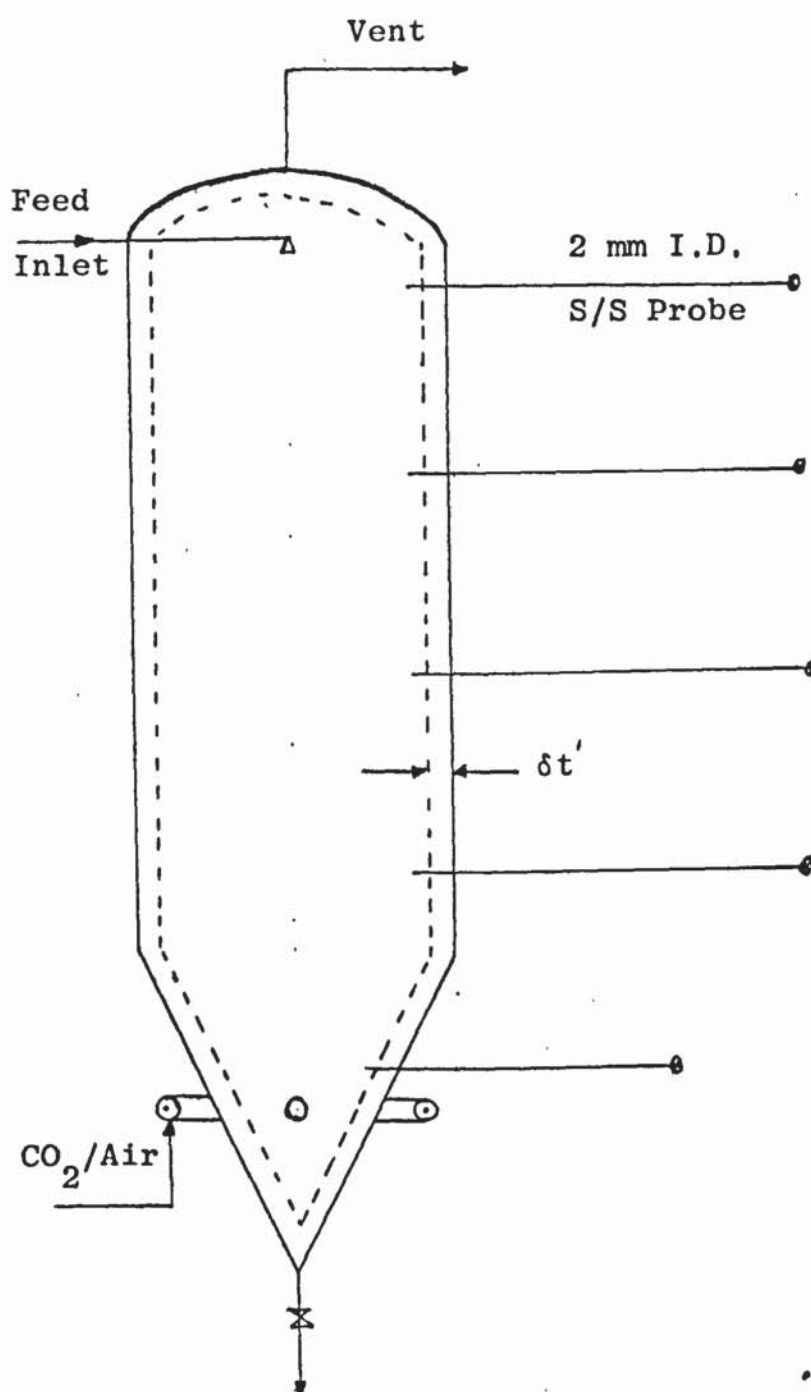


**FIGURE 4.10** Thickness Of By-pass Stream From Spray Chamber Wall

#### 4.4.4 Residence-Time Analysis For Pure Water Spray

A tracer technique was again applied in the experiments on the residence time distribution of pure water sprays in the tower. The feed temperature was kept constant by an Ether temperature controller. A 2.5N iodine solution in potassium iodide was prepared (51). After steady state condition had been attained in the spray tower a shot (10 ml) of the iodine solution was injected into the feed inlet. Samples were then collected from the exit at the bottom of the tower at 10 seconds interval. These samples were then titrated against a standardised solution of sodium thiosulphate (51). Thus the exit concentration profile of iodine tracer in the water spray was calculated. The experiment was repeated with four other flowrates of the feed as well as the air. Care was taken to ensure that all of the tracer was removed from the feed line after every run, by allowing the water to run for about 15 minutes.

#### 4.4.5 Residence Time Analysis - Sodium Carbonate Slurries

A slurry of sodium carbonate decahydrate was prepared and fed into the spray tower. A solution of 2.5 N iodine solution in potassium iodide was also prepared (51) and then mixed with a slurry of sodium carbonate. This mixture was used as tracer in the feed. After steady state condition at the desired air and feed flowrates and temperature had been attained in the tower, the tracer was injected at the feed inlet to the tower and as in the





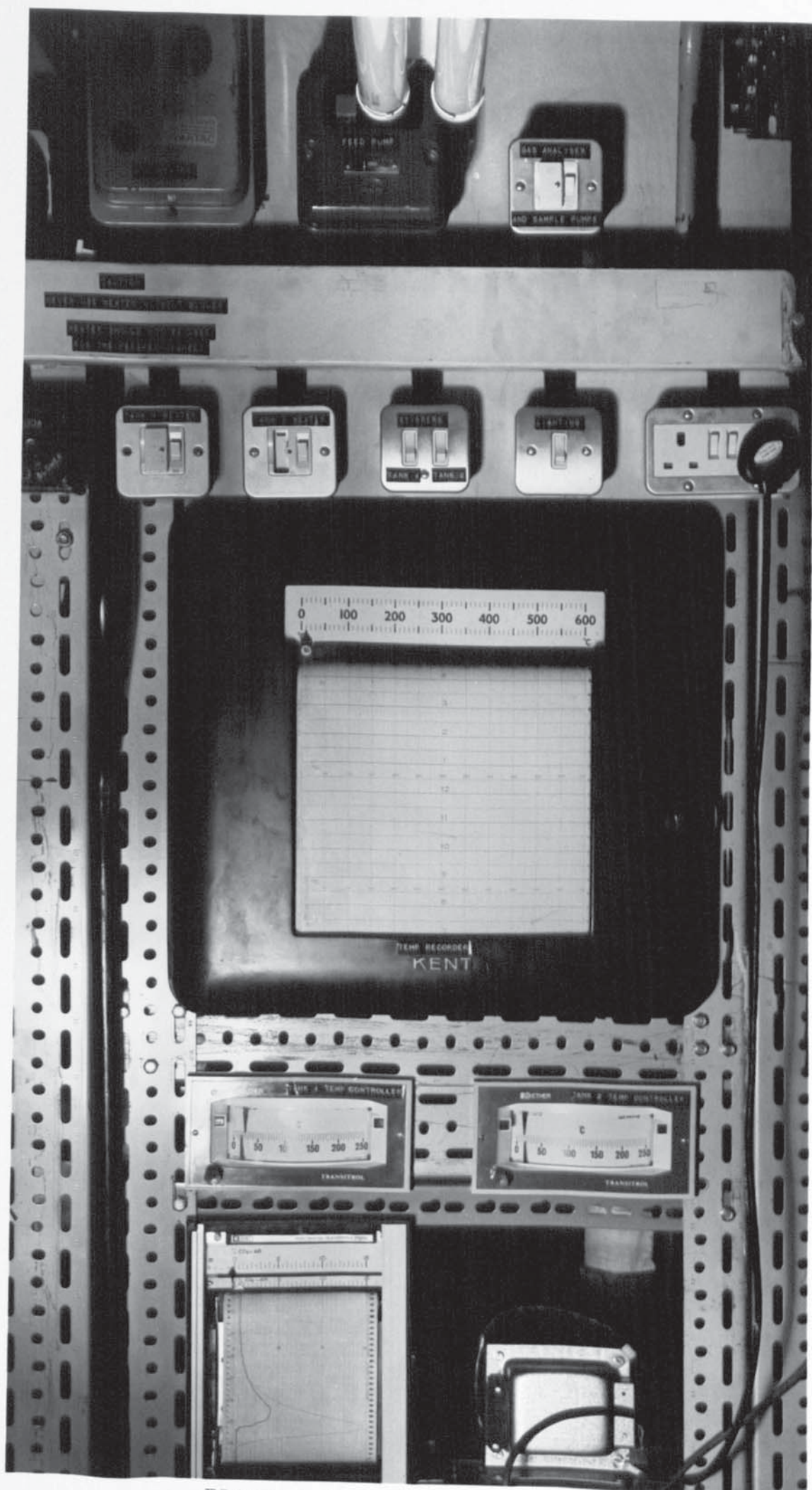


PLATE 4.10 CONTROL PANEL

previous experiments, samples were collected from the exit of the spray tower, at 20 seconds interval. These were then titrated against a standardised sodium thiosulphate solution ( $\text{Na}_2\text{S}_2\text{O}_3 \cdot 5\text{H}_2\text{O}$ ). The concentration profile of the tracer in the sodium carbonate was then calculated. The experiment was repeated with a different air and feed flowrate.

After each run, the spray tower was washed down with water to remove the sodium carbonate that adhered to the inside of the tower.

## CHAPTER FIVE

### PRESENTATION AND ANALYSIS OF EXPERIMENTAL RESULTS

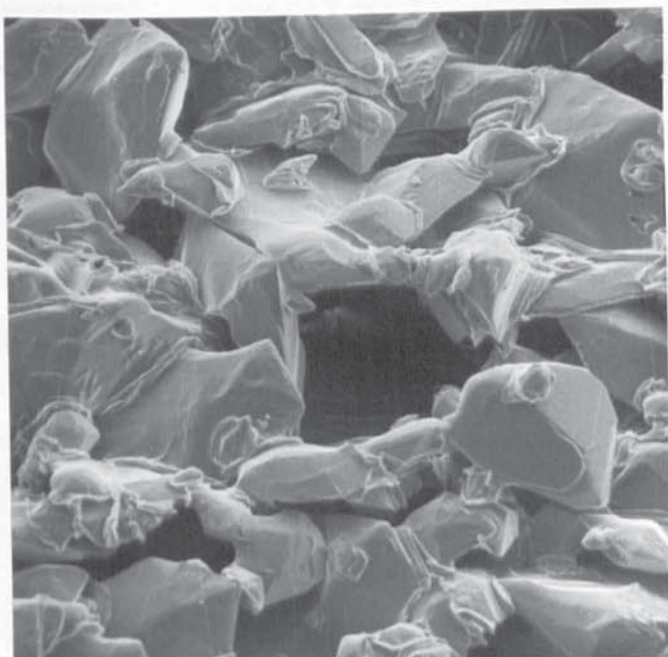




PLATE 5.1

SODIUM SULPHATE CRUST

5.1a: Internal Structure  
Showing Pores  
Magnification = 100X



5.1b: External Structure  
Showing Ruptures  
Magnification = 200X

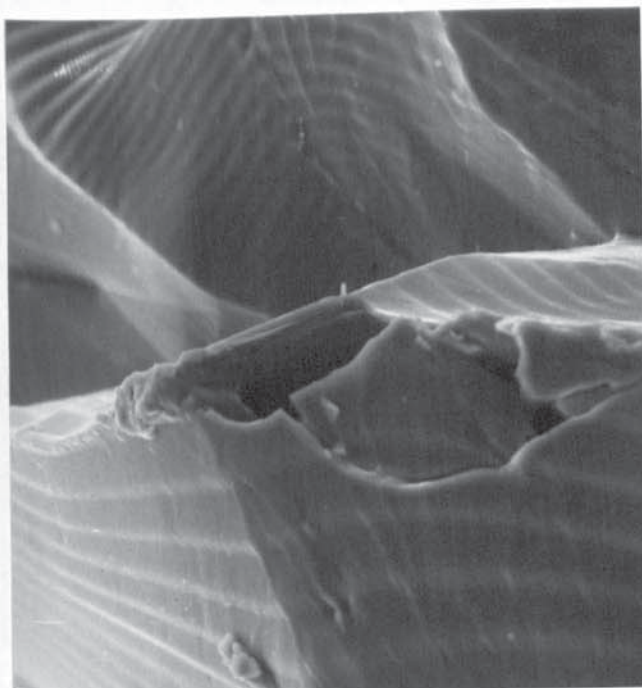
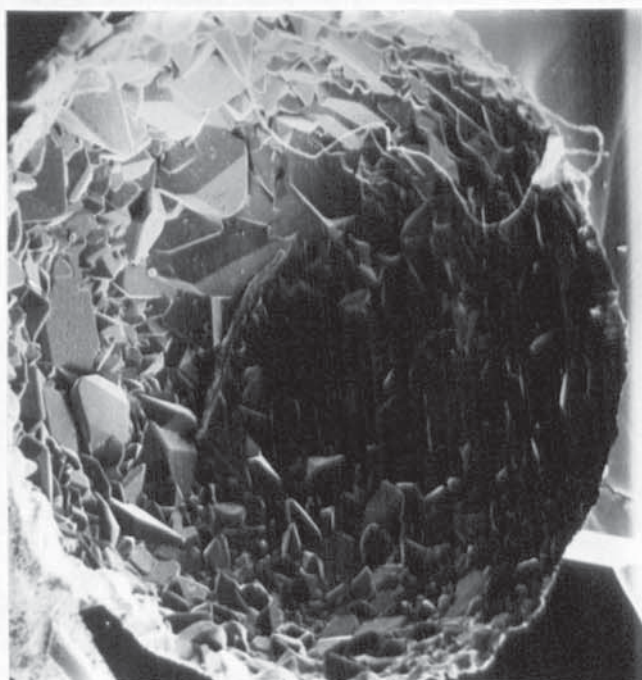






PLATE 5.2  
SODIUM SULPHATE CRUST

5.2a: Internal Structure  
Magnification = 35X



5.2b: External Structure  
Showing Cracks  
and Holes  
Magnification = 50X

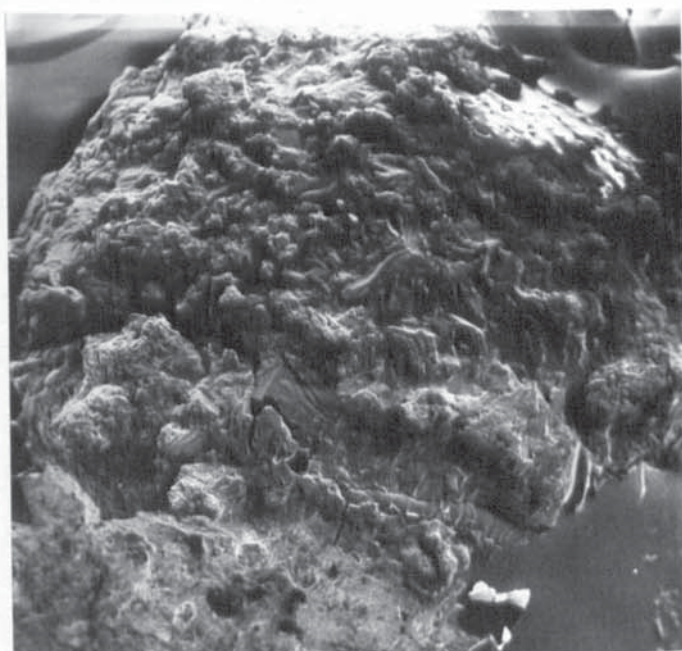
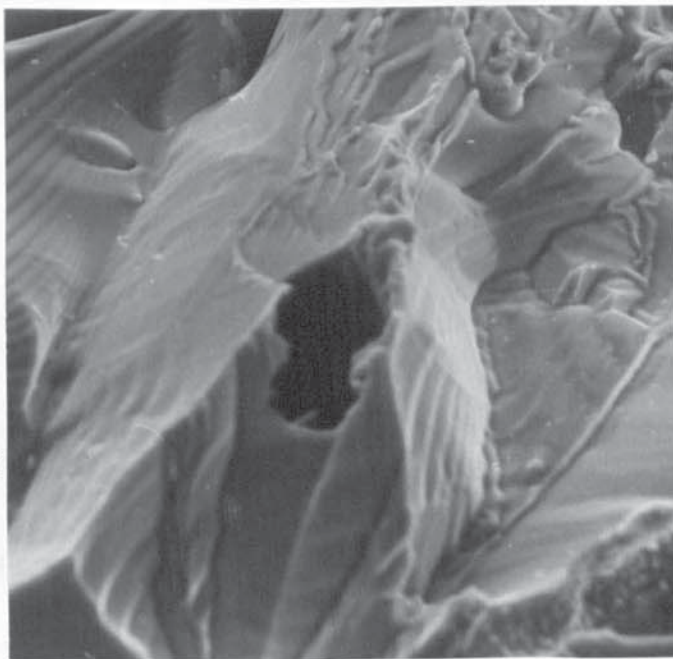




PLATE 5.3

SODIUM SULPHATE CRUST

5.3a: External Structure  
Showing Craters  
Magnification = 120X



5.3b: Internal Structure  
Showing Pores  
Magnification = 60X

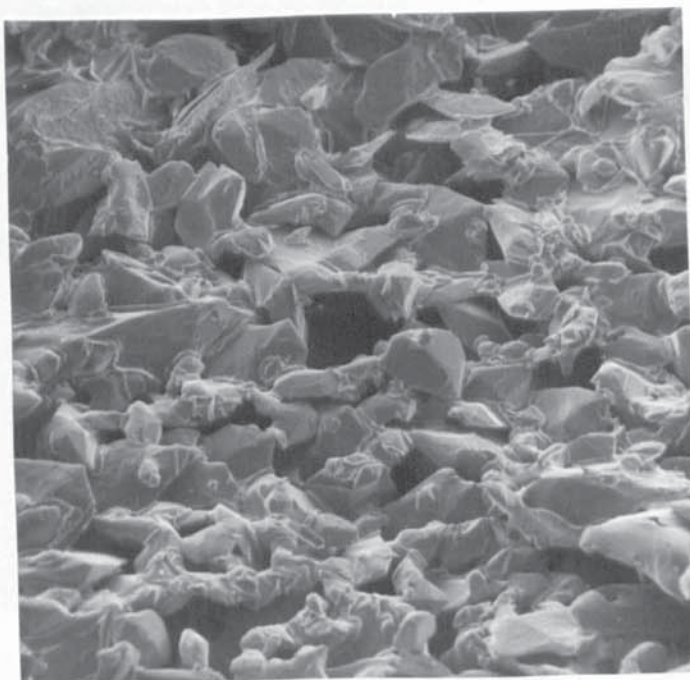


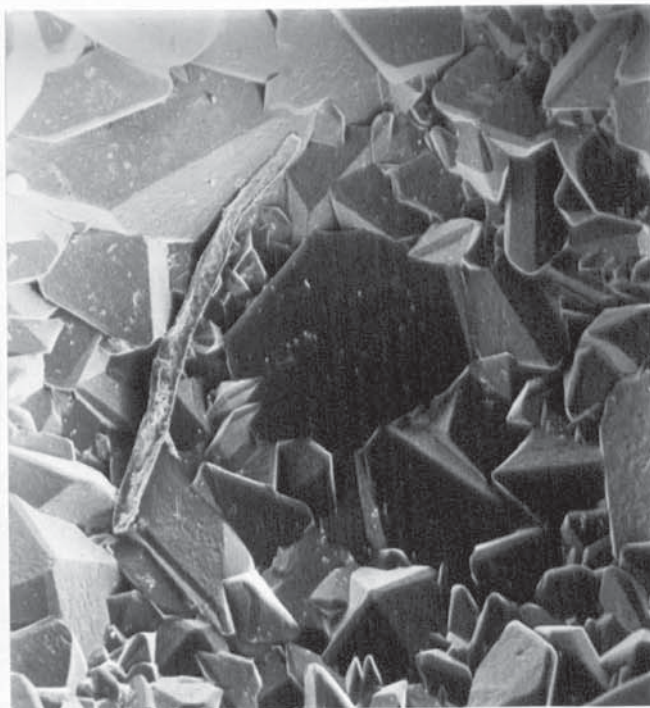




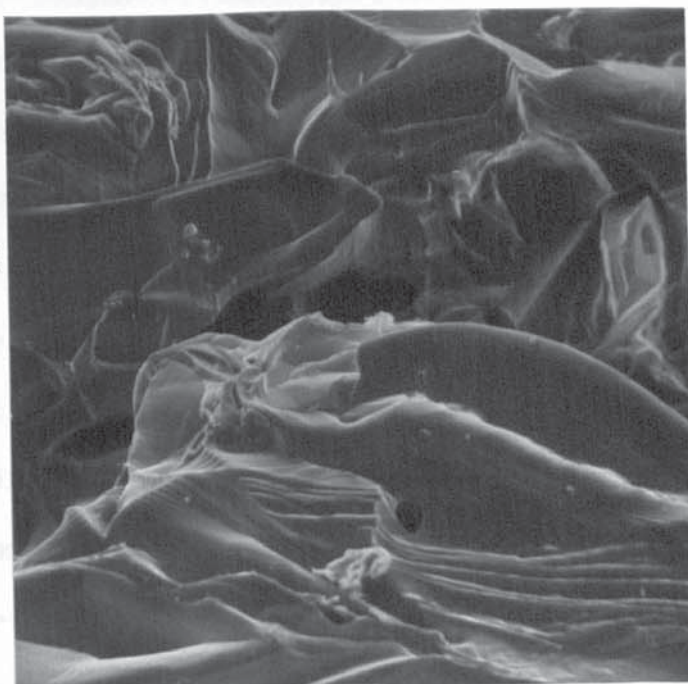
PLATE 5.4

SODIUM SULPHATE CRUST

5.4a: Internal Structure  
Magnification = 110X



5.4b: External Structure  
Magnification = 120X



## 5. PRESENTATION AND ANALYSIS OF EXPERIMENTAL RESULTS

Experiments on the drying of single drops of aqueous sodium sulphate were analysed using the photomicrographs - some of which are presented in Plates 5.1 to 5.4 - obtained from the stereoscan equipment and calculated values of the mass transfer coefficient  $K_G$ , were evaluated from the amount of water evaporated.

The experimental results for the studies of the residence-time distribution of the drops and air in the spray drying tower have been presented graphically and where possible a correlation has been proposed.

### 5.1 Drying Of Single Drops Of Sodium Sulphate Decahydrate

The mass transfer coefficient was calculated from equation (3.8) and the amount of water evaporated was obtained from equations (3.2) and (3.7). The results obtained from the Honeywell H316 "Basic 16" computer program shown in appendix A are presented in Table A6 for four drop diameters. The crust thickness and porosity were obtained from the stereoscan micrography. Typical photomicrographs obtained from the stereoscan equipment are shown in Plates 5.1, 5.2, 5.3 and 5.4. Fractures and holes can be seen on the photomicrograph on plate 5.2b. Plate 5.1b shows a rupture of the crust, which confirms the basis for the theory presented in Section (3.1); that is - steam was ejected from the wet core of the particle through evaporation and pressure build-up as a result of the high rate of heat transfer through the crust. Also it



can be seen that the external structure of the crusts are much smoother than the internal structure. This confirms the work of Charlesworth and Marshall (10) and Audu (11).

The cracks and craters observed in these photomicrographs, are the result of the steam causing explosions of the crust. These observations do not contradict Audu's theory (11) but merely limits his analysis to low rates of heat and mass transfer, conditions that would exist only when there is a small temperature difference.

Figure 5.2.1

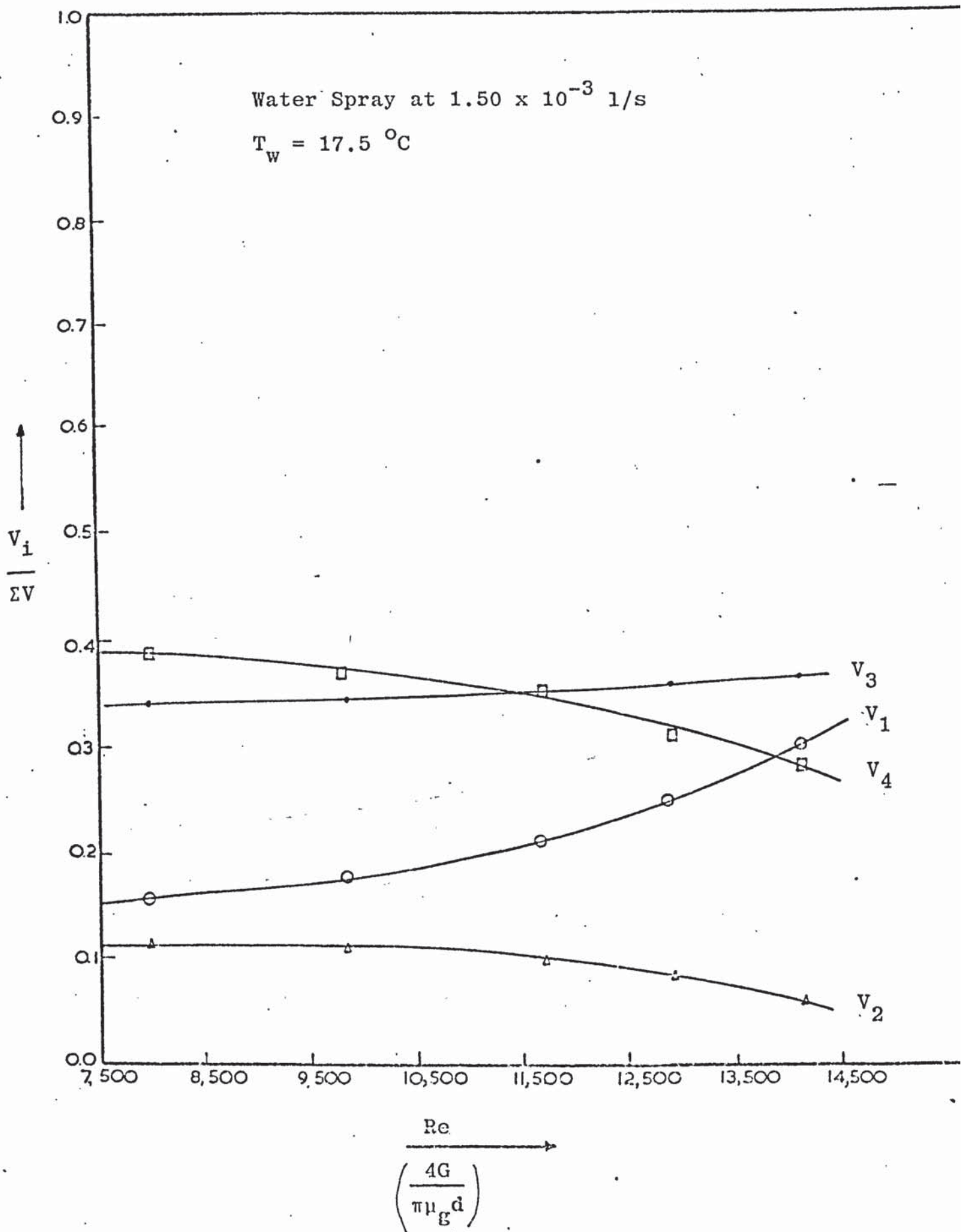


Figure 5.2.2

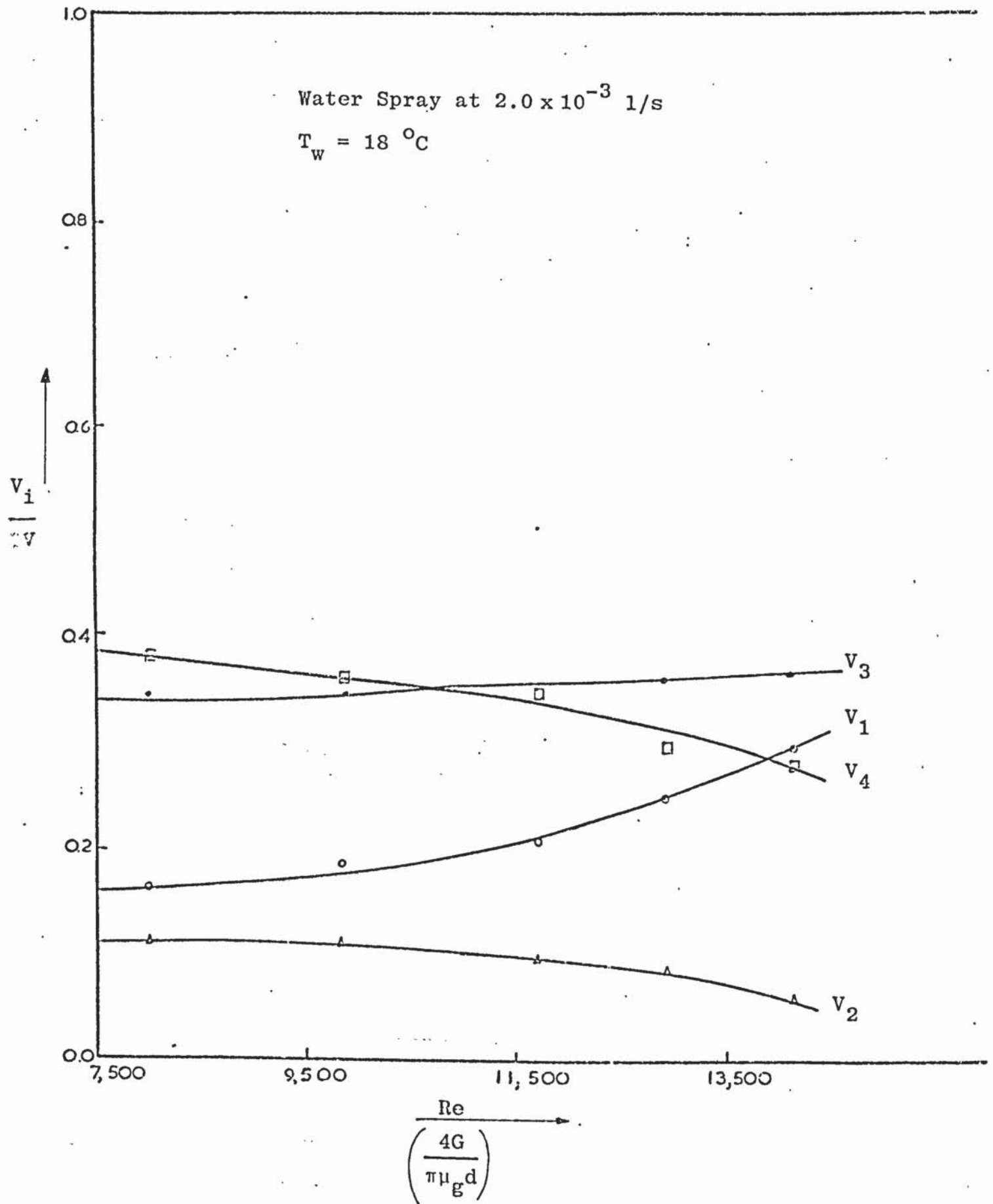




Figure 5.2.3

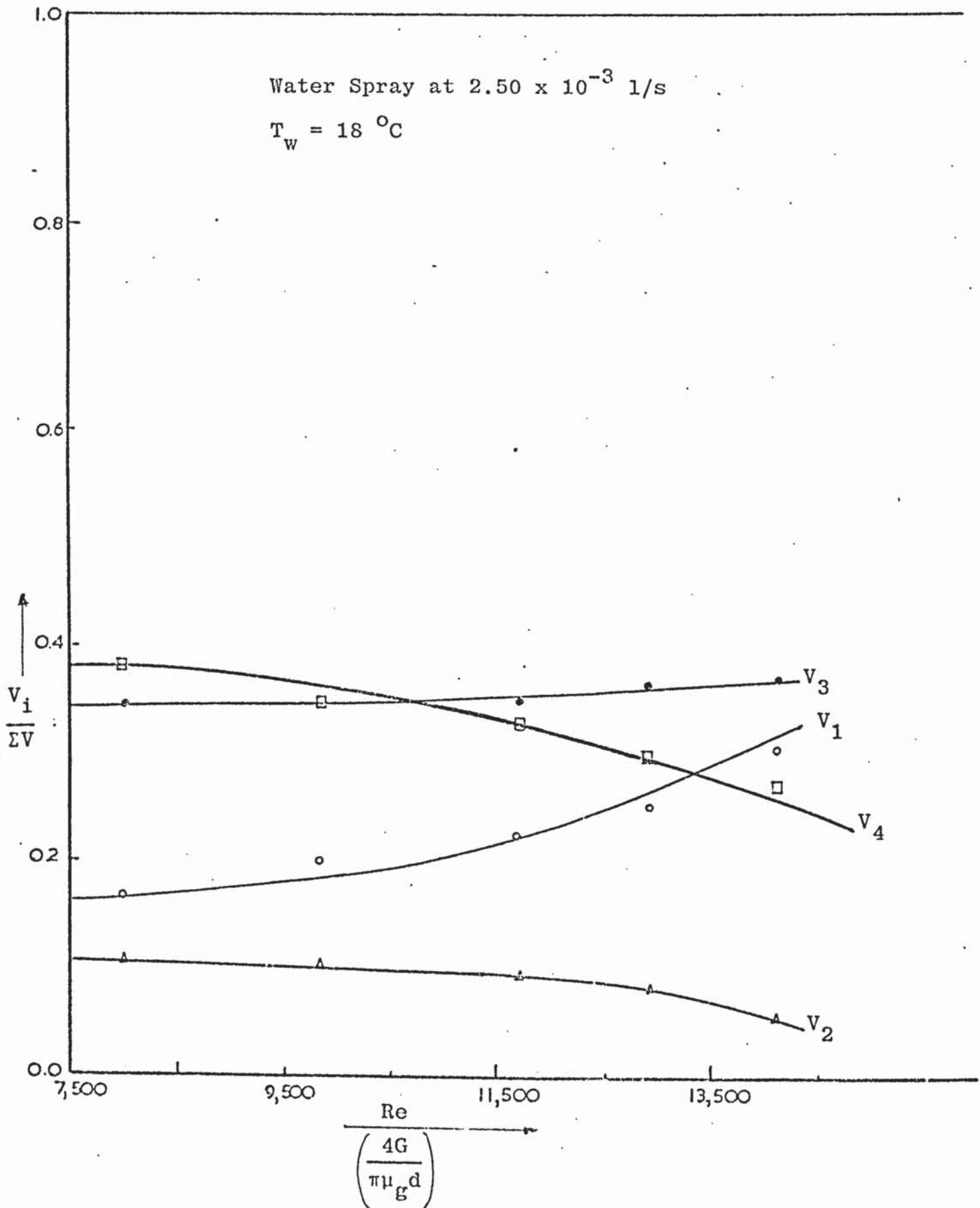


Figure 5.2.4

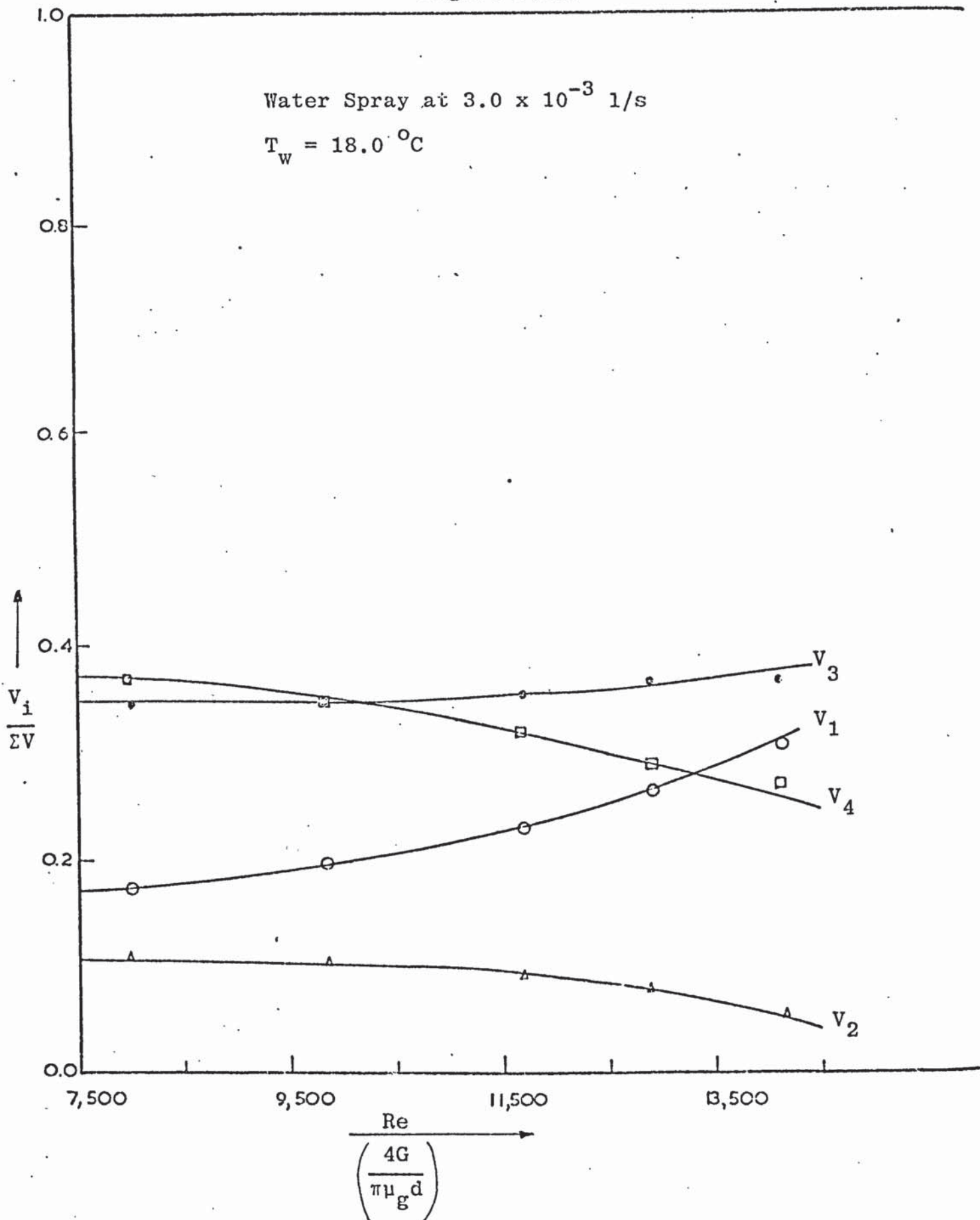
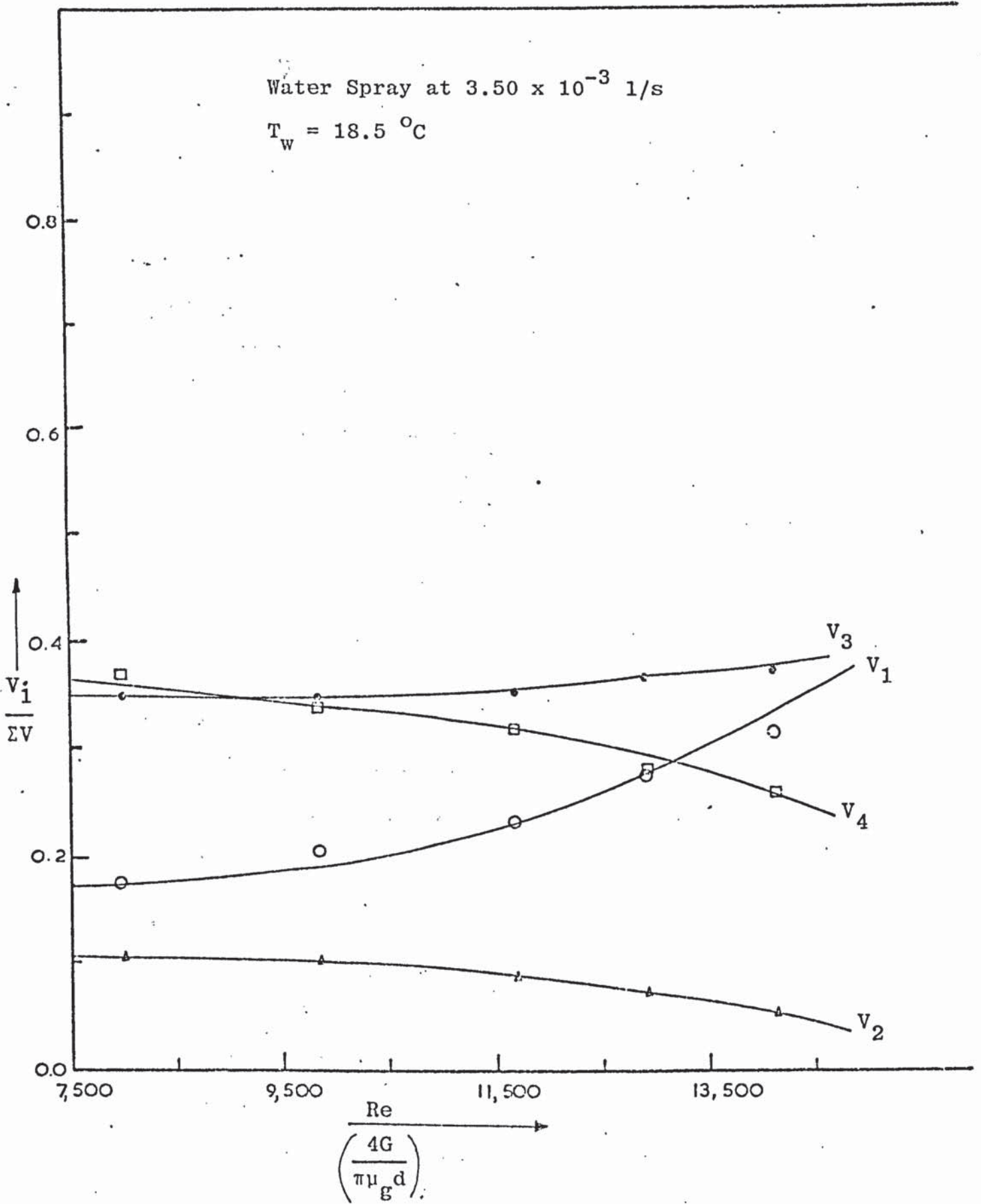


Figure 5.2.5





## 5.2 HYDRODYNAMIC BEHAVIOUR OF DROPS AND AIR IN THE SPRAY TOWER

It is evident from the literature reported in Section (2.5) that the manner in which the sprayed droplets and the drying air contact one another is an important factor in spray drier design (56, 62, 64, 121). Thus the studies of the various flow patterns existing in the transparent spray drier, with the aid of the smoke generator offered the advantage of being able to observe the effect of different operating conditions on the estimated volumes discussed in Section (4.4.2). The results are presented in Tables B1 to B10 in Appendix B.

### 5.2.1 Effect Of Air Flowrate

The effect of air flowrate on the well-mixed, plug flow and by-pass volumes in the spray tower are shown in Tables B1 to B5. The well-mixed volumes both at the top and bottom of the spray tower increased with an increase in air flowrate, while the volume of the plug flow section in the middle of the tower as well as the by-pass stream decreased appreciably with an increase in air flowrate.

### 5.2.2. Effect Of Liquid Feed Flowrate

The volumes of the well-mixed sections were also found to increase with an increase in the flowrate of the water spray. This agreed with the proposal by Masters (56)-

Figure 5.2.6

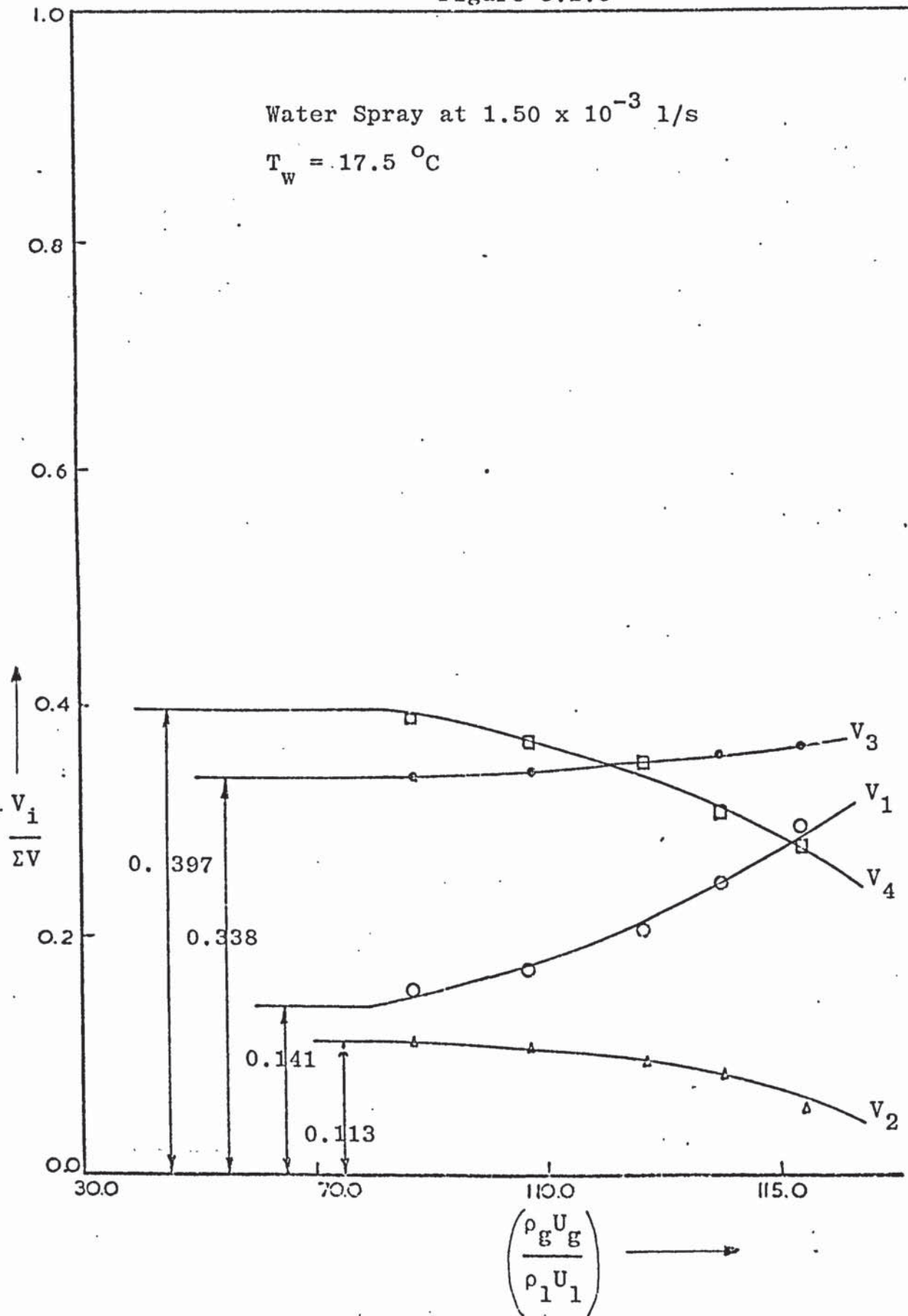


Figure 5.2.7

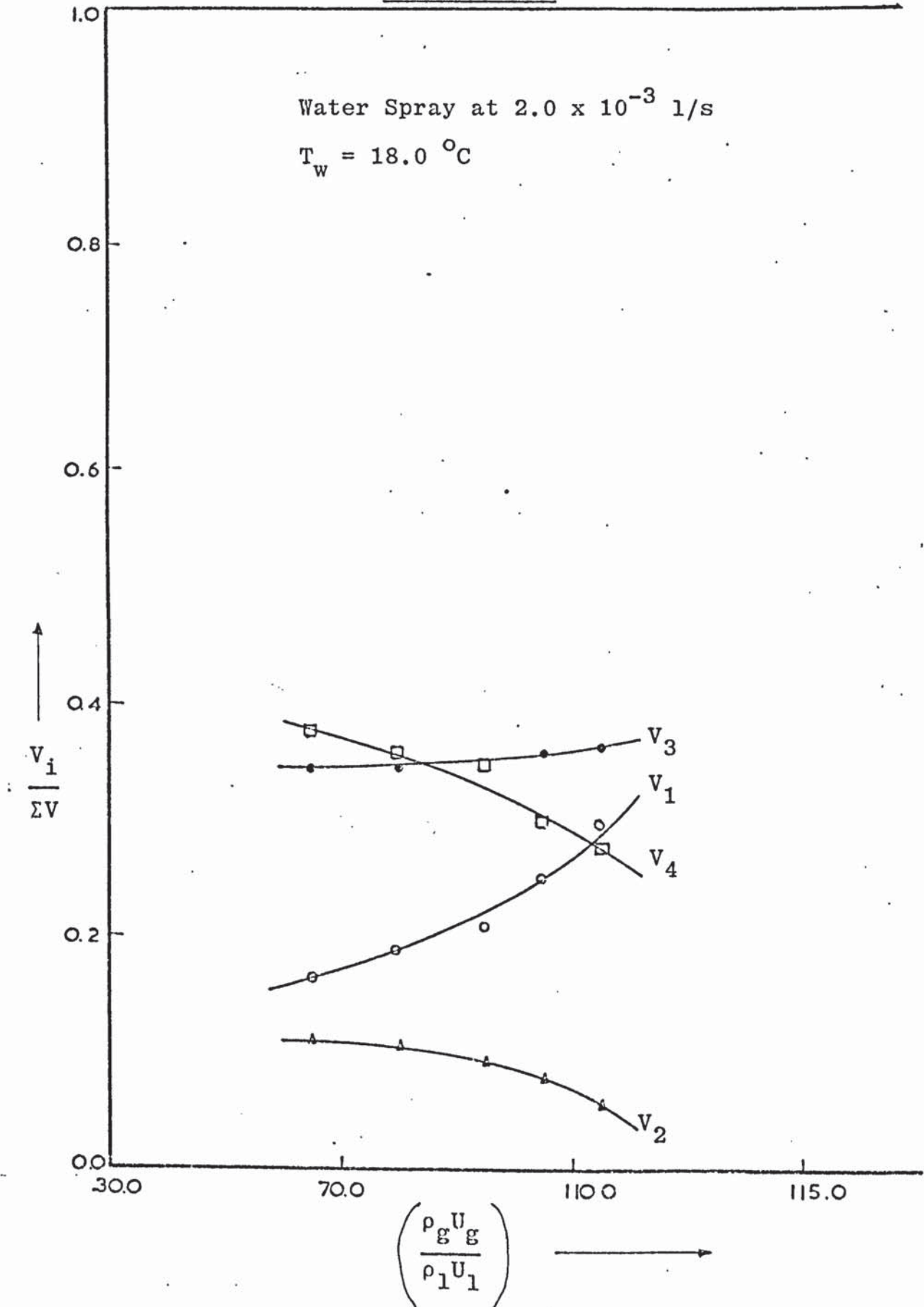
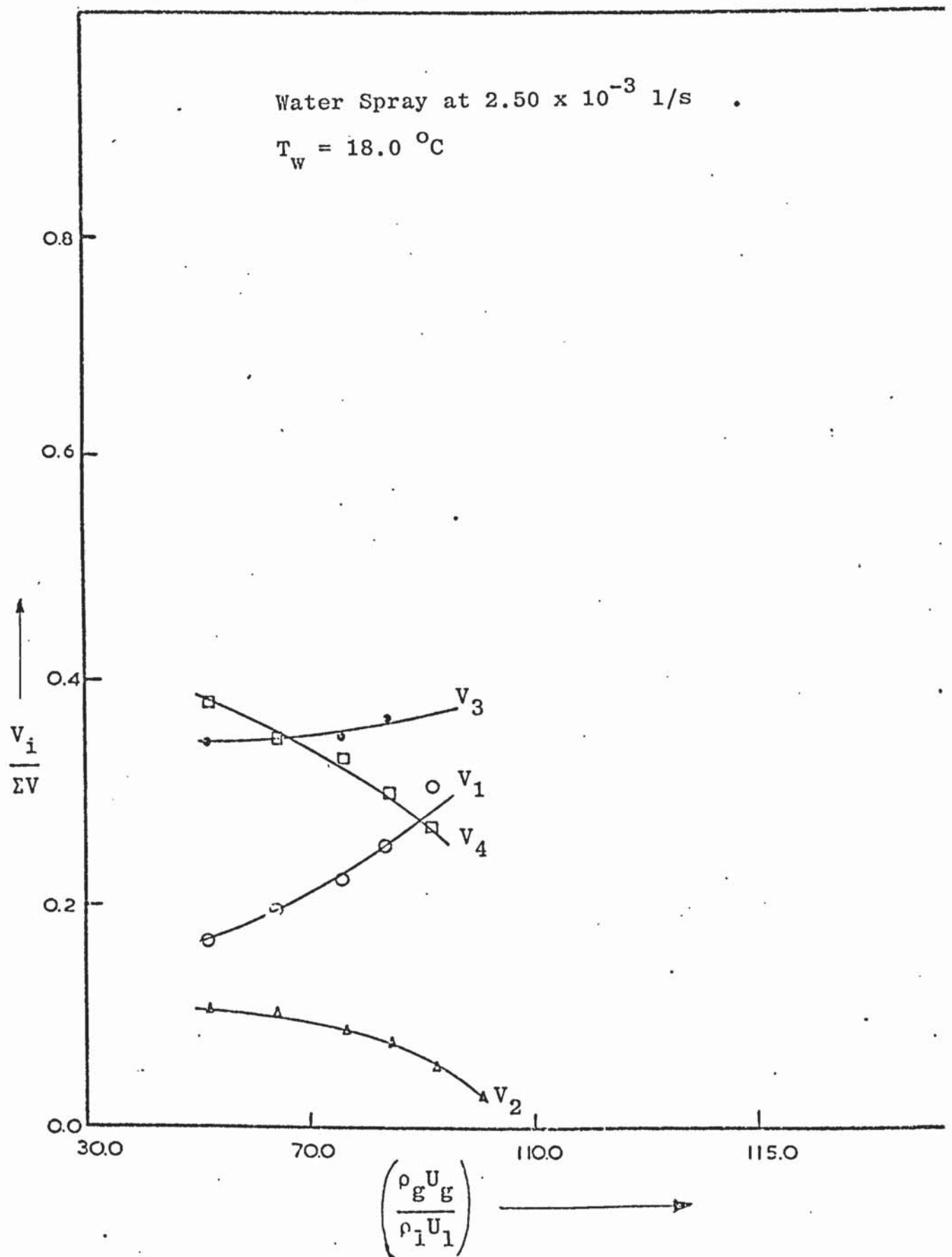




Figure 5.2.8



Figures 5.2.9

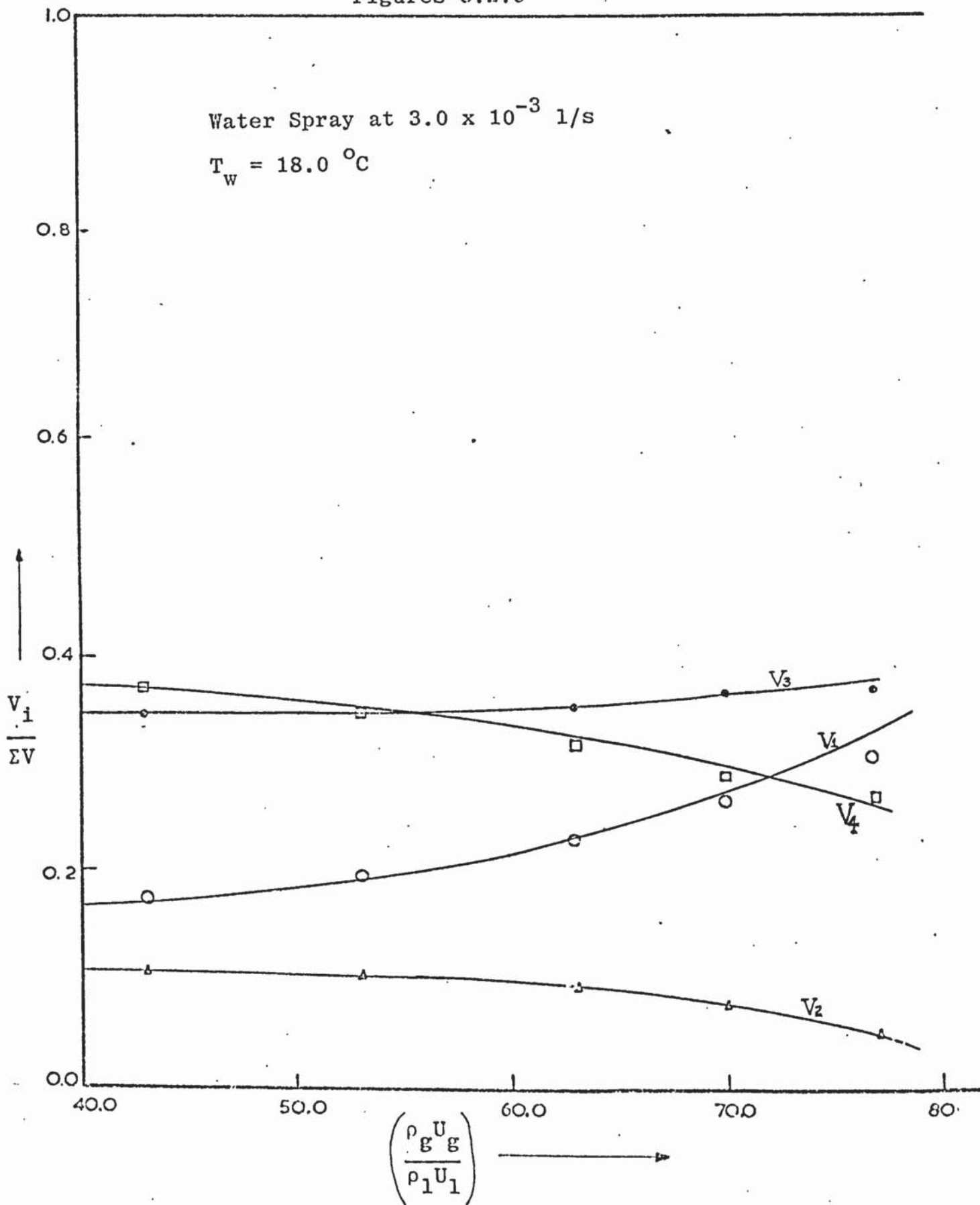
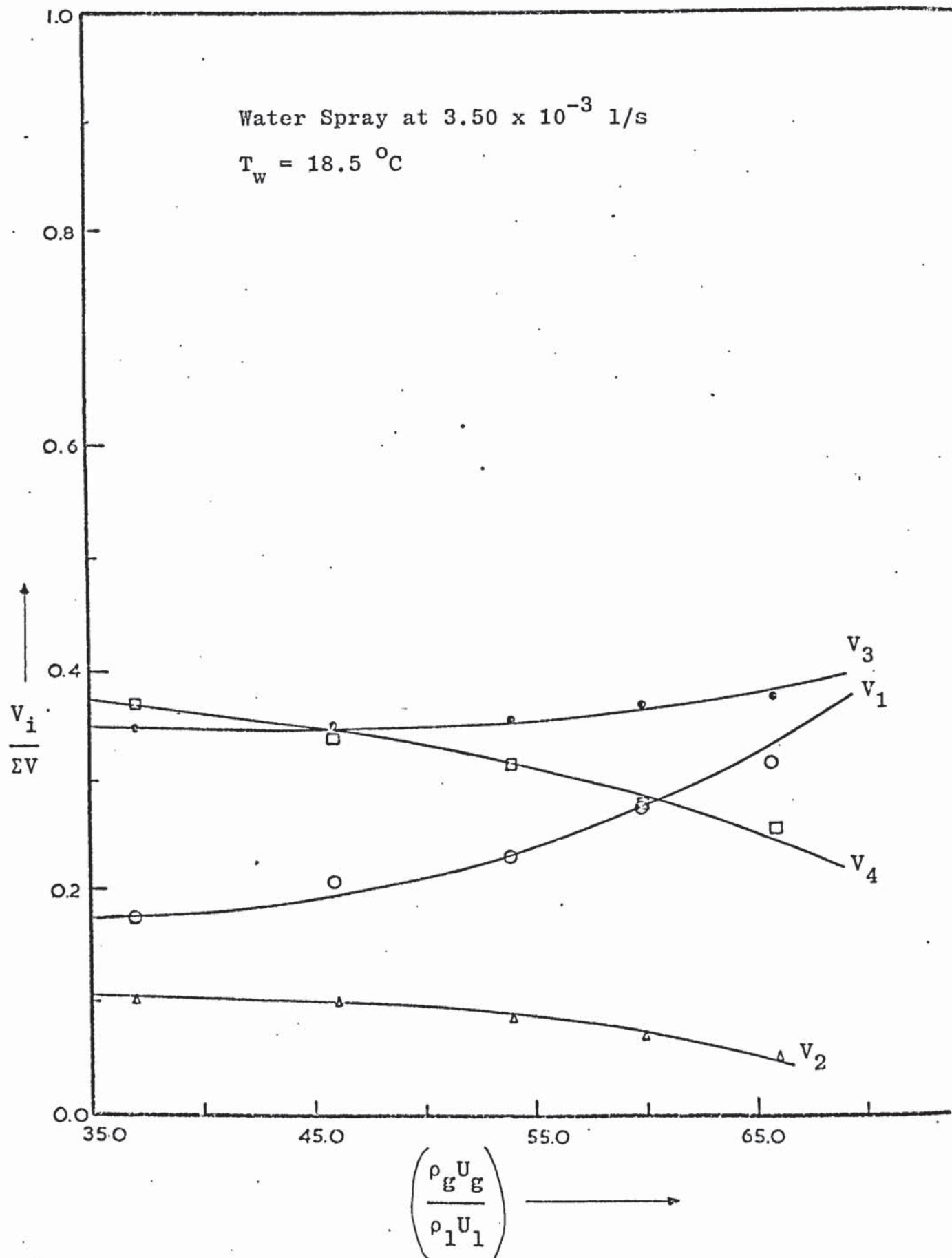


Figure 5.2.10



In counter-current flow driers, the upflowing drying air in the path of the droplets tends to increase the residence time of the droplets. This in turn increases the rate of transfer between the two phases in the spray tower.

The plug flow volume and the volume of the by-pass stream also decreased with increasing feed flowrate.

### 5.2.3 Effect Of Reynolds Number

Figures 5.2.1 to 5.2.5 show the graphs obtained when the volumes of the various sections in the tower divided by the total effective volume were plotted against the Reynolds Number of the drying air for five different liquid feed flowrates. In all cases the two well-mixed volumes,  $V_1/EV$  and  $V_3/EV$  increased with an increase in the Reynolds Number of the air while the volumes of the plug flow and by-pass regions  $V_2/EV$  and  $V_4/EV$  decreased respectively with increasing Reynolds Number.

### 5.2.4 Effect Of Superficial Velocity

As shown in figures 5.2.6 to 5.2.10 the volumes of the stirred-tank sections increased with an increase in the superficial velocity, while the plug flow and by-pass stream volumes decreased at higher values of the superficial velocity.

### 5.2.5 Correlations

As shown in appendix B, dimensional analysis (118) was used to obtain equation;



$$\frac{V_i}{\Sigma V} = \psi \cdot \text{Re}^d \cdot \left( \frac{\mu_1}{\mu_g} \right)^f \cdot \left( \frac{U_1}{U_g} \right)^e \cdot \left( \frac{Z}{D} \right)^g \quad (5.2.1)$$

The above equation was then used to correlate the volumes of the various sections in the tower in terms of the dimensionless groups, using the ICL 1900 Statistical Analysis Computer Package. A copy of this program is also shown in appendix B. The values of  $\psi$ ,  $d$ ,  $f$ ,  $e$ , and  $g$  in equation (5.2.1) were then obtained. The correlations for the volumes are shown in Table 5.2.1.

TABLE 5.2.1

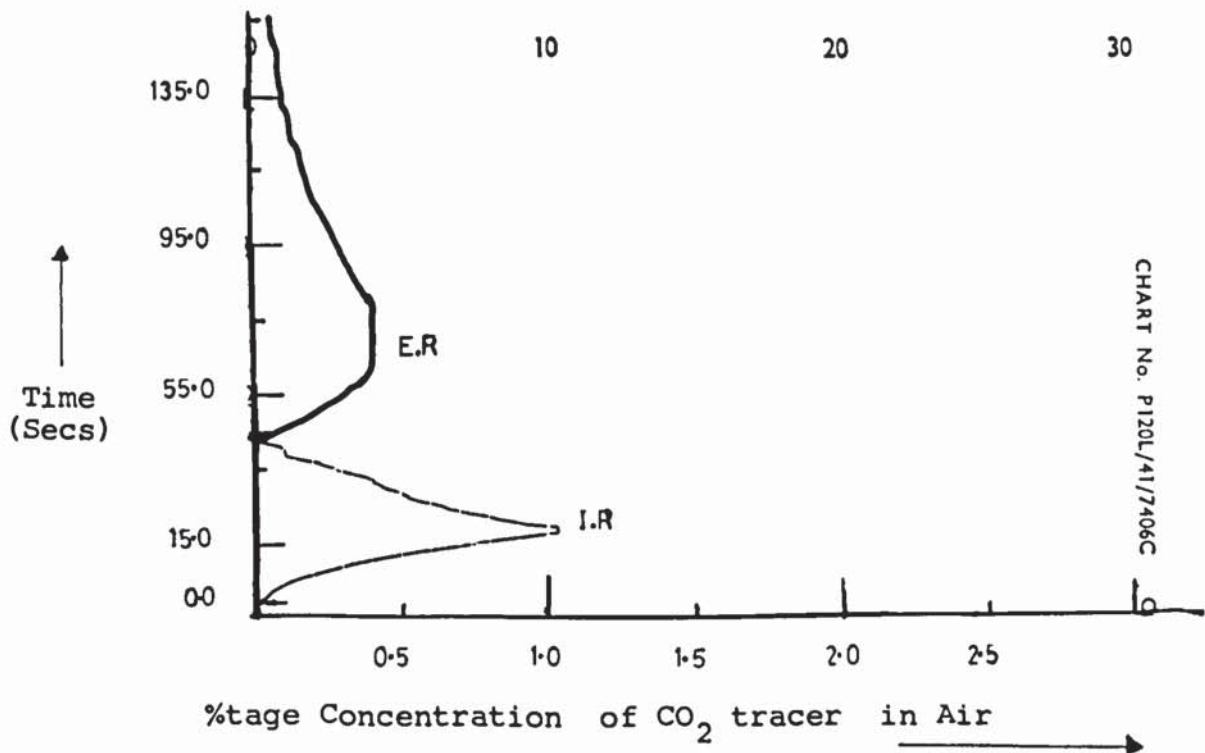
	Correlation	Correlation Coefficient
$\frac{V_1}{\Sigma V} = 13.076 \text{ (Re)}^{1.079} \cdot \left(\frac{\mu_1}{\mu_g}\right)^{1.551} \cdot \left(\frac{U_1}{U_g}\right)^{0.290} \cdot \left(\frac{Z}{D}\right)^{0.835}$		0.978
$\frac{V_2}{\Sigma V} = 17.085 \text{ (Re)}^{-1.096} \cdot \left(\frac{\mu_1}{\mu_g}\right)^{-5.213} \cdot \left(\frac{U_1}{U_g}\right)^{-0.611} \cdot \left(\frac{Z}{D}\right)^{0.752}$		0.989
$\frac{V_3}{\Sigma V} = 3.157 \text{ (Re)}^{0.134} \cdot \left(\frac{\mu_1}{\mu_g}\right)^{0.480} \cdot \left(\frac{U_1}{U_g}\right)^{0.076} \cdot \left(\frac{Z}{D}\right)^{0.893}$		0.996
$\frac{V_4}{\Sigma V} = 5.938 \text{ (Re)}^{-0.619} \cdot \left(\frac{\mu_1}{\mu_g}\right)^{-1.057} \cdot \left(\frac{U_1}{U_g}\right)^{-0.195} \cdot \left(\frac{Z}{D}\right)^{0.374}$		0.994



PLATE 5.5

Typical Input/Exit response graphs obtained from chart on the 2-pen potentiometric indicating Recorder.

Air flowrate,  $G$ , at 0.16 Kg/s  
Air Temperature,  $T_a$ , at 31.5 °C  
Water Spray,  $W$ , at  $3.50 \times 10^{-3}$  l/s  
Feed Temperature,  $T_w$ , at 18.5 °C



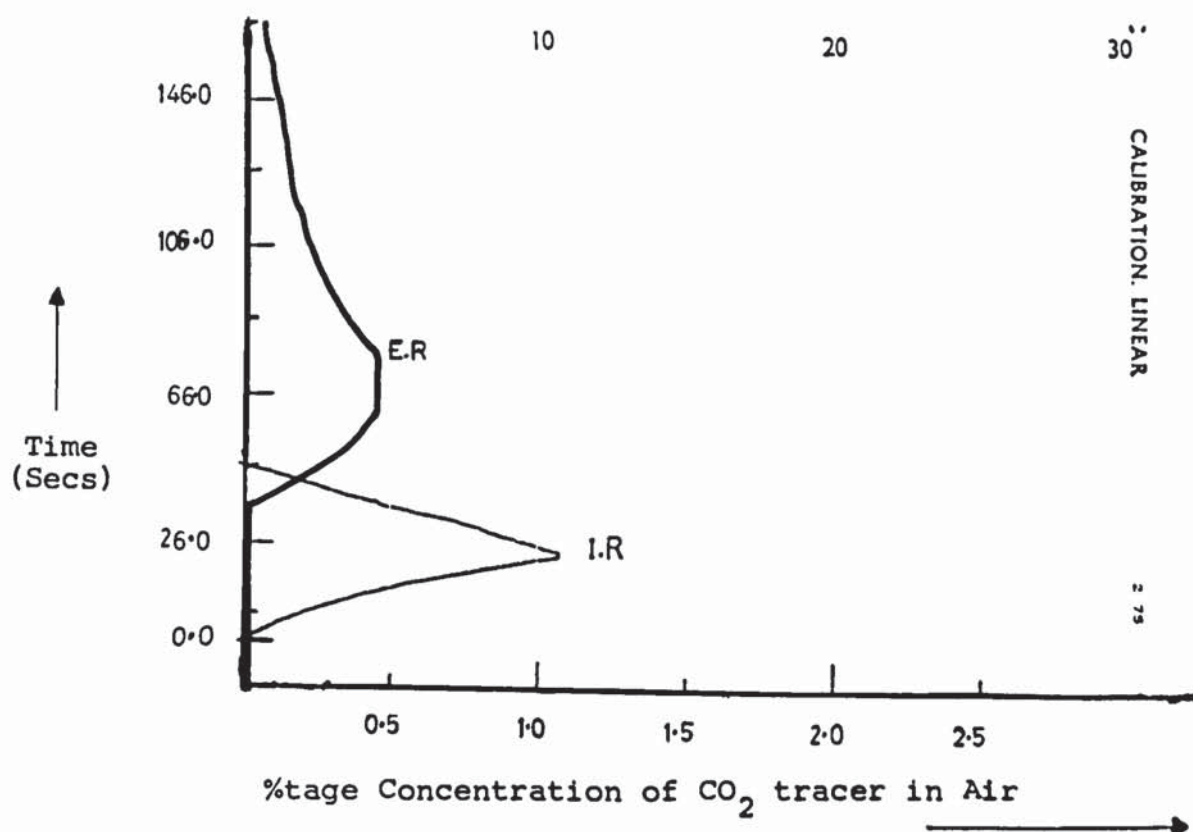




# PLATE 5.6

Typical Input/Exit response graphs obtained from chart on the 2-pen potentiometric indicating Recorder.

Air flowrate,  $G$ , at  $0.19 \text{ Kg/s}$   
 Air Temperature,  $T_a$ , at  $31.0^\circ\text{C}$   
 Water Spray,  $W$ , at  $2.0 \times 10^{-3} \text{ l/s}$   
 Feed Temperature,  $T_w$ , at  $18.0^\circ\text{C}$



### 5.3 EXIT RESPONSE ANALYSIS OF AIR

The exit concentration profile of the tracer of carbon dioxide in the drying air, measured by the katharometer as described in section (4.4.3) was plotted on the two-pen recorder chart. Typical input-output concentration profiles from the recorder chart are shown in the photographs on plates 5.5 and 5.6. The theoretical predictions of the exit concentration profile deduced from equation (3.37) and the experimental values are presented graphically as shown in Figures 5.3.1 to 5.3.25. The results are also presented in Tables C1 to C25 in the appendix.

#### 5.3.1 Effect Of Air Flowrate

The graphical results presented in figures 5.3.1 to 5.3.25 show that when the air flowrate was increased the peak of the exit concentration profile was quickly attained, indicating a shorter residence time of the drying air. Also from the graphs, it is evident that an appreciable amount of mixing exists in the spray tower, as the right hand side of the concentration-time curve was much more prolonged than the first part. This supports the two stirred tanks at the top and bottom of the spray tower, proposed in the model in section (3.2). Thus an increase in the air flowrate in the spray drying tower, would increase turbulence and hence the rate of heat and mass transfer between the two phases in the tower, and thereby

Figure 5.3.1

Water Spray at  $1.50 \times 10^{-3}$  l/s

Air at 0.13 kg/s

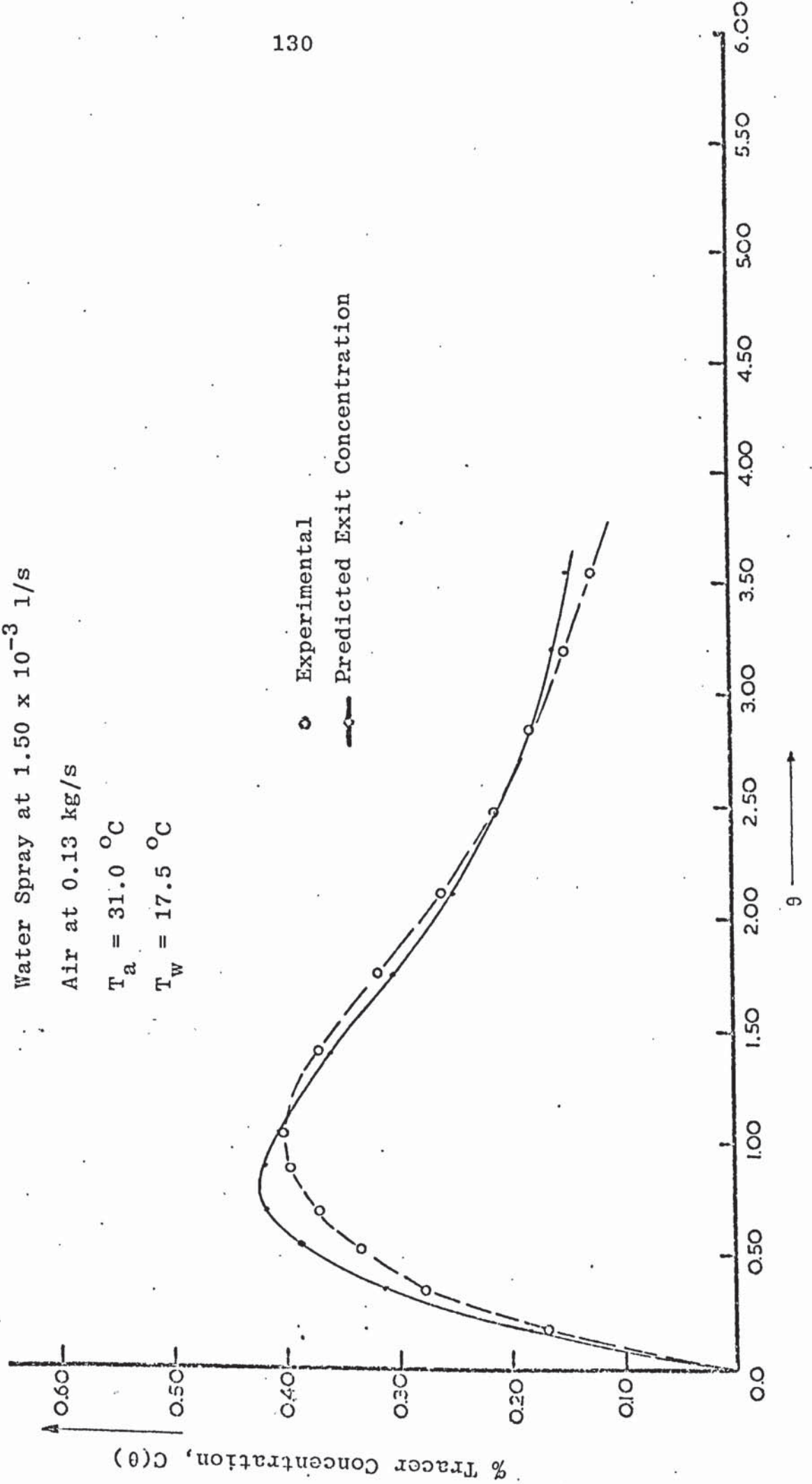
 $T_a = 31.0^\circ\text{C}$  $T_w = 17.5^\circ\text{C}$ 



Figure 5.3.2

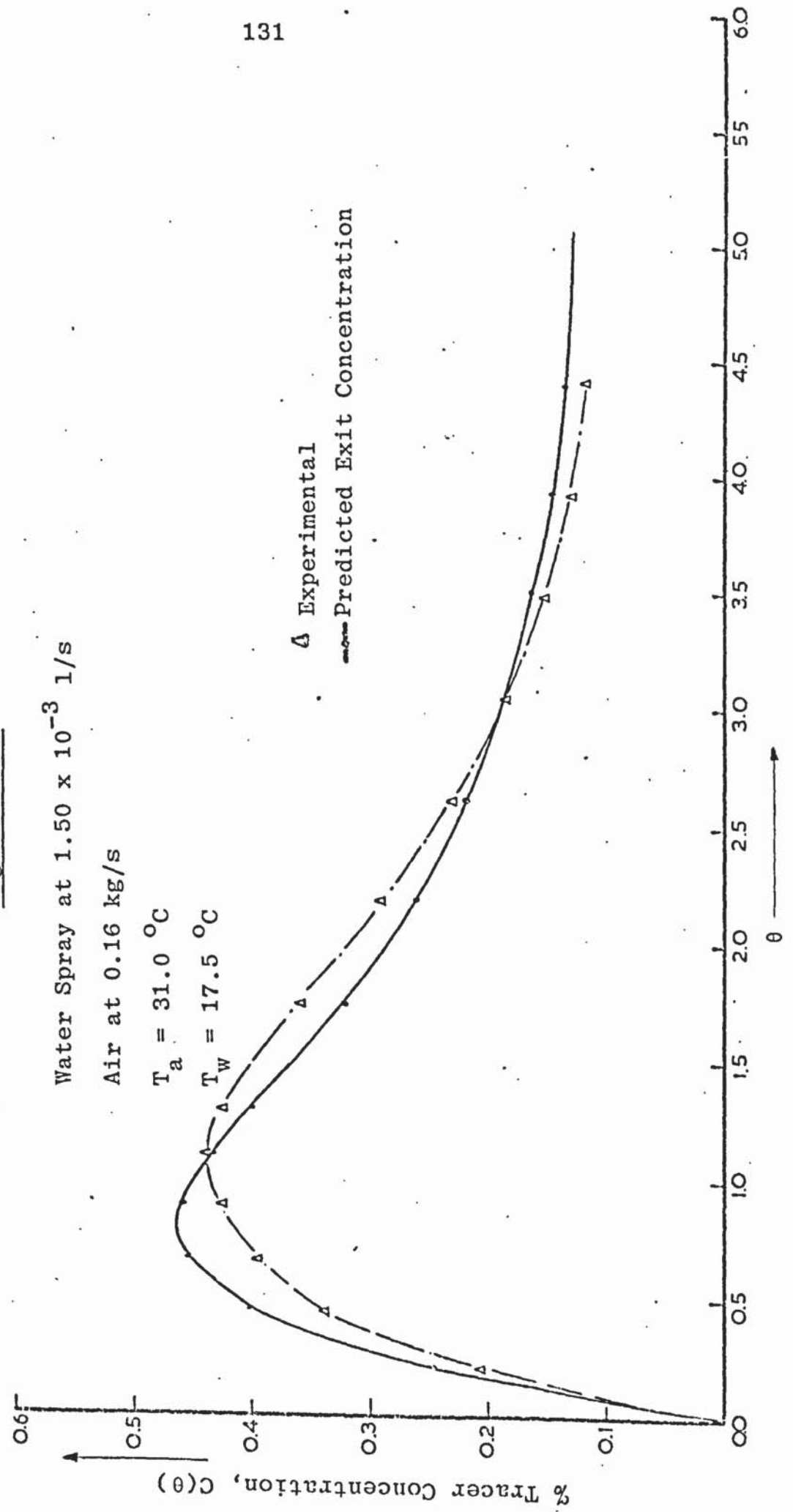


Figure 5.3.3

Water Spray at  $1.50 \times 10^{-3}$  l/s

Air at 0.19 kg/s

$T_a = 31.0^\circ\text{C}$

$T_w = 17.5^\circ\text{C}$

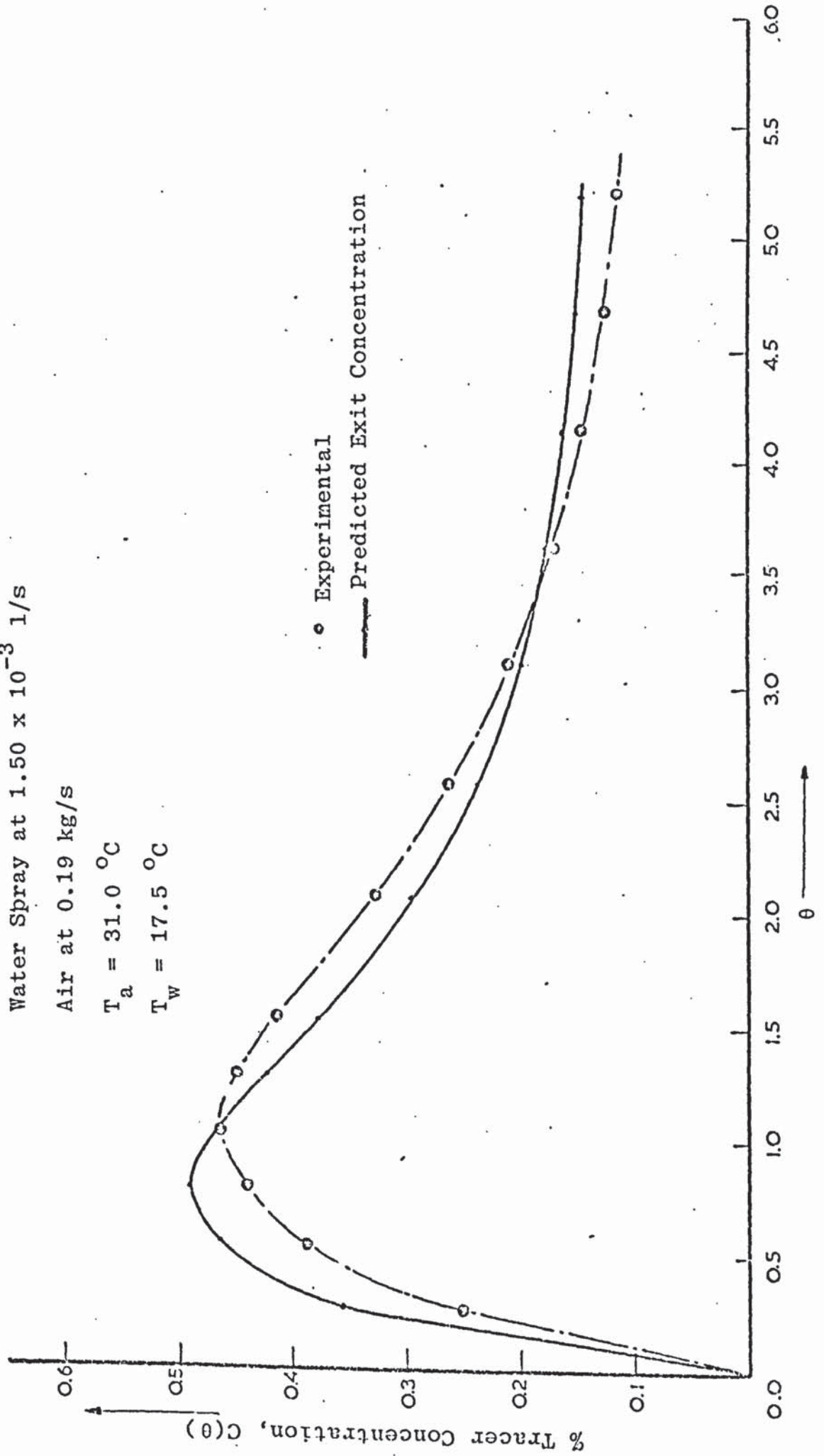


Figure 5.3.4

Water Spray at  $1.50 \times 10^{-3}$  l/s

Air at 0.21 kg/s

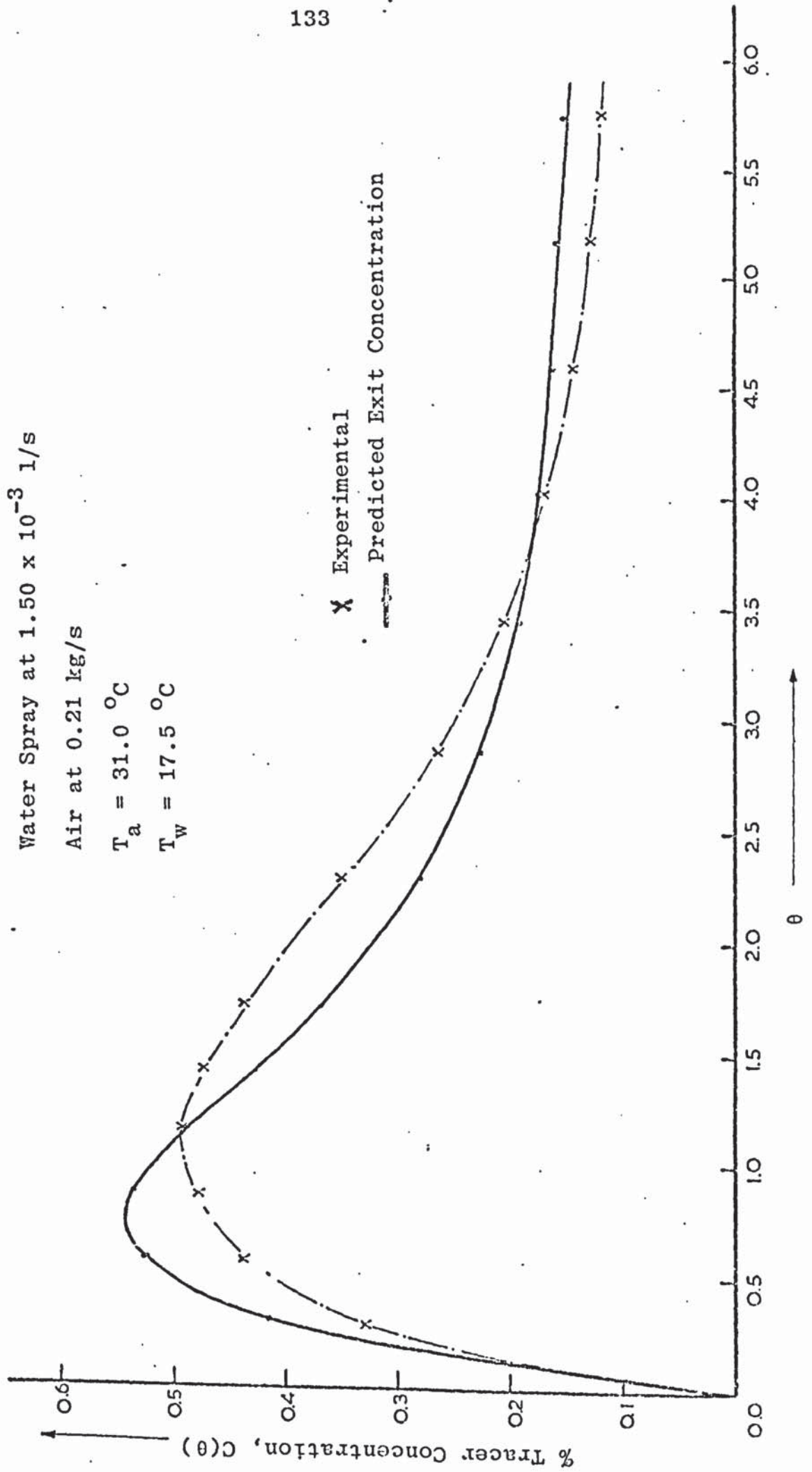
 $T_a = 31.0^\circ\text{C}$  $T_w = 17.5^\circ\text{C}$ 

Figure 5.3.5

Water Spray at  $1.50 \times 10^{-3}$  l/s

Air at 0.23 kg/s

$T_a = 31.5^\circ\text{C}$

$T_w = 17.5^\circ\text{C}$

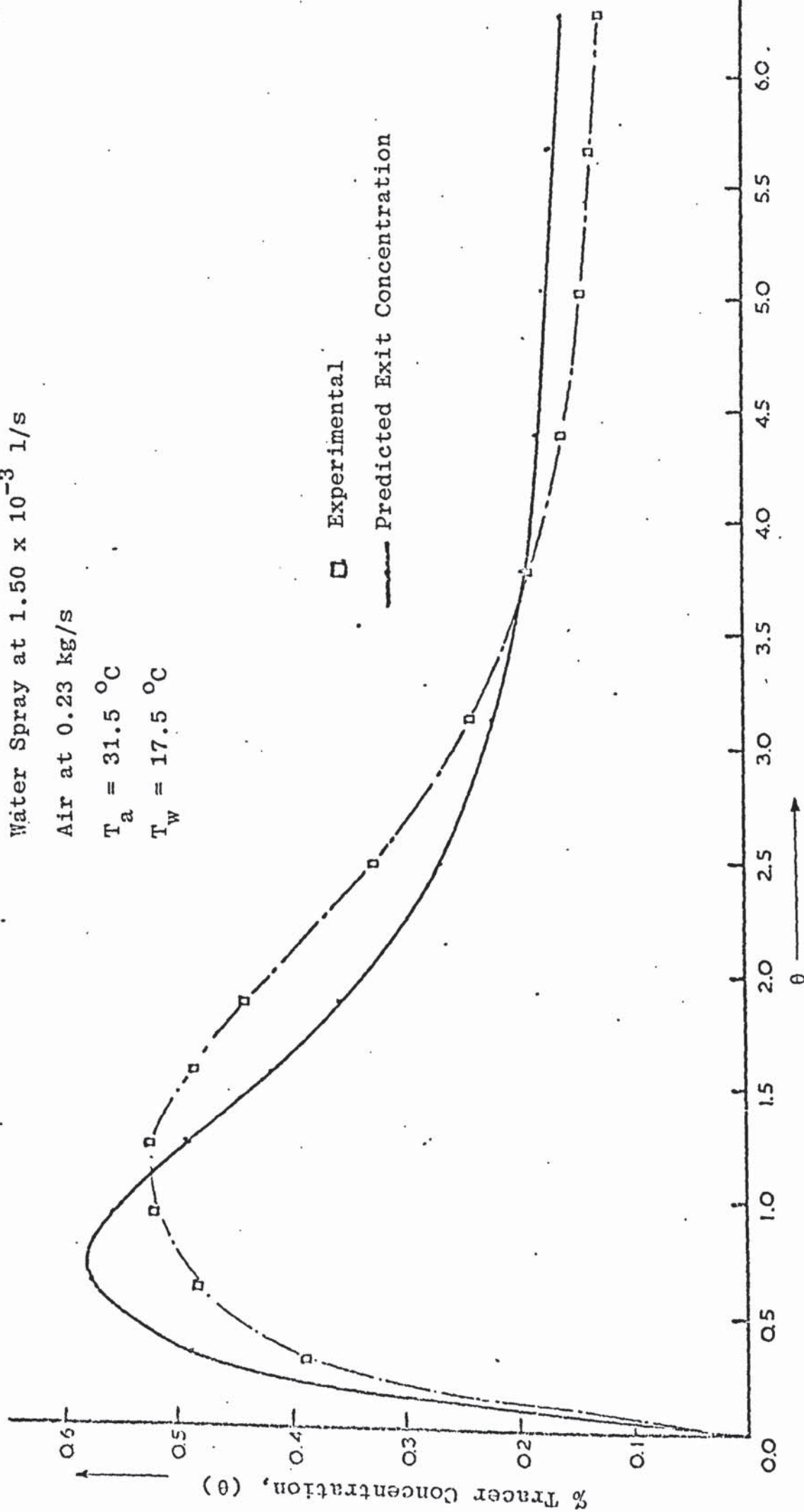




Figure 5.3.6

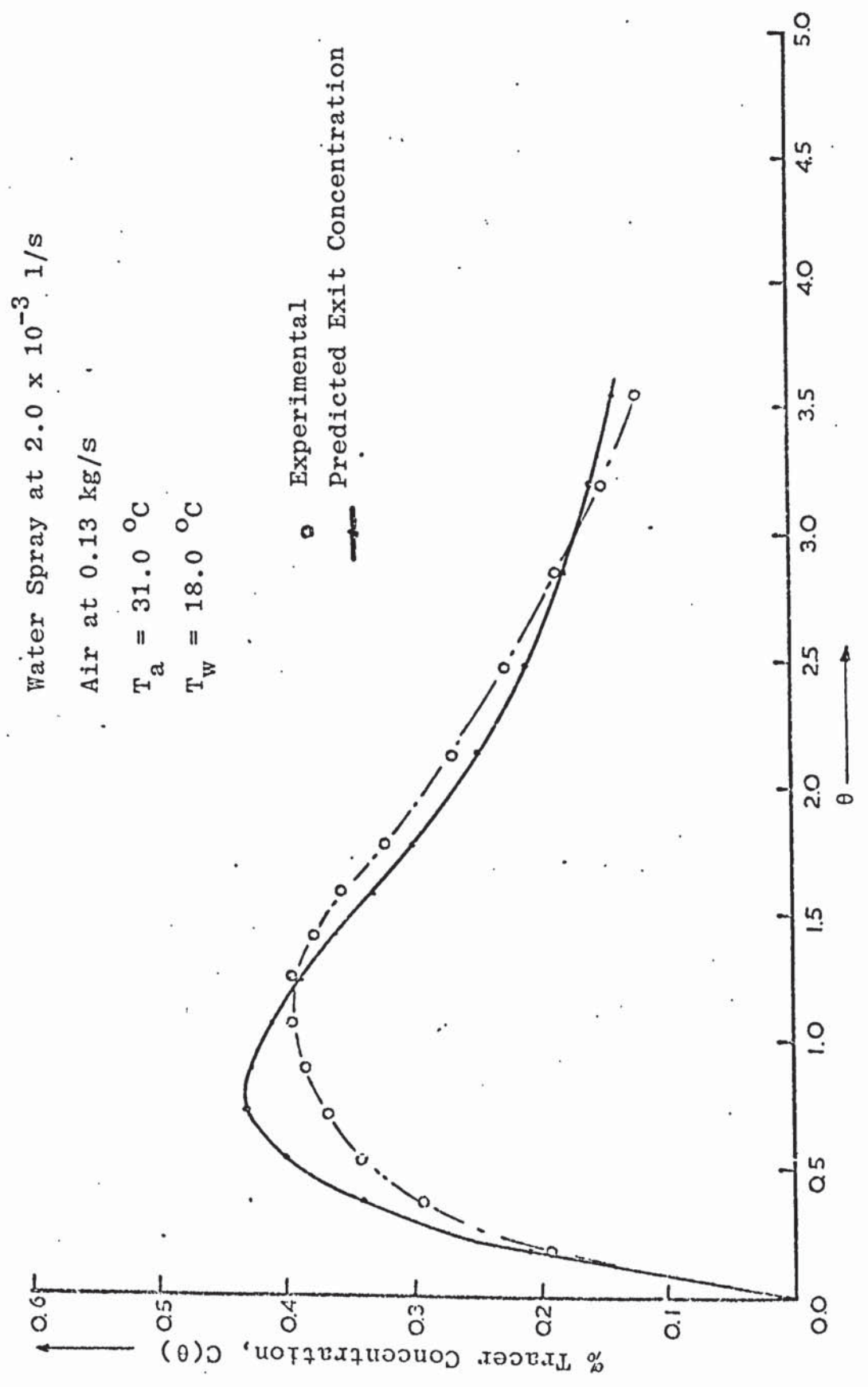


Figure 5.3.7

Water Spray at  $2.0 \times 10^{-3}$  l/s

Air at 0.16 kg/s

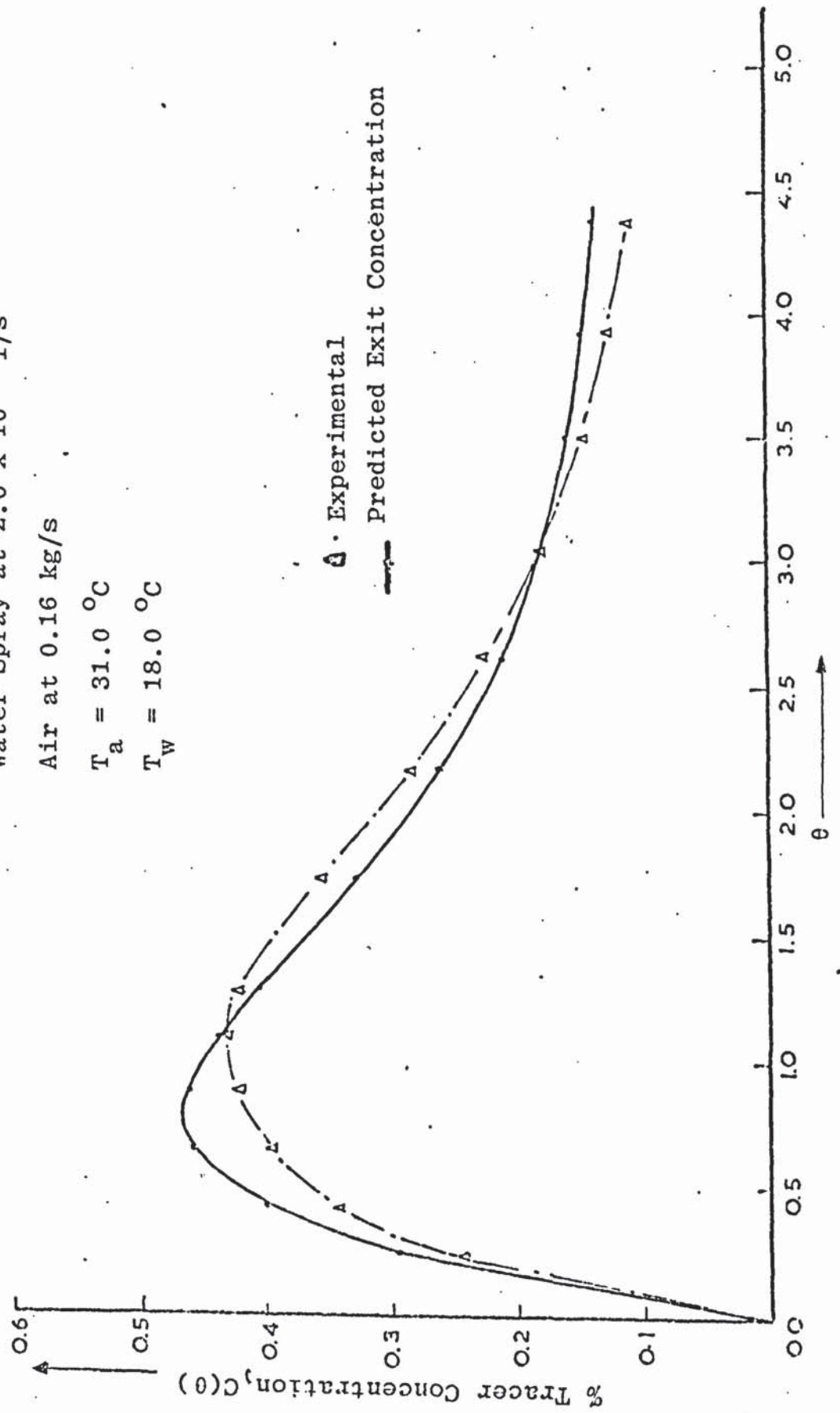
 $T_a = 31.0^\circ\text{C}$  $T_w = 18.0^\circ\text{C}$ 

Figure 5.3.8

Water Spray at  $2.0 \times 10^{-3}$  l/s

Air at 0.19 kg/s

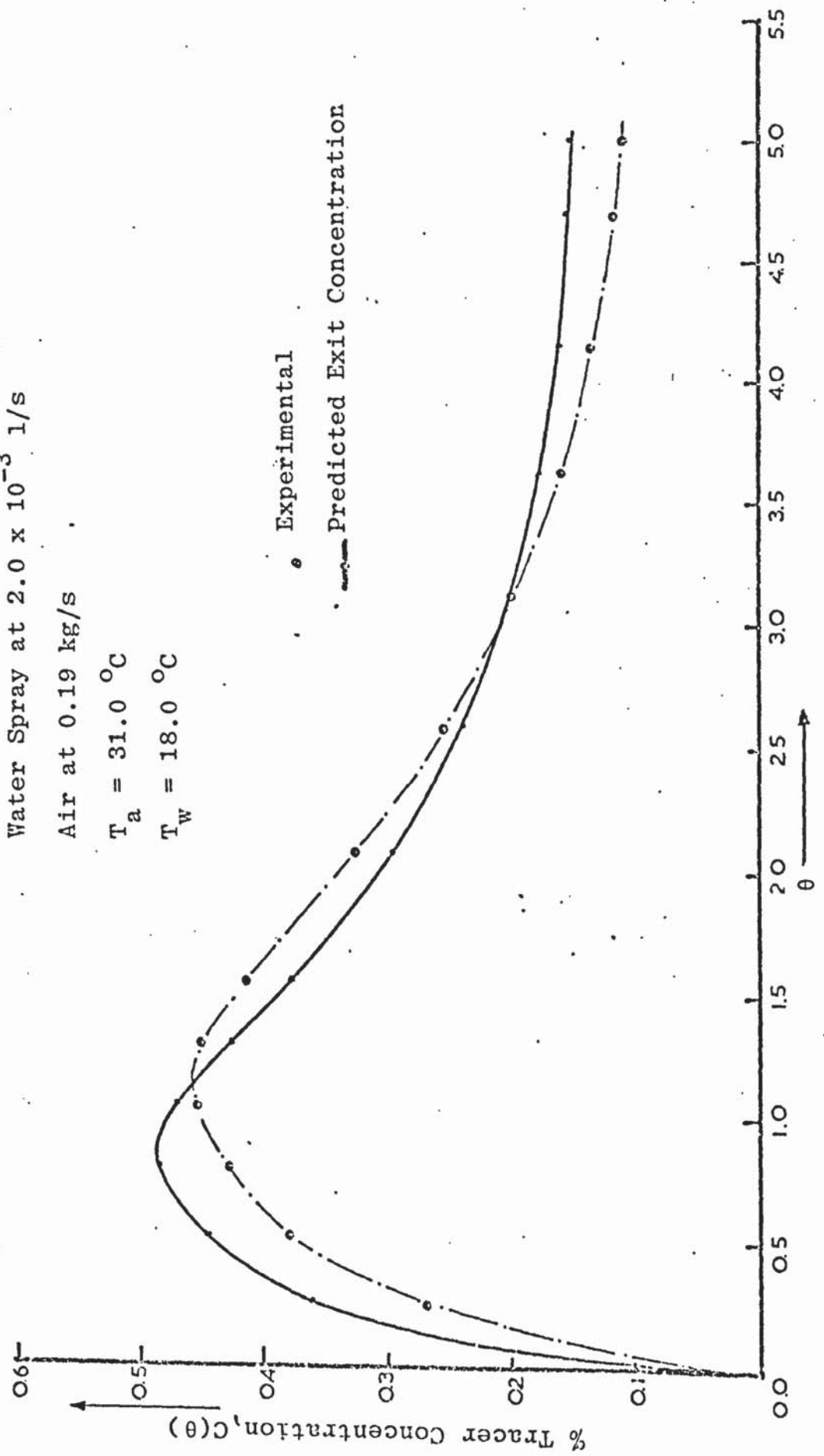
 $T_a = 31.0$  °C $T_w = 18.0$  °C

Figure 5.3.9

Water Spray at  $2.00 \times 10^{-3}$  l/s

Air at 0.21 kg/s

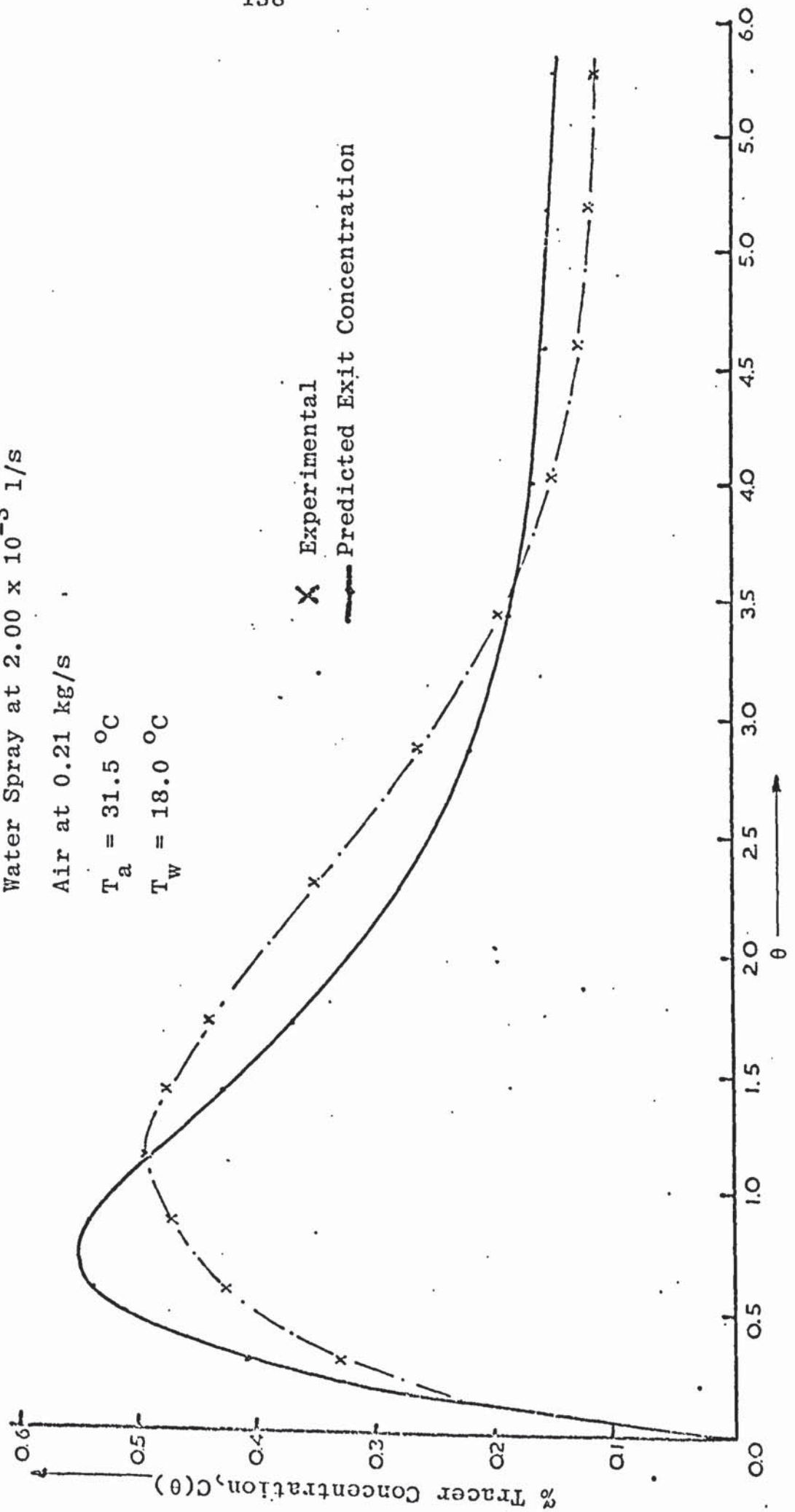
 $T_a = 31.5^\circ\text{C}$  $T_w = 18.0^\circ\text{C}$ 



Figure 5.3.10

Water Spray at  $2.0 \times 10^{-3}$  l/s

Air at 0.23 kg/s

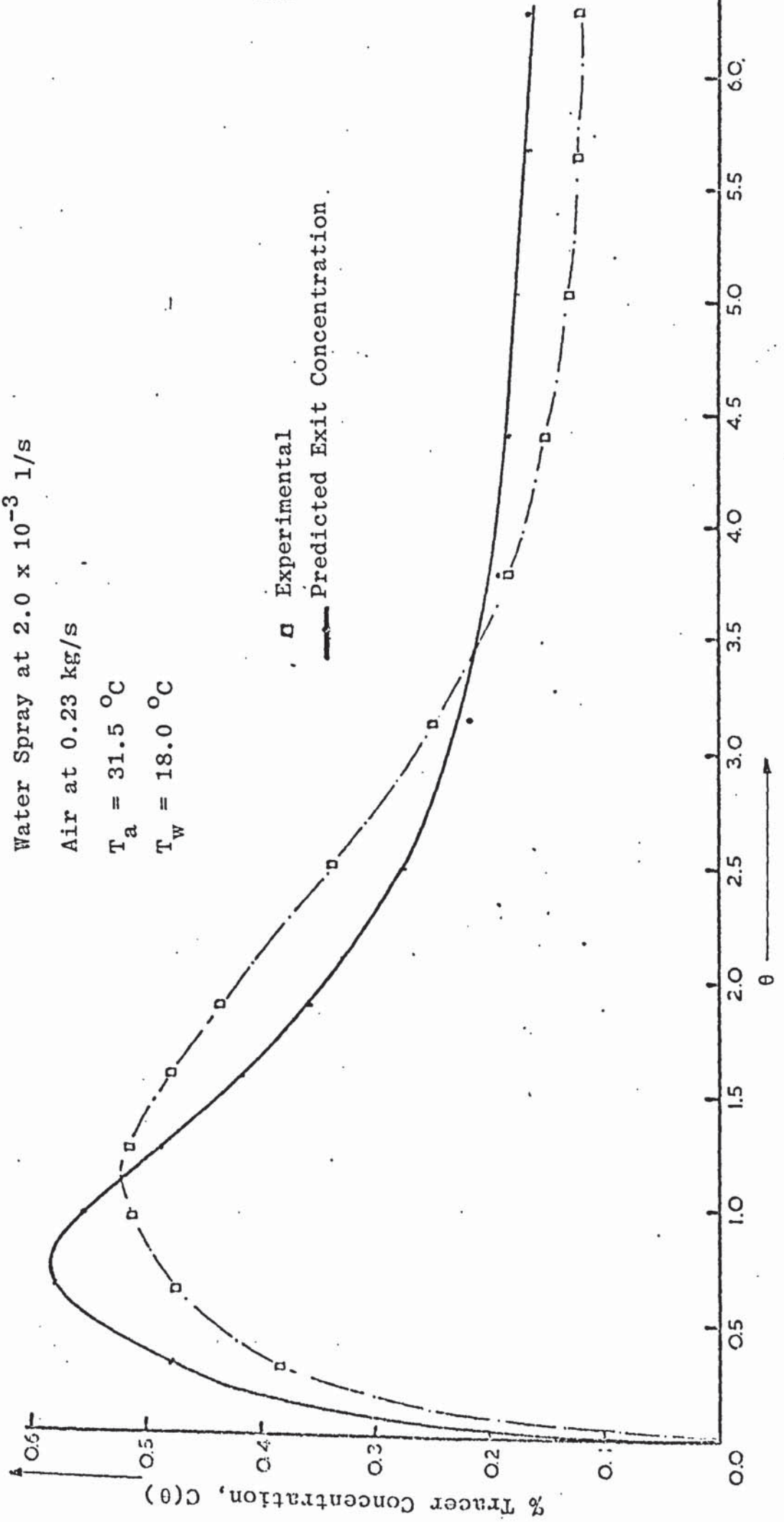
 $T_a = 31.5^\circ\text{C}$  $T_w = 18.0^\circ\text{C}$ 

Figure 5.3.11

Water Spray at  $2.50 \times 10^{-3}$  l/s

Air at 0.13 kg/s

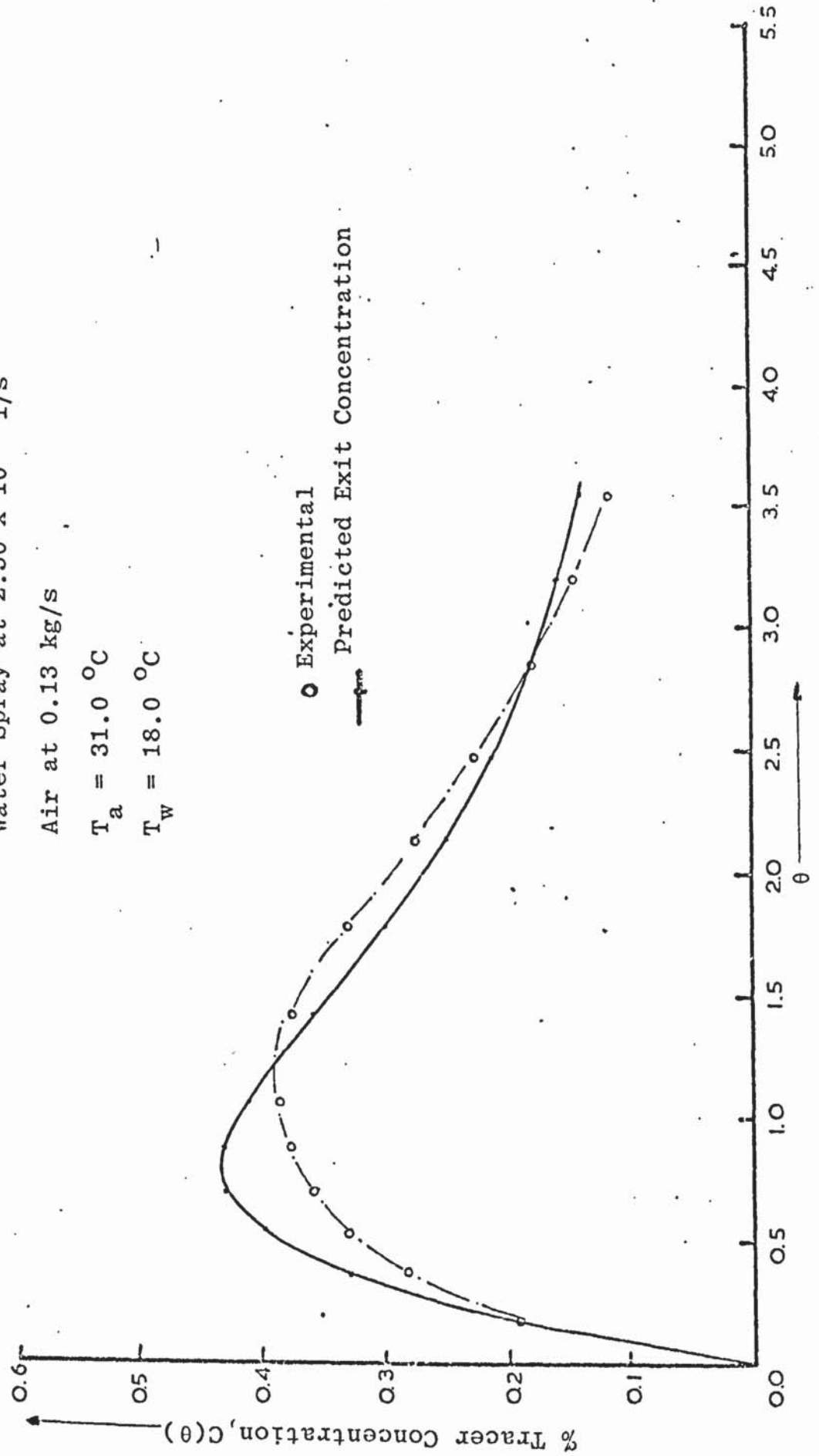
 $T_a = 31.0^\circ\text{C}$  $T_w = 18.0^\circ\text{C}$ 

Figure 5.3.12Water Spray at  $2.50 \times 10^{-3}$  l/s

Air at 0.16 kg/s

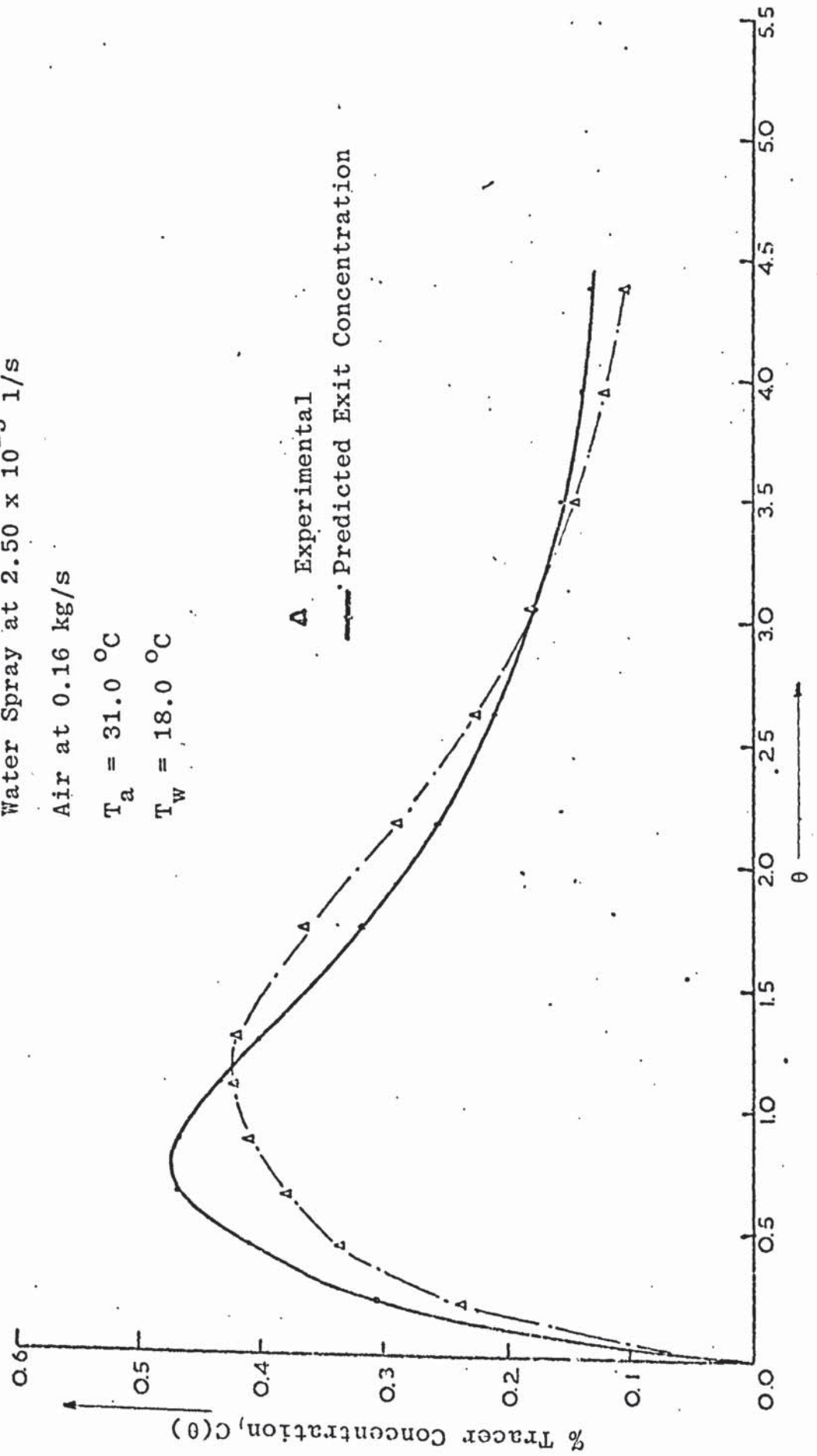
 $T_a = 31.0^\circ\text{C}$  $T_w = 18.0^\circ\text{C}$ 

Figure 5.3.13Water Spray at  $2.50 \times 10^{-3}$  l/s

Air at 0.19 kg/s

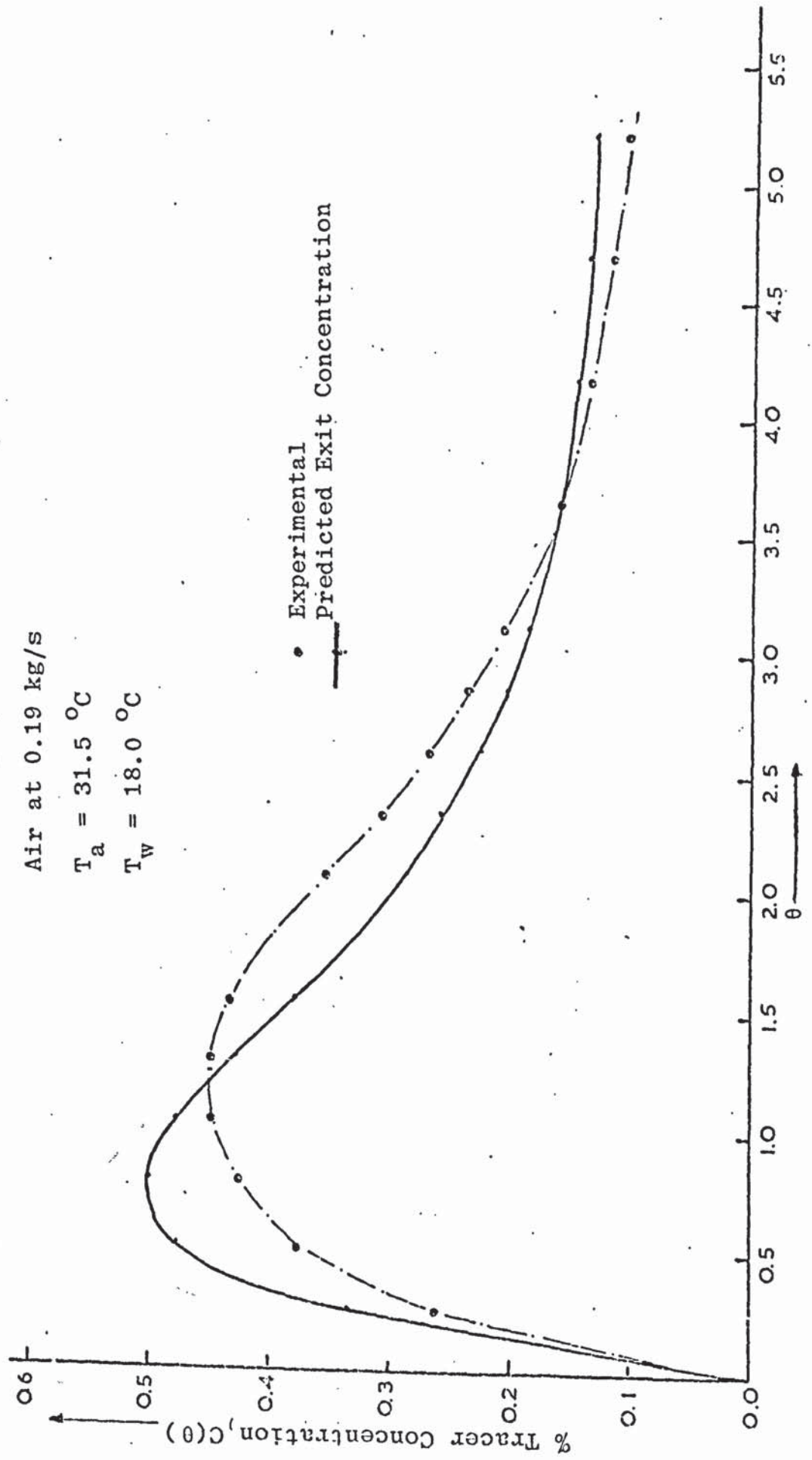
 $T_a = 31.5^\circ\text{C}$  $T_w = 18.0^\circ\text{C}$ 



Figure 5.3.14

Water Spray at  $2.50 \times 10^{-3}$  l/s

Air at 0.21 kg/s

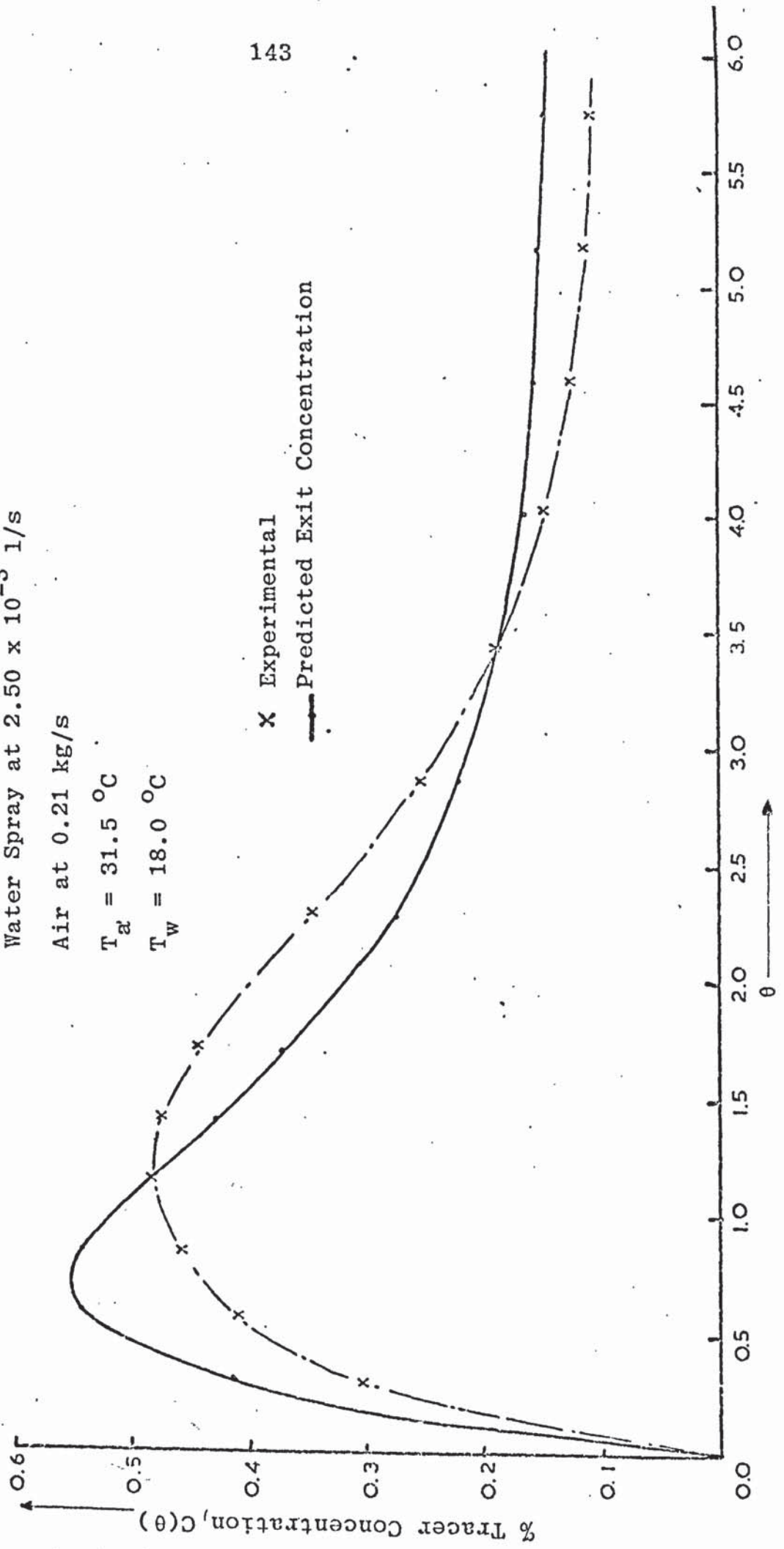
 $T_a = 31.5^\circ\text{C}$  $T_w = 18.0^\circ\text{C}$ 

Figure 5.3.15

Water Spray at  $2.50 \times 10^{-3}$  l/s

Air at 0.23 kg/s

$T_a = 31.5^\circ\text{C}$

$T_w = 18.0^\circ\text{C}$

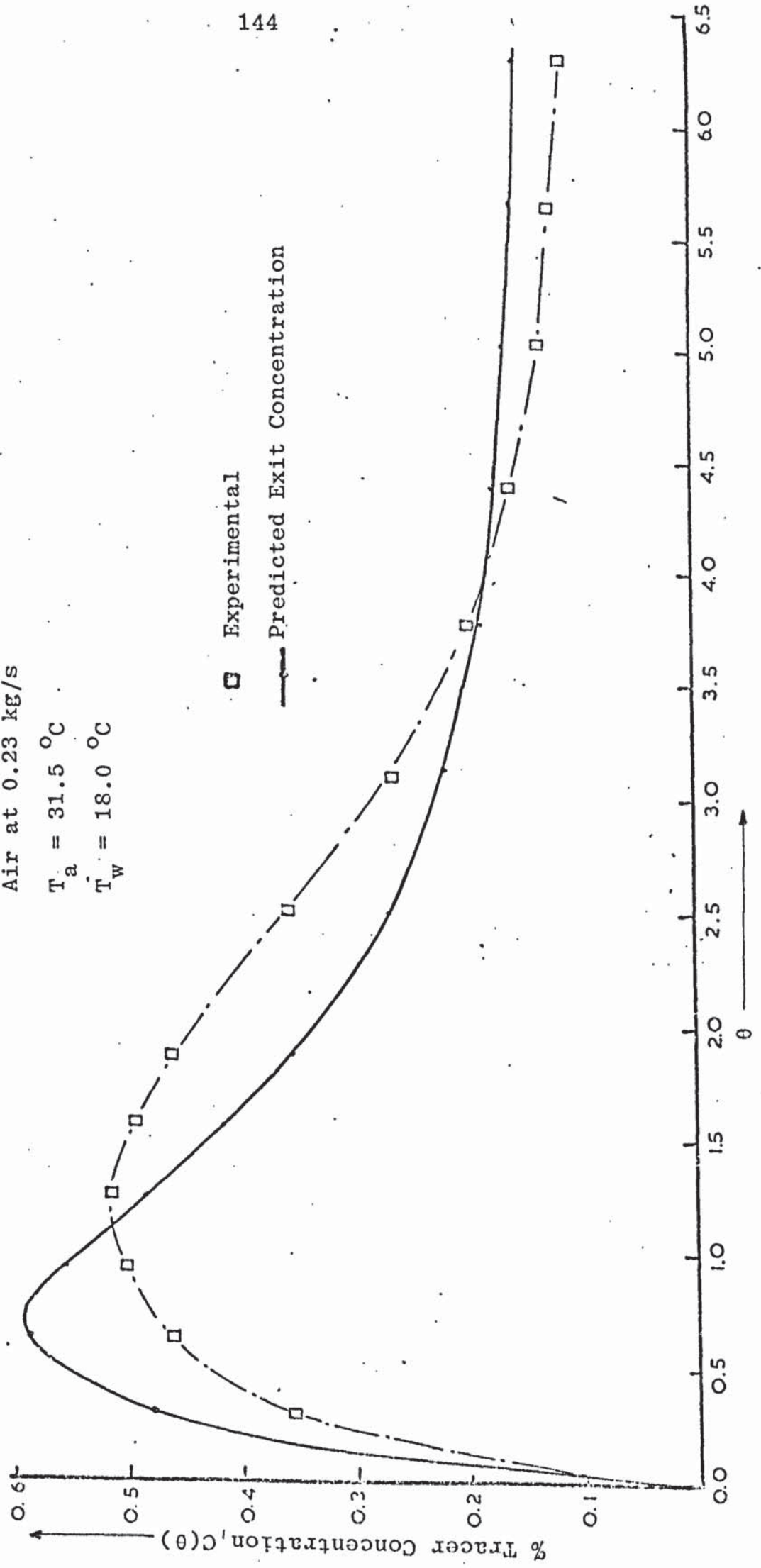


Figure 5.3.16

Water Spray at  $3.00 \times 10^{-3}$  l/s

Air at 0.13 kg/s

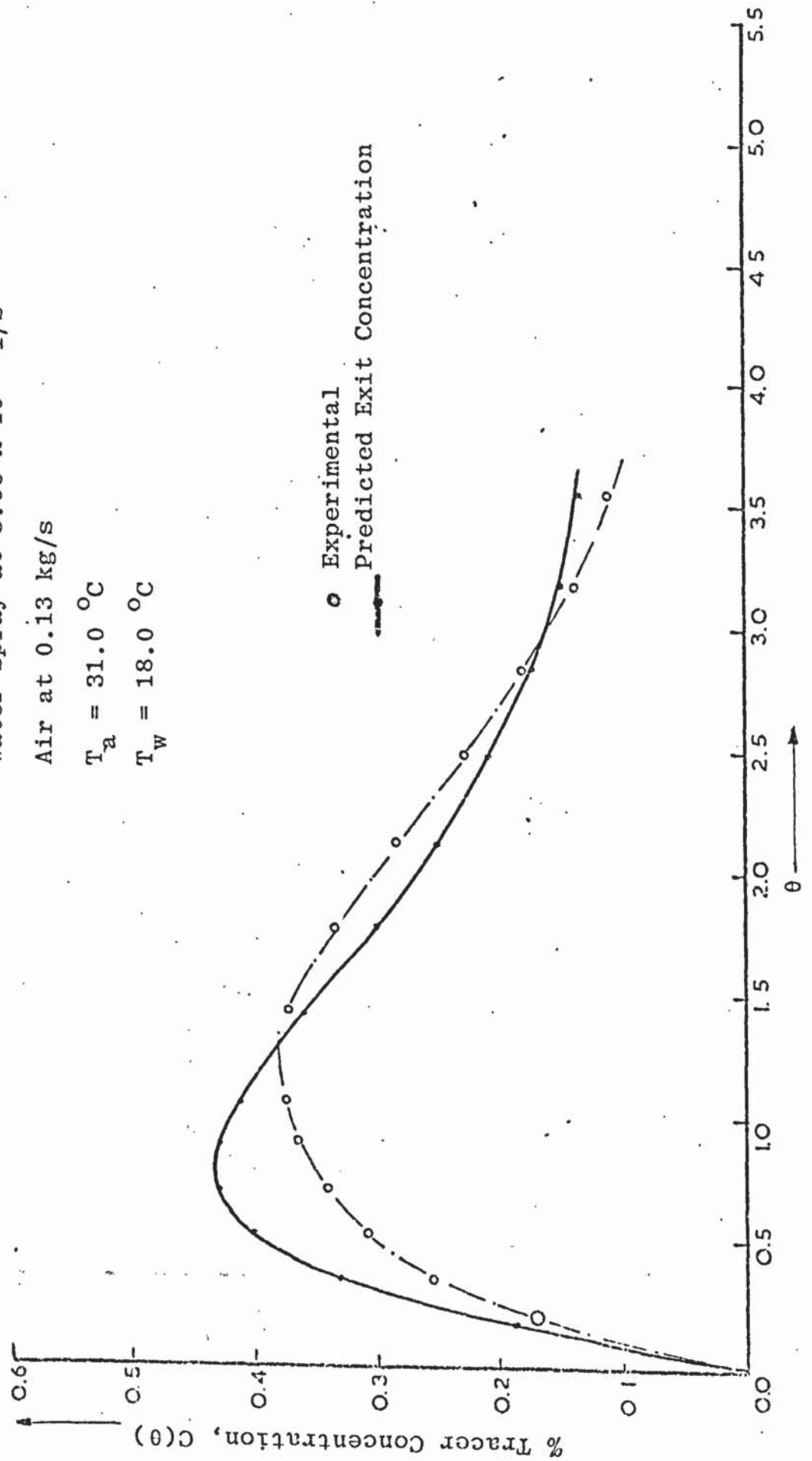
 $T_a = 31.0^\circ\text{C}$  $T_w = 18.0^\circ\text{C}$ 

Figure 5.3.17

Water Spray at  $3.00 \times 10^{-3}$  l/s

Air at 0.16 kg/s

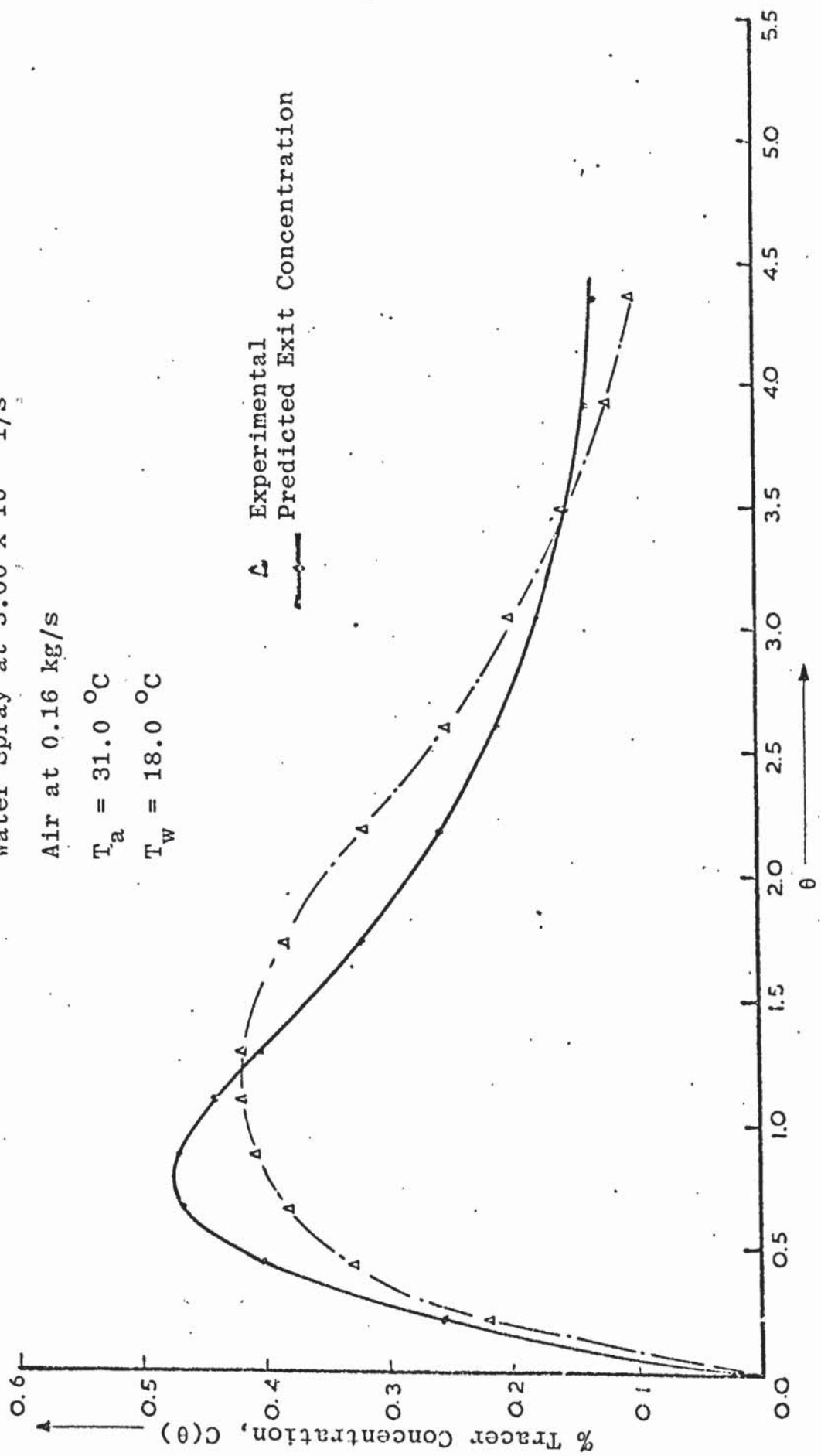
 $T_a = 31.0$  °C $T_w = 18.0$  °C



Figure 5.3.18

Water Spray at  $3.0 \times 10^{-3}$  l/s

Air at 0.19 kg/s

$T_a = 31.5^\circ\text{C}$

$T_w = 18.0^\circ\text{C}$

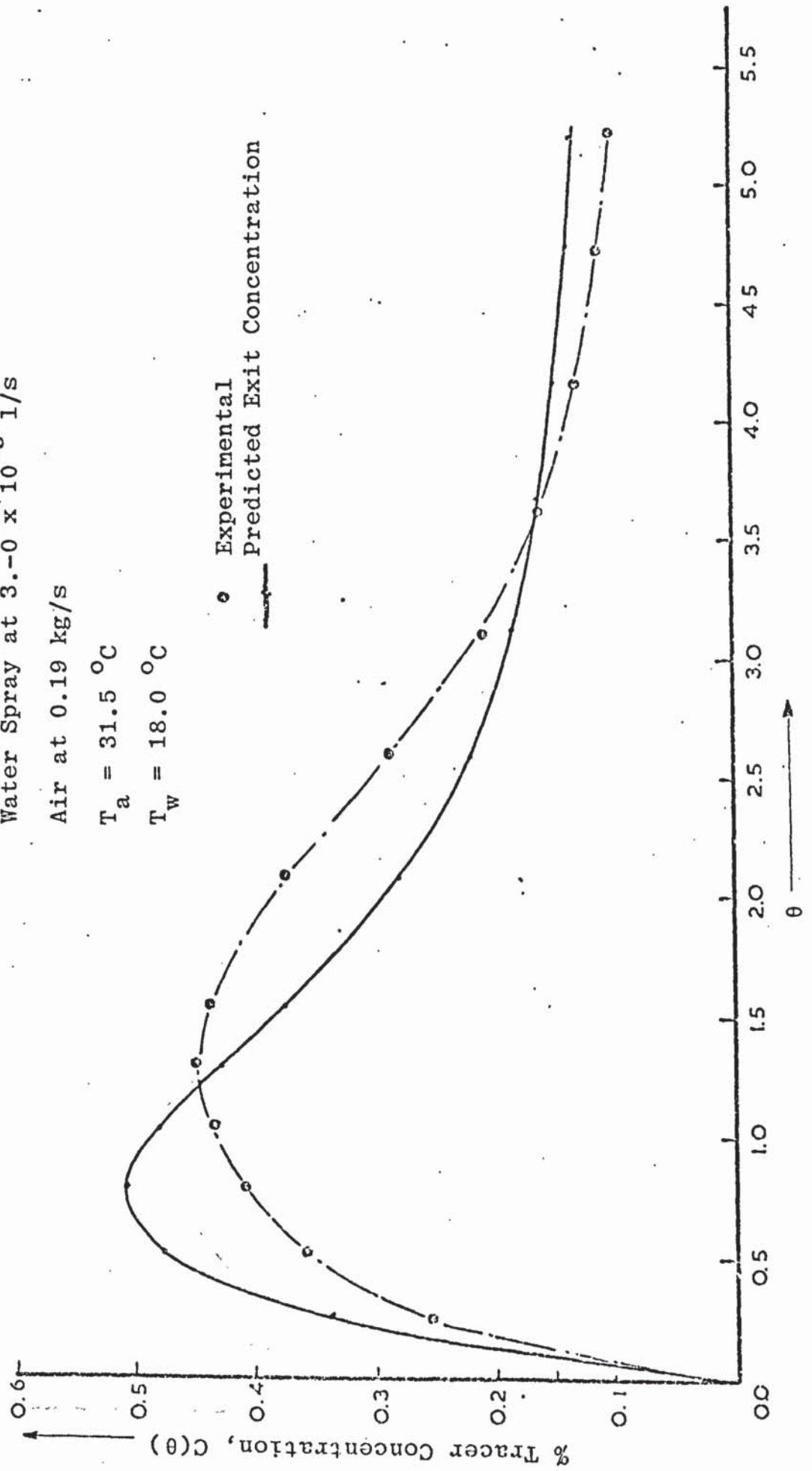


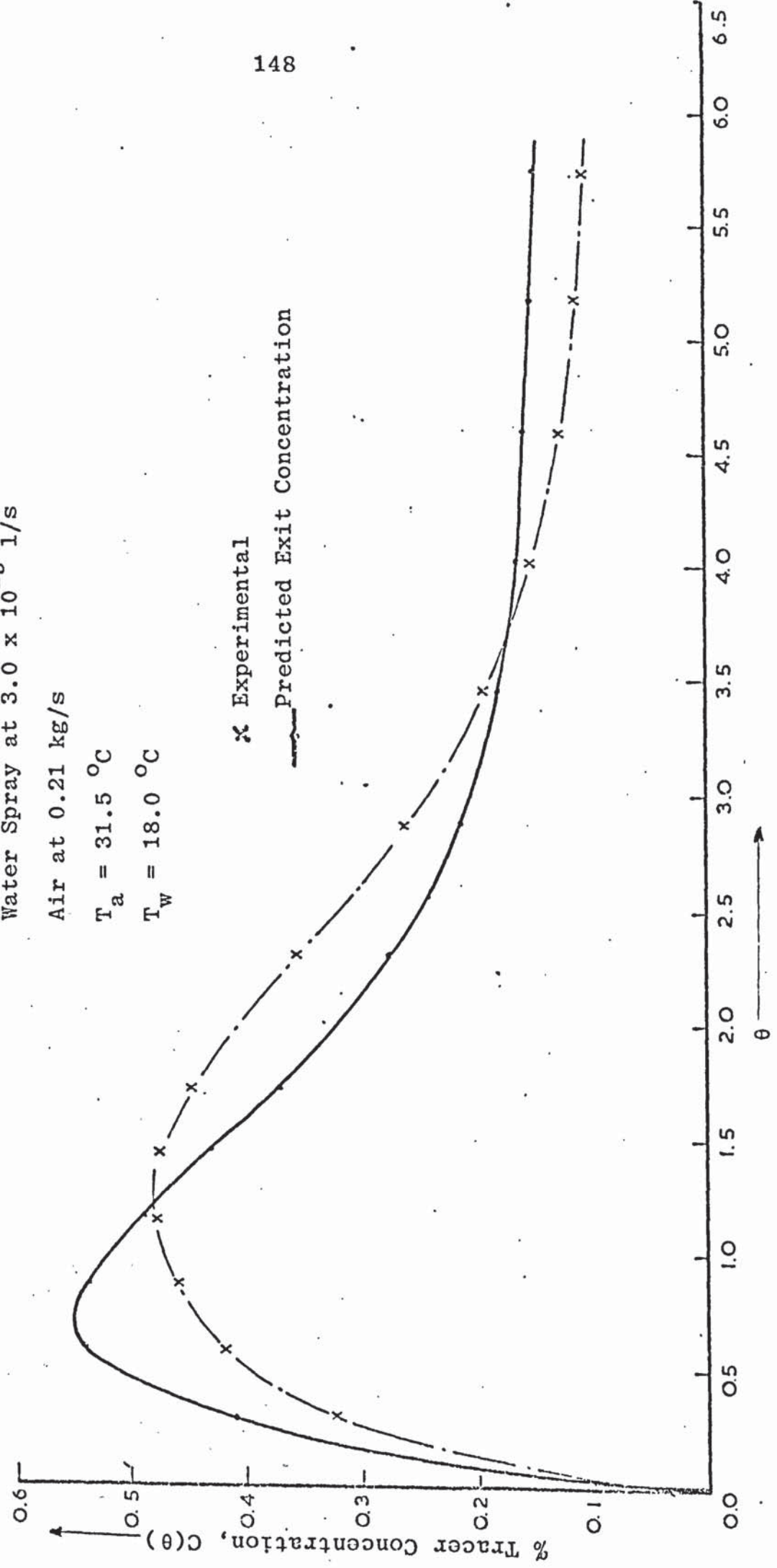
Figure 5.3.19

Water Spray at  $3.0 \times 10^{-3}$  l/s

Air at 0.21 kg/s

$T_a = 31.5^\circ\text{C}$

$T_w = 18.0^\circ\text{C}$



Figures 5.3.20

Water Spray at  $3.0 \times 10^{-3}$  l/s

Air at 0.23 kg/s

$T_a = 31.5^\circ\text{C}$

$T_w = 18.0^\circ\text{C}$

□ Experimental

— Predicted Exit Concentration

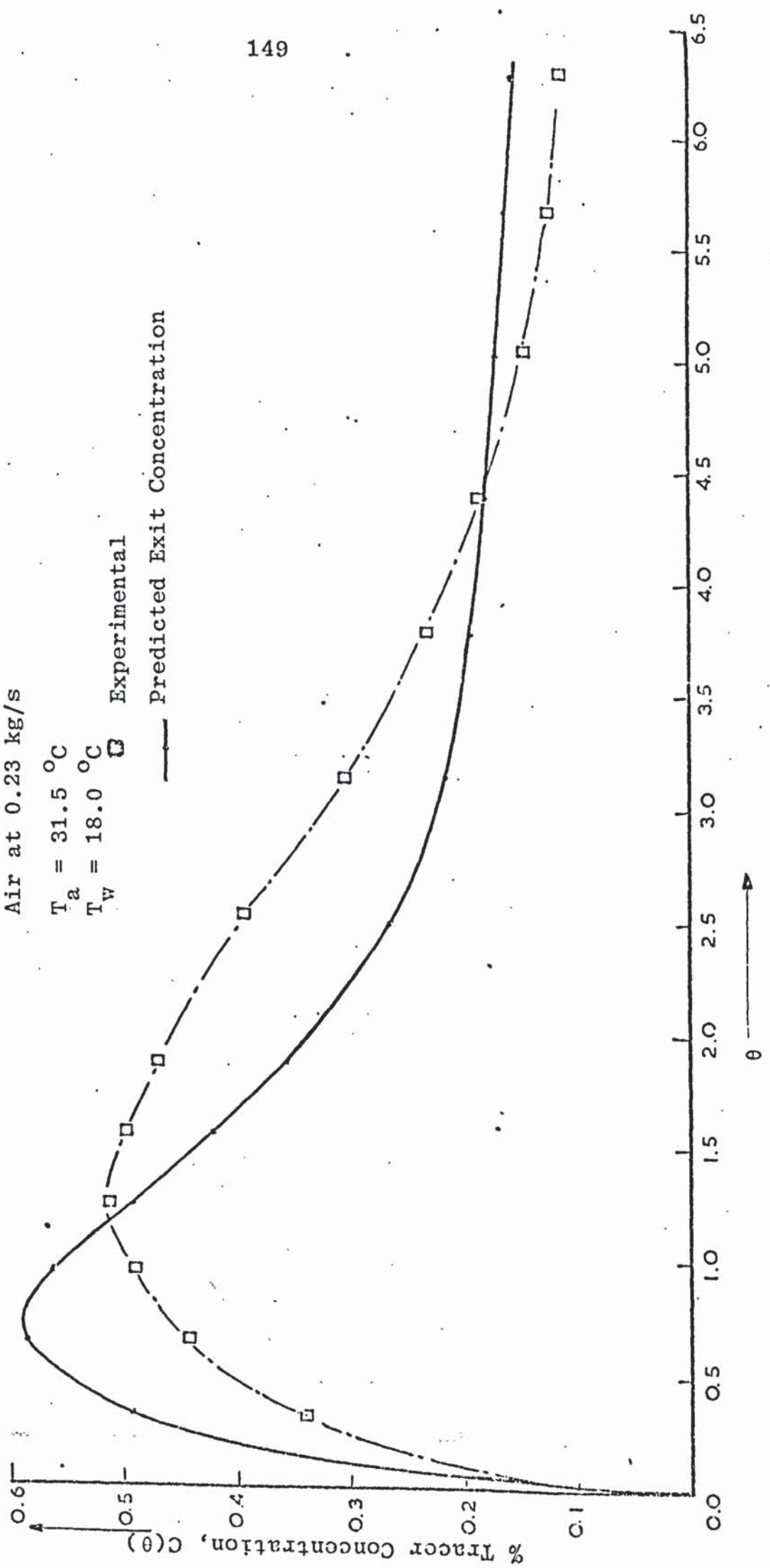


Figure 5.3.21

Water Spray at  $3.50 \times 10^{-3}$  l/s

Air at 0.13 kg/s

$T_a = 31.5^\circ\text{C}$

$T_w = 18.5^\circ\text{C}$

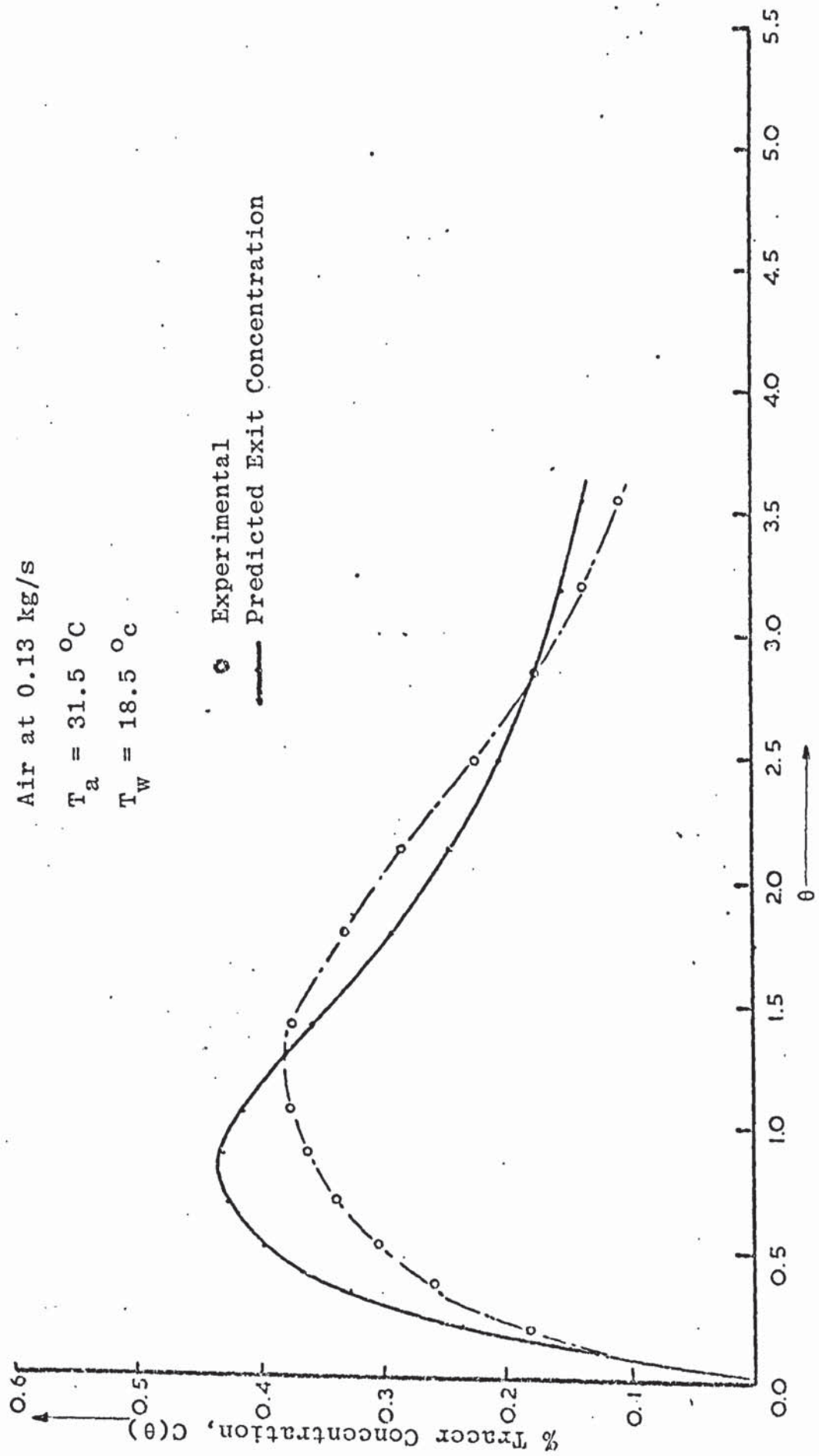




Figure 5.3.22

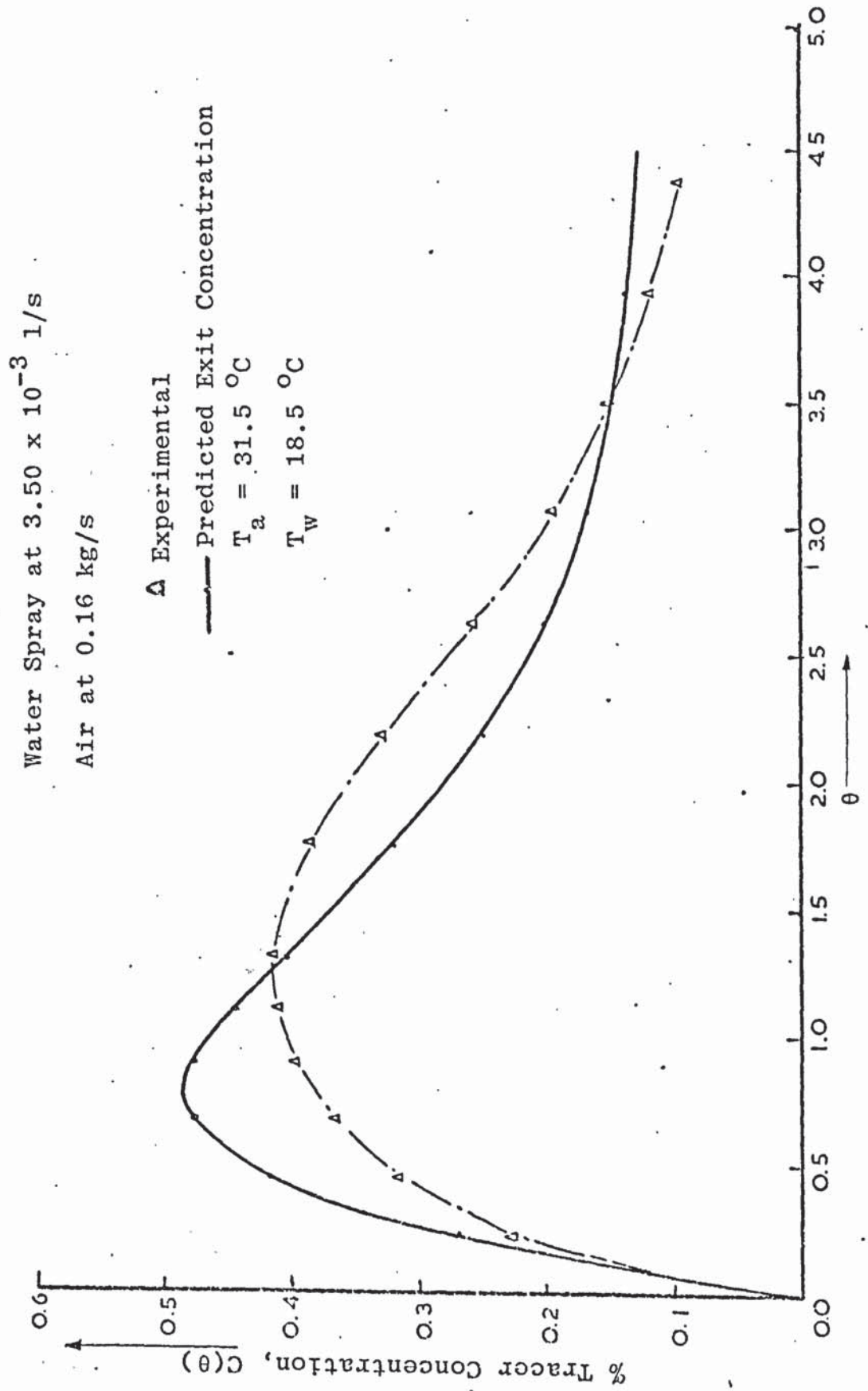


Figure 5.3.23

Water Spray at  $3.50 \times 10^{-3}$  l/s

Air at 0.19 kg/s

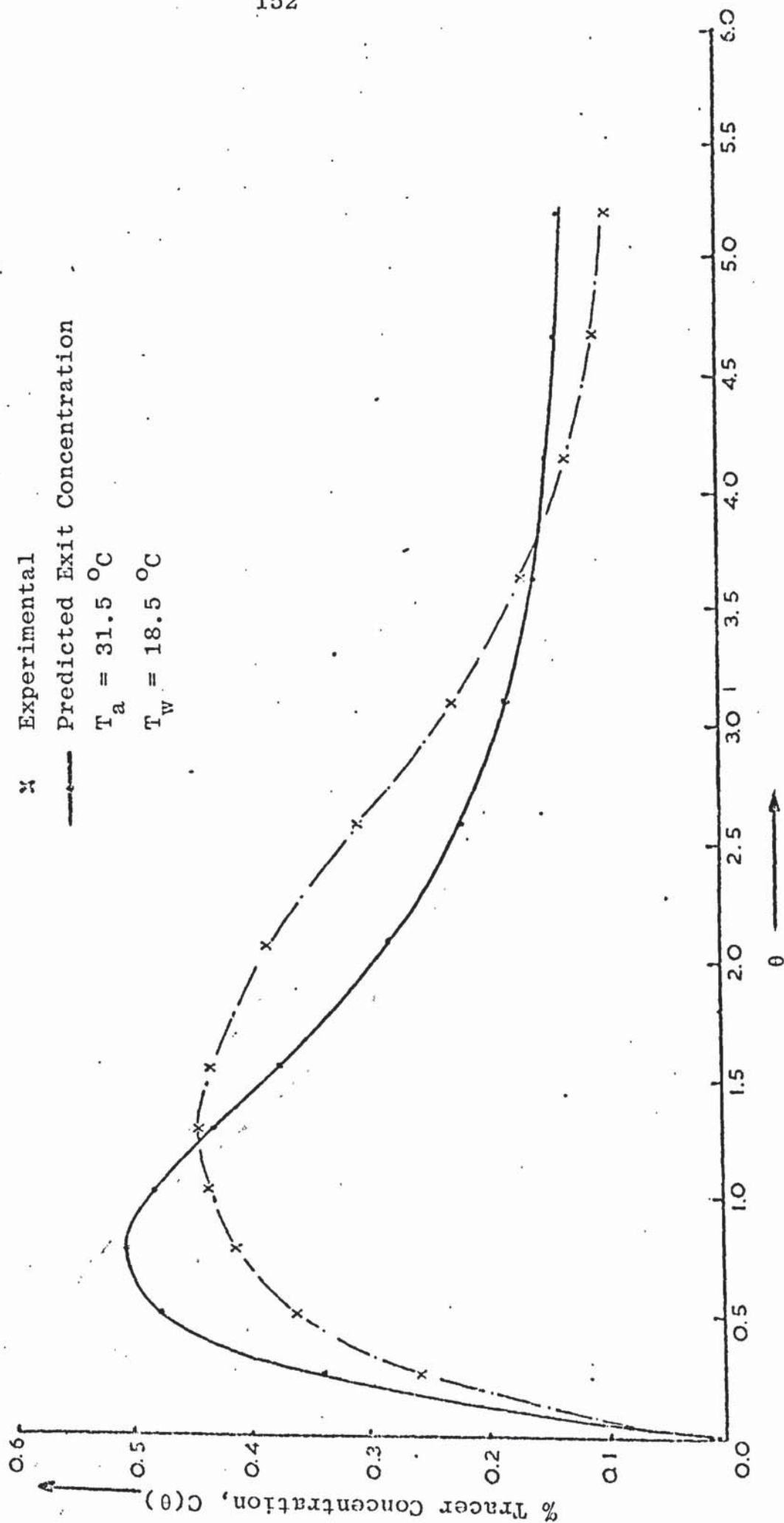


Figure 5.3.24

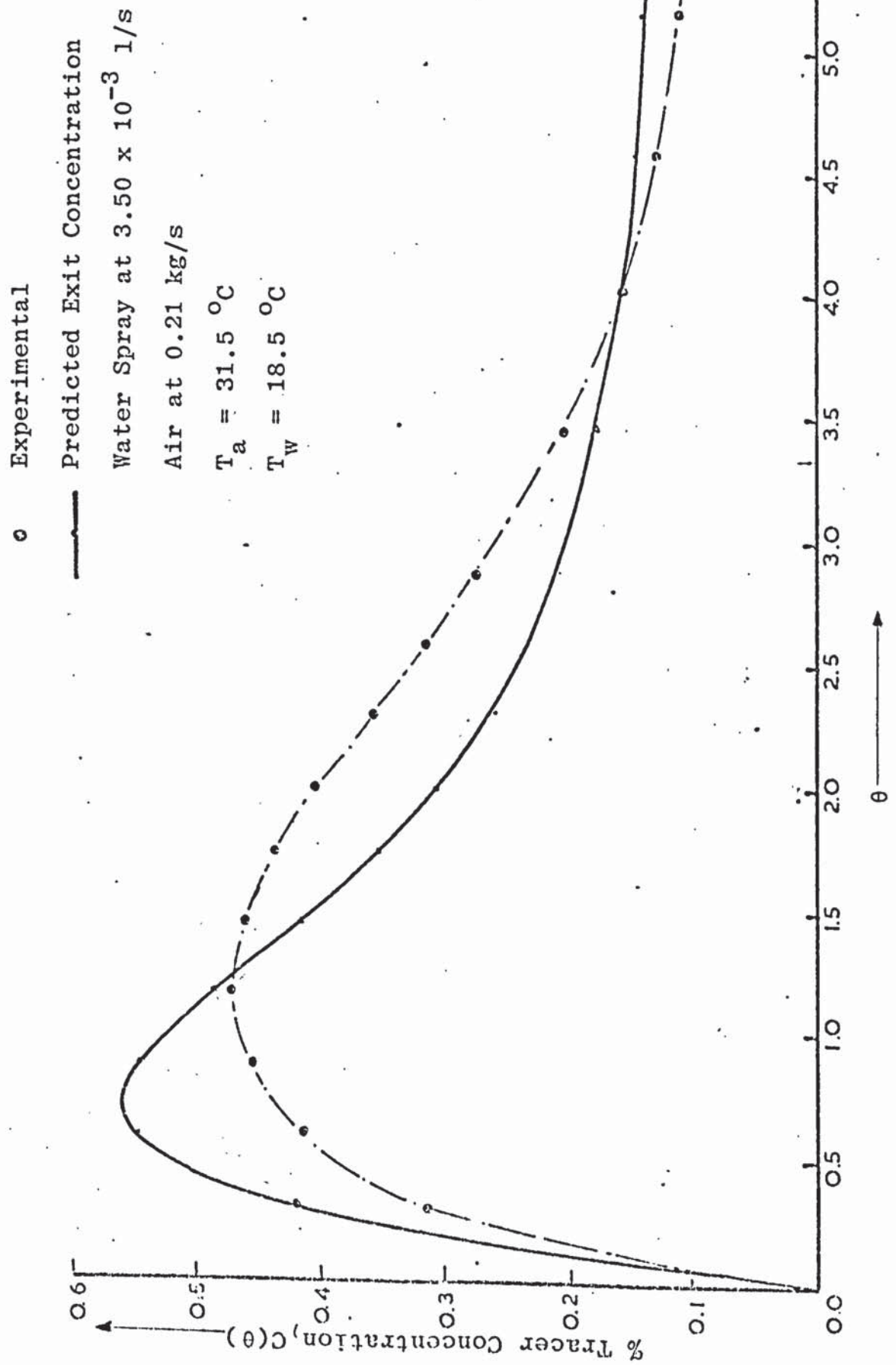
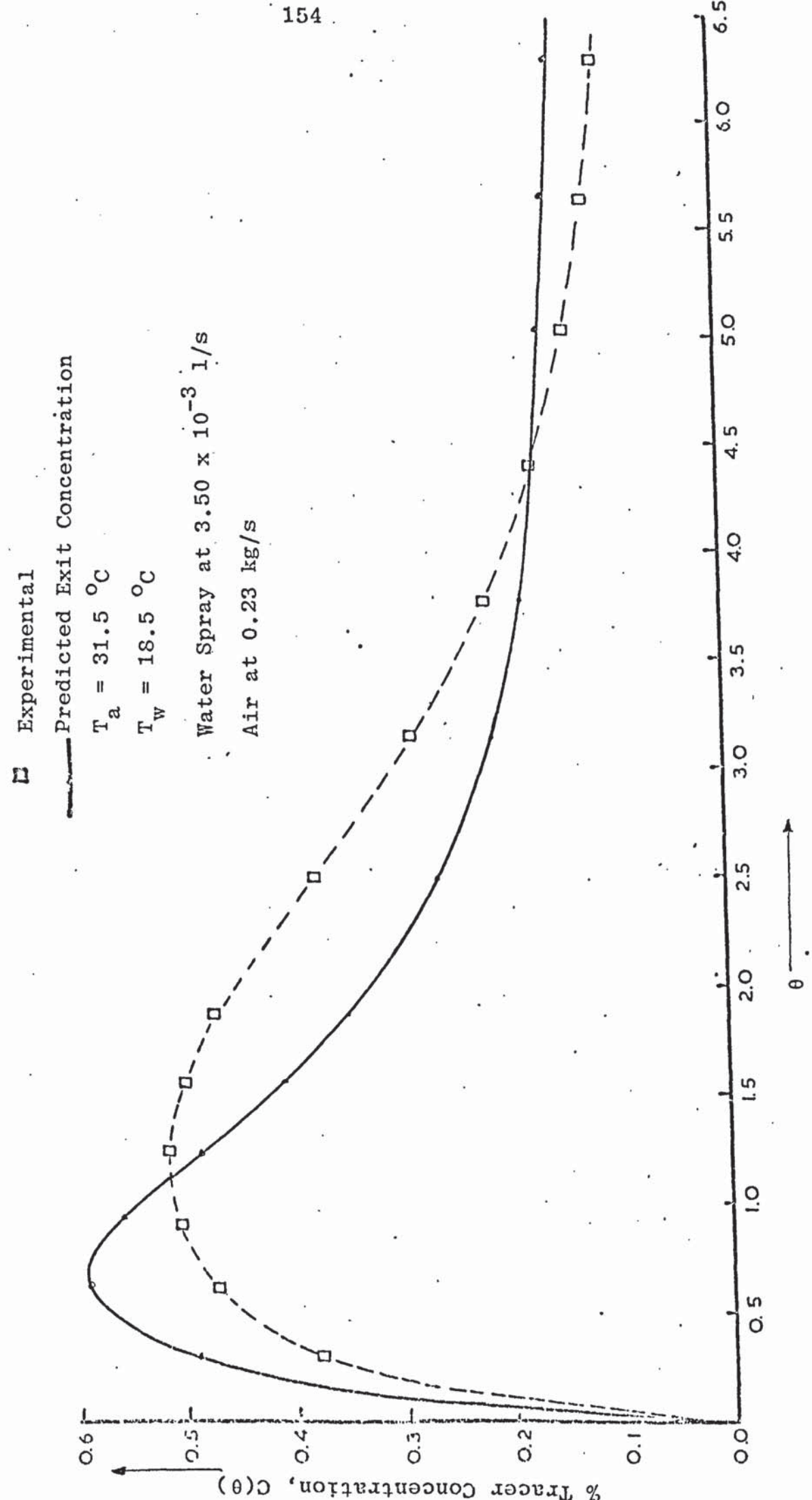


Figure 5.3.25





reduces the difference in air temperature.

### 5.3.2 Comparison Of Predicted With Experimental Exit Concentration Profile

From figures 5.3.1 to 5.3.25, the experimental exit concentration profile obtained from the recorder chart compare favourably with the predicted values deduced from equation (3.37). The standard deviation of the experimental points from the theoretical prediction range from  $1.76 \times 10^{-2}$  to  $1.83 \times 10^{-2}$ . Although it was generally observed that the deviation became more prominent at higher air flowrates.

Figure 5.4.1

Water Spray at  $1.50 \times 10^{-3}$  l/s

◇ Air at 0.13 kg/s

• Air at 0.16 kg/s

△ Air at 0.19 kg/s

□ Air at 0.21 kg/s

● Air at 0.23 kg/s

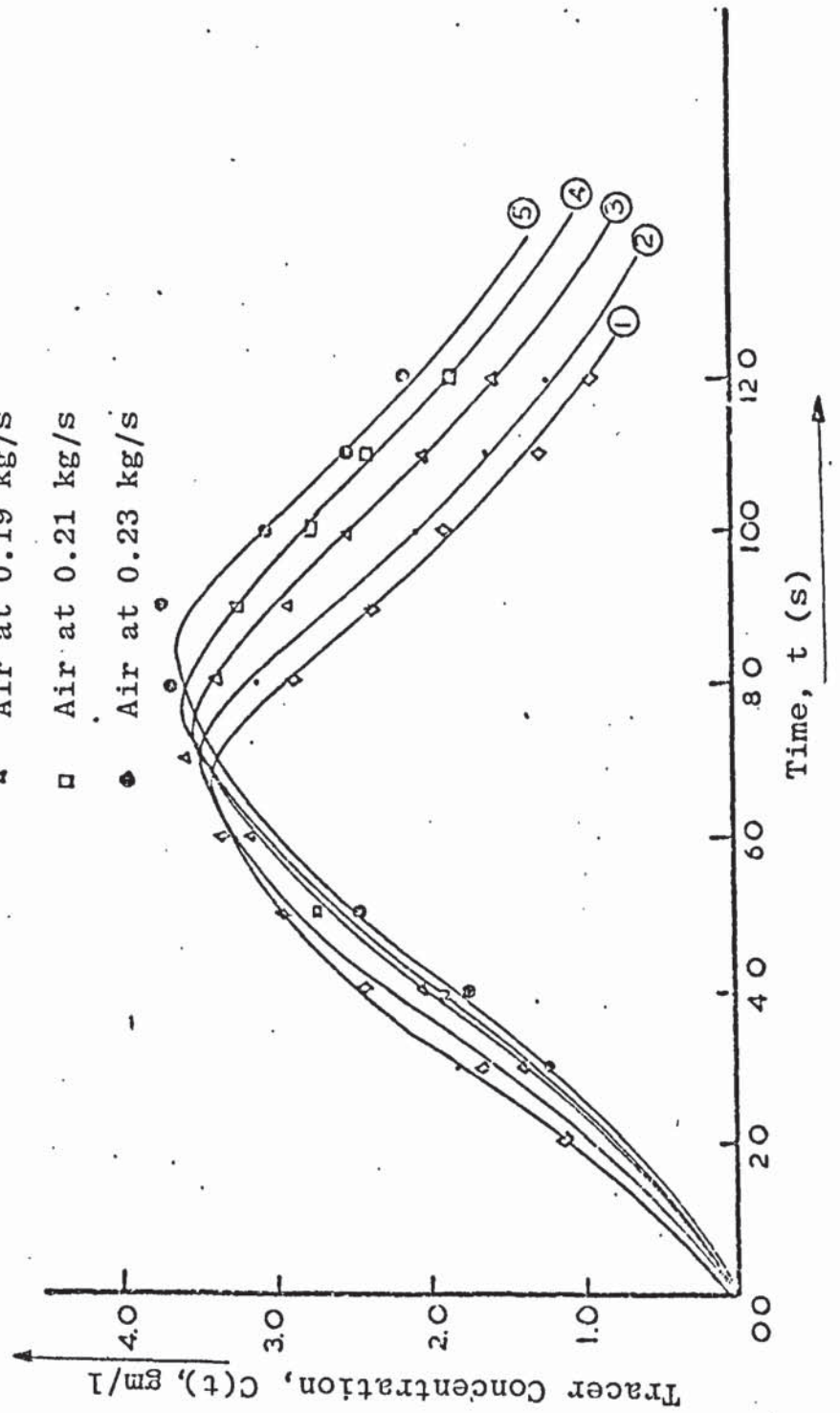


Figure 5.4.2

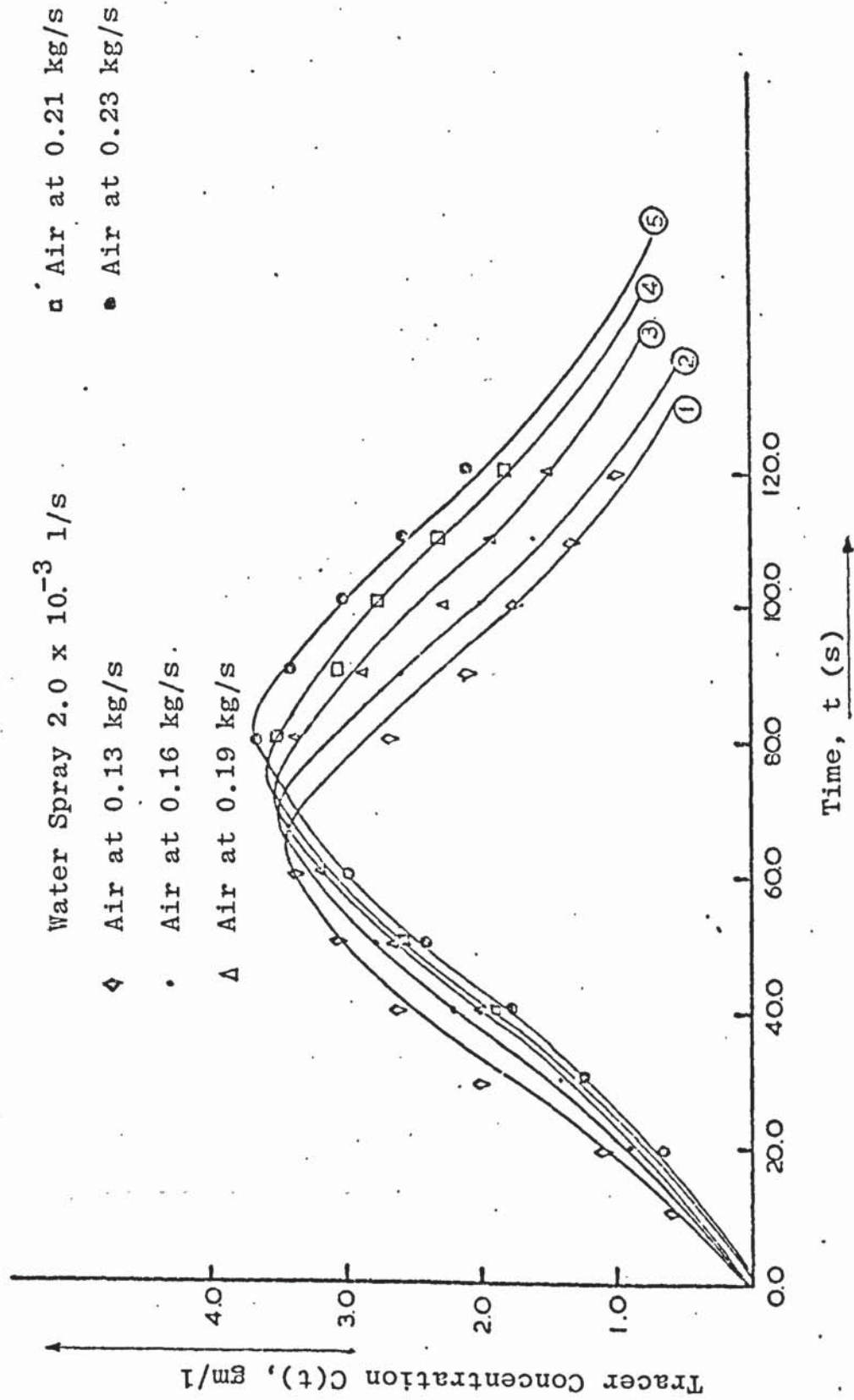


Figure 5.4.3.

Water Spray at  $2.50 \times 10^{-3}$  l/s

□ Air at 0.21 kg/s

● Air at 0.23 kg/s

◇ Air at 0.13 kg/s

• Air at 0.16 kg/s

△ Air at 0.19 kg/s

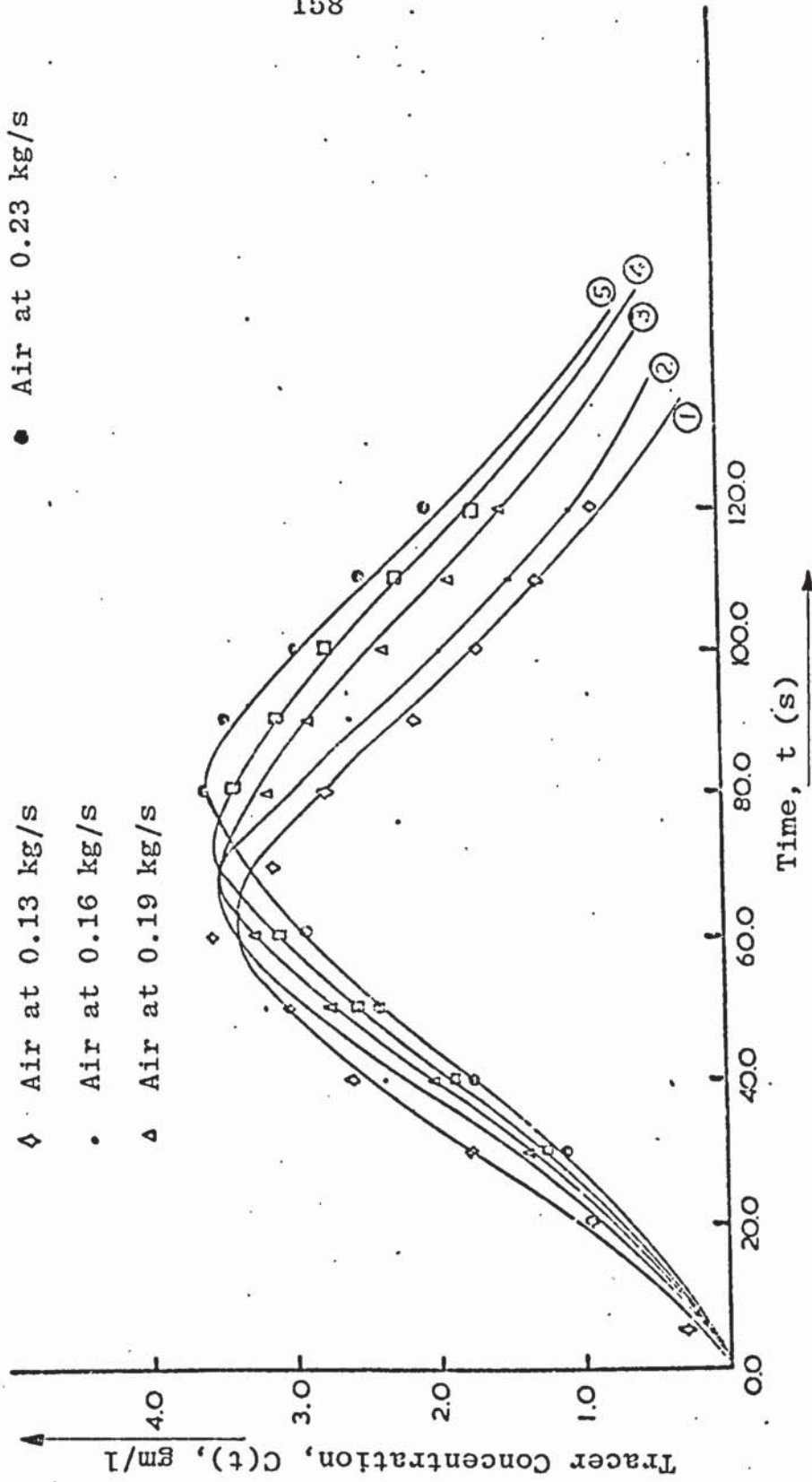




Figure 5.4.4.

Water Spray at  $3.0 \times 10^{-3}$  l/s

◇ Air at 0.13 kg/s

• Air at 0.16 kg/s

△ Air at 0.19 kg/s

□ Air at 0.21 kg/s

● Air at 0.23 kg/s

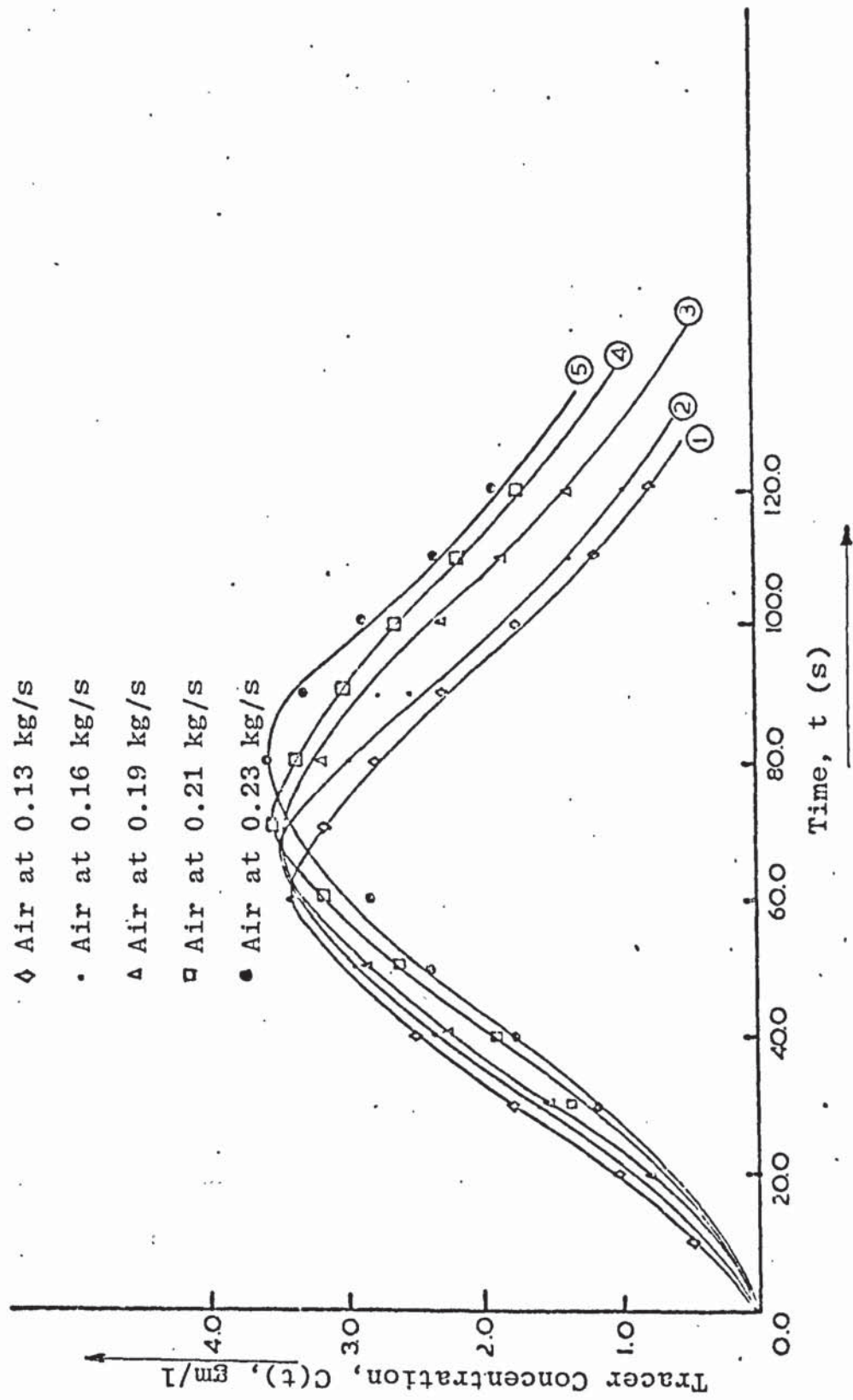
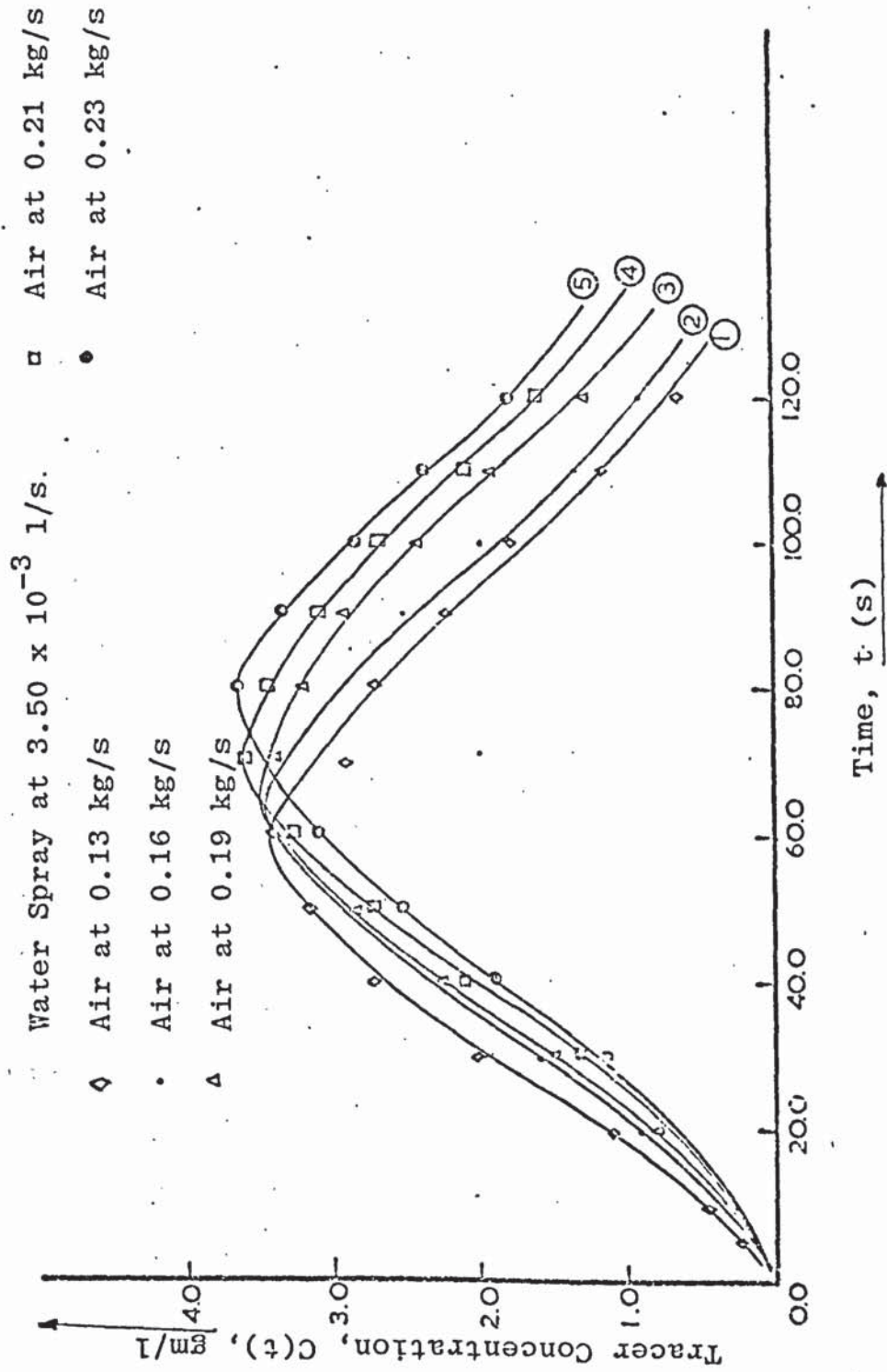


Figure 5.4.5



#### 5.4 EXIT RESPONSE ANALYSIS OF LIQUID SPRAY

The results obtained for the residence time distribution for sprays of pure water and sodium carbonate slurry are presented in figures 5.4.1 to 5.4.7 in graphical form, and in tables D1 to D5 and table E1 in appendix C.

##### 5.4.1 Residence-Time Analysis For Pure Water Spray

The effect of the air flowrate on the residence time of the water spray is shown in figures 5.4.1 to 5.4.5. The residence time increased with increasing air flowrate when the spray was maintained at a constant flowrate as would be expected. This was probably due to the fact that the drag of the drying air on the droplets was much more pronounced at higher air flowrates.

As would be expected, the residence time increased as the rate of flow of the liquid feed was reduced.

##### 5.4.2 Residence-Time Analysis For Sodium Carbonate Slurry Spray

For sprays of sodium carbonate slurry, however, the residence time distribution of the spray was generally longer than that for pure water. This was because some of the sprayed sodium carbonate droplets adhered to the sides of the conical base of the tower and hence took a longer time to get to the exit point.

Figure 5.4.6

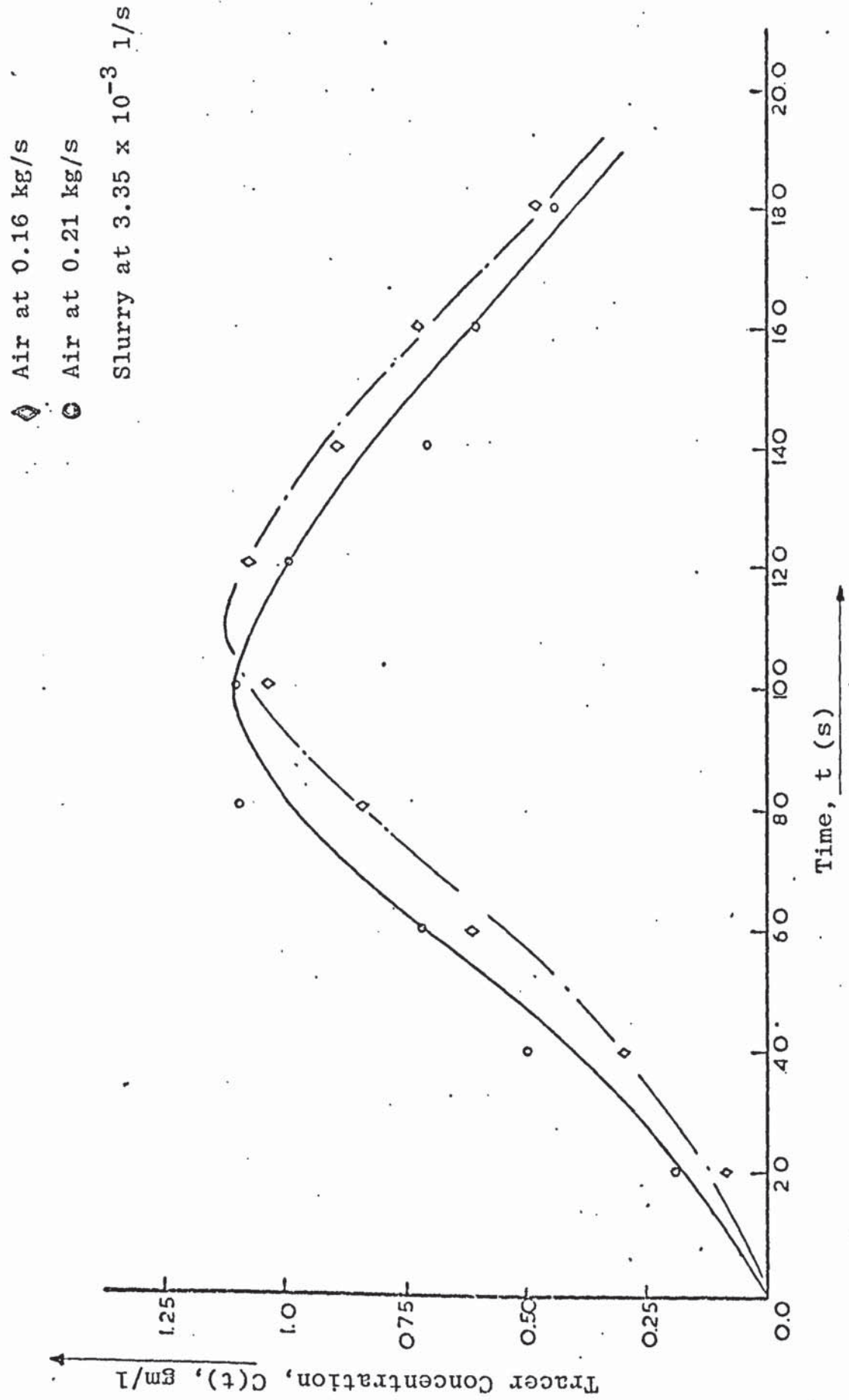
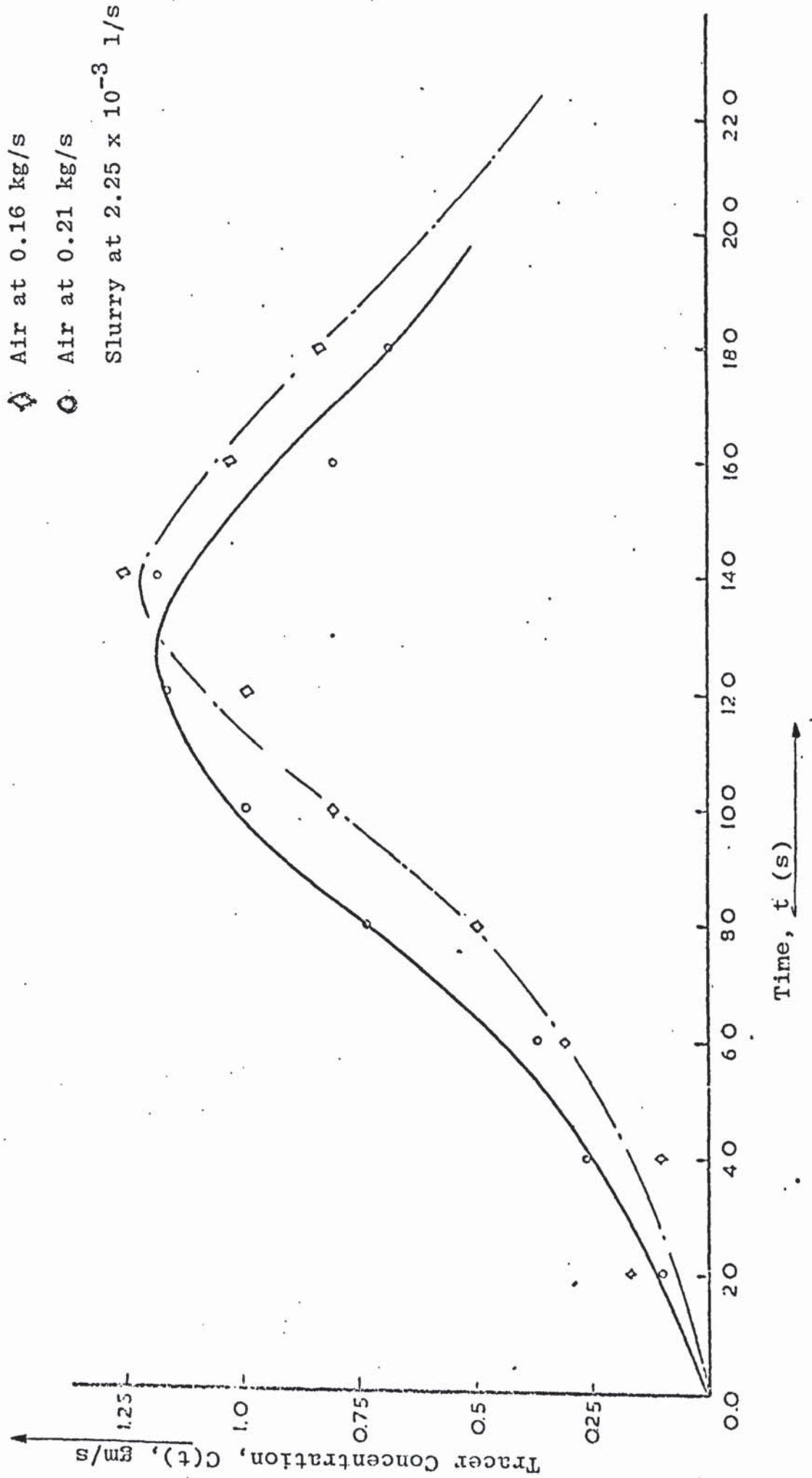




Figure 5.4.7



For the same reasoning given in section (5.4.1) the residence time of the spray increased as the rate of air flow was increased, due to prolonged mixing of the two phases in the spray tower.

CHAPTER SIX

APPLICATION OF THE SPRAY

TOWER DESIGN MODEL

## 6. APPLICATION OF THE SPRAY TOWER DESIGN MODEL

Despite the growing importance of spray drying in industry and its applications in the production of pharmaceuticals, detergents, food products, pigments ceramics, and a large number of organic and inorganic chemical compounds, the design of spray driers has remained largely based on previous experience and the vast amount of operating data which manufacturers have acquired over the years. The lack of information on residence-times and the flow patterns of the drops and air in the tower has been a major difficulty in spray drier design. Schowalter and Johnstone (122), carried out detailed measurements in a vortex tube which provided a clear picture of the flow field, but they failed to correlate their results. Bank (123), Paris et al (125) and Janda (124) have also investigated the flow patterns of the drying air and reported high turbulence intensities in the tower. It is also evident from the work reported by Bank (123), Gauvin and Katta (121) that in the free entrainment zone, the motion of the sprayed droplets is governed by the drying gas.

In the present investigation however, it has been possible to measure the volumes of the various flow patterns existing in the 9' x 4' diameter spray tower and obtain correlations for them in terms of the gas Reynolds Number, the air and liquid feed velocities and other physical properties of the drops and air. These have



been presented in section (5.2.5). Hence in this work, the major design parameters identified are the capacities of the different turbulent zones of the drying tower, the physical properties of both the drops and air, the flowrates, heat balance, the rate of drying and the residence-time distribution of the drops and air.

The model discussed in section (3.3) is hereby tested with a practical spray drying tower.

Data obtained from an industrial company (126), on an existing pilot plant spray drying tower for the drying of an anionic Detergent formulation.

Slurry temperature at jet, $T_o$	43 °C
Inlet air temperature, $t_3$	327 °C
Outlet air temperature, $t_o$	110 °C
Inlet air flowrate $G_a$	(0.73 kg/s)
Slurry flowrate, $G_L$	(0.167 kg/s)
Moisture content of slurry, $C_o$	48%
Final moisture content of powder, $C_3$ .	12%
Tower pressure, P	-0.1 in. WG
Final powder temperature, $T_3$	50°C
Ambient humidity at 25 °C, H	50% R.H
Diameter of spray tower, D	6 ft. (1.83m)
Height of tower, Z	18 ft.(5.49m)
Height of Conical base, $h_1$	3 ft. (0.91m)

Data on humid heat  $s$ , heat capacity  $c_p$ , and latent heat of evaporation were obtained from psychometric, humidity, and heat capacity charts (56,99) at the

corresponding temperatures. Other physical properties of the air have been taken from the International critical Tables. Data on the porosity of the sprayed droplets are obtained from Table (5.8) for the anionic detergent formulation (11).

The results obtained from all the calculations are shown in the Honeywell 'H316' Basic 16 computer program in Appendix C. The volumes  $V_1$ ,  $V_2$ ,  $V_3$  of the bottom stirred-tank, plug flow and top stirred-tank section respectively were calculated from the correlations proposed in section (5.25) in the general form:

$$\frac{V_i}{\Sigma V} = \psi (Re)^d \cdot \left(\frac{\mu_1}{\mu_g}\right)^e \cdot \left(\frac{U_1}{U_g}\right)^f \cdot \left(\frac{Z}{D}\right)^g \quad (5.2.1)$$

The volumes obtained were:

$$V_1 = 5.58 \text{ m}^3$$

$$V_2 = 2.34 \text{ m}^3$$

$$\text{and } V_3 = 5.31 \text{ m}^3$$

Now the volume  $V_T$  of the system was calculated as follows:

$$\begin{aligned} V_T &= \Sigma V = \pi r^2 \cdot Z + 1/3 \pi r^2 h_1 \\ &= \pi r^2 \left( Z + \frac{h_1}{3} \right) \\ &= \pi \cdot (0.9144)^2 \times (5.4864 + \frac{0.9144}{3}) \end{aligned}$$

$$= 0.8361\pi \cdot (5.7912)$$

$$= \underline{15.21 \text{ m}^3}$$

Having obtained the capacities of the various sections in the tower, the residence times of the drying air in these sections were obtained from the relations:

From equation (3.38)

$$\tau_1 = V_1/Q$$

$$\text{where } Q = 0.76 \text{ m}^3/\text{s}$$

$$\begin{aligned} \text{Therefore; } \tau_1 &= \frac{5.58}{0.76} \\ &= \underline{7.33 \text{ s}} \end{aligned}$$

Similarly from equation (3.39)

$$\begin{aligned} \tau_2 &= V_2/Q \\ &= \frac{2.34}{0.76} \\ &= \underline{3.08 \text{ s}} \end{aligned}$$

and from equation (3.40)

$$\tau_3 = V_3/Q$$

$$\begin{aligned}\tau_3 &= \frac{5.31}{0.76} \\ &= \underline{6.99} \text{ s}\end{aligned}$$

The total residence time of the air in the spray tower is given by:

$$\begin{aligned}\tau &= \frac{V_T}{Q} \\ &= \frac{15.21}{0.76} \\ &= \underline{20.01} \text{ s}\end{aligned}$$

From the overall heat balance equation (3.41), the residence-time of the spray droplet is given by:

$$\theta = \left\{ Q \cdot s_f (t_3 - t_o) \times \tau - q_1 \cdot c_{p_l} (T_3 - T_o) \right\} / q_1 \rho_l (C_3 - C_o) \lambda$$

Therefore;

$$\begin{aligned}\theta &= \left\{ \frac{0.76 \times 1.08 \times 20.01 \times (327 - 110) - 1.13 \times 10^{-4} \times 1.674 (50 - 43)}{1.13 \times 10^{-4} \times (1500 - 350) \times 2228.31} \right\} \\ &= \underline{12.31} \text{ s}\end{aligned}$$

From equation (3.48) the mass transfer coefficient is calculated from the amount of water evaporated .



$$\begin{aligned}
 \text{Therefore; } K_G &= \frac{W}{\Delta C \cdot \pi d_p^2} \\
 &= \frac{0.4667 \times 10^{-3}}{1150 \times 3.142 \times (0.2 \times 10^{-2})^2} \\
 &= \underline{3.23 \times 10^{-2} \text{ m/s}}
 \end{aligned}$$

From equation (3.47), the rate of drying within the time interval  $\theta$ , is given by:

$$N_A \theta = K_G \cdot a \cdot \Delta C \cdot \theta.$$

Recall,

Mass Flowrate of slurry = 0.167 kg/s

Density of slurry = 1.08 gm/cc

Drop diameter =  $0.2 \times 10^{-2} \text{ m}$

$$\text{Therefore; Mass of Drop} = \left[ \frac{\pi}{6} \times (0.2)^3 \times 1.08 \right] \text{ gm}$$

$$\text{Therefore; Number of Drops} = \left[ \frac{0.167 \times 1000}{\pi/6 \times (0.2)^3 \times 1.08} \right]$$

$$= \left[ \frac{0.3189 \times 10^3}{1.08 \times 10^{-3}} \right]$$

$$\text{Therefore; Surface Area} = \left[ \frac{0.3189 \times 10^6 \times \pi \cdot (.2)^2}{1.08 \times 10^6} \right] \text{ m}^2/\text{s}$$

$$= \left[ \frac{0.3189 \times 0.04\pi}{1.08} \right] \text{ m}^2/\text{s}$$

$$\begin{aligned}
 \text{Therefore Surface Area} &= 0.4637 \times 10^{-2} \quad \text{m}^2/\text{s} \\
 &= 0.4637 \times 12.31 \times 10^{-2} \quad \text{m}^2 \\
 &= \underline{0.057} \quad \text{m}^2
 \end{aligned}$$

From equation (3.47), water evaporated in the time interval  $\theta$ , is given by:

$$N_A \cdot \theta = (3.23 \times 3.142 \times 0.057 \times 10^{-2} \times 11.50) \times 12.31$$

$$\text{Therefore } X = \underline{0.8188} \text{ kg}$$

$$\begin{aligned}
 \text{Water in feed} &= (0.167 \times 0.48) \text{ kg/s} \\
 &= 0.08016 \text{ kg/s} \\
 &= 0.08016 \times 12.31 \text{ kg} \\
 &= \underline{0.9867} \text{ kg}
 \end{aligned}$$

Therefore Water remaining in drop after drying;

$$\begin{aligned}
 &= 0.9867 - X \\
 &= \underline{0.1680} \text{ kg}
 \end{aligned}$$

Therefore dry solids in feed for the drying time  $\theta$ , is given by:

$$\begin{aligned}
 Y &= (0.167 - 0.08016) \times 12.31 \text{ kg} \\
 &= \underline{1.069} \text{ kg}
 \end{aligned}$$

The total wet solids is given by;

$$\begin{aligned} Z &= Y + (0.9867 - X) \text{ kg} \\ &= 1.069 + 0.1680 \text{ kg} \\ &= \underline{1.237} \text{ kg} \end{aligned}$$

Therefore percentage final moisture content

$$\begin{aligned} &= \frac{0.1680 \times 100 \%}{1.237} \\ &= \underline{13.6 \%} \end{aligned}$$

This agrees favourably with the experimental value of 12% for the final moisture content of the powdered product.

Using these data to calculate the capacities  $V_1$ ,  $V_2$  and  $V_3$  of the 9' x 4' diameter laboratory spray tower, in the same manner the volumes were calculated from the correlations presented in section (5.25). The calculated values are also shown in the Computer Program in Appendix C.

$$V_1 = 1.34 \text{ m}^3$$

$$V_2 = 0.56 \text{ m}^3$$

$$V_3 = 1.27 \text{ m}^3$$

$$\begin{aligned} \text{Now } V_T &= \Sigma V = \pi r^2 Z + 1/3 \pi r^2 h_2 \\ &= \pi r^2 (2.736 + (1.216/3)) \end{aligned}$$

$$\begin{aligned}
 V_T &= \pi (0.608)^2 \times (2.736 + 0.405) \\
 &= \underline{3.65} \text{ m}^3
 \end{aligned}$$

The air residence time  $\tau$ , in the first stirred-tank section is given by;

$$\begin{aligned}
 \tau_1 &= V_1/Q \\
 &= 1.34/0.76 \\
 &= \underline{1.76} \text{ s}
 \end{aligned}$$

For the plug flow section;

$$\begin{aligned}
 \tau_2 &= \frac{V_2}{Q} \\
 &= \frac{0.56}{0.76} \\
 &= \underline{0.74} \text{ s}
 \end{aligned}$$

For the top stirred-tank;

$$\begin{aligned}
 \tau_3 &= V_3/Q \\
 &= \frac{1.275}{0.76} \\
 &= \underline{1.68} \text{ s}
 \end{aligned}$$

The air residence time in the tower is given by;

$$\tau = V_T/Q$$



$$\tau = \frac{3.65}{0.76}$$

$$= \underline{4.80 \text{ s}}$$

From these calculations the volumes of the stirred-tank sections  $V_1$  and  $V_3$  were found to be much higher than that for the plug flow volume  $V_2$ .

This was also the case, with the experimental results obtained from the laboratory spray drier. The results are presented in tables B1-B10 of Appendix B. This indicate that the transfer coefficients between the drops and air in the spray drier are high.

The residence time of both the drops and air,  $\theta$  and  $\tau$  respectively can therefore be determined from this model. The value of the final moisture content calculated from this model agreed closely with the value obtained from the experimental data (126).

## 6.1 DISCUSSION ON THE DESIGN MODEL

In the above calculation, it will be seen that;

1. The drying is based on a mean residence - time  $\theta$ , of the sprayed droplets in the tower. This has been applied for the following reasons:-

(i) The hold-up of each section in the tower was not known.

(ii) Sampling at each section was unreliable.

2. The mean mass-transfer coefficient of the tower has been used. Thus it is recommended that for future work relating to this project, the mass-transfer coefficient at each section of the tower should be determined, and hence

the concentration gradient of the sprayed droplets between each Section should be obtained.

## CHAPTER SEVEN

### DISCUSSION

## 7. DISCUSSION

### 7.1 Single Drops of Sodium Sulphate Decahydrate

The drying of aqueous drops of sodium sulphate decahydrate initially presented a free liquid interface to the hot air stream, so that evaporation took place in a similar manner as was for pure water drops, and this process continued until the crust began to form when the rate of mass transfer decreased dramatically. This confirmed that the formation of crust on the drop presented an additional resistance to mass transfer. This resistance was characteristic of the material and the crust thickness. The material affected the porosity and it was found, as shown in Tables A1 to A4, that the porosity,  $\epsilon'$ , was independent of the drop diameter.

The crust thickness,  $\phi$ , was however found to decrease with an increase in the drop diameter for the same drying rate. Thus the rate of mass transfer, and hence the mass transfer coefficient  $K_G$ , was found to increase with an increase in drop diameter. This was due to the fact that the resistance to mass transfer was much more prominent for smaller drop diameter as a result of the increase in the crust thickness.

The mass transfer coefficient  $K_G$ , calculated on the basis that steam was ejected from the wet core of the drop, due to the high rate of heat transfer through the crust from the drying air, was found to be in reasonable agreement to that obtained by Audu (11).



## 7.2 Hydrodynamic Behaviour of Drop and Air in The Spray Tower

The results obtained from these studies have shown that a considerable amount of swirling of the drying air occurs in the spray tower. The swirl of the air increases with an increase in both the air flowrate and the flowrate of the liquid feed. The advantage of this turbulent action of the drying air in practical spray driers, is that the transfer coefficients between the droplets and air are increased and hence reduces the difference in air temperature from one section of the tower to the other.

The correlations proposed in section (5.2.5) could be used for predicting the volumes of the stirred tanks, plug-flow and by-pass stream sections at various operating conditions of the spray drier.

### 7.2.1 Residence-Time Analysis of Air

The volume of the various sections obtained for the different flow patterns existing in the spray tower were confirmed from the concentration profile of carbon dioxide tracer in the exit drying air. This was verified from the slope of the curve obtained when the plot of exit concentration versus, dimensionless time was plotted for each of the experiment. The curves generally had a gradual descent due to the high rate of mixing in the tower. The time taken to attain the maximum of the concentration-time curve varied from 12 to 25 seconds although this was dependent

upon the operating condition, as explained in section (5.3). When the probes were placed in the region of the by-pass stream close to the chamber wall however, a quicker response was obtained indicating that there was a shorter residence time of the air, unlike that for the well-stirred section. This was due to the channelling of the air to the tower exit. In practical cases however this must be reduced to a minimum as the by-pass stream generally leaves the drier without having made any contribution to the drying process.

#### 7.2.2 Residence-Time Analysis Of Liquid Spray

An important factor which must be taken into consideration in the design of spray driers are the flow patterns of the sprayed droplets. A review of the literature had shown that this has a great bearing on the properties of the dried products as a whole. It is essential in spray drier operation that the droplets should not hit the wall of the drying chamber before drying is complete when they will not stick to the wall. For this investigation, the Delavan hollow cone spray nozzle of known spray angle was used. The maximum spray angle of  $28^{\circ}$  was calculated from the position of the spray nozzle above the conical base in relation to the diameter of the spray tower, so that the sprayed droplets did not hit the cylindrical portion. This was done when no air was flowing in the tower.

As a result of the drag effect of the drying air on the sprayed droplets, it was found that the residence time

of the drops was longer at higher air flowrates for both water and sodium carbonate slurry. This is quite understandable since the sprayed droplets are much more influenced in the free-entrainment zone. The irregularity of points on the graph of exit concentration versus time, for the sodium carbonate slurry could be explained by the fact that some of the sprayed particles adhered to the conical section of the tower. The residence time for the sprayed droplets of sodium carbonate was therefore generally longer than that for pure water drops.



### 7.3 COMPARISON OF EXPERIMENTAL TECHNIQUES

From the work reported in the literature, no one has employed a similar technique for calculating the mass transfer coefficient  $K_G$ , on the drying of single drops containing dissolved and suspended solids. Froessling (5), Ranz and Marshall (1), Charlesworth and Marshall (10) and Trommelen and Crosby (25) carried out studies on the less complex situation of evaporation from single stationary liquid drops suspended from capillary glass tubes, or glass filaments, or the junction of a chromel-constantan thermocouple affixed to a special weighing balance. Although these techniques offered the advantage of being able to measure the weight loss of the drop as drying proceeded and hence the rate of mass transfer; the rate of heat transfer to the whole surface of the suspended drop could not be as uniform as when the drop was rotated. For example Ranz and Marshall (1), reported in their work on the evaporation of suspended single water drops from capillary glass tubes, that the rate of heat transfer was largest on the side facing the air stream as would be expected. They found that, at that position the temperature gradient was steepest and the isotherms were close together.

The investigation made by Audu (11), on single sodium sulphate drops, was based on the theory that mass transfer through the crust occurred by a diffusion mechanism. This theory however limits his analysis to low rates of heat and mass transfer; conditions prevailing at low values of



temperature difference. The analysis employed in this investigation was based on the theory that steam is ejected from the wet core of the particle as a result of the high rate of heat transfer through the crust walls. This hypothesis was confirmed by the occasional appearance of cracks and craters observed in the photomicrographs of crust as shown in plates 5.1 to 5.4. These must have resulted from pressure build-up in the drop and subsequent release of the steam through rupture and explosions of the crust. This is closely related to the conditions existing in spray driers.

Previous work by Place et al (65), Katta and Gauvin (64, 121) on the flow patterns of drops and air in spray driers have shown that an appreciable amount of swirling, stagnation and channelling of the drying air occurs in the tower, but to our knowledge no one has estimated the volumes of these sections. The interactions of these different flows were hitherto not well understood. The advantages of the swirling air had already been discussed in section (7.2). The advantages offered by the use of a P.V.C. spray tower for these studies gave the opportunity to make visual observation of the hydrodynamic behaviour of both the drops and air. Previous investigators (64,65,121) were only able to observe conditions in the spray tower through small sight glasses and postulate a flow model embodying the different sections from the analysis of the responses to tracer injection. In this study the alternative models giving almost the same response analysis have been

investigated by smoke injection, so that it has been possible to measure the actual volumes of the various sections and thereby evaluate the accuracy of the conventional tracer response technique.

## CHAPTER EIGHT

### CONCLUSIONS AND RECOMMENDATIONS

### 8.1. CONCLUSIONS

The main conclusions drawn from this investigation are presented as follows:-

#### 8.1.1. Single Crust-forming Sodium Sulphate Drops

- (1) The analysis of the stereoscan photomicrographs, shows that the porosity of the crust is independent of the drop diameter but dependent on the material being dried.
- (2) The crust thickness increases as the drop diameter decreases.
- (3) The mass transfer coefficient  $K_G$ , increases as the drop diameter increases. Hence the rate of mass transfer also increases with increasing drop diameter.
- (4) The appearance of ruptures and craters in the photomicrographs of the crust confirm that, at high rate of heat transfer through the crust, steam is ejected from the particle as a result of evaporation and pressure build-up inside the drop. This confirms that crystallisation and evaporation take place in the wet core of the particle.
- (5) Resistance to mass transfer is much more pronounced as the drop diameter decreases as would be expected.

#### 8.1.2. Flow Characteristics Of The Drops And Air In The Spray Tower

- (6) The volumes of the stirred-tank sections increase as the air flowrate increases, while the plug flow



volume decreases under the same condition. Thus the rate of transfer between the drops and air increases at higher air flowrates.

- (7) The stirred-tank volumes also increase with an increase in the liquid feed flowrate. This is due to the drag effect caused by the upflow of the drying air. Hence the rate of transfer between the two phases in the tower increases at higher liquid feed flowrates.
- (8) The volumes of the various flow patterns of the drying air in the tower can be correlated by the equations presented in Table 5.2.1.
- (9) The air residence-time could be predicted from equation (3.37), if the volumes of the various flow sections were known.
- (10) The experimental exit concentration of the tracer in air compare favourably with the predicted values. The standard deviation varied from  $1.76 \times 10^{-2}$  to  $1.83 \times 10^{-2}$ . This confirms the existence of a stirred-tank at the top and bottom of the tower, a plug flow in-between and a by-pass stream in the tower.
- (11) The residence time of the sprayed droplets increases as the flowrate of liquid feed decreases.
- (12) The residence time of the sprayed droplets increases as the air flowrate increases, at constant feed flowrate.

## 8.2. RECOMMENDATIONS

- (1) The mathematical model proposed in section (3.1) for calculating the mass transfer coefficient for crust-forming sodium sulphate drops, has been tested and found to be satisfactory. The model should be applied to other drops containing dissolved or suspended organic salts, detergent slurries, skim milk, coffee extract and other food products.
- (2) The model proposed in section (3.2), for predicting the exit concentration profile of a tracer in air, in the 9' x 4' diameter P.V.C. spray tower had been tested with water spray and found to be in good agreement with the experimental values. The model should be tested further with other feeds such as detergent formulations, food products and inorganic salts.
- (3) The present investigation had been carried out with a transparent spray tower. The work should be extended to a stainless steel tower of similar dimension operating under spray drying conditions. So that drying at high air temperature could be studied and compared with the results presented in this work.
- (4) The air residence-time in the tower had been determined by using carbon dioxide as tracer. The model could also be tested with other tracers such as helium or argon, and analysed by spectrometry method.

- (5) The liquid feed residence-time in the tower had been determined using iodine solution in potassium iodide. Future work on the residence time distribution of the sprayed droplets should be carried out using a suitable dye as tracer. The exit concentration should then be obtained much faster by colourimetry.
- (6) The effect of drying in high-humid medium such as steam or superheated vapours should be studied in the stainless steel tower.
- (7) The internal and external structural analysis, porosity and crust thickness measurements had been obtained from the stereoscan photomicrographs for single drops. This analysis should be extended to dried products obtained from the stainless steel tower at the high air temperature. The effect of the various operating conditions on the properties of the dried products should then be investigated.
- (8) The correlations proposed in section 5.2.5, for predicting the volumes of the various sections in the tower, had been based on the experimental data obtained from two spray drying towers. Future work should be extended to spray drying towers of different  $Z/D$  ratio.

## APPENDICES



APPENDIX A

- (i) Tables A1-A6: Data for evaluating The Momentum Heat Transfer Model for aqueous Sodium Sulphate Decahydrate ( $\text{Na}_2\text{CO}_4 \cdot 10\text{H}_2\text{O}$ ) Drops.
- (ii) Honeywell H316 'Basic 16' Computer Program for evaluating the Mass Transfer Coefficient,  $K_G$ .

TABLE A1

Air Temperature Upstream $\theta_{au}$	= 111 °C
Air Temperature Downstream $\theta_{ad}$	= 98 °C
Drop Temperature $\theta_d$	= 68 °C
External Drop Diameter $d_p$	= $0.2 \times 10^{-2}$ m
Air Flowrate G	= $0.577 \times 10^{-3}$ kg/s
Porosity, $\epsilon'$	= 0.334
Crust thickness $\phi$	= $0.133 \times 10^{-3}$ m

Time, t (s)	HUMIDITIES (kg/kg)		
	Hu x 10 <sup>3</sup> Upstream	Hd x 10 <sup>3</sup> Downstream	Hs Saturation
300	0.132	0.334	0.040
600	0.132	0.279	0.040
900	0.132	0.250	0.040
1200	0.130	0.196	0.040
1500	0.130	0.164	0.040
1800	0.130	0.152	0.040

TABLE A2

Air Temperature Upstream $\theta_{au}$	= 111 °C
Air Temperature Downstream $\theta_{ad}$	= 98 °C
Drop Temperature $\theta_d$	= 67.5 °C
External Drop Diameter $D_p$	= $0.4 \times 10^{-2}$ m
Air Flowrate G	= $0.577 \times 10^{-3}$ kg/s
Porosity, $\epsilon'$	= 0.310
Crust thickness $\phi$	= $0.12 \times 10^{-3}$ m

Time, t (s)	HUMIDITIES (kg/kg)		
	$H_u \times 10^3$ Upstream	$H_d \times 10^3$ Downstream	$H_s$ Saturation
300	0.147	0.425	0.039
600	0.147	0.387	0.039
900	0.147	0.312	0.039
1200	0.147	0.276	0.039
1500	0.146	0.215	0.039
1800	0.146	0.193	0.039

TABLE A3

Air Temperature Upstream $\theta_{au}$	= 111 °C
Air Temperature Downstream $\theta_{ad}$	= 97 °C
Drop Temperature $\theta_d$	= 68.5 °C
External Drop Diameter $D_p$	= $0.5 \times 10^{-2}$ m
Air Flowrate G	= $0.577 \times 10^{-3}$ kg/s
Porosity, $\epsilon'$	= 0.306
Crust Thickness, $\phi$	= $0.115 \times 10^{-3}$ m

Time, t (s)	HUMIDITIES (kg/kg)		
	Hu x 10 <sup>3</sup> Upstream	Hd x 10 <sup>3</sup> Downstream	Hs Saturation
300	0.156	0.483	0.041
600	0.157	0.426	0.041
900	0.156	0.381	0.041
1200	0.156	0.334	0.041
1500	0.155	0.296	0.041
1800	0.155	0.243	0.041



TABLE A4

Air Temperature Upstream $\theta_{au}$	= 111 °C
Air Temperature Downstream $\theta_{ad}$	= 98 °C
Drop Temperature $\theta_d$	= 68 °C
External Drop Diameter $D_p$	= $0.6 \times 10^{-2}$ m
Air Flowrate G	= $0.577 \times 10^{-3}$ kg/s
Porosity, $\epsilon'$	= 0.321
Crust Thickness, $\phi$	= $0.096 \times 10^{-3}$ m

Time, t (s)	HUMIDITIES (kg/kg)		
	Hu x 10 <sup>3</sup> Upstream	Hd x 10 <sup>3</sup> Downstream	Hs Saturation
300	0.158	0.501	0.040
600	0.157	0.501	0.040
900	0.157	0.492	0.040
1200	0.158	0.431	0.040
1500	0.158	0.376	0.040
1800	0.158	0.290	0.040

Experiment for the measurement of the thermal conductivity by the use of the Lees' disc apparatus described in Section 4.4.1.

TABLE A5

Room Temperature  $\theta_{amb} = 23.0\text{ }^{\circ}\text{C}$

Thickness of Specimen  $t' = 0.5 \times 10^{-3}\text{m}$

Time (Mins.)	Voltage $V'$ (volts)	Current $I$ (amp)	Temperature of Disc 1 ( $^{\circ}\text{C}$ ) $\theta_1$	Temperature of Disc 2 ( $^{\circ}\text{C}$ ) $\theta_2$	Temperature of Disc 3 ( $^{\circ}\text{C}$ ) $\theta_3$
0	5.8	3.0	23.0	23.0	23.0
5	5.8	3.0	52.0	39.8	35.6
10	3.8	2.0	58.6	46.8	44.0
15	3.8	2.0	61.6	51.8	49.0
20	3.8	2.0	65.0	56.0	53.0
25	3.8	2.0	67.5	59.2	56.4
30	3.8	2.0	70.2	62.0	59.2
35	3.8	2.0	72.4	64.7	61.8
40	3.8	2.0	74.3	66.6	63.6
45	3.8	2.0	75.8	68.0	65.2
50	3.8	2.0	77.1	69.6	66.2
55	3.8	2.0	78.0	70.6	67.7
60	3.8	2.0	79.0	71.6	68.7
70	3.8	2.0	80.0	73.0	70.0
80	3.8	2.0	81.0	73.9	70.7
90	3.8	2.0	81.2	74.4	71.4

From the Basic 16 Computational Program shown in the appendix, the following results were obtained for the Sodium Sulphate Decahydrate drops.

TABLE A6

Drop Diameter $D_p \times 10^2 \text{ m}$	Amount of Water Evap. $W \times 10^3$ (kg)	Calc. Value of $W \times 10^3$ (kg)	Mass-Trans. Coefficient $K_G \times 10^3$ (m/s)
0.6	0.430	0.244	51.736
0.5	0.255	0.194	30.654
0.4	0.155	0.140	18.693
0.2	$0.338 \times 10^{-1}$	0.093	4.069

## LIST

```

10  REM  DRYING OF SINGLE DROPS
20  DIM R(10),T(10),P(10),K(10)
30  READ A1,A2,A3,A4,Q1,Q2,Q3,Q4,Q5,Q,V,I,T1,T,D1,L,D,F,P1,P2,D2
40  E=V*I/(A1*(Q1-Q)+A2*(Q2-Q)+A4*((Q2+Q3)/2-Q)+A3*(Q3-Q))
50  K=E*T/(Q2-Q3)*A4*(A4/2*((Q2+Q3)/2-Q)+A3*(Q3-Q))
60  N=4
70  FOR I=1,N
80  READ R(I),T(I),P(I),K(I)
90  H(I)=K*2*3.142*R(I)+2*(Q4-Q5)*(1-P(I))/T(I)
100 W(I)=K*2*3.142*R(I)+2*(Q4-Q5)*(1-P(I))/T(I)*L
110 U(I)=((.25*F)*(D2/T(I)*D)*(P1-P2))+.5
120 Y(I)=U(I)*D*K(I)*3.142*D2+2
130 K(I)=W(I)*.1/(3.142*D2+2*(P1-P2))
140 NEXT I
150 PRINT : PRINT
160 PRINT "WATER EVAP ","MASS TRANS COEFF."
165 PRINT "(KG) ","(M/S*10+3)"
170 PRINT : PRINT
180 FOR I=1,N
190 PRINT W(I),K(I)
200 NEXT I
210 END
220 STOP
230 DATA .401E-02,.2E-02,.401E-02,.429E-04,81.2,74.4
240 DATA 71.4,111,68,23,3.8,2,.126E-01,.5E-03,.506E-01,1256.04
250 DATA .893,.964E-02,689.4,27.576,.2E-04
260 DATA .3E-02,.96E-04,.321,400,.25E-02,.115E-03,.306,347,.2E-02
270 DATA .12E-03,.31,256,.1E-02,.133E-03,.334,179

```

?RUN

WATER EVAP (KG)	MASS TRANS COEFF. (M/S*10+3)
--------------------	---------------------------------

.430332E-03	51.7362
.254979E-03	30.6546
.155486E-03	18.6931
.33852E-04	4.06983

210 EXIT

?

Typical Computer Program For Calculating  
The Mass Transfer Coefficient



APPENDIX B

- (i) Tables B1-B10: Data for the Estimation of the Volumes.
- (ii) Dimensional Analysis
- (iii) ICL 1900 'Statistical Analysis' Computer Package for correlating the equation:

$$\frac{V_i}{\Sigma V} = \psi \text{ (Re)}^d \cdot \left( \frac{\mu_1}{\mu_g} \right)^f \cdot \left( \frac{U_1}{U_g} \right)^e \cdot \left( \frac{Z}{D} \right)^g$$

TABLE B1

Water Spray at  $1.50 \times 10^{-3}$  l/sAir Temperature  $T_a$  at  $31.0^\circ\text{C}$ Feed Temperature  $T_w$  at  $17.5^\circ\text{C}$ 

$Q_3$ ( $\text{m}^3/\text{s}$ )	$Q_1$ ( $\text{m}^3/\text{s}$ )	$Q_2$ ( $\text{m}^3/\text{s}$ )	$\beta$	$V_1$ ( $\text{m}^3$ )	$V_2$ ( $\text{m}^3$ )	$V_3$ ( $\text{m}^3$ )	$V_4$ ( $\text{m}^3$ )	$V_T$ ( $\text{m}^3$ )	$V_1+V_2+V_3$ ( $\text{m}^3$ )
0.13	0.079	0.057	0.610	0.566	0.410	1.250	1.424	3.650	2.226
0.16	0.101	0.059	0.630	0.640	0.405	1.252	1.350	3.650	2.300
0.19	0.123	0.067	0.650	0.760	0.350	1.262	1.278	3.650	2.372
0.21	0.145	0.065	0.690	0.902	0.310	1.306	1.132	3.650	2.518
0.23	0.166	0.064	0.720	1.092	0.205	1.331	1.022	3.650	2.628

TABLE B2

Water Spray at  $2.0 \times 10^{-3}$  l/sAir Temperature  $T_a$  at  $31.0^\circ\text{C}$ Feed Temperature  $T_w$  at  $18.0^\circ\text{C}$ 

$Q_3$ ( $\text{m}^3/\text{s}$ )	$Q_1$ ( $\text{m}^3/\text{s}$ )	$Q_2$ ( $\text{m}^3/\text{s}$ )	$\beta$	$V_1$ ( $\text{m}^3$ )	$V_2$ ( $\text{m}^3$ )	$V_3$ ( $\text{m}^3$ )	$V_4$ ( $\text{m}^3$ )	$V_T$ ( $\text{m}^3$ )	$V_1+V_2+V_3$ ( $\text{m}^3$ )
0.13	0.081	0.049	0.620	0.603	0.398	1.262	1.387	3.650	2.263
0.16	0.102	0.058	0.640	0.684	0.386	1.266	1.314	3.650	2.336
0.19	0.123	0.067	0.650	0.764	0.347	1.271	1.278	3.650	2.372
0.21	0.147	0.063	0.700	0.926	0.304	1.325	1.095	3.650	2.555
0.23	0.166	0.064	0.720	1.092	0.201	1.335	1.022	3.650	2.628

TABLE B3

Water Spray at  $2.50 \times 10^{-3}$  l/sAir Temperature  $T_a$  at  $31.0^\circ\text{C}$ Feed Temperature  $T_w$  at  $18.0^\circ\text{C}$ 

$Q_3$ ( $\text{m}^3/\text{s}$ )	$Q_1$ ( $\text{m}^3/\text{s}$ )	$Q_2$ ( $\text{m}^3/\text{s}$ )	$\beta$	$V_1$ ( $\text{m}^3$ )	$V_2$ ( $\text{m}^3$ )	$V_3$ ( $\text{m}^3$ )	$V_4$ ( $\text{m}^3$ )	$V_T$ ( $\text{m}^3$ )	$V_1+V_2+V_3$ ( $\text{m}^3$ )
0.130	0.081	0.049	0.620	0.607	0.392	1.264	1.387	3.650	2.263
0.160	0.104	0.056	0.650	0.719	0.381	1.272	1.278	3.650	2.372
0.190	0.127	0.063	0.670	0.817	0.345	1.283	1.205	3.650	2.445
0.210	0.147	0.063	0.700	0.929	0.290	1.336	1.095	3.650	2.555
0.230	0.168	0.062	0.730	1.116	0.200	1.348	0.986	3.650	2.664



TABLE B4

Water Spray at  $3.0 \times 10^{-3}$  l/s  
 Air Temperature  $T_a$  at  $31.0^\circ\text{C}$   
 Feed Temperature  $T_w$  at  $18.0^\circ\text{C}$

$Q_3$ ( $\text{m}^3/\text{s}$ )	$Q_1$ ( $\text{m}^3/\text{s}$ )	$Q_2$ ( $\text{m}^3/\text{s}$ )	$\beta$	$V_1$ ( $\text{m}^3$ )	$V_2$ ( $\text{m}^3$ )	$V_3$ ( $\text{m}^3$ )	$V_4$ ( $\text{m}^3$ )	$V_T$ ( $\text{m}^3$ )	$V_1+V_2+V_3$ ( $\text{m}^3$ )
0.130	0.082	0.048	0.630	0.642	0.388	1.269	1.351	3.650	2.299
0.160	0.104	0.056	0.650	0.723	0.374	1.275	1.278	3.650	2.372
0.190	0.129	0.061	0.680	0.852	0.336	1.294	1.168	3.650	2.482
0.210	0.149	0.061	0.710	0.971	0.279	1.341	1.059	3.650	2.591
0.230	0.168	0.062	0.730	1.120	0.194	1.350	0.986	3.650	2.664

TABLE B5

Water Spray at  $3.50 \times 10^{-3}$  l/sAir Temperature  $T_a$  at  $31.5^\circ\text{C}$ Feed Temperature  $T_w$  at  $18.5^\circ\text{C}$ 

$Q_3$ ( $\text{m}^3/\text{s}$ )	$Q_1$ ( $\text{m}^3/\text{s}$ )	$Q_2$ ( $\text{m}^3/\text{s}$ )	$\beta$	$V_1$ ( $\text{m}^3$ )	$V_2$ ( $\text{m}^3$ )	$V_3$ ( $\text{m}^3$ )	$V_4$ ( $\text{m}^3$ )	$V_T$ ( $\text{m}^3$ )	$V_1+V_2+V_3$ ( $\text{m}^3$ )
0.130	0.082	0.048	0.630	0.642	0.384	1.273	1.351	3.650	2.299
0.160	0.106	0.054	0.660	0.762	0.371	1.276	1.241	3.650	2.409
0.190	0.129	0.061	0.680	0.853	0.330	1.299	1.168	3.650	2.482
0.210	0.151	0.059	0.720	1.012	0.265	1.351	1.022	3.650	2.628
0.230	0.170	0.060	0.740	1.149	0.189	1.363	0.949	3.650	2.701

TABLE B6

Water Spray at  $1.50 \times 10^{-3}$  l/s;  $T_w = 17.5^\circ\text{C}$ 

G (kg/s)	Re $\times 10^{-3}$	$\Sigma V = V_T$ ( $\text{m}^3$ )	$V_1$ $\frac{\quad}{\Sigma V}$	$V_2$ $\frac{\quad}{\Sigma V}$	$V_3$ $\frac{\quad}{\Sigma V}$	$V_4$ $\frac{\quad}{\Sigma V}$	$\frac{\rho_g U_g}{\rho_1 U_1} \times 10^{-3}$
0.13	8.006	3.650	0.155	0.112	0.341	0.390	0.087
0.16	9.854	3.650	0.175	0.110	0.343	0.369	0.107
0.19	11.701	3.650	0.208	0.095	0.346	0.350	0.127
0.21	12.933	3.650	0.246	0.085	0.358	0.310	0.140
0.23	14.165	3.650	0.298	0.056	0.364	0.280	0.154

TABLE B7

Water Spray at  $2.00 \times 10^{-3}$  l/s;  $T_w = 18.0$  °C

G (kg/s)	Re $\times 10^{-3}$	$\Sigma V = V_T$ (m <sup>3</sup> )	$V_1$ $\Sigma V$	$V_2$ $\Sigma V$	$V_3$ $\Sigma V$	$V_4$ $\Sigma V$	$\rho_g U_g$ $\rho_l U_l \times 10^{-3}$
0.13	8.006	3.650	0.164	0.109	0.346	0.380	0.065
0.16	9.854	3.650	0.186	0.106	0.347	0.359	0.080
0.19	11.701	3.650	0.208	0.094	0.348	0.350	0.095
0.21	12.933	3.650	0.253	0.083	0.363	0.300	0.105
0.23	14.165	3.650	0.298	0.055	0.366	0.280	0.115



TABLE B8

Water Spray at  $2.50 \times 10^{-3}$  l/s;  $T_w = 18.0$  °C.

G (kg/s)	Re $\times 10^{-3}$	$\Sigma V = V_T$ (m <sup>3</sup> )	$V_1$ $\frac{V_1}{\Sigma V}$	$V_2$ $\frac{V_2}{\Sigma V}$	$V_3$ $\frac{V_3}{\Sigma V}$	$V_4$ $\frac{V_4}{\Sigma V}$	$\frac{\rho_g U_g}{\rho_l U_l} \times 10^{-3}$
0.13	8.006	3.650	0.166	0.106	0.346	0.380	0.032
0.16	9.854	3.650	0.197	0.104	0.348	0.350	0.064
0.19	11.701	3.650	0.224	0.093	0.351	0.330	0.076
0.21	12.933	3.650	0.253	0.078	0.366	0.300	0.084
0.23	14.165	3.650	0.305	0.055	0.369	0.270	0.092

TABLE B9

Water Spray at  $3.0 \times 10^{-3}$  l/s;  $T_w = 18.0^\circ\text{C}$ 

G (kg/s)	$\text{Re} \times 10^{-3}$	$\Sigma V = V_T$ (m <sup>3</sup> )	$\frac{V_1}{\Sigma V}$	$\frac{V_2}{\Sigma V}$	$\frac{V_3}{\Sigma V}$	$\frac{V_4}{\Sigma V}$	$\frac{\rho_g U_g}{\rho_l U_l} \times 10^{-3}$
0.13	8.006	3.650	0.175	0.106	0.348	0.370	0.043
0.16	9.854	3.650	0.198	0.102	0.349	0.350	0.053
0.19	11.701	3.650	0.232	0.092	0.354	0.320	0.063
0.21	12.933	3.650	0.266	0.076	0.367	0.290	0.070
0.23	14.165	3.650	0.306	0.053	0.370	0.270	0.077

TABLE B10

Water Spray at  $3.50 \times 10^{-3}$  l/s;  $T_w = 18.5$  °C

G (kg/s)	Re $\times 10^{-3}$	$\Sigma V = V_T$ (m <sup>3</sup> )	$V_1$ $\Sigma V$	$V_2$ $\Sigma V$	$V_3$ $\Sigma V$	$V_4$ $\Sigma V$	$\frac{\rho_g U_g}{\rho_l U_l} \times 10^{-3}$
0.13	8.006	3.650	0.175	0.105	0.349	0.370	0.037
0.16	9.854	3.650	0.207	0.102	0.350	0.340	0.046
0.19	11.701	3.650	0.234	0.088	0.356	0.320	0.054
0.21	12.933	3.650	0.277	0.072	0.370	0.280	0.060
0.23	14.165	3.650	0.315	0.052	0.373	0.259	0.066

### Dimensional Analysis

A dimensional analysis, was undertaken to correlate the volume  $V_i$ , of each section  $i$ , in the tower, as a fraction of the total effective volume  $V$ , in terms of dimensionless groups (118) as follows:-

$$\text{If } \frac{V_i}{\Sigma V} = f(\rho, U_g, D, \mu_g, U_1, \mu_1, Z)$$

This could also be written in the form,

$$F_1 = f(\rho^a, U_g^b, D^c, \mu_g^d, U_1^e, \mu_1^f, Z^g) \quad (1)$$

$$F_2 = C \left( \frac{M}{L^3} \right)^a \left( \frac{L}{T} \right)^b \left( L \right)^c \left( \frac{M}{LT} \right)^d \left( \frac{L}{T} \right)^e \left( \frac{M}{LT} \right)^f \left( L \right)^g$$

For terms with M;

$$0 = a + d + f \quad (2)$$

For terms with L;

$$0 = -3a + b + c - d + e - f + g \quad (3)$$

For terms with T;

$$0 = -b - d - e - f \quad (4)$$

Giving 3 equations with 7 unknowns



From equation (2)

$$a = - (d + f) \quad (5)$$

From equation (3)

$$c = 3a - b + d - e + f - g \quad (6)$$

From equation (4)

$$b = - (d + e + f) \quad (7)$$

substituting for a and b in equation (6) therefore,

$$c = - (d + f + g)$$

From equation (1)

$$\text{Therefore } F_1 = C \left\{ \rho^{-(d+f)} \cdot U_g^{-(d+e+f)} \cdot D^{-(d+f+g)} \cdot \mu_g^d \cdot U_1^e \cdot \mu_1^f \cdot Z^g \right\}$$

Grouping them together

$$\text{Therefore } \frac{V_i}{\Sigma V} = \psi \left( \frac{\mu_g}{\rho U_g D} \right)^d \left( \frac{\mu_1}{\mu_g} \right)^f \left( \frac{U}{U_g} \right)^e \left( \frac{Z}{D} \right)^g$$

$$\text{Therefore } \frac{V_i}{\Sigma V} = \psi (Re)^{-d} \left( \frac{\mu_1}{\mu_g} \right)^f \left( \frac{U_1}{U_g} \right)^e \left( \frac{Z}{D} \right)^g$$

The ICL 1900 statistical analysis computer package was then used to evaluate the values of  $\psi$ ,  $d$ ,  $f$ ,  $e$  and  $g$ . A typical program used for the correlation is included in the appendix.

A TYPICAL COMPUTER PROGRAM FOR CORRELATING THE VOLUMES

2	#####	#	#####	#####	UUUUUUUUUUUUUUUUUUUUUUUUUUUUUU
	.	#	#	#	UUUU
4	..	#	#	#	UUUU
	#####	#####	#####	#####	UUUU
6	#	#	#	#	UUUU
	#	#	#	#	UUUU
8	#####	#####	#####	#####	UUUUUUUUUUUUUUUUUUUUUUUUUUUUUU

10 #LISTING OF :ECP2658.ADE-JOHN(1/B1B0) PRODUCED ON 8SEP76

12 #G8.42F AT ASTON IN: ECP2658, ADE-JOHN: ON 8SEP76 AT 10

14 DOCUMENT : ECP2658, ADE-JOHN(1B1B0)

16 STARTED :ECP2658,ADE-JOHN, 8SEP70 16.43.44 TYPE:BACK IO

18 16.43.44+ JGB : ECP2628.ADE-JOHN,JD(JT 60,MZ 20000)

20

16/4/42 08/09/76 ICL 1900 STATISTICAL ANALYSIS  
2 = PROBLEM NAME IS TISS 1

DATA ON CARDS

4 OUTPUT FILE NAME IS: ICL STATFILE

REEL SEQUENCE NUMBER IS

6 FILE GENERATION NUMBER IS

RETENTION PERIOD IS

8 OBSERVATION MATRIX TIMEM1

WEIGHTS ARE NOT USED

10 COL NAMES TIME M1

10 - GOLD - DIMVOL

12

DENSIL

14 DIAMETER

14 DIAMETER  
HEIGHT

16

VISCOI

18

VELOC  
VELOC

20. NUMBER OF COL NAMES IS 9

20 NUMBER OF VEC NAMES 13  
MATRIX 6 TIME M1

22 TRANSFORMATIONS      TIME1      SQUARE      TIME2

DIMVOL=DIMVOL

24 DIM EN=(DENSIL)/(DENSIG)

```

DIMVEL=(VELOCL)/(VELOC6)

```

26 DIMVIS=(VISCOL)/(VISCOG)

```
REYNOL=((DENSIG)*(VELOCG)*(PIAIDTR))/(VISCOG)
```

28 DIM LEN=(HEIGHT)/(DIAMTR)

```

20 DIM VOL=(HEIGHT)/2
  DEMVOL=ALOG(DIMVOL)

```

```
30 DEMDEN=ALOG(DIMDEN)
```

```
DEMVEL=ALOG(DIMVEL)
```

```

32      DEMVIS=ALOG(DIMVIS)

```

DEMSEY=ALOG(REYNOL)

```
34      DEMLN=ALOG(DIMLEN)
```

NUMBER OF TRANSFORMATIONS 0012

```

36 PRINT OBSERVATIONS

```



16/45/29 08/09/76 ICL 1900 STATISTICAL ANALYSIS XDS3/25

OBSERVATION MATRIX TIMEM1

	R01	R02	R03	R04	R05	R06
2	CONST	1	100000E	1	100000E	1
4	DIMVOL	0	208000E	0	298000E	0
6	DENSIG	0	993000E	0	986000E	0
8	DENSIL	4	100000E	4	100000E	3
10	DIAHTR	1	121600E	1	121600E	1
12	HEIGHT	1	273600E	1	273600E	1
14	VISCOG	3	165000E	3	161000E	3
16	VISCOL	2	100000E	2	100000E	3
	VELOC	1	765000E	1	765000E	2
	VELUCG	0	162500E	0	197200E	0

16/45/30 08/09/76 ICL 1900 STATISTICAL ANALYSIS XDS3/25

OBSERVATION MATRIX TIMEM1

	R07	R08	R09	R10	R11	R12
2	CONST	1	100000E	1	100000E	1
4	DIMVOL	0	208000E	0	166000E	0
6	DENSIG	0	993000E	0	908000E	0
8	DENSIL	3	999000E	3	997000E	3
10	DIAHTR	1	121600E	1	121600E	1
12	HEIGHT	1	273600E	1	273600E	1
14	VISCOG	3	165000E	3	170000E	3
16	VISCOL	3	980000E	3	970000E	3
	VELOC	2	101700E	2	127500E	2
	VELUCG	0	162500E	0	111300E	0



16/45/30 08/09/76 ICL 1900 STATISTICAL ANALYSIS XDS3/25

OBSERVATION MATRIX TIME#1

	R13	R14	R15	R16	R17	R18
2						
4						
6						
8						
10						
12						
14						
16						
CONST	100000E	100000E	100000E	100000E	100000E	100000E
DIMVOL	224000E	253000E	305000E	175000E	198000E	232000E
DENSIG	993000E	980000E	986000E	998000E	996000E	993000E
DENSIL	997000E	997000E	997000E	993000E	993000E	993000E
DIAHTR	121600E	121600E	121600E	121600E	121600E	121600E
HEIGHT	273600E	273600E	273600E	273600E	273600E	273600E
VISLOG	165000E	163000E	161000E	170000E	168000E	165000E
VISCOL	970000E	970000E	970000E	940000E	940000E	940000E
VELUCL	127500E	127500E	127500E	152700E	152700E	152700E
VELUCG	162500E	180000E	197200E	111500E	136600E	162500E

16/45/30 08/09/76 ICL 1900 STATISTICAL ANALYSIS XDS3/25

OBSERVATION MATRIX TIME#1

	R19	R20	R21	R22	R23	R24
2						
4						
6						
8						
10						
12						
14						
16						
CONST	100000E	100000E	100000E	100000E	100000E	100000E
DIMVOL	266000E	306000E	175000E	207000E	234000E	277000E
DENSIG	989000E	986000E	998000E	996000E	995000E	989000E
DENSIL	993000E	993000E	991000E	991000E	991000E	991000E
DIAHTR	121600E	121600E	121600E	121600E	121600E	121600E
HEIGHT	273600E	273600E	273600E	273600E	273600E	273600E
VISLOG	163000E	161000E	170000E	165000E	165000E	163000E
VISCOL	940000E	940000E	920000E	920000E	920000E	920000E
VELUCL	152700E	152700E	178300E	178300E	178300E	170300E
VELUCG	180000E	197200E	111500E	156600E	162500E	180000E

XDS3/25

ICL 1900 STATISTICAL ANALYSIS

08/09/76

16/45/30

OBSERVATION MATRIX TIMEM1

R25

1	CONST	.100000E
2	DIMJOL	.315000E
3	DENIG	.986000E
4	DENSIL	.991000E
5	DIANTR	.121600E
6	HEIGHT	.273600E
7	VISLOG	.161000E
8	VISCOL	.920000E
9	VELUCL	.178300E
10	VELUGG	.197200E

TOTAL NUMBER OF OBSERVATIONS = 25

	CROSS PRODUCT	TIMEM2	CROSS PRODUCT IS	TIMEM2
20				
22				
24				
26				
28				
30				
32				
34				
36				

PRINT CORRELATION



16/46/17 08/09/76 ICL 1900 STATISTICAL ANALYSIS XDS3/25

# CORRELATION MATRIX

	DIMVOL	DINDEN	DIMVEL	DIMVIS	REYNOL	DIMLEN
2	.100000E 1	.658994E 0	-.396032E 0	.584414E 0	.959602E 0	.000000E 0
4	.658994E 0	.100000E 1	-.912475E 0	.940046E 0	.774187E 0	.000000E 0
6	-.396032E 0	-.912475E 0	.100000E 1	-.964974E 0	-.582096E 0	.000000E 0
8	.584414E 0	.940046E 0	-.964974E 0	.100000E 1	.551178E 0	.000000E 0
10	.959682E 0	.774187E 0	-.582096E 0	.551178E 0	.100000E 1	.000000E 0
12	.000000E 0	.000000E 0	.000000E 0	.000000E 0	.000000E 0	.100000E 1
14	.995635E 0	.651618E 0	-.397247E 0	.380659E 0	.970407E 0	.000000E 0
16	.658605E 0	.100000E 1	-.913202E 0	.940214E 0	.774128E 0	.000000E 0
18	-.378891E 0	-.912502E 0	.978855E 0	-.976423E 0	-.560949E 0	.000000E 0
20	.382742E 0	.939655E 0	-.967594E 0	.999808E 0	.550425E 0	.000000E 0
22	.959638E 0	.759409E 0	-.588927E 0	.542833E 0	.996177E 0	.000000E 0
24	.000000E 0	.000000E 0	.000000E 0	.000000E 0	.000000E 0	.000000E 1

213

16/46/18 08/09/76 ICL 1900 STATISTICAL ANALYSIS XDS3/25

# CORRELATION MATRIX

	DEMVOL	DENDEN	DEMVEL	DEMVIS	DEMREY	DEMLEN
2	.995635E 0	.658605E 0	-.378891E 0	.582742E 0	.939638E 0	.000000E 0
4	.651618E 0	.100000E 1	-.912302E 0	.939655E 0	.759409E 0	.000000E 0
6	-.397247E 0	-.912502E 0	.978855E 0	-.967594E 0	-.588927E 0	.000000E 0
8	.380659E 0	.940214E 0	-.976423E 0	.999808E 0	.545833E 0	.000000E 0
10	.970407E 0	.774128E 0	-.560949E 0	.550425E 0	.996177E 0	.000000E 0
12	.000000E 0	.000000E 0	.000000E 0	.000000E 0	.000000E 0	.000000E 1
14	.100000E 1	.651251E 0	-.380299E 0	.578670E 0	.957368E 0	.000000E 0
16	.651251E 0	.100000E 1	-.912493E 0	.939679E 0	.759457E 0	.000000E 0
18	-.580299E 0	-.912493E 0	.100000E 1	-.972237E 0	-.565527E 0	.000000E 0
20	.378870E 0	.939879E 0	-.975237E 0	.100000E 1	.545443E 0	.000000E 0
22	.957368E 0	.759457E 0	-.563527E 0	.545443E 0	.100000E 1	.000000E 0
24	.000000E 0	.000000E 0	.000000E 0	.000000E 0	.000000E 0	.100000E 1

# REGRESSION ANALYSIS

XDS3/25

ICL 1900 STATISTICAL ANALYSIS

08/09/76

16/46/28

REGRESSION ANALYSIS

2 REGRESSION ANALYSIS COVA TIME2 CUT OFF PARAMETER .100000E-5

4 DEPENDENT VARIABLE DEMVOL DEGREES OF FREEDOM 21

6 INDEPENDENT VARIABLES AT SIGNIFICANT LEVEL 98.99 %

8 DEMDEN DEMVEL DEMVIS DEMREY DEMLPN

10 VARIABLES IN THE REGRESSION SET

12

14 VAR	16 NAME	REGRESSION	COEFF	STANDARD	ERROR	CONFIDENCE	INTERVAL	T STAT	PART	CORR	MULTIPLE	CORRELATION	E S S
18 DEMVEL		0.2895764		.124597E-0		2.32		0.45	0.973		.637888E-1		
20 DEMVIS		1.5509747		.124449E-1		1.25		0.26	0.977		.544970E-1		
22 DEMREY		1.0790825		.542966E-1		19.87		0.97	0.382		.100503E-1		



VAR NAME	T STAT	PART CORR	MULTIPLE CORRELATION	E S S
28 DIMVOL	20.07	0.98	0.999	.239951E-2
30 DIMDEN	4.89	0.74	0.990	.230908E-1
32 DIMVEL	2.45	0.48	0.983	.389995E-1
34 DIMVIS	2.69	0.51	0.984	.572910E-1
36 REYNOL	8.22	0.88	0.995	.115906E-1
38 DIMLEN	0.00		0.952	.109519E 0
40 DEMDEN	4.81	0.73	0.990	.235408E-1
42 DEMLEN	0.00		0.835	.355597E 0
44 E.S.S.				.507583E-1
46 RESIDUAL ERROR				.491539E-1
48 MULT CORR				0.978
50 INTERCEPT TERM				13.0765288
52				

APPENDIX C

- (i) Tables C1-C25: Air Residence-Time Distribution in Spray Tower.
- (ii) Honeywell H316 'GRASP' Computer Program for Predicting the exit concentration of CO<sub>2</sub> tracer in Air.
- (iii) Tables D1-D5: Residence-Time Distribution for Water Spray.
- (iv) Table E1: Residence-Time Distribution for sprayed Droplets of Sodium Carbonate Decahydrate (Na<sub>2</sub>CO<sub>3</sub> · 10H<sub>2</sub>O) Slurries.
- (v) Honeywell H316 'Basic 16' Computer Program for Testing the Spray Tower Design Model.

TABLE C1Water Spray at  $1.50 \times 10^{-3}$  l/s

Air Flowrate at 0.13 kg/s

Air Temperature  $T_a$  at 31.0 °CFeed Temperature  $T_w$  at 17.5 °C

Time (s)	Dimensionless Time ( $\theta$ )	Exit Concentration $C(\theta)$ (V%)	
		Calculated	Experimental
0	0.0	0.0	0.0
5	0.178	0.184	0.170
10	0.356	0.318	0.275
15	0.534	0.388	0.335
20	0.712	0.417	0.370
25	0.890	0.419	0.395
30	1.068	0.405	0.400
35	1.247	0.383	0.390
40	1.425	0.356	0.370
45	1.603	0.328	0.345
50	1.781	0.301	0.320
55	1.959	0.276	0.290
60	2.137	0.252	0.260
65	2.315	0.232	0.235
70	2.493	0.213	0.215
75	2.671	0.197	0.190
80	2.849	0.184	0.180
85	3.027	0.172	0.160
90	3.205	0.162	0.150
95	3.384	0.154	0.135
100	3.562	0.147	0.125

TABLE C2Water Spray at  $1.50 \times 10^{-3}$  l/s

Air Flowrate at 0.16 kg/s

Air Temperature  $T_a$  at 31.0 °CFeed Temperature  $T_w$  at 17.5 °C

Time (s)	Dimensionless Time ( $\theta$ )	Exit Concentration $C(\theta)$ (V%)	
		Calculated	Experimental
0	0.0	0.0	0.0
5	0.219	0.252	0.210
10	0.438	0.399	0.340
15	0.657	0.455	0.400
20	0.877	0.460	0.430
25	1.096	0.438	0.440
30	1.315	0.403	0.430
35	1.534	0.365	0.395
40	1.753	0.328	0.360
45	1.973	0.294	0.325
50	2.192	0.264	0.295
55	2.411	0.238	0.260
60	2.630	0.217	0.230
65	2.849	0.199	0.210
70	3.068	0.185	0.190
75	3.288	0.173	0.170
80	3.507	0.164	0.155
85	3.726	0.157	0.145
90	3.945	0.151	0.130
95	4.164	0.146	0.125
100	4.383	0.142	0.115



TABLE C3Water Spray at  $1.50 \times 10^{-3}$  l/s

Air Flowrate at 0.19 kg/s

Air Temperature  $T_a$  at  $31.0^\circ\text{C}$ Feed Temperature  $T_w$  at  $17.5^\circ\text{C}$ 

Time (s)	Dimensionless Time ( $\theta$ )	Exit Concentration $C(\theta)$ (V%)	
		Calculated	Experimental
0	0.0	0.0	0.0
5	0.260	0.327	0.250
10	0.520	0.461	0.385
15	0.781	0.491	0.440
20	1.041	0.470	0.465
25	1.301	0.428	0.450
30	1.562	0.380	0.415
35	1.822	0.335	0.375
40	2.082	0.296	0.330
45	2.342	0.263	0.295
50	2.603	0.237	0.265
55	2.863	0.215	0.235
60	3.123	0.199	0.210
65	3.384	0.186	0.185
70	3.644	0.176	0.170
75	3.904	0.169	0.155
80	4.164	0.163	0.145
85	4.425	0.159	0.135
90	4.685	0.156	0.125
95	4.945	0.154	0.120
100	5.205	0.152	0.115

TABLE C4

Water Spray at  $1.50 \times 10^{-3}$  l/s

Air Flowrate at 0.21 kg/s

Air Temperature  $T_a$  at 31.0 °CFeed Temperature  $T_w$  at 17.5 °C

Time (s)	Dimensionless Time ( $\theta$ )	Exit Concentration $C(\theta)$ (V%)	
		Calculated	Experimental
0	0.0	0.0	0.0
5	0.288	0.403	0.330
10	0.575	0.534	0.440
15	0.863	0.539	0.480
20	1.151	0.493	0.495
25	1.438	0.432	0.475
30	1.726	0.372	0.440
35	2.014	0.321	0.395
40	2.301	0.280	0.350
45	2.589	0.249	0.300
50	2.877	0.224	0.265
55	3.164	0.207	0.235
60	3.452	0.193	0.210
65	3.740	0.184	0.185
70	4.027	0.177	0.170
75	4.315	0.172	0.160
80	4.603	0.169	0.145
85	4.890	0.166	0.135
90	5.178	0.164	0.130
95	5.466	0.163	0.125
100	5.753	0.162	0.120

TABLE C5Water Spray at  $1.50 \times 10^{-3}$  l/s

Air Flowrate at 0.23 kg/s

Air Temperature  $T_a$  at 31.5 °CFeed Temperature  $T_w$  at 17.5 °C

Time (s)	Dimensionless Time ( $\theta$ )	Exit Concentration $C(\theta)$ (V%)	
		Calculated	Experimental
0	0.0	0.0	0.0
5	0.315	0.479	0.390
10	0.630	0.583	0.480
15	0.945	0.559	0.520
20	1.260	0.493	0.525
25	1.575	0.421	0.490
30	1.890	0.358	0.440
35	2.205	0.308	0.380
40	2.520	0.269	0.330
45	2.836	0.241	0.285
50	3.151	0.221	0.245
55	3.466	0.207	0.215
60	3.781	0.197	0.190
65	4.096	0.190	0.175
70	4.411	0.186	0.160
75	4.726	0.182	0.150
80	5.041	0.180	0.145
85	5.356	0.178	0.140
90	5.671	0.177	0.135
95	5.986	0.177	0.132
100	6.301	0.176	0.130

TABLE C6Water Spray at  $2.0 \times 10^{-3}$  l/s

Air Flowrate at 0.13 kg/s

Air Temperature  $T_a$  at  $31.0^\circ\text{C}$ Feed Temperature  $T_w$  at  $18.0^\circ\text{C}$ 

Time (s)	Dimensionless Time ( $\theta$ )	Exit Concentration $C(\theta)$ (V%)	
		Calculated	Experimental
0	0.0	0.0	0.0
5	0.178	0.187	0.190
10	0.356	0.328	0.290
15	0.534	0.400	0.340
20	0.712	0.428	0.365
25	0.890	0.428	0.385
30	1.068	0.412	0.395
35	1.247	0.387	0.395
40	1.425	0.358	0.375
45	1.603	0.329	0.355
50	1.781	0.300	0.320
55	1.959	0.273	0.295
60	2.137	0.249	0.270
65	2.315	0.227	0.250
70	2.493	0.208	0.225
75	2.671	0.192	0.205
80	2.849	0.178	0.185
85	3.027	0.167	0.165
90	3.205	0.157	0.145
95	3.384	0.148	0.130
100	3.562	0.141	0.120



TABLE C7Water Spray at  $2.0 \times 10^{-3}$  l/s

Air Flowrate at 0.16 kg/s

Air Temperature  $T_a$  at  $31.0^\circ\text{C}$ Feed Temperature  $T_w$  at  $18.0^\circ\text{C}$ 

Time (s)	Dimensionless Time ( $\theta$ )	Exit Concentration $C(\theta)$ (V%)	
		Calculated	Experimental
0	0.0	0.0	0.0
5	0.219	0.258	0.240
10	0.438	0.403	0.345
15	0.657	0.458	0.395
20	0.877	0.461	0.425
25	1.096	0.438	0.435
30	1.315	0.403	0.425
35	1.534	0.364	0.390
40	1.753	0.326	0.355
45	1.973	0.292	0.315
50	2.192	0.262	0.285
55	2.411	0.236	0.255
60	2.630	0.215	0.225
65	2.849	0.197	0.200
70	3.068	0.183	0.180
75	3.288	0.171	0.160
80	3.507	0.162	0.145
85	3.726	0.154	0.135
90	3.945	0.148	0.125
95	4.164	0.144	0.115
100	4.384	0.140	0.110

TABLE C8

Water Spray at  $2.0 \times 10^{-3}$  l/s

Air Flowrate at 0.19 kg/s

Air Temperature  $T_a$  at 31.0 °CFeed Temperature  $T_w$  at 18.0 °C

Time (s)	Dimensionless Time ( $\theta$ )	Exit Concentration $C(\theta)$ (V%)	
		Calculated	Experimental
0	0.0	0.0	0.0
5	0.260	0.327	0.270
10	0.520	0.461	0.380
15	0.781	0.491	0.430
20	1.041	0.470	0.455
25	1.301	0.428	0.460
30	1.562	0.380	0.460
35	1.822	0.336	0.455
40	2.082	0.296	0.430
45	2.342	0.263	0.390
50	2.603	0.237	0.355
55	2.863	0.216	0.225
60	3.123	0.199	0.300
65	3.384	0.186	0.280
70	3.644	0.176	0.220
75	3.904	0.169	0.195
80	4.164	0.163	0.165
85	4.425	0.159	0.155
90	4.685	0.156	0.150
95	4.945	0.154	0.135
100	5.205	0.152	0.110

TABLE C9

Water Spray at  $2.0 \times 10^{-3}$  l/s

Air Flowrate at 0.21 kg/s

Air Temperature  $T_a$  at 31.5 °CFeed Temperature  $T_w$  at 18.0 °C

Time (s)	Dimensionless Time ( $\theta$ )	Exit Concentration C( $\theta$ ) (V%)	
		Calculated	Experimental
0	0.0	0.0	0.0
5	0.288	0.407	0.325
10	0.575	0.540	0.425
15	0.863	0.543	0.470
20	1.151	0.494	0.495
25	1.438	0.430	0.475
30	1.726	0.369	0.440
35	2.014	0.317	0.395
40	2.301	0.275	0.350
45	2.589	0.243	0.305
50	2.877	0.219	0.265
55	3.164	0.201	0.230
60	3.452	0.188	0.195
65	3.740	0.178	0.170
70	4.027	0.172	0.155
75	4.315	0.167	0.140
80	4.603	0.163	0.130
85	4.890	0.161	0.125
90	5.178	0.159	0.120
95	5.466	0.158	0.117
100	5.753	0.157	0.115

TABLE C10Water Spray at  $2.0 \times 10^{-3}$  l/s

Air Flowrate at 0.23 kg/s

Air Temperature  $T_a$  at  $31.5^\circ\text{C}$ Feed Temperature  $T_w$  at  $18.0^\circ\text{C}$ 

Time (s)	Dimensionless Time ( $\theta$ )	Exit Concentration $C(\theta)$ (V%)	
		Calculated	Experimental
0	0.0	0.0	0.0
5	0.315	0.479	0.385
10	0.630	0.583	0.475
15	0.945	0.559	0.515
20	1.260	0.493	0.515
25	1.575	0.421	0.480
30	1.890	0.358	0.440
35	2.205	0.308	0.390
40	2.520	0.270	0.340
45	2.836	0.242	0.290
50	3.151	0.221	0.250
55	3.466	0.207	0.215
60	3.781	0.197	0.190
65	4.096	0.190	0.170
70	4.411	0.186	0.155
75	4.726	0.182	0.145
80	5.041	0.180	0.135
85	5.356	0.179	0.130
90	5.671	0.177	0.125
95	5.986	0.177	0.122
100	6.301	0.176	0.120



TABLE C11Water Spray at  $2.50 \times 10^{-3}$  l/s

Air Flowrate at 0.13 kg/s

Air Temperature  $T_a$  at  $31.0^\circ\text{C}$ Feed Temperature  $T_w$  at  $18.0^\circ\text{C}$ 

Time (s)	Dimensionless Time ( $\theta$ )	Exit Concentration $C(\theta)$ (V%)	
		Calculated	Experimental
0	0.0	0.0	0.0
5	0.178	0.189	0.190
10	0.356	0.328	0.280
15	0.534	0.400	0.330
20	0.712	0.427	0.360
25	0.890	0.428	0.375
30	1.068	0.412	0.387
35	1.247	0.387	0.390
40	1.425	0.358	0.375
45	1.603	0.328	0.355
50	1.781	0.300	0.330
55	1.959	0.273	0.305
60	2.137	0.249	0.275
65	2.315	0.227	0.250
70	2.493	0.209	0.225
75	2.671	0.192	0.200
80	2.849	0.178	0.180
85	3.027	0.167	0.170
90	3.205	0.157	0.145
95	3.384	0.148	0.130
100	3.562	0.141	0.115

TABLE C12Water Spray at  $2.50 \times 10^{-3}$  l/s

Air Flowrate at 0.16 kg/s

Air Temperature  $T_a$  at 31.0 °CFeed Temperature  $T_w$  at 18.0 °C

Time (s)	Dimensionless Time ( $\theta$ )	Exit Concentration $C(\theta)$ (V%)	
		Calculated	Experimental
0	0.0	0.0	0.0
5	0.219	0.261	0.240
10	0.438	0.412	0.335
15	0.657	0.467	0.380
20	0.877	0.469	0.410
25	1.096	0.443	0.427
30	1.315	0.405	0.420
35	1.534	0.364	0.395
40	1.753	0.324	0.365
45	1.973	0.289	0.335
50	2.192	0.257	0.290
55	2.411	0.231	0.260
60	2.630	0.209	0.225
65	2.849	0.192	0.200
70	3.068	0.177	0.180
75	3.288	0.166	0.160
80	3.507	0.156	0.145
85	3.726	0.149	0.130
90	3.945	0.143	0.120
95	4.164	0.139	0.110
100	4.384	0.135	0.105

TABLE C13Water Spray at  $2.50 \times 10^{-3}$  l/s

Air Flowrate at 0.19 kg/s

Air Temperature  $T_a$  at  $31.5^\circ\text{C}$ Feed Temperature  $T_w$  at  $18.0^\circ\text{C}$ 

Time (s)	Dimensionless Time; ( $\theta$ )	Exit Concentration $C(\theta)$ (V%)	
		Calculated	Experimental
0	0.0	0.0	0.0
5	0.260	0.335	0.260
10	0.520	0.476	0.375
15	0.781	0.504	0.425
20	1.041	0.478	0.450
25	1.301	0.430	0.450
30	1.562	0.378	0.435
35	1.822	0.330	0.405
40	2.082	0.288	0.355
45	2.342	0.254	0.310
50	2.603	0.226	0.270
55	2.863	0.205	0.235
60	3.123	0.188	0.217
65	3.384	0.175	0.180
70	3.644	0.166	0.165
75	3.904	0.159	0.150
80	4.164	0.153	0.137
85	4.425	0.149	0.127
90	4.685	0.146	0.120
95	4.945	0.144	0.112
100	5.205	0.143	0.107

TABLE C14Water Spray at  $2.50 \times 10^{-3}$  l/s

Air Flowrate at 0.21 kg/s

Air Temperature  $T_a$  at  $31.5^\circ\text{C}$ Feed Temperature  $T_w$  at  $18.0^\circ\text{C}$ 

Time (s)	Dimensionless Time ( $\theta$ )	Exit Concentration $C(\theta)$ (V%)	
		Calculated	Experimental
0	0.0	0.0	0.0
5	0.288	0.408	0.305
10	0.575	0.538	0.410
15	0.863	0.541	0.460
20	1.151	0.493	0.487
25	1.438	0.430	0.475
30	1.726	0.369	0.445
35	2.014	0.317	0.400
40	2.301	0.275	0.350
45	2.589	0.243	0.300
50	2.877	0.219	0.255
55	3.164	0.201	0.220
60	3.452	0.188	0.190
65	3.740	0.179	0.170
70	4.027	0.172	0.150
75	4.315	0.167	0.140
80	4.603	0.163	0.127
85	4.890	0.161	0.120
90	5.178	0.159	0.115
95	5.466	0.158	0.112
100	5.753	0.157	0.110



TABLE C15

Water Spray at  $2.50 \times 10^{-3}$  l/s

Air Flowrate at 0.23 kg/s

Air Temperature  $T_a$  at 31.5 °CFeed Temperature  $T_w$  at 18.0 °C

Time (s)	Dimensionless Time ( $\theta$ )	Exit Concentration $C(\theta)$ (V%)	
		Calculated	Experimental
0	0.0	0.0	0.0
5	0.315	0.483	0.355
10	0.630	0.587	0.465
15	0.945	0.561	0.505
20	1.260	0.492	0.520
25	1.575	0.418	0.497
30	1.890	0.353	0.460
35	2.205	0.302	0.415
40	2.520	0.263	0.360
45	2.836	0.235	0.315
50	3.151	0.215	0.270
55	3.466	0.201	0.230
60	3.781	0.191	0.200
65	4.096	0.184	0.180
70	4.411	0.180	0.160
75	4.726	0.176	0.145
80	5.041	0.174	0.137
85	5.356	0.173	0.130
90	5.671	0.172	0.125
95	5.986	0.171	0.117
100	6.301	0.171	0.115

TABLE C16

Water Spray at  $3.0 \times 10^{-3}$  l/s

Air Flowrate at 0.13 kg/s

Air Temperature  $T_a$  at 31.0 °CFeed Temperature  $T_w$  at 18.0 °C

Time (s)	Dimensionless Time ( $\theta$ )	Exit Concentration C( $\theta$ ) (V%)	
		Calculated	Experimental
0	0.0	0.0	0.0
5	0.178	0.190	0.170
10	0.356	0.333	0.255
15	0.534	0.406	0.310
20	0.712	0.433	0.340
25	0.890	0.432	0.362
30	1.068	0.415	0.375
35	1.247	0.389	0.382
40	1.425	0.359	0.375
45	1.603	0.328	0.357
50	1.781	0.300	0.335
55	1.959	0.272	0.310
60	2.137	0.247	0.285
65	2.315	0.225	0.260
70	2.493	0.206	0.230
75	2.671	0.190	0.205
80	2.849	0.176	0.180
85	3.027	0.164	0.160
90	3.205	0.154	0.140
95	3.384	0.145	0.122
100	3.562	0.138	0.110

TABLE C17Water Spray at  $3.0 \times 10^{-3}$  l/s

Air Flowrate at 0.16 kg/s

Air Temperature  $T_a$  at 31.0 °CFeed Temperature  $T_w$  at 18.0 °C

Time (s)	Dimensionless Time ( $\theta$ )	Exit Concentration $C(\theta)$ (V%)	
		Calculated	Experimental
0	0.0	0.0	0.0
5	0.219	0.263	0.220
10	0.438	0.412	0.335
15	0.657	0.466	0.385
20	0.877	0.468	0.405
25	1.096	0.442	0.420
30	1.315	0.405	0.420
35	1.534	0.364	0.405
40	1.753	0.324	0.385
45	1.973	0.289	0.355
50	2.192	0.258	0.320
55	2.411	0.231	0.287
60	2.630	0.210	0.255
65	2.849	0.192	0.220
70	3.068	0.177	0.200
75	3.288	0.166	0.175
80	3.507	0.156	0.155
85	3.726	0.149	0.135
90	3.945	0.143	0.120
95	4.164	0.139	0.110
100	4.384	0.135	0.100

TABLE C18Water Spray at  $3.0 \times 10^{-3}$  l/s

Air Flowrate at 0.19 kg/s

Air Temperature  $T_a$  at 31.5 °CFeed Temperature  $T_w$  at 18.0 °C

Time (s)	Dimensionless Time ( $\theta$ )	Exit Concentration $C(\theta)$ (V%)	
		Calculated	Experimental
0	0.0	0.0	0.0
5	0.260	0.340	0.255
10	0.520	0.484	0.357
15	0.781	0.509	0.410
20	1.041	0.481	0.437
25	1.301	0.431	0.450
30	1.562	0.377	0.437
35	1.822	0.327	0.412
40	2.082	0.284	0.375
45	2.342	0.249	0.335
50	2.603	0.221	0.290
55	2.863	0.200	0.247
60	3.123	0.183	0.210
65	3.384	0.170	0.185
70	3.644	0.161	0.160
75	3.904	0.154	0.145
80	4.164	0.148	0.130
85	4.425	0.144	0.120
90	4.685	0.142	0.110
95	4.945	0.139	0.105
100	5.205	0.138	0.100



TABLE C19Water Spray at  $3.0 \times 10^{-3}$  l/s

Air Flowrate at 0.21 kg/s

Air Temperature  $T_a$  at 31.5 °CFeed Temperature  $T_w$  at 18.0 °C

Time (s)	Dimensionless Time ( $\theta$ )	Exit Concentration $C(\theta)$ (V%)	
		Calculated	Experimental
0	0.0	0.0	0.0
5	0.288	0.414	0.325
10	0.575	0.544	0.420
15	0.863	0.544	0.460
20	1.151	0.493	0.480
25	1.438	0.427	0.475
30	1.726	0.365	0.445
35	2.014	0.312	0.405
40	2.301	0.270	0.355
45	2.589	0.238	0.305
50	2.877	0.213	0.260
55	3.164	0.195	0.225
60	3.452	0.182	0.195
65	3.740	0.173	0.170
70	4.027	0.166	0.150
75	4.315	0.162	0.137
80	4.603	0.158	0.125
85	4.890	0.156	0.115
90	5.178	0.154	0.110
95	5.466	0.153	0.107
100	5.753	0.152	0.105

TABLE C20Water Spray at  $3.0 \times 10^{-3}$  l/s

Air Flowrate at 0.23 kg/s

Air Temperature  $T_a$  at 31.5 °CFeed Temperature  $T_w$  at 18.0 °C

Time (s)	Dimensionless Time ( $\theta$ )	Exit Concentration $C(\theta)$ (V%)	
		Calculated	Experimental
0	0.0	0.0	0.0
5	0.315	0.483	0.340
10	0.630	0.586	0.445
15	0.945	0.560	0.490
20	1.260	0.491	0.515
25	1.575	0.417	0.500
30	1.890	0.353	0.470
35	2.205	0.302	0.435
40	2.520	0.263	0.395
45	2.836	0.235	0.345
50	3.151	0.215	0.305
55	3.466	0.201	0.267
60	3.781	0.191	0.235
65	4.096	0.184	0.205
70	4.411	0.180	0.185
75	4.726	0.176	0.160
80	5.041	0.174	0.145
85	5.356	0.173	0.132
90	5.671	0.172	0.122
95	5.986	0.171	0.115
100	6.301	0.171	0.110

TABLE C21Water Spray at  $3.50 \times 10^{-3}$  l/s

Air Flowrate at 0.13 kg/s

Air Temperature  $T_a$  at 31.5 °CFeed Temperature  $T_w$  at 18.5 °C

Time (s)	Dimensionless Time ( $\theta$ )	Exit Concentration $C(\theta)$ (V%)	
		Calculated	Experimental
0	0.0	0.0	0.0
5	0.178	0.191	0.180
10	0.356	0.333	0.260
15	0.534	0.406	0.305
20	0.712	0.433	0.337
25	0.890	0.432	0.365
30	1.068	0.415	0.375
35	1.247	0.389	0.380
40	1.425	0.359	0.375
45	1.603	0.328	0.357
50	1.781	0.300	0.332
55	1.959	0.272	0.315
60	2.137	0.247	0.285
65	2.315	0.225	0.260
70	2.493	0.206	0.225
75	2.671	0.190	0.200
80	2.849	0.176	0.175
85	3.027	0.164	0.155
90	3.205	0.154	0.137
95	3.384	0.145	0.125
100	3.562	0.138	0.105

TABLE C22Water Spray at  $3.50 \times 10^{-3}$  l/s

Air Flowrate at 0.16 kg/s

Air Temperature  $T_a$  at  $31.5^\circ\text{C}$ Feed Temperature  $T_w$  at  $18.5^\circ\text{C}$ 

Time (s)	Dimensionless Time ( $\theta$ )	Exit Concentration $C(\theta)$ (V%)	
		Calculated	Experimental
0	0.0	0.0	0.0
5	0.219	0.267	0.225
10	0.438	0.422	0.315
15	0.657	0.476	0.365
20	0.877	0.476	0.395
25	1.096	0.447	0.410
30	1.315	0.407	0.415
35	1.534	0.363	0.402
40	1.753	0.322	0.385
45	1.973	0.285	0.360
50	2.192	0.253	0.330
55	2.411	0.226	0.295
60	2.630	0.204	0.260
65	2.849	0.186	0.225
70	3.068	0.172	0.195
75	3.288	0.160	0.170
80	3.507	0.151	0.152
85	3.726	0.144	0.135
90	3.945	0.138	0.120
95	4.164	0.134	0.105
100	4.384	0.130	0.095



TABLE C23Water Spray at  $3.50 \times 10^{-3}$  l/s

Air Flowrate at 0.19 kg/s

Air Temperature  $T_a$  at  $31.5^\circ\text{C}$ Feed Temperature  $T_w$  at  $18.5^\circ\text{C}$ 

Time (s)	Dimensionless Time ( $\theta$ )	Exit Concentration $C(\theta)$ (V%)	
		Calculated	Experimental
0	0.0	0.0	0.0
5	0.260	0.340	0.250
10	0.520	0.483	0.360
15	0.781	0.509	0.412
20	1.041	0.480	0.435
25	1.301	0.430	0.445
30	1.562	0.377	0.432
35	1.822	0.327	0.412
40	2.082	0.284	0.380
45	2.342	0.249	0.350
50	2.603	0.221	0.305
55	2.863	0.200	0.265
60	3.123	0.183	0.225
65	3.384	0.170	0.190
70	3.644	0.161	0.167
75	3.904	0.154	0.145
80	4.164	0.148	0.130
85	4.425	0.145	0.115
90	4.685	0.105	0.105
95	4.945	0.139	0.100
100	5.205	0.138	0.095

TABLE C24Water Spray at  $3.50 \times 10^{-3}$  l/s

Air Flowrate at 0.21 kg/s

Air Temperature  $T_a$  at 31.5 °CFeed Temperature  $T_w$  at 18.5 °C

Time (s)	Dimensionless Time ( $\theta$ )	Exit Concentration C( $\theta$ ) (V%)	
		Calculated	Experimental
0	0.0	0.0	0.0
5	0.288	0.419	0.315
10	0.575	0.549	0.415
15	0.863	0.547	0.455
20	1.151	0.493	0.472
25	1.438	0.425	0.462
30	1.726	0.361	0.440
35	2.014	0.308	0.405
40	2.301	0.265	0.360
45	2.589	0.232	0.315
50	2.877	0.208	0.275
55	3.164	0.190	0.240
60	3.452	0.177	0.205
65	3.740	0.168	0.180
70	4.027	0.161	0.155
75	4.315	0.156	0.145
80	4.603	0.153	0.130
85	4.890	0.151	0.120
90	5.178	0.149	0.110
95	5.466	0.148	0.105
100	5.753	0.147	0.100

TABLE C25Water Spray at  $3.50 \times 10^{-3}$  l/s

Air Flowrate at 0.23 kg/s

Air Temperature  $T_a$  at  $31.5^\circ\text{C}$ Feed Temperature  $T_w$  at  $18.5^\circ\text{C}$ 

Time (s)	Dimensionless Time ( $\theta$ )	Exit Concentration $C(\theta)$ (V%)	
		Calculated	Experimental
0	0.0	0.0	0.0
5	0.315	0.487	0.380
10	0.630	0.590	0.470
15	0.945	0.561	0.507
20	1.260	0.490	0.515
25	1.575	0.414	0.500
30	1.890	0.348	0.470
35	2.205	0.296	0.425
40	2.520	0.257	0.380
45	2.836	0.229	0.330
50	3.151	0.209	0.285
55	3.466	0.195	0.250
60	3.781	0.185	0.215
65	4.096	0.178	0.190
70	4.411	0.174	0.170
75	4.726	0.171	0.155
80	5.041	0.169	0.140
85	5.356	0.167	0.130
90	5.671	0.166	0.120
95	5.986	0.166	0.110
100	6.301	0.165	0.105

```

10 REM      ADE-JOHN STUDIES OF THE DRYING OF DROPS
20 DIM T(100),C(100)
30 READ Q1,Q2,Q3,V1,V2,V3,V4,D
40 J=V4/Q3
50 N=100
60 FOR I=1,N
70 T(I)=I/J
80 NEXT I
90 I=V2/V4
100 E=V3/V4
110 B=Q1/Q3
120 A=B/(1-I-E)
130 K=B/E
131 PRINT : PRINT
132 PRINT "      IAD      ","      EBS      ","      BETA      "
133 PRINT T,E,B
134 PRINT : PRINT : PRINT
140 G=(B*A*K)/(K-A)
150 F=D/J
152 FOR I=1,N
155 C(I)=G*(EXP(A*(I-T(I)))-EXP(K*(T-T(I))))+F*(1-B)
158 NEXT I
160 PRINT : PRINT
170 PRINT "      T(SECS)      ","      0      ","      C(0)      "
180 PRINT : PRINT
190 FOR I=1,N
200 PRINT I,T(I),C(I)
210 NEXT I
220 REM INITIALISE AND SET WINDOW
222 CALL (1)
240 X0=0:X1=T(N):Y0=0:Y1=.6
250 CALL (2,X0,X1,Y0,Y1)
260 REM DRAW AXES
270 CALL (3,2,X0,Y0,E)
280 CALL (3,1,X0+X1,Y0,E)
290 CALL (3,1,X0+X1,Y0+Y1,E)
295 CALL (3,1,X0+X1,Y0+Y1,E)
300 CALL (3,1,X0,Y0+Y1,E)
310 CALL (3,1,X0,Y0,E)
320 REM PLOT CURVE
330 FOR I=1,N
340 CALL (3,1,T(I),C(I),E): NEXT I
360 REM PLOT DONE-SOUND BELL AND LEAVE GRAPHICS.
370 CALL (4,7)
380 CALL (5)
390 STOP
400 END
410 DATA .104,.56E-01,.16,.719,.381,1.272,3.65,K

```

Computer Program For Predicting The  
Exit Concentration Of Tracer In Air



RUN

TAU	EBS	BETA
.104384	.348493	.65

T(SECS)	$\theta$	C( $\theta$ )
1	.438356E-01	.270793E-01
2	.876712E-01	.980459E-01
3	.131507	.160222
4	.175342	.21446
5	.219178	.261538
6	.263014	.302165
7	.306849	.336989
8	.350685	.366596
9	.394521	.391523
10	.438356	.412257
11	.482192	.42924
12	.526027	.442875
13	.569863	.453525
14	.613699	.461524
15	.657534	.467172
16	.70137	.470739
17	.745206	.472474
18	.789041	.472598
19	.832877	.471312
20	.876712	.468799
21	.920548	.465222
22	.964384	.460729
23	1.00822	.455452
24	1.05205	.44951
25	1.09589	.443012
26	1.13973	.436051
27	1.18356	.428714
28	1.2274	.421077
29	1.27123	.413208
30	1.31507	.405168
31	1.3589	.39701
32	1.40274	.388781
33	1.44658	.380523
34	1.49041	.372272
35	1.53425	.364061
36	1.57808	.355917
37	1.62192	.347865
38	1.66575	.339924

210 BREAK

?

A Typical Output From The Computer Program  
(As Per Table C.12)

## CONTINUE

39	1.70959	.332113
40	1.75342	.324446
41	1.79726	.316936
42	1.8411	.309593
43	1.88493	.302425
44	1.92877	.29544
45	1.9726	.288641
46	2.01644	.282034
47	2.06027	.275619
48	2.10411	.269399
49	2.14795	.263374
50	2.19178	.257543
51	2.23562	.251906
52	2.27945	.24646
53	2.32329	.241204
54	2.36712	.236134
55	2.41096	.231247
56	2.45479	.22654
57	2.49863	.22201
58	2.54247	.217651
59	2.5863	.213461
60	2.63014	.209433
61	2.67397	.205565
62	2.71781	.201852
63	2.76164	.198288
64	2.80548	.19487
65	2.84932	.191593
66	2.89315	.188452
67	2.93699	.185443
68	2.98082	.182561
69	3.02466	.179801
70	3.06849	.17716
71	3.11233	.174633
72	3.15616	.172216
73	3.2	.169904
74	3.24384	.167695
75	3.28767	.165582
76	3.33151	.163564
77	3.37534	.161636
78	3.41918	.159795
79	3.46301	.158036
80	3.50685	.156357

210 BREAK

?

## CONTINUE

81	3.55068	.154755
82	3.59452	.153226
83	3.63836	.151767
84	3.68219	.150375
85	3.72603	.149047
86	3.76986	.147781
87	3.8137	.146574
88	3.85753	.145423
89	3.90137	.144325
90	3.94521	.14328
91	3.98904	.142283
92	4.03288	.141333
93	4.07671	.140429
94	4.12055	.139567
95	4.16438	.138746
96	4.20822	.137964
97	4.25205	.137219
98	4.29589	.13651
99	4.33973	.135835
100	4.38356	.135193

!

TABLE D1Water Spray at  $1.50 \times 10^{-3}$  l/s

Time, t (s)	Tracer Concentration (gm/l)				
	Air Flowrate (kg/s)				
	0.13	0.16	0.19	0.21	0.23
0	0.0	0.0	0.0	0.0	0.0
5	0.203	0.250	0.150	0.173	0.150
10	0.500	0.420	0.350	0.302	0.296
20	1.152	0.950	0.865	0.770	0.704
30	1.670	1.843	1.400	1.300	1.230
40	2.401	2.250	2.037	1.950	1.750
50	2.950	2.850	2.603	2.730	2.460
60	3.350	3.198	3.151	3.050	3.002
70	3.299	3.480	3.570	3.456	3.273
80	2.880	3.102	3.382	3.572	3.654
90	2.370	2.630	2.930	3.240	3.740
100	1.900	2.080	2.550	2.750	3.050
110	1.250	1.619	2.039	2.400	2.510
120	0.950	1.225	1.564	1.834	2.140



TABLE D2Water Spray at  $2.0 \times 10^{-3}$  l/s

Time, t (s)	Tracer Concentration (gm/l)				
	Air Flowrate (kg/s)				
	0.13	0.16	0.19	0.21	0.23
0	0.0	0.0	0.0	0.0	0.0
5	0.150	0.210	0.290	0.120	0.150
10	0.561	0.423	0.330	0.280	0.301
20	1.070	0.870	0.752	0.675	0.636
30	2.000	1.400	1.270	1.260	1.332
40	2.621	2.175	2.003	1.903	1.770
50	2.998	2.780	2.650	2.568	2.402
60	3.375	3.102	3.170	3.125	3.000
70	3.302	3.460	3.520	3.450	3.370
80	2.674	3.076	3.748	3.500	3.620
90	2.103	2.563	2.883	3.047	3.401
100	1.720	2.020	2.276	2.771	3.004
110	1.316	1.610	1.937	2.293	2.562
120	0.983	1.098	1.486	1.804	2.064

TABLE D3Water Spray at  $2.50 \times 10^{-3}$  l/s

Time, t (s)	Tracer Concentration (gm/l)				
	Air Flowrate (kg/s)				
	0.13	0.16	0.19	0.21	0.23
0	0.0	0.0	0.0	0.0	0.0
5	0.310	0.168	0.147	0.139	0.100
10	0.400	0.332	0.423	0.250	0.270
20	0.953	0.501	0.771	0.671	0.634
30	1.750	1.162	1.402	1.253	1.107
40	2.603	2.376	2.036	1.870	1.750
50	3.014	3.207	2.704	2.568	2.381
60	3.520	3.380	3.280	3.094	2.900
70	3.100	3.381	3.517	3.506	3.307
80	2.750	3.267	3.149	3.427	3.602
90	2.102	2.584	2.887	3.121	3.450
100	1.701	1.950	2.338	2.750	2.950
110	1.280	1.447	1.876	2.250	2.506
120	0.870	1.034	1.531	1.703	2.008

TABLE D4Water Spray at  $3.0 \times 10^{-3}$  l/s

Time, t (s)	Tracer Concentration (gm/l)				
	Air Flowrate (kg/s)				
	0.13	0.16	0.19	0.21	0.23
0	0.0	0.0	0.0	0.0	0.0
5	0.297	0.175	0.126	0.130	0.128
10	0.486	0.378	0.304	0.270	0.239
20	1.004	0.903	0.803	0.704	0.630
30	1.750	1.667	1.580	1.379	1.230
40	2.469	2.372	2.267	1.912	1.800
50	2.941	2.940	2.870	2.658	1.402
60	3.372	3.337	2.278	2.190	2.830
70	3.150	3.420	3.427	3.520	3.350
80	2.800	2.987	3.173	3.340	3.550
90	2.316	2.530	2.870	3.006	3.300
100	1.762	1.870	2.326	2.630	2.871
110	1.160	1.346	1.865	2.210	2.360
120	0.760	0.948	1.400	1.743	1.870

TABLE D5Water Spray at  $3.50 \times 10^{-3}$  l/s

Time, t (s)	Tracer Concentration (gm/l)				
	Air Flowrate (kg/s)				
	0.13	0.16	0.19	0.21	0.23
0	0.0	0.0	0.0	0.0	0.0
5	0.250	0.183	0.128	0.119	0.103
10	0.438	0.360	0.300	0.204	0.241
20	1.087	0.921	0.819	0.697	0.650
30	2.004	1.596	1.500	1.330	1.125
40	2.720	2.330	2.250	2.100	1.926
50	3.160	2.840	2.910	2.750	2.550
60	3.397	3.378	3.370	3.288	3.130
70	2.902	3.250	3.450	3.575	3.362
80	2.728	2.950	3.203	3.430	3.637
90	2.230	2.521	2.950	3.100	3.350
100	1.760	1.987	2.420	2.704	2.847
110	1.152	1.360	1.930	2.089	2.403
120	0.624	0.890	1.281	1.630	1.789



TABLE E1

Residence Time Distribution For Sprayed Droplets  
Of Sodium Carbonate Slurries.

Time, t (s)	Tracer Concentration (gm/l)			
	Spray At $2.25 \times 10^{-3}$ l/s		Spray At $3.35 \times 10^{-3}$ l/s	
	Air Flowrate (kg/s)		Air Flowrate (kg/s)	
	0.16	0.21	0.16	0.21
0	0.0	0.0	0.0	0.0
20	0.101	0.173	0.187	0.087
40	0.252	0.100	0.503	0.302
60	0.375	0.302	0.712	0.611
80	0.737	0.504	1.104	0.852
100	1.004	0.799	1.103	1.037
120	1.172	1.003	1.000	1.087
140	1.179	1.256	0.698	0.896
160	0.801	1.025	0.601	0.725
180	0.687	0.837	0.437	0.487

?LIST

```

10 REM      SPRAY DRYING OF DROPLETS AND SLURRIES
20 READ Q,D,L,U1,U2,M1,M2,Z,Q2,H3,C,A3,A0,C3,C0,E,L,U3,D1,N
30 READ L1,P1,R,V5,H0
40 V1=13.076*V5*(((U2*D*L)/M2)+1.079*(.11/M2)+1.551*(U1/U2)+.29)
50 V2=V1*(Z/L)+.335
60 V3=17.035*V5*(1/(((U2*D*L)/M2)+1.076*(.11/M2)+3.21*(U1/U2)+.61))
70 V4=V3*(Z/L)+.752
80 V7=3.153*V5*(((U2*D*L)/M2)+.134*(.11/M2)+.45*(U1/U2)+.76E-01)
90 V3=V7*(Z/L)+.393
100 V6=5.033*V5*(1/(((U2*D*L)/M2)+.61)*(11/M2)+1.957*(U1/U2)+.125))
110 V9=V6*(Z/L)+.374
120 T1=V2/Q
130 T2=V4/Q
140 T3=V3/Q
150 PRINT : PRINT
160 PRINT "V1 "," V2 "," V3 "
170 PRINT V2,V4,V3
180 PRINT : PRINT
190 PRINT "TAU 1","TAU 2","TAU 3"
200 PRINT T1,T2,T3
210 T=V5/Q
220 G=((Q*S*(H3-H0)*T)-(Q2*C*(A3-A0)))/(Q2*(C3-C0)+1)
230 PRINT : PRINT
240 PRINT "TAU ","THETA"
250 PRINT T,G
255 J1=(4*R+2*N)/L1+2
260 W=U3*D1*N1*P1*L1+2
270 K=W/(P1*(L1)+2*(C3-C0))
280 J2=(K*4*P1*R+2*(C3-C0))*G
290 PRINT : PRINT
300 PRINT "W "
310 PRINT W
315 PRINT : PRINT
320 PRINT " MASS TRANSFER COEFF."
330 PRINT K
335 PRINT : PRINT
340 PRINT " RATE OF DRYING"
350 PRINT J2
360 END
370 STOP
380 DATA .76,.96,1.33,3.59,.29,.1E-02,.17E-16,5.4,.113E-03
390 DATA 327,1.674,50.43,353,1500,1.03,2225.31,.54,.393,.77E-01
400 DATA .2E-04,3.142,.1E-02,15.21,113

```

?

Computer Program For Testing  
The Spray Tower Design Model

? RUN

V1	V2	V3
5.57713	2.33992	5.31136

TAU 1	TAU2	TAU3
7.33334	3.07335	6.93923

TAU	THETA
20.0132	12.3101

W  
 .466661E-03

MASS TRANSFER COEFF.  
 3.22378

RATE OF DRYING  
 .574464

360 EXIT  
 ?

Computer Output ( $V_T = 15.21 \text{ m}^3$ )

RUN

V1  
1.33337V2  
.56152V3  
1.27471TAU 1  
1.76191TAU2  
.733342TAU3  
1.67724TAU  
4.33263THETA  
2.95489Computer Output ( $V_T = 3.65 \text{ m}^3$ )



NOMENCLATURE

List of symbols used in this thesis, unless otherwise stated.

$A$	area of hemispherical drop ( $2\pi R^2$ )	$(m^2)$
$A_1$	emissive area of disc 1	$(m^2)$
$A_2$	emissive area of disc 2	$(m^2)$
$A_3$	emissive area of disc 3	$(m^2)$
$A_p$	projected area of droplet on a plane normal to mean flow	$(m^2)$
$A_x$	emissive area of specimen	$(m^2)$
$C$	moisture content (kg moisture/ $m^3$ solution)	
$\Delta C$	concentration driving force (kg moisture/ $m^3$ solution)	
$C_s$	specific heat of particle per unit weight of solid	$(kJ/kg^{\circ}K)$
$C_D$	drag coefficient	
$c_p$	specific heat	$(kJ/kg^{\circ}K)$
$D$	diameter of spherical or cylindrical objects	$(m)$
$D_v$	diffusivity of vapour in air	$(m^2/s)$
$D_p$	drop diameter	$(m)$
$D_{pc}$	critical diameter of drop and dried particle	$(m)$
$D_{p1}$	original atomised diameter of drop	$(m)$
$d_p$	mean pore diameter	$(m)$
$d_{vs}$	Sauter mean diameter ( $\sum n_i d_i^3 / \sum n_i d_i^2$ )	$(m)$

$d_m$	diameter of largest drop	(m)
$d_i$	diameter of each class of droplets	(m)
$\Delta d$	the spread of droplet size distribution	(m)
$e$	emissivity	
$F_L$	lift force	(N)
$f$	Fanning friction factor	$\left( \frac{R}{\rho V^2} \right)$
$G$	air mass flowrate	(kg/s)
$G_s$	superficial mass velocity	
$Gr$	Grashof Number	$(D_p^3 \rho_g^2 g_c \sigma \Delta \theta) / \mu^2$
$g_c$	acceleration due to gravity	(m/s <sup>2</sup> )
$H$	humidity	(kg/kg)
$h_c$	rate of heat transfer by conduction and convection per unit area of interface per unit temperature difference across transfer path	(W/m <sup>2</sup> .s. <sup>o</sup> K)
$I$	current	(amp.)
$K_G$	mass transfer coefficient	(m/s)
$k$	thermal conductivity	(W/m <sup>2</sup> .s. <sup>o</sup> K)
$l_t$	total length ( $l_o + l_x$ ) of heated or wetted section of plate, from front edge to downstream edge	(m)
$l_o$	length of unheated or dry plate	(m)
$l_x$	length of heated or wetted plate	(m)
$M$	average molecular weight of gas mixture in transfer path	
$Nu$	Nusselt Number for heat transfer	$(h_c D_p / k)$
$Nu'$	Nusselt Number for mass transfer	$(K_G M D_p p_f) / D_v \rho_g$

N	total number of pores	
$N_A$	rate of mass transfer	$(\text{kg}/\text{m}^2\text{s})$
$n_i$	number of each class of droplet	
Pr	Prandtl Number	$(c_p\mu/k)$
P	total pressure	$(\text{N}/\text{m}^2)$
$p_b$	log mean partial pressure of air in film	$(\text{N}/\text{m}^2)$
$p_{av}$	average partial pressure of air in transfer path adjacent to drop	$(\text{N}/\text{m}^2)$
$p_f$	average value of $(\Pi - p_A)$ across transfer path	$(\text{N}/\text{m}^2)$
$p_d$	partial pressure of steam at $\theta_d$	$(\text{N}/\text{m}^2)$
$p_A$	partial pressure of diffusing vapour	$(\text{N}/\text{m}^2)$
$\Delta P$	pressure driving force	$(\text{N}/\text{m}^2)$
$p_a$	air pressure	$(\text{N}/\text{m}^2)$
p	parameter related to the extent of mixing	
$Q_1$	volumetric flowrate of main stream	$(\text{m}^3/\text{s})$
$Q_2$	volumetric flowrate of by-pass stream	$(\text{m}^3/\text{s})$
$Q_T$	total air volumetric flowrate	$(\text{m}^3/\text{s})$
$Q_a$	volumetric flowrate of atomising air	$(\text{m}^3/\text{s})$
q	rate of heat transfer to droplet	$(\text{J}/\text{s})$
$q_1$	liquid volumetric flowrate	$(\text{l}/\text{s})$
Re	Reynolds Number	$(\rho_g V D_p)/\mu$
$R_c$	universal gas constant	$(8.314 \text{ kJ}/\text{kmol}^\circ\text{K})$
R	external radius of drop	$(\text{m})$
r	internal radius of drop	$(\text{m})$
$r'$	radial position of droplet	$(\text{m})$
$r_1$	radial distance where the nozzle velocity becomes half	$(\text{m})$

Sh	Sherwood Number	$(K_G D_p / D_v)$
Sc	Schmidt Number	$(\mu / \rho_g D_v)$
s	humid heat	$(\text{kJ/kg}^\circ\text{K})$
t	time	(s)
$\bar{t}$	mean residence time	(s)
U	mean velocity of flow of liquid or vapour	(m/s)
V	velocity	(m/s)
$V_o$	average velocity in conduit	(m/s)
$V_1$	volume of first stirred-tank	(m <sup>3</sup> )
$V_2$	volume of plug-flow section	(m <sup>3</sup> )
$V_3$	volume of second stirred-tank	(m <sup>3</sup> )
$V_4$	volume occupied by the by-pass stream	(m <sup>3</sup> )
V'	voltage	(volts)
$V_T$	total volume ( $\Sigma V$ )	(m <sup>3</sup> )
$V_f$	velocity of droplet relative to fluid	(m/s)
$V_{rel}$	relative velocity between the air stream and liquid stream	(m/s)
W	mass of water evaporated	(kg)
$W_d$	mass of droplet	(kg)
$W_c$	critical moisture content	(kg moisture/m <sup>3</sup> solution)
$W_f$	final moisture content	(kg moisture/m <sup>3</sup> solution)
Z	height of tower	(m)
$T_0, T_1, T_2, T_3$	liquid feed temperature at stage 0, 1, 2, 3 respectively	(°K)
$t_0, t_1, t_2, t_3$	air temperature at stage 0, 1, 2, 3 respectively	(°K)



GREEK LETTERS

$\beta$	fraction of flow entering the main stream	
$\epsilon$	dimensionless residence time in top stirred-tank section	
$\epsilon'$	porosity of crust	
$\tau$	dimensionless residence time in plug flow section	
$\theta$	dimensionless time	$(t/\bar{t})$
$\Gamma$	gamma function	
$\nu_a$	kinematic viscosity of air	$(m^2/s)$
$\nu$	parameter which relates to the mean residence time of the system	
$\mu$	viscosity	$(Ns/m^2)$
$\eta$	surface tension	$(N/m)$
$\psi$	constant	
$\delta t'$	thickness of by-pass stream from wall of spray tower	$(m)$
$\delta\theta$	tracer injection time (dimensionless)	
$\sigma$	temperature coefficient of expansion for the gas	$(^{\circ}K^{-1})$
$\pi$	constant (3.1416)	
$\rho$	density	$(kg/m^3)$
$\rho_s$	particle density	$(kg/m^3)$
$\theta_1$	final temperature of disc 1	$(^{\circ}K)$
$\theta_2$	final temperature of disc 2	$(^{\circ}K)$
$\theta_3$	final temperature of disc 3	$(^{\circ}K)$
$\theta_i$	temperature inside particle	$(^{\circ}K)$

$\theta_o$	temperature of main stream	(°K)
$\theta_d$	drop temperature	(°K)
$\Delta\theta$	temperature difference	(°K)
$\lambda$	latent heat	(kJ/kg)
$\lambda_i$	latent heat of evaporation at interface	(kJ/kg)
$\omega$	angular velocity of droplet	(rad/s)
$\alpha, \gamma$	constants depending upon the operating conditions	
$a, b, q$	constants	

#### SUBSCRIPT

a	air
u, au	upstream
d, ad	downstream
l	liquid
g	gas
s	saturation
av	average
i	interfacial
amb	ambient
t	tangential
r	radial
a	axial

REFERENCES

1. RANZ, W.E., and MARSHALL, W.R., Jnr; Chem. Eng. Prog; 48, 141, 173 (1952).
2. FUCHS, N., Phys. Z. Sowjet; 6, 224 (1934), available in translation as Tech. Mem. 1160, Nat. Advisory Comm. Aeronaut.
3. KRAMERS, H., Physica; 12, 61 (1946)
4. MEYER, P., Trans Inst. Chem. Eng; 15, 127 (1937).
5. FROESSLING, N., Gerlands Beitr. Geophys; 52, 170 (1938).
6. CHILTON, T.H., and COLBURN, A.P., Ind. Eng. Chem; 26, 1183 (1935).
7. COLBURN, A. P., Trans. Am. Inst. Chem. Eng; 29 174 (1933).
8. McADAMS, W.H., "Heat Transmission"; McGraw-Hill Book Co. Inc; New York (1942).
9. COLBURN, A. P., and PIGFORD, R. L., 8, "Chemical Engnr's Handbook" 3rd Edition McGraw-Hill Book Co; Inc; New York (1950).
10. CHARLESWORTH, D. H., and MARSHALL, W. R., A.I.Ch.E. Journal; 6, 9, (1960).
11. AUDU, T.O.K., Ph.D. Thesis; University of Aston in Birmingham (1973).
12. DLOUHY, J., and GAUVIN, W. H., A.I.Ch.E. Journal; 6, 29, (1960).
13. WILLIAMS, G.C., and SCHMIT, R. O., Ind. Eng. Chem. 38, 967, (1946).

14. WILLIAMS, G. C., Ph.D. Thesis M.I.T. (1943).  
Available in Abridged form as P.B. Report 6538, by  
T. K. SHERWOOD, and G. C. WILLIAMS.
15. KEEN, B.A., J. Agric. Sci; 6, 456, (1914).
16. FISHER, E. A., *ibid*; 13, 121, (1923).
17. FISHER, E. A., *ibid*; 17, 407, (1927).
18. SHERWOOD, T.K., Ind. Eng. Chem; 21, 12, 976, (1929).
19. SHERWOOD, T.K., *ibid*; 22, 132, (1930).
20. SHERWOOD, T.K., and COMINGS, E.W., *ibid*; 25, 311,  
(1933).
21. COULSON, J. M., and RICHARDSON, J. F., Chem.  
Engineering, Vol. 2; 2nd Edition, Pergamon Press,  
(1968).
22. PERRY, J. H., Chem. Engineers Handbook, 4th Edition  
McGraw-Hill, (1936).
23. GILLILAND, E. R., Ind. Eng. Chem; 30, 406, (1938).
24. KIRK-OTHMER, Encyclopedia of Chem. Tech., Vol. 7,  
2nd Edition.
25. TROMMELEN, A. M., and CROSBY, E. J., A.I.Ch.E. Journal  
16, 857, (1970).
26. CHU, J. C., LANE, A. M., and CONKLIN, D., Ind. Eng.  
Chem; 45, 1586 (1953).
27. CHU, J. C., FINELT, S., HOERRNER, W., and LIN, M. S.,  
*ibid*; 51, 275, (1959).
28. TOEI, R., et al; Chem. Eng. (Japan), 30, 43 (1966).
29. WENZEL, L., and WHITE, R. R., Ind. Eng. Chem; 43,  
1829, (1951).



30. KEEY, R. B., and GLEN, J. B., Can. J. Chem. Eng; 42, 227, (1964).
31. ROWE et al; Trans. Inst. Chem. Engrs; 43, T14 (1965).
32. HUGHMARK, G. A., A.I.Ch.E.J; 13, 1219, (1967).
33. LEE, K., and RYLEY, D. J., J. Heat Transfer, Trans. Am. Soc. Mech. Engrs. 90, 445, (1968).
34. ZAK, E. G., Zhur. Geofiz. (U.S.S.R.), 6, 452 (1936).
35. VAN KREVELIN, D. W., and HOFTIJZER, P. J., J. Soc. Chem. Ind; 68, 59, (1949).
36. MAISEL, D. S., and SHERWOOD, T. K., Chem. Eng. Prog; 46, 131, 172, (1950).
37. SHERWOOD, T. K., Trans. Am. Inst. Chem. Engrs.; 36, 817, (1940).
38. GILLILAND, E. R., and SHERWOOD, T. K., Ind. Eng. Chem; 26, 516, (1934).
39. POHLHAUSEN, E., Zeit. fur Angewardte Math. und. Mech; 1, 115, (1921).
40. JACOB, M., and DOW, W., Trans. Am. Soc. Mech. Engrs; 68, 123 (1946)
41. POWELL, R. W., Trans. Inst. Chem. Engrs. 18, 26, (1940).
42. LINTON, W. H., and SHERWOOD, T. K., Chem. Eng. Prog; 46, 258, (1950).
43. POWELL, R. W., and GRIFFITHS, E., Trans. Inst. Chem. Engrs; 13, 175 (1935).
44. COLBURN, A. P., Ind. Eng. Chem., 22, 967 (1930).
45. AUDU, T. O. K., and JEFFREYS, G. V., Trans. Inst. Chem. Engrs; 53, 165, (1975).
46. COULSON, J. M., and RICHARDSON, J. F., Chem. Engineering, Vol. 1, 2nd Edition, Pergamon Press (1970).

47. MAXWELL, J. C., Coll. Sci. Papers, Cambridge; 11, 625, (1890).
48. WHITMAN, W. G., Chem. and Met. Eng; 29, 147, (1923).
49. GOODRIDGE, F., and BRICKNELL, D. J., Trans. Int. Chem. Engrs; 40, 54 (1962).
50. HIGBIE, R., Trans. Am. Inst. Chem. Eng; 31, 365, (1935).
51. BELCHER, R., and NUTTEN, A. J., Quantitative Inorganic Analysis; Butterworth and Co. (Publishers) Ltd; 3rd Edition (1970).
52. KISHINEVSKIJ, M. K., J. Appl. Chem. U.S.S.R; 24, 593; and Zhur Priklad. Khim; 24, 542, (1951).
53. DANCKWERTS, P. V., A.I.Ch.E.J; 1, 456, (1955).
54. TOOR, H. L., and MARCHELLO, J. M., ibid; 4, 97, (1958).
55. RANZ, W. E., Trans. A.S.M.E; 54, 909, (1956).
56. MASTERS, K., Spray Drying; Leonard Hill Books London (1972).
57. BELCHER, D. W., et al; Chem. Eng; 70, 20, 83 (1963).
58. MARSHALL, W. R., Chem. Eng. Prog. Monograph Series; 2, 50 (1954).
59. MASTERS, K., Brit. Chem. Eng; 13, 88, 242, (1968).
60. LAPPLE, C. E., and SHEPHERD, C. B., Ind. Eng. Chem; 32, 605, (1940).
61. CHARM, S. E., "Fundamentals of Food Eng." Avi Publishing Co., Westport, Conn; (1963).
62. MASTERS, K., and MOHTADI, M. F., Chem. Eng., 12, 12, (1967).
63. FRIEDMAN, J. J. et al; Chem. Eng. Prog. 48, 181, (1952).

64. KATTA, S., and GAUVIN, W. H., A.I.Ch.E.J; 21, 143, (1975).
65. PLACE, G. et. al; Trans. Inst. Chem. Eng.; 37 268, (1959).
66. MASTERS, K., Ind. Eng. Chem.; 60, 53, (1968).
67. KESSLER, H. G., Chem. Ing. Tech; 36, 479 (1964).
68. BUCKHAM, J. A., and MOULTON, R. W., Chem. Eng. Prog; 51, 126 (1955).
69. ARNI, V. R. S., "Production, Movement, and Evaporation in Spray Dryers"; U. Washington; Inc; Ann Arbor, Mich. (1959).
70. CHALLOUD, et al.; Chem. Eng. Prog; 53, 593 (1957).
71. DANCKWERTS, P. V.. Chem. Eng. Sc; 9, 78 (1958).
72. TAYLOR, G. I., Proc. Roy. Soc; A223, 446 (1954).
73. FRAZER, R. P. et al.; Brit. Chem. Eng; 2, 496 (1957).
74. SITVEZ, M. S., and FOOTE, H., "Coffee Processing Tech.", Avi Publishing Co., Westport, Conn. (1963).
75. BALTAS, L., and GAUVIN, W. H., A.I.Ch.E.J; 15, 764 (1969).
76. GAUVIN, W. H. et. al., "Drop Trajectory Predictions and Their Importance in the Design of Spray Dryers", Intern. J. Multi-Phase Flow (1974).
77. NAKIYAMA, S., and TANASAWA, Y., Trans Soc. Mech. Engrs. (Japan) 4, 86, 138 (1938); 5, 63, 68 (1939); II-7 and II-8 (1940).
78. LEWIS, H. C. et. al., Ind. Eng. Chem; 40, 67 (1948).
79. KIM, K. Y., and MARSHALL, W. R., Jnr; A.I.Ch.E.J; 17, 575 (1971).

80. MUGELE, R. A., and EVANS, H. D., Ind. Eng. Chem; 43, 1317 (1951).
81. GWYN, J. E. et. al., Ind. Eng. Chem. Fundamentals; 4, 204 (1965).
82. BALTAS, L., and GAUVIN, W. H., A.I.Ch.E.J; 15, 772 (1969).
83. LICHT, W., ibid; 20, 595 (1974).
84. MIYASAKA, Y., J. Mech. Eng. Japan; 15, 34 (1959).
85. BEARD, K. V., and PRUPPACHER, H. R., J. atm. Sci; 26, 1066 (1969).
86. SAFFMAN, P. G., J. Fluid Mech; 22, 385 (1965).
87. KEEY, R. B., and PHAM, Q. T., The Chemical Engineer; 311, 516 (1976).
88. MARSHALL, W. R., Jnr; Trans. A.S.M.E; 1377, November (1955).
89. CROSBY, E. J., and MARSHALL, W.R., Chem. Eng. Prog; 54, 56 (1958).
90. MARSHALL, W. R., and SELTZER, E., Chem. Eng. Prog; 46, 501, 575 (1950).
91. CROSBY, E. J., and MARSHALL, W. R., ibid; 53, 347, (1957).
92. PROBERT, R. P., Phil. Mag.; 37, 94, (1946).
93. MIESSE, C. C., J. Franklin Inst.; 264, 391, (1957).
94. SHAPIRO, A. H., and ERICKSON; Trans. Am. Soc. Mech. Engrs.; 79, 775 (1957).
95. MANNING, W. P., and GAUVIN, W. H., A.I.Ch.E.J; 6, 184, (1960).
96. BOSE, A. K., and PEI, D. C. T., Can. J. Chem. Eng.; 42, 259 (1964).



97. DICKINSON, D. R., and MARSHALL, W. R., A.I.Ch.E.J.; 14, 541 (1968).
98. KIRSCHBAUM, E., Chem. Eng. Tech.; 24, 3 (1952).
99. KEEY, R. B., "Drying Principles And Practice"; 1st Edition, Pergamon Press (1972).
100. LANGMUIR, I., Phys. Rev.; 12, 368 (1918).
101. DLOUHY, J., and GAUVIN, W. H., Canadian J. Chem. Eng.; 113, (August 1960).
102. DUFFIE, J. A. and MARSHALL, W. R. Jnr; Chem. Eng. Prog; 49, 417, 480 (1953).
103. WALLMAN, H., and BLYTH, H. A., Ind. Eng. Chem.; 43, 1480 (1951).
104. ADE-JOHN, A. O., M.Sc. Thesis; University of Aston in Birmingham, 1974.
105. WEN, C. Y., and FAN, L. T., "Models for Flow Systems and Chemical Reactors"; Chem. Proc. and Eng. Series Vol. 3, Marcel Dekker Inc., New York (1975).
106. JENSON, V. G., and JEFFREYS, G. V., "Mathematical Methods in Chemical Engineering"; 7th Edition, Academic Press Inc. London (1973).
107. JOHNSON, J. L., FAN, L. T., and WU, Y. S., Ind. Eng. Chem. Proc. Des. Dev.; 10, 4 (1971).
108. BAKOWSKI, S., Trans. I. Chem. Eng.; 32, S.37 (1954).
109. COOPER, A. R., and JEFFREYS, G. V., Chemical Kinetics and Reactor Design, Oliver and Boyd, Edinburgh (1971).
110. KOZENY, J., Ber. Wien Akad; 136a, 271, (1927).
111. CHIU, K. F., Chemical Engineering Report; University of Aston in Birmingham (1975).
112. CARMAN, P. C., Trans. I.Ch. Engrs.; 15, 150, (1937).
113. SHALHOUB, N. G., Ph.D. Thesis; University of Aston

- in Birmingham (1975).
114. D'ARCY, H. P. G., "Les Fontaines Publiques de la Ville de Dijon"; Victor Dalmont, Paris (1856).
  115. ERGUN, S., Chem. Eng. Prog; 48, 89, (1952).
  116. BLAKE, F. C., Trans. Am.I.Ch.Eng; 14, 415, (1922).
  117. CARSLAW, H. S., and JAEGER, J. C., "Operational methods in Applied Mathematics"; 2nd Edition, Oxford University Press (1948).
  118. MASSEY, B. S., Units, Dimensional Analysis and Physical Similarity; Van Nostrand Reinhold Company, London (1971).
  119. DANCKWERTS, P. V., Chem Eng. Sc.; 2, 1, (1953).
  120. SPALDING, D. B., ibid; 9, 74 (1958) .
  121. GAUVIN, W. H., and KATTA, S., A.I.Ch.E.J; 22, 713 (1976).
  122. SCHOWALTER, W. R., and JOHNSTONE, H. F., "Characteristics of the Mean Flow Patterns and Structure of Turbulence in Spiral Gas Streams", A. I. Chem.E.J., 6, 648 (1960).
  123. BANK, N., M. Eng. Thesis, "Measurements of Flow Characteristics in a Confined Vortex Flow", McGill Univ., Montreal Canada (1975).
  124. JANDA, F., "Calculation of the Dimension of Disc Spray Driers with Intensive Circulation of the Drying Medium", Intern. Chem. Eng., 13, 649 (1973).
  125. PARIS, J. R; et. al. "Modelling of the Air Flow in a Countercurrent Spray Drying Tower", Ind. Eng. Chem. Proc. Des. Dev.; 10, 157 (1971).

126. JEFFREYS, G. V., By Private Communication with an Industrial Company.